EXPRESSION AND CHARACTERISATION OF A NOVEL MANGANESE PEROXIDASE FROM *PHLEBIA RADIATA*

by

Usenobong Friday Ufot

A thesis submitted for the degree of

Doctor of Philosophy (Biochemistry)

at the University of Sussex

September, 2010

This page is deliberately left blank

Declaration

This thesis has never been submitted in whole
or in part to this University or any other
University for a degree. This work is my own
except where otherwise stated

Signed.....

Usenobong Friday Ufot M.Sc. (Calabar, Nigeria)

Dedication

This work is dedicated to my beautiful twin daughters, Inyene and Uduak for their understanding and endurance of my long absence from home.

Acknowledgement

I am first all most grateful to the Almighty God who made this training opportunity possible through Akwa Ibom State University of Technology staff training programme. All my successes, achievements and sustenance I received from you.

I am grateful to my supervisor Professor Andrew T. Smith for giving me the opportunity to work in his laboratory. His guidance, suggestions and ideas were invaluable and enhanced the successful completion of this study. He taught me independence, patience and endurance, which have ensured my success. It has been a great opportunity to work in a very stimulating and multidisciplinary scientific environment. The scientific competence and encouragement made this training a rich and fruitful time for me. I am thankful to my co-supervisor Dr. Neil Crickmore for always being there for me whenever I needed help or advice.

The author is extremely thankful to Dr. Wendy Doyle for her wonderful role throughout the period of my PhD studies. I am particularly humbled by her selfless and sacrificial support. I will not forget in a hurry Wendy's pain-staking guidance and involvement particularly during the writing of this thesis. In the absence of my supervisor, you gave me hope. Your advice was invaluable. I am grateful to Prof. Mike Wallis for his advice and guidance in the writing of thesis. Present and former members of Lab. 13 and particularly Andy's group are thanked Maria, Khasim, Sarah, Elodie and Falah deserve many thanks for the various supports I received from them during my study.

My friends both at home and abroad I wish to thank for just being there. Kevin, Daniel, Udorohs, Oworens, Akpanabiatu have shared memorable moments and experiences with me. Your encouragement and prayers have been immense. Thanks also to all those I do not mention but do not forget.

I am much indebted to my family, wife, children, my brothers, sisters, and other relations for prayers and support. My in-laws are highly acknowledged for all the assistance and support given to my family during these years of my absence from home. Of particular mention are the patience, sacrifice, endurance, encouragement and understanding shown by my wife, Mboso and children, Unwana, Ifiok, Inyene and Uduak.

“It always seems impossible until it’s done”.

Expression and characterisation of a Novel Manganese Peroxidase from *Phlebia radiata.*

Summary

Manganese peroxidase 3 (MnP3) is an extracellular peroxidase from the white-rot fungus, *P. radiata* that is a well-studied wood/lignin degrader from Scandinavian forest (Hilden *et al.*, 2005). Unlike the *Phanerochaete chrysosporium* MnP's previously characterised, the *P. radiata* MnP3 is a 'short' MnP with a truncated C-terminus evolutionarily more related to the newly characterised versatile peroxidase. The cDNA for the full length MnP3 from *P. radiata* was optimised at the 5' end for *E.coli* expression and cloned into the expression vector pFLAG1. Five site-directed mutants targetting the Mn binding site (E40H, E44H, E40H/E44H, D186H and D186N) were constructed and characterised. The recombinant MnP3's, both wild-type and variants were isolated from *E.coli* inclusion bodies after expression in W3110 and active soluble proteins recovered after *in vitro* refolding and extensively characterised.

In this work, the characteristics of the *P. radiata* wild type MnP3 were compared with those of the mutant enzymes and the 'classical' *Phanerochaete* enzyme described in the literature. The molecular weight of the enzymes was 36kDa with UV/Vis absorption spectra typical of a six-coordinate high spin haem peroxidase. In contrast to the literature on these enzymes, the *Phlebia* MnP3 was found to have a maximum efficacy (k_{cat}/K_m) at pH 5.0 rather than the more typical optimum at 4.5. Consistent with the high oxidation potential of these enzymes, the Compound I form of the enzyme was found to be unstable decaying rapidly to a Compound II-like intermediate. Mutations to the manganese (II)-binding ligands change the catalytic properties of the *Phlebia* MnP3 dramatically and reactivity towards Mn (II) were greatly decreased particularly at lower pH. Interestingly, much of the activity in the higher pH region was maintained, showing that carboxylate Mn ligands are not essential at higher pH when tighter binding of Mn^{2+} is favoured. The *pKa*'s for the activity dependence matches those expected for the deprotonation of the surrogate His ligands.

The results confirm that the mutated Mn (II) binding site is the only productive catalytic site for Mn (II) oxidation. The specificity of metal binding by MnP3 was examined; Cu ions were found to be strongly inhibitory and Zinc ions bound particularly tightly and somewhat non-specifically to MnP3 with stoichiometries as high as 5:1 suggestive of multiple metal-binding sites other than the specific manganese-binding site. Use of Zn ions in crystallisation media clearly has the potential to complicate metal ion assignment in the structures of these enzymes. Interestingly, Cobalt ions were able to enhance the activity of MnP3 but were not rapidly oxidised by the enzyme itself.

The *P. radiata* enzymes have been found to be active in acidic and alkaline regions, being stable over a large pH range (5.0 – 8.5) and are readily additionally stabilised by addition of excess Ca^{2+}, both desirable features in such an enzyme that could be applied to the 'biorefinery' concept.

Table of Contents

Chapter 1: Introduction and Review literature

Chapter 2: Materials and Methods

Chapter 3: Cloning and expression of manganese peroxidase 3 of *Phlebia radiata* in *E.coli* and production of MnP3 mutant genes.

Chapter 4: General characterisation of *P. radiata* wild-type MnP3 and mutants

Chapter 5: Binding of manganese (II) and other divalent metals to MnP3 from *Phlebia radiata*

Chapter 7: Effect of temperature on the stability of MnP3

LIST OF ABBREVIATIONS

5c	Five-coordinated
6c	Six-coordinated
AAO	Aryl alcohol oxidase
ABTS	2, 2'-azino-bis (2-ethylbenzthiozoline-6-sulphonic) acid
APX	Ascorbate peroxidase
ATCC	American Type Culture Collection
BSA	Bovine serum albumin
CcP	Cytochrome *c* peroxidase
CD	Circular dichroism
CDM	Continuum Dielectric Method
CiP	*Coprinus cinereus* peroxidase
CPO	Chloroperoxidase
CTI	Charge transfer band I
CTII	Charge transfer band II
D186H	MnP3 with aspartate 186 replaced with histidine
D186N	MnP3 with aspartate 186 replaced with asparagine
DFT	Density Functional Theory
DHP	Dehydrogenation polymer (synthetic lignin)
DNA	Deoxyribonucleic acid
dNTP	Deoxynucleotide triphosphate
DTT	Dithothreitol
E40H	MnP3 with glutamate 40 replaced by histidine
E40H/E44H	MnP3 with glutamate 40 and 44 replaced by histidine
E44E	MnP3 with glutamate 44 replaced by histidine
EDTA	Ethylenediaminetetraacetic acid
EPR	Electron paramagnetic resonance
FPLC	Fast Performance Liqiud Chromatography
GLOX	Glyoxal oxidase
GSSG	Oxidize glutathione
HRP	Horseradish peroxidase
HS	High spin
ICP-MS	Inductively coupled plasma mass spectrometry
IPTG	Isopropyl β-D- thiogalactopyranoside
LiP	Lignin peroxidase
CiP	*Coprinus cinereus* peroxidase
LPO	Lactoperoxidase
LS	Low spin
m/z	Mass to charge ratio
MALDI	Matrix Assisted Laser Desorption Ionisation
MCO	Multicopper oxidase
MnP	Manganese peroxidase
MOPS	3-Morpholinopropanesulfonic acid
MS	Mass spectrometry
MYCOR	Mycelial Colour Removal process
NC-IUB	Nomenclature Committee of the International Union of Biochemistry
NMR	Nuclear magnetic resonance spectroscopy
PAH	Polycyclic aromatic hydrocarbon
PCB	Polychlorinated biphenyl

PCR	Polymerase Chain Reaction
PNK	Polynucleotide kinase
PNP	Peanut peroxidase
RZ	Reinheitszahl number
SDS-PAGE	Sodium Dodecyl Sulphate Polyacrylamide Gel Electrophoresis
TB	Terrific broth
TEMED	N, N, N, N-tetramethylethylenediamine
TNT	Trinitroluene
TOF	Time of flight
Tris	Tris (hydroxymethyl) aminomethane
VP	Versatile peroxidase
WPAM	Whole Plasmid Amplification Method
WTMnP3	Wild-type recombinant manganese peroxidase3

List of Figures

Where figures are not included in the main body of the text numbers refer to the page following the figure.

Chapter 1

Chapter 2

Chapter 3

Chapter 4

Chapter 6

Chapter 7

List of Tables

CHAPTER One

Introduction and literature review

1.1 Introduction

A concern over the long-term availability and costs of petroleum-based fuels and feedstock chemicals has sparked interest in the utilisation of readily available, renewable sources of fuels and chemicals (Ng *et al*., 1983). One such potential source of fuels and chemicals is lignocellulosic plant material, the world's most abundant renewable source of organic carbon. The feasibility of greater utilisation of lignocellulosic materials relies on the conversion of the polymeric components, (cellulose, and hemicelluloses) to fermentable sugars.

Figure 1.1 shows the 'biorefinery concept' and chemicals that could be obtained from wood on degradation.

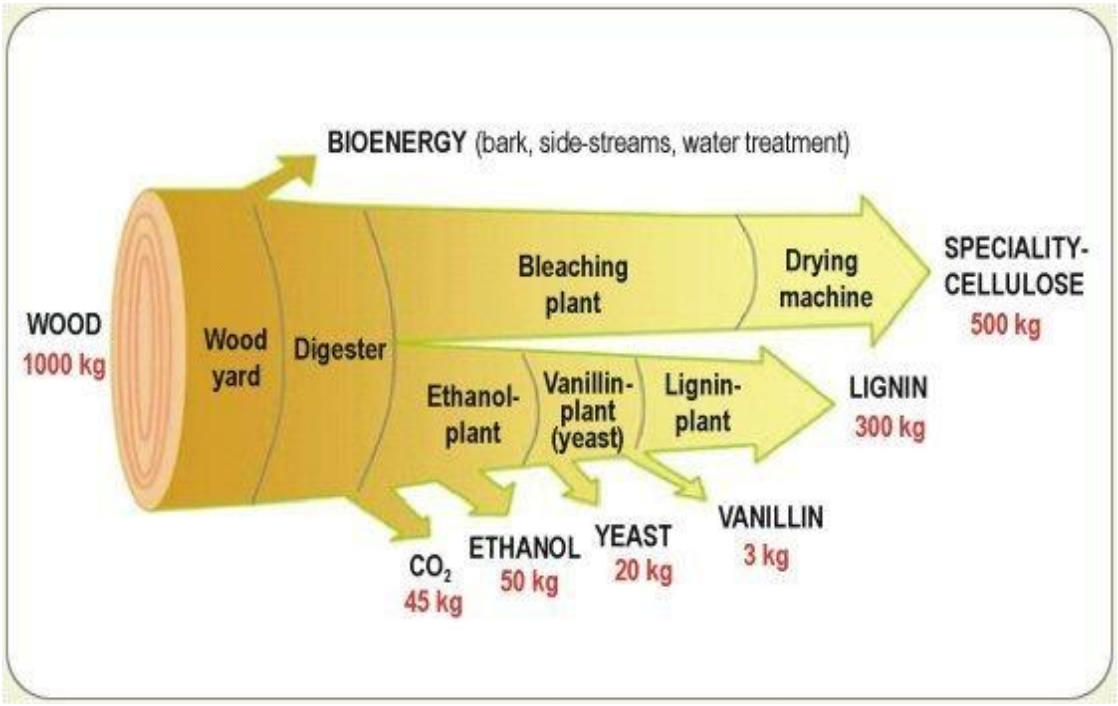

Figure 1.1: The lignocelluloses Biorefinery: Wood-based chemicals in an integrated concept (taken from Biorenew, Sixth Framework programme).

White-rot fungi have been found to be unusual among microorganisms in that they are capable of fully degrading the plant cell wall (Farrell, 1987; Bushwell and Odier, 1987; Gold *et al*., 1989). The ligninolytic enzymes of white-rot fungi are effective, nonspecific catalysts, and thus, these fungi are also considered to be potential microorganisms for bioremediation of polluted soils or water (Orth *et al*., 1994; Paszczynski and Crawford, 1995; Hatakka, 2001; Pointing, 2001). The possible application of these enzymes in a range of different fields has stimulated much research into the biochemistry of the white-rot fungi.

Because of climate change, interest in the use of abundant renewable lignocellulose as energy source has been kindled worldwide. Lignocellulosic biomasses, such as agricultural and forestry residues, have been recognised as a potential source of energy (biorefinery concept, Figure 1.1) that could replace future petroleum based fossil fuels (Himmel *et al*., 2007). The most common renewable fuel is ethanol, which could be derived from lignocellulosic materials, cellulose and hemicellulose, by fermentation (Wyman 2003; Gray *et al*., 2006).

1.2 Wood composition

Wood is a porous plant material made up of various types of xylem cells. Softwoods consist mainly of long tracheids and smaller ray parenchyma cells that give strength to the wood stem and sustain water transport. Hardwoods have more diverse types of xylem cells including fibers, vessels, and ray parenchyma cells that are connected by bordered or simple pits (Sjostrom, 1993; Kuhad *et al*., 1997). These cells are responsible for support and nutrient storage as well as water and nutrient transport between plant roots and the photosynthesizing leaves (Eriksson *et al*., 1990). Wood cell walls, in particular the long tracheids and fibers, consist of several layers, which differ, in their structure and chemical composition.

The woody cell wall is composed of secondary and primary walls (Figure 1.2). The secondary wall has three distinct layers; thin outer (S1) and inner layers (S3) and a thick middle layer (S2) (Sjostrom, 1993). Adjacent cells are separated by the pectin-rich middle lamella. The major components of wood cell walls are three biopolymers, namely cellulose, hemicellulose, and lignin (Harris and Stone, 2008). They are chemically linked in the plant cell wall, so isolating these compounds in a pure state is virtually impossible (Fengel and Wegener, 1989). Fengel and Wegener (1989) and Argyropoulos and Menachem (1997) estimated that there is $2.5{-}4{\times}10^{11}$ tons of cellulose and $2{-}3{\times}10^{11}$ tons of lignin on the earth, representing 40% and 30% of the total organic matter carbon, respectively, with other polysaccharides comprising 26%. The biopolymers are not uniformly distributed in the plant cell wall; the S2-layer of the secondary wall has the highest percentage of cellulose, and the middle lamella has the highest percentage of lignin, but all three compounds can be found in every cell wall layer (Sjostrom 1993; Kuhad *et al*., 1997; see Figure 1.2 for cell wall layers).

Lignin distribution among plant species is also not uniforms (Kuhad *et al*., 1997), gramineous plants having more variation than woody plants. In addition, some grasses contain considerable amounts of pectin in the middle lamella, whereas wood contains only small quantities of extractives, inorganic compounds, and pectin compounds (Fengel and Wegener, 1989; Hatfield, 1989; McDougall *et al*., 1993). Fungal hyphae penetrate from one cell to another through existing pores and pits in the cell walls (Eriksson *et al.* 1990).

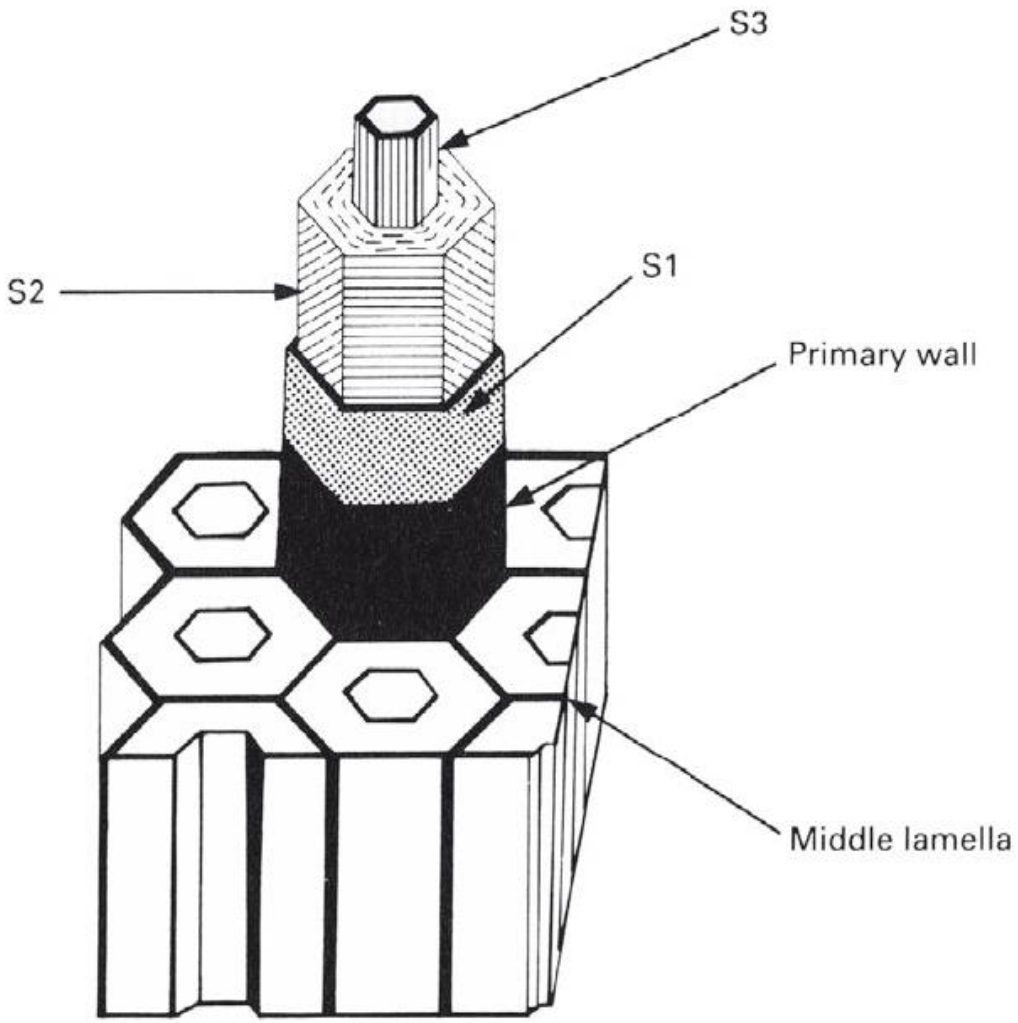

Figure 1.2: Model of the cell wall structure of wood. S1 = outer layer, S2 = middle layer, S3 = inner layer of secondary wall (taken from Dix and Webster (1995).

1.2.1 Cellulose

The main structural component in the cell wall of green plants is cellulose. Cellulose molecules form linear homopolysaccharide chains of β-D-glucopyranose units, which are joined together by β (1–>4)-glycosidic bonds. Cellulose molecules are strongly associated through inter- and intramolecular hydrogen bonds and bundles of cellulose molecules form microfibrils. They are organized into strong fibrous structures, in which the highly oriented regions are called crystalline cellulose and the less oriented region amorphous cellulose. Most

of the plant cell wall cellulose is crystalline. Cellulose microfibrils are embedded in a lignin-hemicellulose matrix (Teeri, 1997; Daniel, 2003).

The cellulose-degrading ability of microorganisms, especially fungi, is widespread, with a synergistic action produced by several enzymes or microorganisms acting in concert (Eriksson *et al*., 1990; Carlile and Watkinson, 1994). The most efficient cellulose degraders are filamentous fungi (Teeri *et al*., 1992). Cellulose-degrading fungi include basidiomycetous (white-rot and brown-rot), ascomycetous, deuteromycetous (soft-rot), and anaerobic (rumen) fungi, of which only brown-rot fungi are capable of degrading crystalline cellulose together with the lignocellulose matrix (Rayner and Boddy, 1988; Gordon and Phillips, 1989).

Typically, endoglucanases and cellobiohydrolases first hydrolyse crystalline cellulose to cellobiose, and *β*-endoglucanases degrade cellobiose to glucose. Finally, aerobic fungi and bacteria oxidize glucose to carbon dioxide (Beguin and Aubert, 1994). During anaerobic degradation glucose originating from cellulose is first fermented to hydrogen, carbon dioxide, and simple organic compounds, then these compounds are converted to acetate and carbon dioxide, and finally acetate is converted to methane and carbon dioxide by microbial co-cultures of anaerobic fungi and bacteria (Beguin and Aubert, 1994).

1.2.2 Hemicellulose

Hemicelluloses are a mixed group of short chain, linear and branched heteropolymers, mainly comprising monomeric sugars, both hexoses and pentoses. Hemicelluloses are named after their main sugar constituents, such as galactoglucomannans, which are the

principal hemicelluloses in softwoods and which are formed of galactose, glucose and mannose units. Glucuronoxylans predominate in the hemicelluloses of hardwood, and are composed of *β*-Dixylose and 4-O-methyl-α-D-glucopyranosyluronic acid units (Fengel and

Wegener, 1989; Kuhad *et al*., 1997). They are linked together mostly by β-1, 4-glycosidic bonds, but β-1, 3-, β-1, 6-, α-1, 2-, α-1, 3-, and α-1, 6-glycosidic bonds can also be found (Eriksson *et al*., 1990)

The degree of polymerization of hemicelluloses is 100-200, which is much less than that of cellulose (Fengel and Wegener 1989). Hemicelluloses and lignin are covalently bound together; this binding gives the cell structure rigidity, thereby providing additional strength for the plant (Sjostrom, 1993; Kuhad *et al*., 1997). As a result of lower degree of polymerization and their amorphous nature, hemicelluloses are believed to be broken down more easily than cellulose. However, the variable nature of hemicellulose requires a complex enzymatic system, such as different xylanolytic and mannan-degrading enzymes (Kuhad *et al*., 1997). The ability to degrade hemicellulose is probably more common than the ability to break down cellulose, although hemicellulase producing microbes commonly also produce cellulase (Eriksson *et al*., 1990; Dix and Webster, 1995).

1.3 Lignin

Next to cellulose, lignin is the second most abundant renewable biopolymer in nature. Structurally, lignin is an amorphous, aromatic, water-insoluble, heterogeneous, three-dimensional, and cross-linked polymer with low viscosity (Fengel and Wegener, 1989; Sjostrom, 1993; Brunow, 2001). Lignin is a natural composite material in all vascular plants, providing the plant with structural integrity, strength and rigidity. Other

important roles of lignin in plants include water transport and protecting cellulose and hemicelluloses from attack by pests and pathogens by reducing the surface area available of these to enzymatic attack (Brown, 1985; Eriksson *et al*., 1990). By decreasing water permeation across the cell wall, lignin renders the plant resistant to biodegradation as well as to environmental stresses (Eriksson *et al*. 1990; Argyropoulos and Menachem, 1997).

The molecular mass of lignin is high (600–1000 kDa), although not uniform, varying greatly within isolated samples; thus making it difficult to determine and the use of conventional formula not possible (Kirk and Farrell, 1987; Fengel and Wegener, 1989; Brunow, 2001). Lignin is highly reduced and its carbon content is 50% higher than that of polysaccharides, which makes lignin energy-rich (Brown, 1985). The complex structure and properties of the lignin polymer make studies on their degradation difficult. Isolation of native lignin is complicated; if at all possible (Hatakka, 2001) and therefore suitable model compounds are needed for study. This problem can be overcome by using ^{14}C-labeled artificial lignin preparations such as the dehydrogenation polymer (DHP). The chemical properties of DHP resemble those of natural lignin. Labelled DHP can be prepared by polymerising specifically labelled coniferyl alcohol with horseradish peroxidase (Kirk and Brunow, 1988), resulting in guaiacyl (G) lignin. However, G-type lignin synthetic or natural is more recalcitrant to breakdown than other types of lignin (Faix *et al*., 1985).

The secondary reactions of polymerisation link lignin with hemicelluloses, thus lignin and polysaccharides form a lignin-polysaccharide complex, from which the components cannot be totally separated from each other (Kirk and Farrell, 1987; Monties and Fukushima, 2001). The bonds between lignin and hemicellulose are formed mainly with the arabinose part of arabinoxylan or the galactose part of galactoglucomannan in wood and in gramineous plants, but these interactions remain inadequately understood (McDougall *et al*., 1993; Monties and Fukushima, 2001). Microorganisms do not gain energy from lignin degradation as such but the degradation enables efficient utilization of carbohydrates (Eriksson *et al*., 1990).

1.3.1 Structure and synthesis of lignin

The lignin polymer arises from enzyme-initiated oxidation of three phenolic precursors and building units, coumaryl (H), coniferyl (G) and sinapyl (S) alcohols (see Figure 1.3), which differ in their degree of methoxylation. These precursors are synthesized initially from L-

phenylalanine and L-tyrosine (Higuchi *et al*., 1977). Enzymic reactions, deamination and several successive hydroxylations and methylation results in the formation of intermediates, *p*-coumaric, caffeic, ferulic, 5-hydroxyferulic and sinapyl acids. Enzyme-catalysed reductions then convert the above intermediates into the primary precursors in Figure 1.3 below.

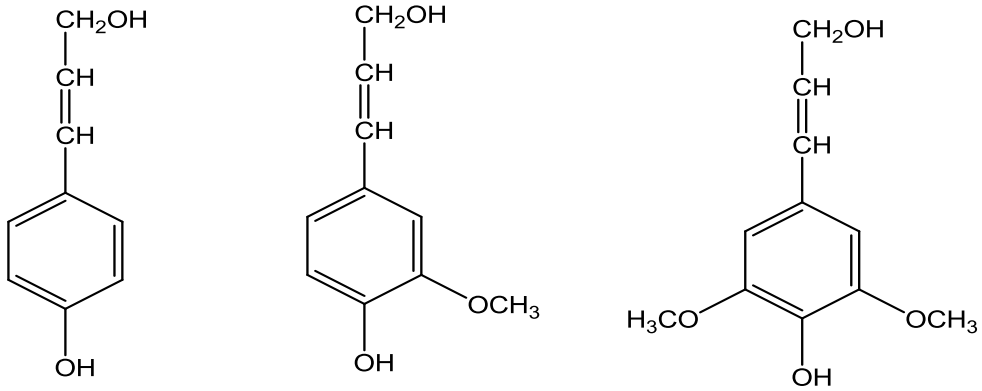

P– Coumaryl alcohol (p-hydroxylphenol, H)

coniferyl alcohol (guaiacyl, G)

sinapyl alcohol (syringyl, S)

Figure 1.3: *p*-Hydroxycinnamyl alcohols, the precursors of lignin (Modified from Buswell and Odier 1987; Dean and Eriksson, 1992). Names in parentheses refer to the corresponding phenylpropanoid units in a lignin molecule.

The G-type of lignin dominates in softwoods and the middle lamella of hardwoods, the G-S type in hardwoods, and the G-S-H type in gramineous plants (Brown, 1985; Besle *et al*., 1989; Brunow, 2001) (see Figure 1.4) for precursors. In addition to methoxyl groups that distinguish various lignin types, lignin has other functional groups, including hydroxyl, benzyl alcohol, and carbonyl group (Sjostrom, 1993; Brunow, 2001). Lignin is synthesized finally by the polymerisation of radicals generated by the one-electron oxidation of the lignin precursors (Kirk and Brunow, 1988; Eriksson *et al*., 1990; Chiang, 2006). Because of the almost random series of bonding, the lignin polymer has no single repeating bond between the subunits. This makes lignin compact, water-insoluble, with non-hydrolysable bonds.

The units of lignin are linked together by different types of bonds (Figure 1.4), which the commonest is β-aryl ether (β-O-4) linkage amounting to 50% and 60% of intermonomeric bonds in softwood lignin and hardwood lignin, respectively (Argyropoulos and Menachem, 1997; Kuhad *et al*., 1997). The monomers usually couple with the phenolic end groups of the growing lignin polymer, not with each other (Sjostrom, 1993).

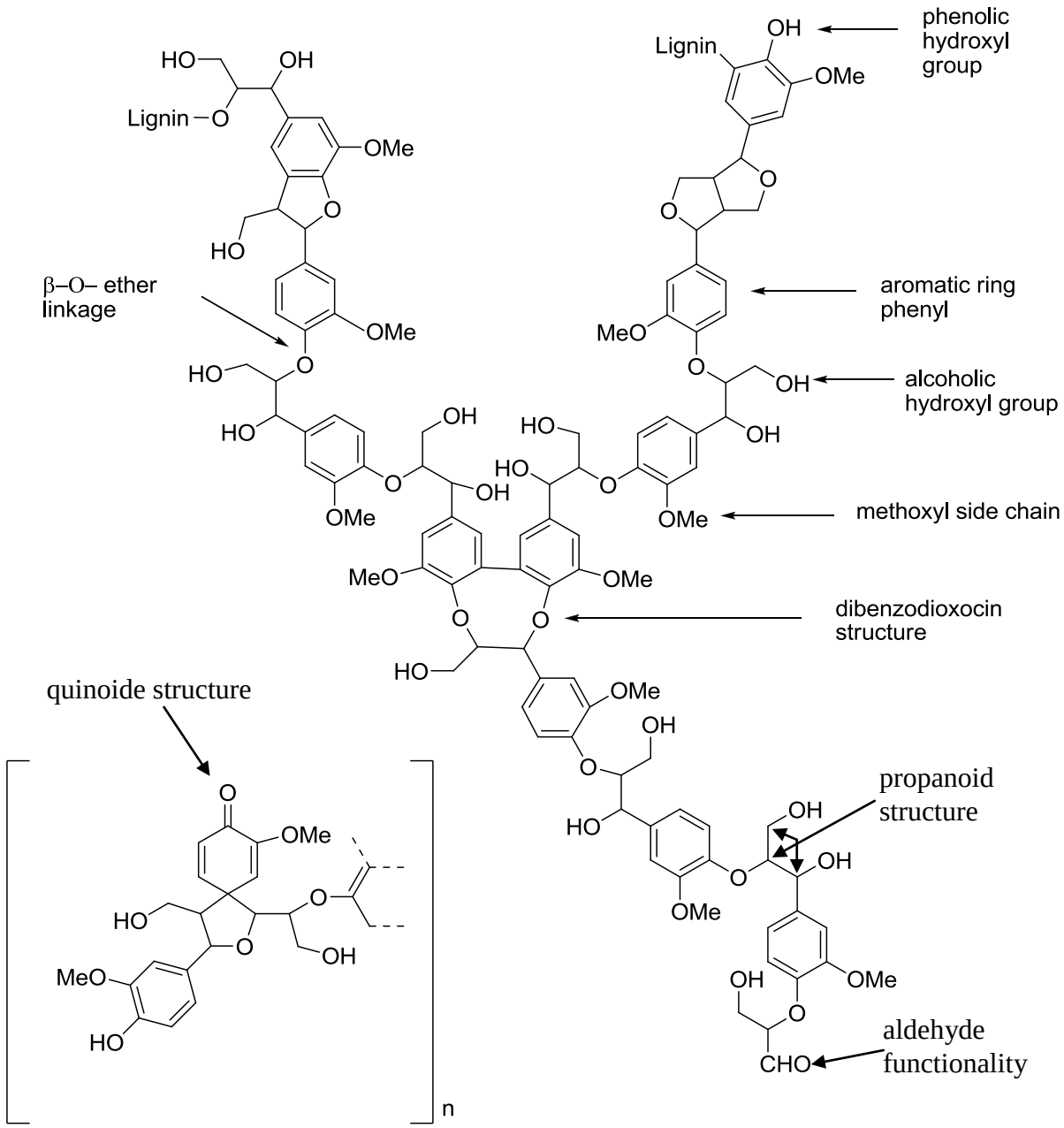

Figure 1.4: Structural model of lignin. The model shows some structure, linkages and functionalities that can the present in lignin molecules (taken from Brunow, 2001).

1.4 Wood and lignin degradation by fungi

The biological degradation of wood/ lignin contributes immensely to earth's carbon cycle, because most renewable carbon is either in lignin form or in compounds protected by lignin from enzymatic degradation (Kirk, 1983; Hatakka, 2001). Wood, being poor in nutrients other than organic carbon, is a demanding growth environment for microorganisms. In addition, the

lignocellulose complex efficiently hinders the access of microbes and their enzymes into wood cell walls. Other wood components, such as extractives, also restrict growth of many microbes. Of all organisms, fungi are the most powerful degraders of wood polymers (Eriksson *et al*., 1990; Carlile *et al*., 2001).

Studies on lignin degradation have revealed that lignin is depolymerized outside the fungal hyphae by the combined oxidative action of lignin-degrading enzymes, oxygen radicals, and small metabolites, after which at least some of the resulting fragments are converted intracellularly (Lundell, 1993; Hofrichter *et al*., 1999b; Kapich *et al*., 1999; Hatakka, 2001; Hammel and Cullen, 2008). Lignin-degrading enzymes considered to be involved in lignin biodegradation include oxidative enzymes that catalyze nonspecific reactions, *i.e.* manganese peroxidase (MnP, EC 1.11.1.13), lignin peroxidase (LiP, EC 1.11.1.14), versatile peroxidase (VP, EC 1.11.1.16) (Martínez 2002; Hammel and Cullen, 2008), laccase (benzenediol: oxygen oxidoreductase, EC 1.10.3.2) and diarylpropane peroxidase, EC 1.11.1.14). Numerous H_2O_2-generating enzymes, such as aryl alcohol oxidase, glyoxal oxidase and pyranose-2 oxidase are also regarded as part of the white-rot fungal lignin-degrading machinery (de Jong *et al*., 1994; Kersten and Cullen, 2007).

In nature, lignin is most likely degraded by an array of microorganisms, although abiotic degradation may also occur in special environments, such as those due to alkaline chemical spills (Blanchette *et al*., 1991) or UV radiation (Vahatalo *et al*., 1999). The environment governs which lignocellulose-utilizing organisms dominate, and thus, the speed of the degradation (Blanchette, 1995). In a forest ecosystem, temperature, moisture content and pH are the major factors influencing lignin transformation and breakdown activities (Donnelly *et al*., 1990; Criquet *et al*., 2000). The abiotic oxidation by transition metals such as Cu, Ni and Zn in calcareous soils also participates in the incorporation of phenolic and lignin-related compounds into humus (Kaschl *et al*., 2002). In aerobic conditions, lignin is decomposed

considerably but in aqueous or anaerobic environment, lignin losses are negligible and wood may persist in non-degraded form for many years (Blanchette, 1995).

Three different types of wood decay caused by fungi can be distinguished: white rot, brown rot, and soft-rot (Eriksson *et al*. 1990). White-rot and brown–rot fungi both belong to the basidiomycetes, and are taxonomically so close to each other, that both may sometimes appear in the same genus (Hatakka, 2001). However, less than 10% of wood-degrading basidiomycetous fungal species are brown-rot fungi (Eaton and Hale, 1993; Dix and Webster, 1995). Soft-rot fungi, on the other hand, are ascomycetes, and their activity is usually related to particularly high or low moisture content of wood (Blanchette, 1995).

1.4.1 White-rot fungi

White-rot fungi are a heterogeneous group of fungi classified in the basidiomycota, which under natural conditions mostly colonize dead wood (Eriksson *et al*., 1990). While most of white-rot fungi grow on hardwoods, certain species grow on softwoods, such as *Heterobasidion annosum*, *Phellinus pini*, and *Phlebia radiata* (Blanchette, 1995). White-rot fungi inhabit the wood cell lumen and the fungal hypha move from cell to cell through intercellular spaces or directly through the cell wall.

The presence of multiple, functionally-related genes in these fungi may have a role in maintaining lignin-degrading activity under changing environmental conditions or time within wood substrate decay (Kersten and Cullen, 2007). The unique capacity of white-rot fungi to efficiently degrade lignin is dependent on the production of their oxidative extracellular lignolytic enzyme system (Kirk and Farrell, 1987; Hatakka, 2001; Hammel and Cullen, 2008). This enzyme system primarily comprises lignin peroxidase (LiP), manganese peroxidase (MnP), laccase, and hydrogen peroxide-generating oxidases (Hatakka, 1994). In

addition to the lignolytic enzymes, white-rot fungi also produce cellulases, xylanases, and other hemicellulases (Hatakka, 1994; 2001).

White-rot fungi can either degrade lignin selectively or non-selectively. Selective white-rot fungi degrade lignin rather than the cellulose components whereas in non-selective fungi all components of lignocelluloses are degraded. Selective lignin degraders are especially interesting from the standpoint of biotechnological applications, since they remove lignin and leave the valuable cellulose intact. Lignin degradation by these fungi is thought to occur during secondary metabolism, typically under nitrogen starvation. Such lignin-selective fungi include, *Phanerochaete chrysosporium*, *Ceriporiopsis Subvermispora* (Otjen and Blanchette, 1987), *Pleurotus ostreatus* (Martinez *et al*., 1994), *Pleurotus eryngii* (Martinez *et al*., 1994; Dorado *et al*., 1999), *Dichomitus squalens* (Eriksson *et al*., 1990) and *Phlebia radiata* (Ander and Eriksson, 1977)

1.5 *Phlebia radiata*

Figure 1.5: Picture of *Phlebia radiata* (taken from Kuo, 2008**).**

Phlebia radiata (Figure 1.5) is a selective and effective degrader of lignin (Hatakka *et al*., 2003; Vares *et al*., 1995). It is a common white-rot fungus that typically grows on dead deciduous trees in temperate forests and is particularly common and well known in Scandinavian (Julich and Stalper 1980; Eriksson *et al*., 1981).

Molecular analysis of rDNA has placed *P. radiata* near to *Pleurotus* eryngii, but well separated from the more extensively studied *Phanerochaete chrysosporium* (Nakasone and Sytsma, 1993; Hilden *et al*., 2008; Piontek *et al*, 2009). *Phlebia radiata* has been shown under certain conditions to be an even more effective lignin degrader than *P. chrysosporium* (Hatakka and Uusi-Rauva, 1983).

The wood and lignin-degrading features of this fungus, and its capacity to degrade complex aromatic compounds, have been the focus of various studies. Particular interest has been focused on the efficient Finnish isolate (79, American Type Culture Collection (ATCC) 64658) (Hatakka and Uusi-Rauva 1983). This strain has been used to degrade synthetic lignins, and lignin model compounds (Hatakka *et al*., 1983; Lundell *et al*. 1990; Niemenmaa *et al*. 2006) and has been studied under various culture conditions (Hatakka *et al*., 1989; Kantelinen *et al*., 1989; Niku-Paavola *et al*., 1990; Vares *et al*., 1995; Moilanen *et al*., 1996). As a white-rot fungus, *P. radiata* expresses a multitude of extracellular lignin-modifying enzymes (Lundell 1993; Hatakka, 1994) including 1 – 4 isoforms of LiP, 1-3 isoforms of MnP and laccase (Hatakka *et al*., 1987; Hatakka and Lundell, 1989; Karhunen *et al*., 1990; Vares *et al*., 1995). While manganese peroxidase will be discussed more fully in later section, a brief description of lignin peroxidase and laccases is given here.

1.5.1 Lignin peroxidase (LiP)

Lignin peroxidase (LiP; EC 1.11.1.14,) is an extracellular oxidative fungal enzyme, first found in cultures of *Phanerochaete chrysosporium*, and connected to direct degradation of the aromatic plant heteropolymer lignin and lignin-like aromatic model compounds (Tien and Kirk 1984; Renganathan *et al*. 1985; Paszczynski *et al*. 1986). This extracellular enzyme is a glycoprotein and has been described in only few species of wood-decaying basidiomycetous fungi (Lundell *et al*., 1993). LiP is produced by several white rot fungi such *Phlebia radiata* (Hilden *et al*., 2006), *Trametes trogii* (Vares and Hatakka, 1997) and *Bjerkandera* sp. BOS55 (ten Have *et al*., 1998). Till now, there is limited knowledge on LiP production in fungi other than white rot basidiomycetes. However, three isoforms of LiP have been purified from the ascomycete *Chrysonilia sitophila* (Rodriguez *et al*., 1997). LiP-like peroxidase from the lignin degrading fungus *Penicillium decumbens* P6 has recently been characterized (Yang *et al*. 2006). *Phlebia radiata* 79 readily produces a versatile set of lignin-oxidizing enzymes

including LiPs, MnPs and laccases. Studies by Hilden *et al,* (2005) showed that translated LiP 1 and LiP 4 shares the highest protein sequence identity (74 and 86%) with *Phlebia radiata* LiP 3.

LiP remains the first enzyme connected to oxidative degradation of the aromatic plant heteropolymer lignin and related xenobiotics (Hilden *et al*., 2006). LiP oxidise a wide variety of substrates including both phenolic and non-phenolic aromatic compounds structurally related to lignin (Krk and Farrell, 1987; Hatakka, 2001). The phenolic substrates are oxidized to yield products similar to those produced by peroxidases, while oxidation of nonphenolic methoxybenzenes is unique to LiP (Kersten *et al*., 1985). The oxidation of these substrates to yield aryl cation radicals can result in either demethylation, Cα-Cβ cleavage of lignin model compounds, benzylic alcohol oxidation, or hydroxylation of aromatic rings and side chains (Kirk and Farrell 1987).

Phlebia radiata produces at least three species of LiPs known as ligninases I, II, III that resemble those of *P chrysosporium* with respect to prosthetic group (Niku-Paavola *et al*., 1988), antigenic determinants (Kantelinen *et al*., 1988), and amino acid sequence (Saloheimo *et al*., 1989).

1.5.2 Laccase

Laccases (benzenediol: oxygen oxidoreductase, EC 1.10.3.2) are copper-containing proteins, which belong to the large and diverse superfamily of multicopper oxidases (Hoegger *et al*., 2006; Arora and Sharma, 2010). They are widely distributed in higher plants and fungi (Messerschmidt and Huber, 1990; Leontievsky *et al*., 1997; Kiiskinen *et al*., 2004) and have also been found in insects and bacteria (Diamantidi *et al*., 2000; Zhulin, 2000; Martins *et al*., 2002; Suzuki *et al*., 2003; Arias *et al*., 2003). Fungal laccases degrade lignocellulosic

materials/phenolic compounds with the concomitant reduction of molecular oxygen to water (Makela, 2009).

Although laccase strongly prefers O_2 as its oxidizing substrate, it usually has low specificity toward its reducing substrates (Arora and Sharma, 2010). Therefore a number of quite different organic and inorganic compounds including diphenols, polyphenols, substituted phenols, diamines and aromatic amines can be oxidized (Thurston 1994). Laccase catalyzes the cleavage of the Cα- Cβ bonds in phenolic β-1 and β-O-4 lignin model dimers by oxidizing the Cα and by splitting the aryl-alkyl bonds (Eriksson *et al*. 1990).

1.6 Applications of ligninolytic fungi, and their enzymes, in biotechnology.

Several biotechnological applications have already taken advantage of white-rot fungi and their lignin degrading enzymes. An engineered form of *Coprinus cinereus* peroxidase was successfully produced in a heterologous system (Cherry *et al*., 1999) and sold as a bleaching agent for laundry detergents.

Purified enzymes, crude enzyme preparations and cultures of ligninolytic fungi have been widely studied for biopulping (review by Messner and Srebotnik, 1994), degradation of toxic compounds (review by Kremer and Anke, 1997) and dye removal (review by Shah and Nerud, 2002). These potential applications are based on the concomitant and nonspecific action of the fungal ligninolytic system (review by Pointing, 2001; Ralph and Catcheside, 2002).

1.6.1 Biopulping, and biografting

The use of lignin-degrading fungal cultures and their lignin-degrading enzymes in the pulp and paper industry has been intensively studied and commercial applications have been developed (review Scott *et al.*, 2000). Selective lignin-degrading white-rot fungi are regarded

as the most suitable organisms for biopulping, to minimize cellulose loss during the fungal pretreatment (Blanchette, 1984; Hakala, 2007). Laccases have potential in wood, paper and pulp industry as it has been used in biopulping and in biografting of low molecular weight compounds onto lignocellulosic materials, and in cross-linking of fibers and lignin moieties for the production of wood composite products (reviewed by Widsten, and Kandelbauer, 2008a). Currently, commercial laccase and laccase-mediator applications for pulp and paper (delignification) and textile industry (bleaching) are already available (Morozova *et al*., 2007). Manganese peroxidase has been also demonstrated to improve pulp bleaching (Moreira *et al*., 2003; Feijoo *et al*., 2008) and decreases consumption of refining energy (Maijala *et al*., 2008) during paper manufacturing.

1.6.2 Biobleaching

Bleaching of industrial effluent and dye colours by white-rot fungi and their ligninolytic enzymes is a promising biotechnological application. Laccase from *Phlebia* species have been successfully employed for biodecolourization of many synthetic and industrial dyes (Gill *et al*., 2002; Chander and Arora, 2007). LiP was reported to be effective in decolourising kraft pulp mill effluents (Ferrer *et al*., 1991). Moreira *et al*., (1998) considered MnP as the most important enzyme in biobleaching experiments with *Bjerkandera* sp. strain BOS55. The utilization of fungi and/ or their enzymes with the combination of mediators and cellobiose dehydrogenase for the decolourization of azo textile dyes proved to be a valid alternative to more expensive and less environmentally friendly chemical treatments of textile dye wastes (Ciullini *et al*., 2008).

1.6.3 Bioremediation

Lignin-degrading peroxidases have been extensively studied in bioremediation; example is soil and industrial effluents contaminated with various harmful compounds of natural and anthropogenic origin (reviewed by Hofrichter, 2002; Husain, 2006; Raghukumar *et al*., 2008;

Haritash and Kaushik, 2009). Organopollutants such as 2,4,6-trinitrotoluene (TNT), polychlorinated biphenyls (PCBs), organochlorines, wood preservatives and Polycyclic aromatic hydrocarbons (PAHs), which arise from natural oil deposits and utilization of fossil fuels being major soil contaminants were shown to be degraded by white-rot fungi (review by Pointing, 2001). Also highly efficient and safe desulphurisation of fossil fuels has been possible through the use of laccase (Villaasenor *et al*., 2004; Xu *et al*., 2006).

1.6.4 Biorefinery concept

The global demand for the use of renewable materials for production of energy and consumables has been expanded. The main aim of biorefinery concept is to use advanced biotechnological processes to coproduce various value-added end products such as biofuels and chemicals from renewable biomass. Forest and agricultural waste lignocelluloses form a large source of renewable biomass that can be used as a feedstock for biorefining (reviewed by Kamm and Kamm, 1994; Kumar *et al*. 2008; Foust *et al*., 2008). Being that lignin in plant cell walls prevents the effective use of cellulose and hemicellulose, its removal is a key step for the use of cellulosic biomass. Hence, the implication of white-rot fungi and their enzymes as environmentally friendly biocatalysts for the pretreatment of lignocelluloses (Ruiz-Duenas and Martinez, 2009).

1.6.5 Limitations

Development of recombinant DNA technologies has modified traditional reaction routes and production-organisms. Heterologous expression systems have been introduced to aid in the manufacture of recombinant proteins and bioactive compounds (review by Bennet, 1998). However, the industrial use of fungal peroxidases is still hindered by their high cost and low yields so far gained using heterologous expression systems. The lack of an efficient heterologous production system for biotechnological fungi at bioreactor scale is constraining

more bulky and industrial applications (Couto and Toca-Herrera, 2007). Also the limited availability and low stability of the enzymes as well as their inactivation by H_2O_2 and elevated temperatures are problems in large-scale production and in industrial applications (reviewed by Martínez *et al*. 2009).

1.7 Metalloproteins and metal ion binding sites

About one-third of all structurally characterised proteins contain metals, while over 50% of all proteins are estimated to be metalloproteins (Jernigan *et al*., 1994; Lovell *et al.*, 2003). Metals commonly found binding to proteins under physiological conditions are potassium, sodium, calcium, magnesium, iron and the trace metals including copper, cobalt, manganese, zinc, molybdenum and nickel (Frausto da Silva and William, 1991; Bertini *et al*., 2001). The role of metals in proteins ranges from protein structure stabilization to enzyme catalysis and signal transduction, (Lippard and Berg, 1994; Christianson and Cox, 1999; Bertini *et al*., 2001). Metalloenzymes exploit the unique properties of metal ion such as small size and simple structure, electron acceptor ability; positive charge, flexible coordination sphere, specific ligand affinity, varying valence state and electron spin configuration, and high mobility, to perform a wide variety of chemical reactions.

Two types of metal-binding site can be found in metalloproteins, "structural" and "catalytic" metal sites. Some proteins possess only one binding site (mononuclear) while other proteins contain more sites (binuclear or polynuclear), with either the same or different ions bound in separate binding locations. If two metal-binding sites are involved in catalysis in a metalloenzymes, the two metal ions are usually connected by bridging ligands such as water hydrolysing formate or imidazole (Osterberg, 1974; Ibers and Holm, 1980; Bertini *et al*., 1995).

A common feature of metal-binding sites is that the metal ion binds to a preformed protein pocket whose composition, size, shape and flexibility play an important role in selecting a particular metal cation (Falke *et al*., 1991; Huang *et al*., 1999; Lee *et al*., 2000; Dudev & Lim, 2003). Ligands often found coordinated to metal ions in metalloproteins are formate from deprotonated aspartic acid and glutamic acid side chains interaction which is thermodynamically favourable (Garner and Gresh, 1994; Harding, 2001; Rulisek and Havlas, 2002). In addition, imidazole from histidine side chains, formamide from asparagine, and glutamine side chains and backbone peptide groups on the other hand, are the most abundant non-charged residues flanking the metal-binding sites (Jernigan *et al*., 1994; Rulisek and Vondrasek, 1998; Dudev and Lim, 2006).

1.8 Mechanism of metal ion binding to proteins

The engineering of metalloproteins with new characteristics requires good knowledge of the mechanism of metal binding to proteins. Unfortunately, so far, mechanisms of metal binding are poorly understood for the vast majority of metalloproteins and metalloenzymes (Kuchar and Hausinger, 2004).

According to Yamashita *et al* (1990), metals bind to proteins in an inner-sphere mode and at centres of high hydrophobicity contrast; *i.e.* the metal ions generally bind directly to a shell of polar hydrophilic amino acid residues surrounded by a shell of nonpolar hydrophobic groups (Yamashita *et al*., 1990; Black *et al.*, 1994; Cowan, 1995; Dudev and Lim, 2000). The hydrophobic outer sphere has been hypothesized to restrict flexibility of the site (Serpersu *et al*., 1986), and limit solvent accessibility, thus providing a low dielectric cavity that thermodynamically enhances the electrostatic interactions between the metal and hydrophilic ligands (Harvey and Hockstra, 1972; Gilson and Honig, 1986; Yamashita *et al*., 1990; Dudev and Lim, 2000). The metal ion most likely binds to the protein in a stepwise process, starting

when the hydrated metal ion positions itself in a protein pocket characterised by a low dielectric constant value, and subsequently some of its inner-shell water molecules are replaced by negatively charged protein ligands.

1.9 Haem peroxidase enzymes

Peroxidases are enzymes that utilize hydrogen peroxide (H_2O_2) to catalyse oxidation of a variety of inorganic and organic substrates including aromatic compounds (Everse *et al*., 1991; Nakayama and Amachi, 1999; Ana *et al*., 2002). Peroxidases are ubiquitous in nature, and have molecular weights ranging from 35 kDa to 100 kDa with 251 to 726 residues respectively (Dunford, 1982; Banci, 1997). Most peroxidases contain a protoporphyrin IX haem as a prosthetic group (with exception of myeloperoxidase) (Sibbet and Hurst, 1984; Ikeda-Saito and Prince, 1985; Dunford, 2010).

The overall reaction catalyzed by peroxidases is shown in the equation below:

$$H_2O_2 + AH_2 \longrightarrow 2H_2O + A^{\bullet}$$

The importance of peroxidases is emphasized by their multiplicity of physiological activities. Studies have shown that plant peroxidases function in auxin catabolism, plant defence against pathogen attack and wound healing (Birecka *et al*., 1979), while fungal peroxidases are particularly ligninolytic.

Peroxidases also play a significant physiological role in the disposal of activated oxygen species that are released by normal metabolic processes in the aerobic cell. The use of oxygen by aerobic organism brings with it the unwanted production of strong oxidants as the by-products of metabolic reactions. For example, oxidative phosphorylation by mitochondria results in the production of superoxide free radicals ($O_2^{\bullet}$) (Loschen *et al*., 1974). Other enzymes produce superoxide as a by-product of their catalytic cycle, including aldehyde

oxidases, xanthine oxidases, and cytochrome P450s. It is beneficial for organisms to reduce superoxide quickly so that other more dangerous oxidants do not accumulate, as these radicals damage cellular components including proteins, DNA and lipids (Faraggi and Houee- Levin, 1999; Moller, 2001). Indeed, the damage induced by reactive oxygen species can have a deleterious effect on human health and has been associated with degenerative diseases (Faraggi and Houee- Levin, 1999).

Enzymatically mediated detoxification of these oxidative species is achieved through the action of superoxide dismutases, catalases, and peroxidases (Fridovich, 1998). Superoxide dismutases are known to exert a cytoprotective effect by catalysing the disproportionation of two superoxide radicals, reducing them to hydrogen peroxide. But while hydrogen peroxide is not as potent an oxidizing agent as superoxide, it is still dangerous to the cell. Both peroxidases and catalases play an important role in the removal of hydrogen peroxide. Catalases convert hydrogen peroxide into water and oxygen Peroxidases in effect act as electron donors; once they have reacted with peroxide they dissipate their oxidative potential via reaction with substrates (Smith and Veitch, 1998). Therefore, peroxidases are able to detoxify hydrogen peroxide and also use its oxidative power to perform essential task.

1.10 Classification of haem peroxidases

Many peroxidases have been isolated, sequenced and characterized. These proteins have been classified essentially based on biological functionality, tertiary structures and primary sequence correlation (Dunford, 1999; Welinder, 1991). Peroxidases are firstly divided into haem and non-haem peroxidases, with a number of subdivisions of each classification (Figure 1.6). The non-haem peroxidases contain no haem but possess vanadium (Butler, 1998; Littlechild, 1999) or selenium (Stadman, 1990) as prosthetic group, and generate peroxidase activity by means of an active site cysteine (Choi *et al*., 1998).

Some haem peroxidases (e.g. C*c*P, MnP, etc) utilise hydrogen peroxide (H_2O_2) in the peroxidative cycle to produce radical substrate products (Passardi *et al*., 2007). The precise ferriprotoporphyrin IX haem moiety contained in each haem peroxidase differs between two superfamilies (Furtmuller *et al*., 2005).

The haem peroxidases are divided into two main superfamilies, mammalian and plant with grouping based on a combination of similarity of sequence and tertiary structure, origin of species and function. The third subdivision of the haem peroxidase superfamily is a grouping of "indistinct" peroxidases that do not fit well in either the plant or mammalian superfamilies (Smith and Veitch, 1998). This group contain chloroperoxidase, a haem peroxidase that functions in a way similar to cytochrome P-450s and di-haem cytochrome *c* peroxidases.

The mammalian peroxidase and plant superfamilies are believed to have developed the same peroxidative function through convergent evolution (Taurog, 1999) rather than sharing recent common ancestors (Passardi *et al*., 2007). The mammalian and plant superfamilies do not share significant sequence homology despite having catalytically similar mechanisms. The nature of the prosthetic group is also different between the two superfamilies.

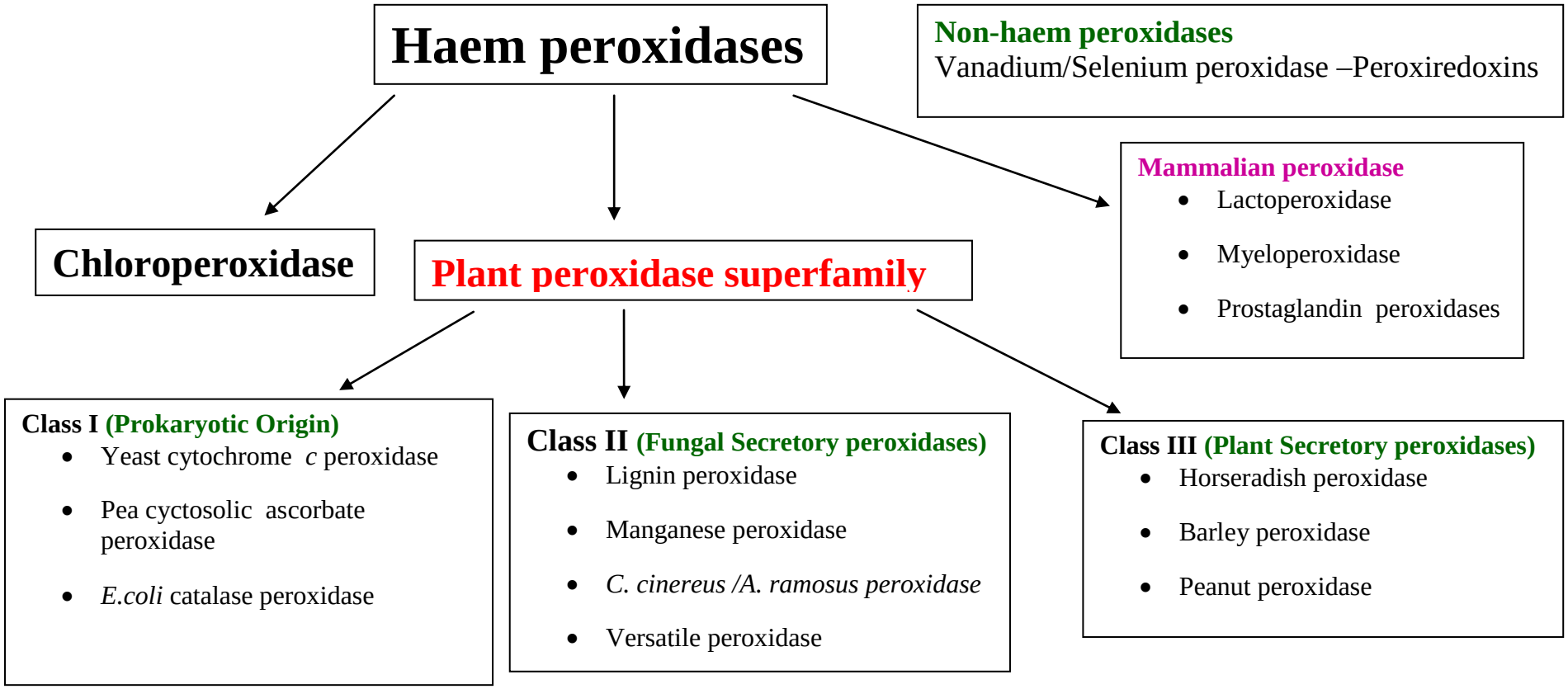

Figure 1.6: Classification of peroxidases. Peroxidases are grouped into two groups, haem and non-haem. Then the haem peroxidases further grouped into two main superfamilies, mammalian and plant (Dunford, 1999). Members of the plant superfamily have been further divided into three classes on the basis of similarities in structure and sequence. Despite the presence of less than 20% sequence identity between some members of the superfamily, all possess ten core conserved α-helices (Welinder, 1992).

1.10.1 Mammalian peroxidases

Mammalian peroxidases include amongst others glutathione peroxidase (GPO), myeloperoxidase (MPO) thyroid peroxidase (TPO), eosinophil peroxidase (EPO) and lactoperoxidase (LPO) (English and Tsaprailis, 1995; Welinder *et al*., 1992). However, mammalian peroxidase-like sequences are also present in a variety of invertebrates including arthropods, molluscs, crayfish and *Drosophila* (Taurog, 1999). Mammalian peroxidases have a unique ability in catalyzing the H_2O_2-dependent peroxidation of halides and pseudohalides to produce antimicrobial agents and hypohalous acids e.g. lactoperoxidase which is found in milk for this reason (Kimura and Ikeda-Saito, 1988; Mayeno *et al*., 1989). The primary and tertiary structures (based on MPO), as well as the nature of prosthetic group differ greatly from those of plant or fungal peroxidases. It is thought that the mammalian peroxidase arose independently of the plant and is an example of convergent evolution (Taurog, 1999).

It has been suggested by modelling studies that the regions corresponding to helices in MPO are well conserved in other members of the superfamily, although some are monomers (Thomsen *et al*., 2000; Wolf *et al*., 2000). Disulphide bridges and calcium binding sites are in good agreement and the peroxidases also share conserved glycosylation sites at Asn 189 and Asn 225. However, Asn 317 that may be responsible for the dimer interaction in MPO is missing in the other peroxidases (Fiedler *et al*., 2000).

The haem peroxidases from plant fungi and bacteria have similar protein folds and constitute the plant peroxidase superfamily. They are different in structure from haem peroxidase of animal origin (Welinder, 1992). The haem group in mammalian peroxidases is a derivative of protoporphyrin IX (Dunford, 2010). The properties of the

haem in mammalian peroxidases have been characterized by a wide variety of spectroscopic techniques, including optical absorption, stopped-flow, electron paramagnetic resonance, and resonance Raman spectroscopy (Ortiz de Montellano, 1992; Marquez and Dunford, 1995; Abu-Soud *et al*., 2001; Furtmuller *et al*., 2004). These techniques, with a combination of structure analysis (Davey and Fenna, 1996) and advanced computer modelling (De Gioia *et al*., 1996), have shown that the haem pockets of mammalian peroxidases are envisioned to form the catalytic site where the stepwise reduction of H_2O_2 occurs. There is biochemical and biophysical evidence for covalent haem linkage through esters in MPO, Glu242 and Asp94 (Fiedler *et al*., 2000), EPO, Asp232 and Glu380 (Oxvig *et al*., 1999), LPO, Asp225 and Glu375 (Andersso *et al*., 1996; Colas *et al*., 2002; DePhillis *et al*., 1997; Rae and Goff, 1996; Surino *et al*., 2001), and TPO, Asp238 and Glu399 (Taurog, 1999).

The unusual haem binding is responsible for the peculiar red shifted spectroscopic features of mammalian peroxidases. The sulfonium ion linkage serves two roles, firstly, it serves as an electron withdrawing group using its positive charge, and secondly, together with its neighbouring residue Glu242, it appears to be responsible for lack of symmetry of the haem group and distortion from the planar conformation. Generally, the spectral properties of mammalian peroxidases, EPO, LPO, and TPO are very similar, underlining that they share an identical way of haem binding. UV/Vis absorption and EPR spectroscopy both suggest that the haem plane undergoes the same distortion in all these enzymes (Carlstrom, 1969; Bolscher *et al*., 1984; Kohler *et al*., 1988; Ferrari *et al*., 1995; Watanabe *et al*., 2000).

The proximal histidine in haem peroxidases is important in maintaining the redox properties of the haem iron for catalysis. In plant peroxidases, a conserved aspartate

serves to deprotonate the proximal histidine thus providing a strong axial ligand with H-acceptor which produces a Fe (III)/Fe (II) reduction potential, typical for haem peroxidases, of between -180 and 300 mV (Dunford, 1999c).

Below is the reaction scheme for mammalian peroxidase:

1) [Fe (III) .....Por.....aa] + H_2O_2 → [Fe^{IV} = O.....$Por^{\bullet+}$ .....aa] + H_2O (Reaction

2) [FeIV= O.....$Por^{\bullet+}$ .....aa] + H_2O_2 → [Fe^{IV} = O....Por.....aa] + $H_2O^{\bullet}$ (Reaction 2)

3) [FeIV = O..... Por•+ .....aa] → [Fe^{IV} = O.....Por.....$aa^{\bullet+}$] (Reaction

4)[Fe (III) .....Por....aa] + HOCl → [Fe^{IV} = O.....Por....$aa^{\bullet+}$] + Cl^- + H^+ (Reaction

Scheme 1.1: Reaction scheme for mammalian peroxidase, aa represents an amino acid from the protein.

In mammalian peroxidases, both peroxidase and halogenations cycles start by the reaction of resting state ferric enzyme with peroxides to form Compound I. The mechanism of Compound I formation in mammalian peroxidase is similar to that proposed by Poulos and Kraut, (Poulos and Kraut, 1980), or that proposed for HRPC (Rodriguez-Lopez *et al*., 2001). As with plant superfamily peroxidases, the resulting high oxidation state intermediate (Compound I) has an oxy-ferryl (Fe (IV) =O) haem (Moss *et al*., 1969) and porphyrin π cation radical (Browett and Still, 1981; Dolphin *et al*., 1971). In addition, hypochlorous acid can be used to oxidise ferric mammalian peroxidases to Compound I (Reaction 4) (Furtmuller *et al*., 2000). Independent of the oxidant, the half-life of Compound I is short, and in the absence of suitable electron donors, it can react or decay via Reaction 2 and 3, with reaction 2 being specifically for MPO. It has also been demonstrated that superoxide is generated from the one-electron

oxidation of hydrogen peroxide by Compound I (Bolscher and Wever, 1984; Marquez *et al*., 1994).

An alternative isomeric Compound I can be formed, via Reaction 3 by an intermolecular electron transport from the protein to protein to the porpphyrin π cation radical. This Compond I isomer contains the same number of oxidising equivalents as conventional Compound I. Several pieces of evidence suggest the existence of two Compound I isomers in MPO and LPO (Laureti and Ghibaudi, 2003). First, the standard reduction potential of the couple Compound I/Compound II of MPO (Arnhold *et al*., 2003; Furtmuller *et al*., 2003) and LPO (Furtmuller *et al*., 2005) are high enough to make the oxidation of an amino acid residue on the polypeptide chain possible. In addition, the EPR spectrum of a spin trapped radical in MPO Compound I, generated only in the presence of hydrogen peroxide, has been reported, and was suggested to either a Tyr or Trp radical (Laurdinois and Ortiz de Montellano, 2000). This is contrary to that obtained in HRP-C and other plant peroxidases.

1.10.2 Plant peroxidase superfamily

The members of the plant peroxidase superfamily are believed to be evolutionally related and have been subdivided into three classes on the basis of sequence and structural homology (Welinder, 1992; Welinder and Gadjhede, 1993). The subclasses comprise the intracellular prokaryotic (Class I), extracellular fungal (Class II) and the "classical plant secretory peroxidase (Class III). The primary amino acid sequences of peroxidases are highly variable among the members of the plant peroxidase superfamily, with less than 20% identity for the most divergent cases (Hiraga *et al*., 2001). Crystal structures are now available for many peroxidases, including cytochrome *c* peroxidase (Finzel *et al*., 1984), pea ascorbate peroxidase (Patterson and Poulos,

1995), ascorbate peroxidase-salicylhydroxamic acid complex (2004), *Arthromyces rasmosus* peroxidase (Kunishima *et al*., 1994), *Coprinus cinereus* peroxidase (CiP, Petersen *et al*., 1994), lignin peroxidase (LiP, Poulos *et al*., 1993; Piontek *et al*., 1993), manganese peroxidase (MnP, Sundaramoorthy *et al*., 1994), peanut peroxidase (Schuller *et al*., 1996), barley peroxidase (Henriksen *et al*., 1998b), recombinant horseradish peroxidase (HRPC) (Gajhede *et al*., 1997). Comparison has revealed that the overall folding and organization of the secondary structure is conserved (Li and Poulos, 1994; Poulos *et al*., 1995; Welinder., and Gajhede, 1993).

1.10.2.1 Class I plant peroxidases

Members of Class I include the intracellular enzymes of prokaryotic origin (plants, bacteria and yeast). Enzymes in this class include *Saccharomyces cerevisae* cytochrome *c* peroxidase (C*c*P), chloroplast or cytosolic ascobate peroxidase (APX) and bacterial catalase-peroxidase. Peroxidases in this class do not contain disulphide bridges; structural calcium ions, carbohydrate attachments or secretory signal sequences.

Poulos *et al* (1980) first resolved the X-ray crystal structure of C*c*P at 2.5 Å resolution, which was later refined to a resolution of 1.7 Å (Finzel *et al*., 1984). As in other peroxidases, the C*c*P haem prosthetic group is located in the active site cavity between two domains, distal and proximal. Both domains are mostly α-helical in structure, with only 12% of the molecule present as β sheet structure. The enzyme contains ten major helices, A-J and three minor α-helices, B1, F1 and J1, see Figure 1.7a for ribbon representation. The resolved structure of this enzyme revealed that the catalytic residues Arg48, Trp51 and His52 protrude into the distal haem cavity from helix B, while helix F contains the proximal haem-attaching histidine, His175. The side chain of His175 and a

structural water molecule occupy the fifth and sixth coordination positions of the haem iron, respectively (Finzel *et al*., 1984).

1.10.2.2 Class II plant peroxidases

The Class II peroxidases are extracellular peroxidases from fungi and include lignin peroxidase (LiP), manganese peroxidase (MnP) and *Coprinus cinereus* peroxidase (CiP). These peroxidases have two structural calciums, four or five disulphide bridges, about 5% carbohydrate content and N-terminal secretory signal sequences. Peroxidases of this class are general involved in lignin degradation. A member of this peroxidase class, MnP from *Phlebia radiata* is the focus of this study.

1.10.2.3 Class III plant peroxidases

Class III plant peroxidases consists of the plant secretory peroxidases, a typical example is the widely studied horseradish peroxidase (HRP). These peroxidases are secreted outside cells or transported into vacuoles (Hiraga *et al*., 2001). Peroxidases of this class contain two calcium ions, four disulphide bridges and are generally highly glycosylated (Welinder *et al*., 1992).

The first Class III peroxidase X-ray crystal structure to be resolved was that of peanut peroxidase (PNP) (Schuller *et al*., 1996), which was followed by the structure of HRP C* see Figure1.7c (Gajhede *et al*., 1997). The crystal structures of PNP and HRPC*(Gajhede *et al*., 1997) confirmed that Class III peroxidases possess ten helices, A-J, in similar positions to Class I and II peroxidases. However, HRPC* and PNP also contain an additional three helices, D′, F′, and F′′. The F′ and F′′, helices are located in a long insertion between helices F and G, and the local structure in this region is maintained by a disulphide bridge, (Cys177-Cys209 HRPC). This insertion is hypervariable within the Class III enzymes and is believed to affect the character and

accessibility of the substrate access channel. In HRPC* the catalytic residue side chains of Arg38 and His42 extend into the haem cavity from helix B, whilst the haem iron proximal ligand, His170, is found in the connecting loop between the F and F′ helices. Class III peroxidase also contain two calcium binding sites, one distal and one proximal to the haem plane, as shown in Figure 1.7c, as in the Class II peroxidases.

1.11 Manganese peroxidase

Manganese peroxidase (MnP; EC 1.11.1.13) is a glycosylated; haem-containing enzyme that was first discovered along with LiP, in the lignin-degrading fungus, *Phanerochaete chrysosporium* (Huynh and Crawford, 1985; Glenn and Gold, 1985). This enzyme is also produced by many other lignolytic fungi, including *Phlebia radiata* (Hofrichter *et al*; 1999; van-Aken *et al*., 1999), *Nematoloma frowardii* (Schneegaβ *et al*., 1997; Hofrichter *et al*., 1999), *Pleurotus eryngii* (Caramelo *et al*., 1999), and *Bjerkandera adusta* (Mester and Field, 1998; Wang *et al*., 2002; Hatakka, 1994). Manganese peroxidase is so named because of its requirement for divalent manganese in carrying out peroxide-dependent oxidations (Kuwahara *et al*., 1984; Glenn and Gold, 1985).

MnP occurs as a series of isoenzymes encoded by a large number of structurally related genes (Kirk *et al*., 1986; Pease *et al*., 1989; Mayfield *et al*., 1994; Alic *et al*., 1997). The significance of the multiplicity of isoenzymes is unknown, but considerable effort has focused on characterizing individual isoenzymes as their activities vary. Efficient expressions of individual isozymes in heterologus hosts have greatly facilitated investigations.

Studies with different white-rot fungi have shown that MnP appears to be more common than LiP (Orth *et al*., 1993; Hatakka, 1994; Vares and Hatakka, 1997), and during recent years, the characteristics and role of MnP have been extensively studied.

Manganese peroxidase has an essential role in the depolymerisation of lignin (Warrishi *et al*., 1991) and chlorolignin (Lackner *et al*., 1991), as well as in the demethylation of lignin and bleaching of pulp (Paice *et al*., 1993). Moreover, the enzyme mediates initial steps in the degradation of high-molecular weight lignin (Perez and Jeffries, 1992). Recently, it has been shown that MnP in the presence of suitable organic acids is even able to mineralize lignin and lignin model compound to a considerable amount (Hofrichter *et al*., 1990a).

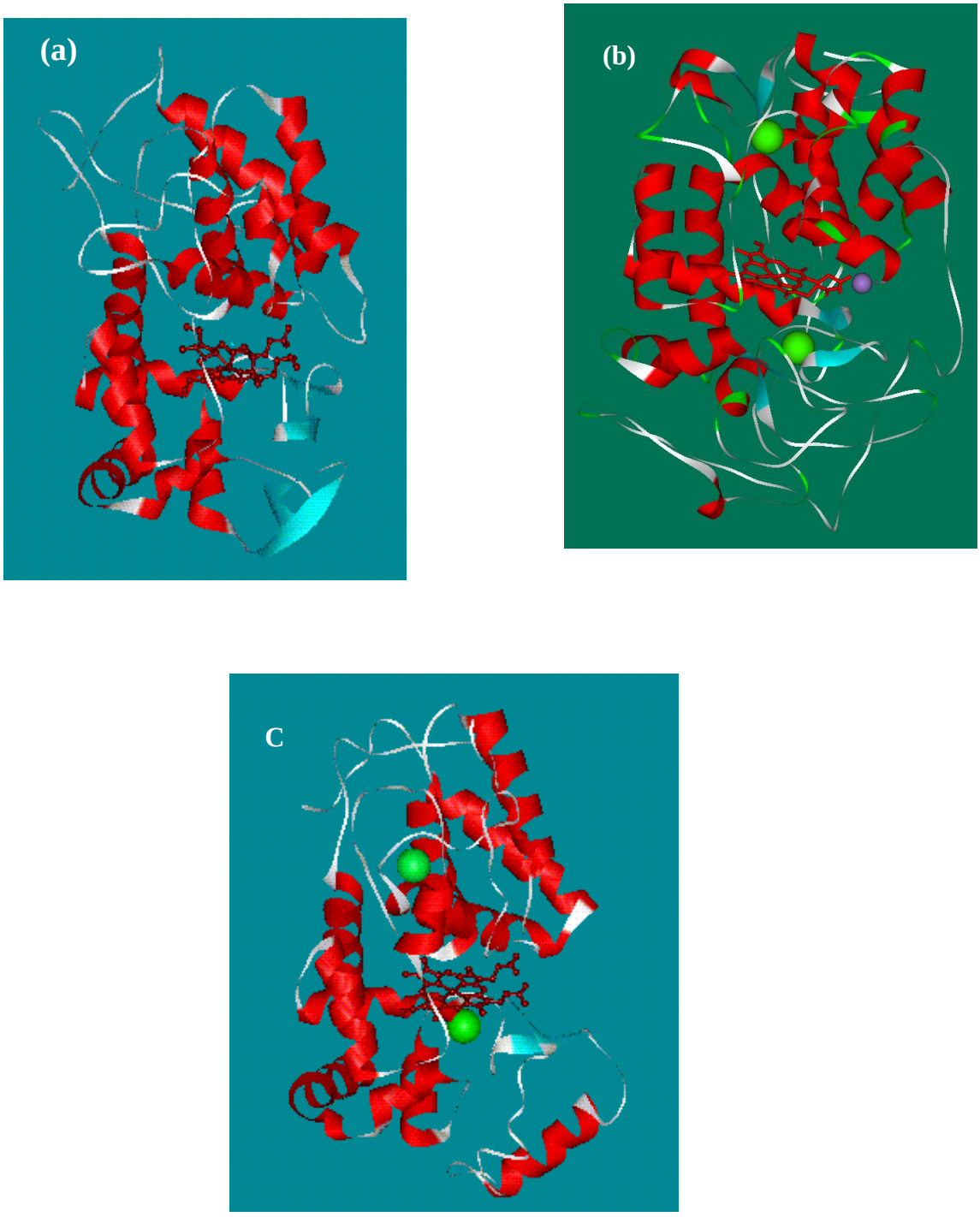

Figure 1.7: Ribbon model representations of enzymes of the plant peroxidase superfamily Classes I, II, III, ¥. (a) *Saccharomyces cerevisiae* cytochrome *c* peroxidase (C*c*P), **(b)** *Phanerochaete chrysosporium* manganase peroxidase (MnP) and **(c)** recombinant horseradish peroxidase isoenzyme C (HRPC*). Helices and central haem group are shown in red in Figures a, b and c.; β structure in light green and calcium ions as green van der Waals spheres, while Mn^{2+} (Figure b) is in pink.

¥ Drawn using Swiss-Pdb Viewer V3.7 b2 (http://www.expasy.ch/spddv/) (Guex and Peitsch, 1997) and the PDB (Berman *et al*., 2000) file **(a)** 2CYP, **(b)** 1MnP, and **(c)** 1ATJ.

1.11.1 General structure of MnP

Figure 1.7b shows the resolved X-ray crystal structure of MnP (Sundaramoorthy *et al*., 1994) and it reveals that the overall folding of the MnP polypeptide chain is similar to that of other plant and fungal peroxidases. MnP has two domains proximal and distal with the haem located in between them (Welinder and Gajhede, 1993). The enzyme has 10 major helices and minor helices, all of which are also present in LiP (Sundaramoorthy *et al*., 1994). The cysteine residues in MnP participate in five disulfide bonds; the first four, Cys3 –Cys15, Cys33- Cys117, Cys14 - Cys289 and Cys253 -Cys319 (*P. chrysosporium* MnP numbering), are the same as those found in LiP but the fifth disulphide bond, Cys341- Cys348 is specific to MnP (Sundaramoorthy *et al*., 1994). *The disulphide bonds in P. radiata are C3: C16, C15: C286, C35: C121 and C250: C315 (Hilden et al., 2005).* The fifth disulphide bond is part of the longer C–terminal tail in MnP and is partially responsible for forcing the C–terminal tail further away from the main body of the protein.

A 3D molecular model of MnP3 from *Phlebia radiata* the enzyme studied here, revealed a shorter C-terminal and this enzyme is structurally more related to *P.chrysosporium* LiP (LiPH8/H2) (Hilden *et al*., 2005) than *P. chrysosporium* MnP. In addition, a structure based sequence alignment showed that the *Pleurotus eryngii* versatile peroxidase (VP) (PDB entry 3FJWA) the closest homology to MnP3 with 68% identity (See section 1.11.2). In MnP3, an alanine replaces the exposed tryptophan present in LiP and versatile peroxidases.

1.11.2 Homology modelling of *P. radiata* MnP3.

The online resources at SWISS MODEL (http://swissmodel.expasy.org/) were used to generate a model structure of MnP3. Structure based alignment identified the *Pleurotus*

eryngii Versatile peroxidase structure (PDB entry 3FJWA) as the closest structural neighbour with 68% identity. The short MnPs such as the *Phlebia radiata* MnP3 have been identified as phylogentically more similar to the versatile enzymes than to the classical *Phanerochaete chysosporium* MnP's (Piontek *et al*., 2009), which have the longer C-termimal region and an additional disulphide bond. The alignment used for model building is shown in Figure 1.8. The energy optimised MnP3 structure (100 steps steepest decent using GROMOS96 (Peitsch, 1996) was viewed in RasWin Molecular Graphics version 2.7.5 (http://www.rasmol.org/) and the coordinates for the haem group, Ca and Mn ions were copied manually from the text file of the versatile structure and appended directly to the MnP3 model structure file. Images of Mn (II)-binding site and haem and associated axial ligands were then generated using Accelrys dv visualize 2.0 (http://accelrys.com/).

```
3FJW_A          ---ATCDDGR-TTANAACCILFPILDDIQENLFDGAQCGEEVHESLRLTFHDAIGFSPTL 56
ENG_MnP3        MLTVACPDGVNTATNAVCCSLFAVRDLIQDQLFDGGECGEEVHESLRLTFHDAIGISPTI 60
                   .:* **  *::**.** **.: * **::****.:******************:***:

3FJW_A          G------GGGADGSIIAFDTIETNFPANAGIDEIVSAQKPFVAKHNISAGDFIQFAGAVG 110
ENG_MnP3        ASTGVFGGGGADGSIAIFAEIETNFHANNGVDEIIGEQAPFIQMTNMTTADFIQFAGAVG 120
                .      ********  *  ***** ** *:***:. * **:   *:::.**********

3FJW_A          VSNCPGGVRIPFFLGRPDAVAASPDHLVPEPFDSVDSILARMGDAG-FSPVEVVWLLASH 169
ENG_MnP3        VSNCPGAPALPVFVGRPDATQPAPDKTVPEPFDTVDSILARFADAGGFSSAEVVALLASH 180
                ******.  :*.*:*****. .:**: ******:*******:.*** **..*** *****

3FJW_A          SIAAADKVDPSIPGTPFDSTPGVFDSQFFIETQLKGRLFPGTADNKGEAQSPLQGEIRLQ 229
ENG_MnP3        TIAAADHVDPSIPGTPFDSTPEIFDTQFFIETQLRGILFPGTGGNQGEVESPLHGEIRLQ 240
                :*****:************** :**:********:* *****..*:**.:***:******

3FJW_A          SDHLLARDPQTACEWQSMVNNQPKIQNRFAATMSKMALLGQDKTKLIDCSDVIPTPPALV 289
ENG_MnP3        SDSELARDSRTACEWQSFVNNQAKIQSAFKAAFRKMTILGHSESSLIECSEVIQTPPALE 300
                **  ****.:*******:****.***. * *:: **::**:.::.**:**:** *****

3FJW_A          GAAHLPAGFSLSDVEQACAATPFPALTADPGPVTSVPPVPGS 331
ENG_MnP3        GNAHLPAGQTMNDIEQACATTPFPSLSADPGPATSVAPVPPS 342
                * ****** ::.*:*****:****:*:*****.***.*** *
```

Figure 1.8: Structure based alignment of *Pleurotus eryngii* versatile peroxidase translated sequence (3FJW_A) with engineered MnP3 sequence (ENG_MnP3) generated using Swiss model online facility (http://swissmodel.expansy.org/). Identical base pairs are represented by the symbol '*'. Mismatch base pairs are indicated by the symbol '•' , '**:** 'very identical and ' ' no relationship at all.

The model below shows the overall fold of the engineered MnP3 from *Phlebia radiata*.

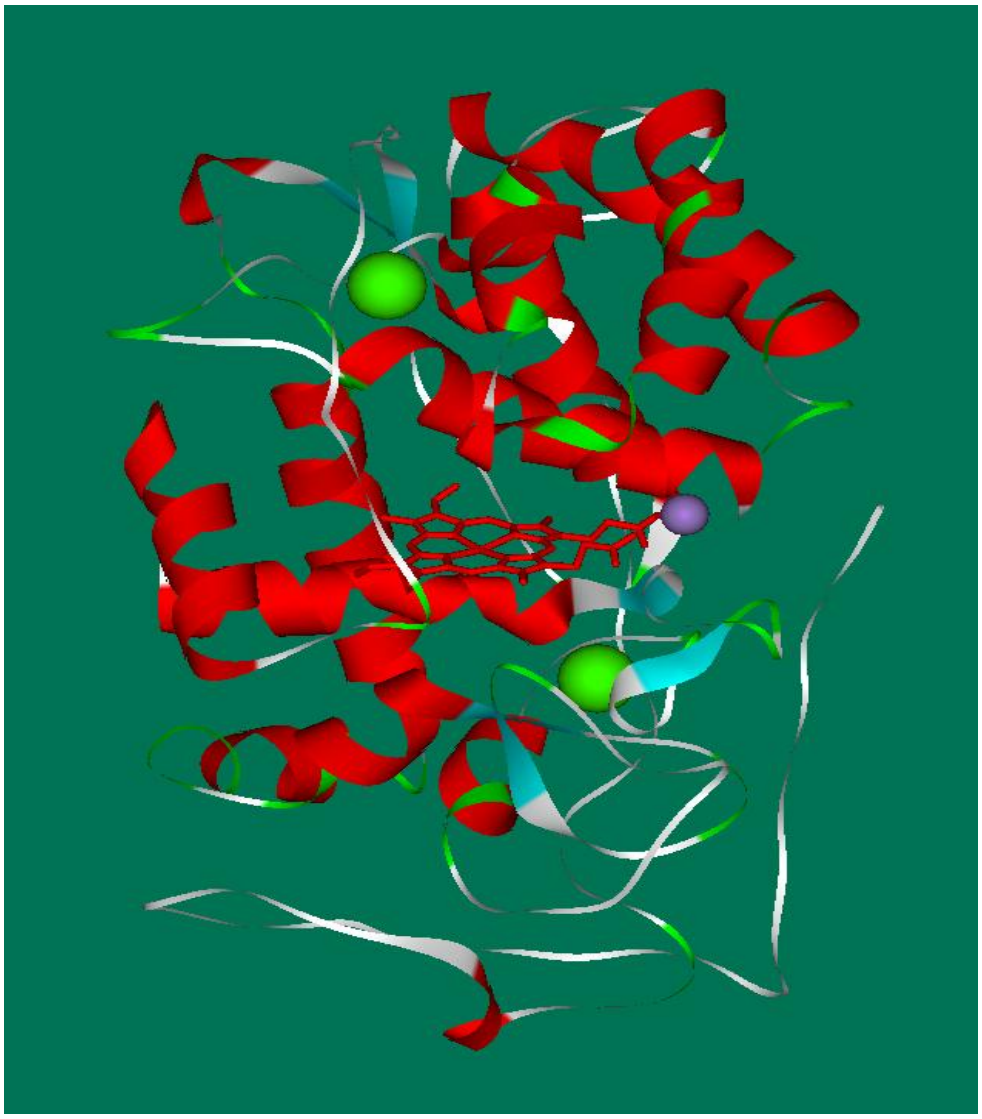

Figure 1.9: Ribbon Model showing the overall fold of engineered MnP3 from *Phlebia radiata*. α-Helices are shown in red, β-strands in white, haem, distal and proximal calcium in green, manganese in pink. Image generated using Web Lab Viewer (Raswin) and the haem, Mn, and Ca obtained from crystal structure of versatile peroxidase from *Pleurotus eryngii* deposited in the protein Data Bank, entry code 3FJWA.

1.11.3 Haem active site of MnP

As shown by the crystal structure of MnP from *P. chrysosporium* (Sundaramoorthy *et al*., 1994), the active site environment of MnP is similar to those of other plant and fungal peroxidases. The distal histidine (His48) functions as an acid-base catalyst in the formation of intermediate, Compound I (Poulos and Krasut, 1980; Poulos and Finzel 1984). Two hydrogen bonds are also present, that are conserved among plant and fungal peroxidases; the H-bond between the distal histidine and Asn80, which ensures that Nε2 of the distal histidine is available for accepting a proton from the peroxide and the second H-bond between the proximal ligand, His173 and the buried side chain of Asp242 that is thought to impact a greater anionic character to the proximal histidine ligand **(**Poulos and Finzel (1984), which, in turn helps to lower the redox potential of the haem iron (Goodin and McRee, 1993; Banci *et al*., 1995). This stabilizes high oxidation states (oxyferryl (Fe^{4+}) iron) required for the stabilization of the MnP intermediates, Compound I and Compound II**.**

MnP enzymes contain a single high-spin protoporphyrin IX (haem b) as a prosthetic group (Dunford, 1999) (Figures1.9 and 1.10). In the resting state, the iron in MnP3 has an oxidation state of +3 (ferric) and is coordinated to the four pyrrole nitrogens of the haem, and to the nitrogen in the imidazole group of the proximal histidine (His173 in *P.chrysosporium*) (Cramer *et al*., 1978). In MnP the sixth (distal) Fe coordination position is occupied by a water molecule, *i.e.* six–coordinated. In addition to the Fe-His173 interaction, the haem is uniquely stabilized in MnP by the interaction of propionates with Mn^{2+}. The outer propionate in MnP indirectly interacts with Lys180 through an unusual carboxylate-carboxylate H-bond (Poulos *et al*., 1993). However, the propionate also rotates about 60° to make hydrogen bonds with the main chain peptide nitrogens of Asp179 and Lys180 and two water molecules. Due to the orientation of this

propionate in MnP, the distal arginine, Arg42 cannot form a hydrogen bond with this propionate. The second (inner) propionate interacts with the Mn^{2+} ion, water molecules, and the peptide NH group of Arg177.

The spin state of the ferric iron atom (Fe (III) is determined by the orbital occupancy of its d-orbital electrons, and in turn the nature of this occupancy is influenced by the ligand bonding electrons at the fifth and sixth haem coordination positions. Ferric iron has 5 d electrons and its porphyrin complexes can be generally divided up into two classes (Orgel, 1966). The 6^{th} coordination position is usually free, thus determining a high spin S= 5/2 state for the iron, with the possession of five unpaired electrons, while a low spin ferric porphyrin has one unpaired electron, spin ½. However, a purely high spin or low spin species seldom exist as ferric porphyrin is a thermal equilibrium mixture of high and low spins (Taumura and Hori, 1972).

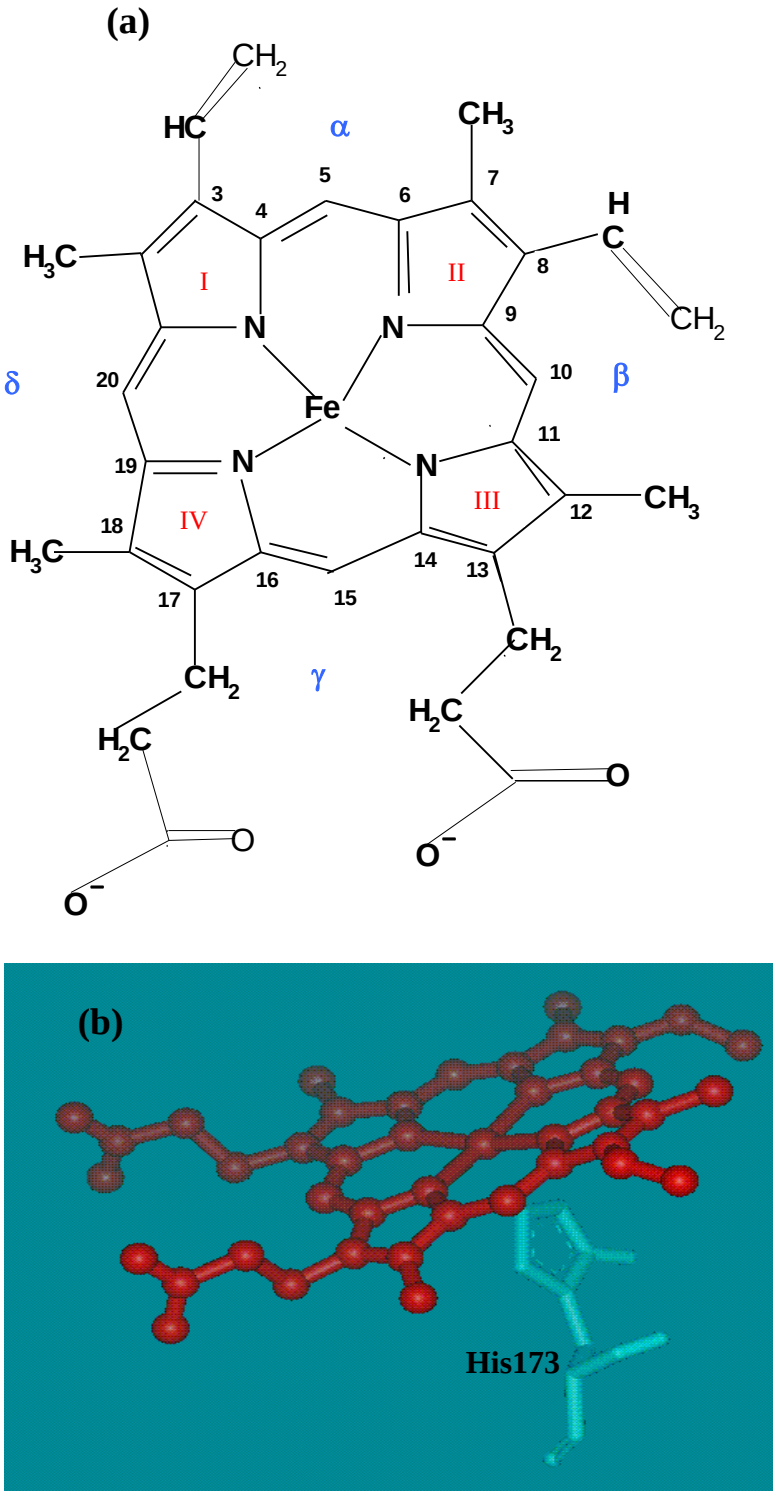

Figure 1.10 Haem structure and haem iron coordination. (a) Chemical structure of haem, ferriprotoporphyrin IX, with porphyrin ring carbon atoms numbered (IUPAC) in black and pyrrole rings in red (I-IV). Greek symbols in blue denote haem edge nomenclature.[ϒ] **(b)** Image showing occupation of the fifth iron coordination position by the imidazole side chain His173 in 1MNP[ƒ]

[ϒ] Drawn using ISIS™ /Draw V2.5 (http://www.mdl.com/downloads/public/isis.draw/2.5/en/draw25.jsp. [ƒ] Drawn using Swiss-Pdb Viewer V3.7 b2 (http://www.expasy.ch/spddv/) (Guex and Peitsch, 1997) and the PDB (Sundaramoorthy *et al.*, 1994) file 1MNP

Also present in MnP and other plant peroxidases of Class II and III are conserved calcium-binding and variable glycosylation sites. The two highly conserved, Ca^{2+} - binding sites are present in MnP (see Figure 1.7b and 1.9) one in each of the proximal and distal domains (Kunishima *et al.*, 1994; Poulos *et al*., 1993; Sundaramoorthy *et al*., 1994). The proximal Ca^{2+} has most of its ligands within a single loop from Asp191 to Trp196, is tightly bound with its binding site not accessible to the bulk solvent. The distal calcium-binding site is formed by seven oxygen atoms, which belong to the backbone and the side chains of residues Gly66 - Ser70, by the backbone and the side chain oxygen atoms of Asp48 and by two water molecules. The distal calcium ion is less tightly bound, as the binding site is close to the surface and is solvent exposed. Calcium ions have been shown to be important for MnP stability (Sutherland and Aust, 1996), and in maintaining the structural environment of the active site (Reviewed in Banci, 1997).

MnP is a glycoprotein (Paszcynski *et al*., 1986), and has three potential O- and N-glycosylation sites. Differences in glycosylation are, in some cases, responsible for the appearance of isozymes in extracellular peroxidases (Konigsberg *et al*., 1987; Kjalke *et al*., 1992). Deglycosylation studies and expression in *E.coli* (Whitwam *et al*., 1995; Dalton *et al*., 1996; Doyle and Smith, 1996) have shown that glycan groups are not essential for activity, but they do improve both enzyme stability (Nie *et al*., 1999) and solubility (Tams *et al*., 1999).

1.11.5 Manganese-binding Site

With the availability of X-ray crystal data, it became possible to locate a highly specific binding site for Mn (II) in the *P. chrysosporium* MnP structure (Sundaramoorthy *et al*.,

1994) (Figure 1.11). It is a unique anionic environment, present in MnP, that is absent in other homologous peroxidases e.g. LiP, CiP and C*c*P. (Sundaramoorthy *et al*., 1994).

The manganese-binding site in MnP is situated near the internal propionate of the haem (Kusters-van Someren *et al*., 1995; Kishi *et al*., 1996; Sundaramoorthy *et al*., 1997). The Mn (II) ion is coordinated to one oxygen atom of the carboxylic group of this propionate. The Mn^{2+} coordination sphere is further completed by 3 other oxygens from 3 different carboxylate groups, the side chains of acidic residues Glu35, Glu39 and Asp 179, and by two water molecules, thereby giving a six-coordinate octahedron. The coordination between Mn^{2+} and it ligands as octahedral is typical of Mn^{2+} complexes (Demmer *et al*., 1980; Sundaramoorthy *et al*., 1994; 2005). The presence of specific ligands (Gold *et al*., 2000; Sundaramoorthy *et al*., 1994) is an indication of conservation of the topology required for Mn (II) coordination and for a similar role in catalysis (Kusters-van Someren *et al*., 1995; Gold *et al*., 2000). Note that the Mn (II) ligands for the *P. radiata* MnP3 enzyme of the current study will be Glu40, Glu44 and Asp186 (see Figure 1.11).

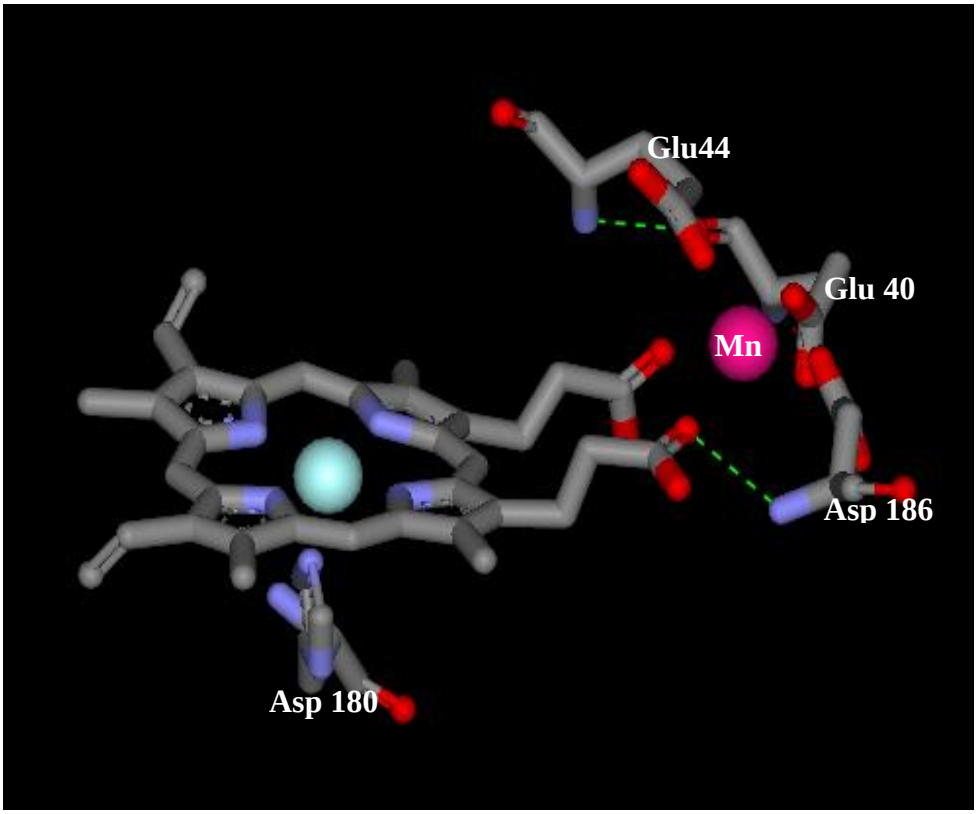

Figure 1.11: A model of manganese (II) binding site, with its associated amino acids ligands, of engineered *P. radiata* MnP3. The Mn (II) (pink) at the edge of the haem priopionate is sorrounded by ligands, Glu40, Glu44 and Asp186. Image generated using WebLab Viewer (Accelrys) and the haem, Mn, and ligands obtained from crystal structure of versatile peroxidase from *Pleurotus eryngii* deposited in the protein Data Bank, entry code 3FJWA (Piontek *et al*., 2009).

1.12 Reaction mechanism of peroxidases

Peroxidase catalysis involves three key steps (Everse and Everse, 1991, see Figure 1.12). Firstly, hydrogen peroxide reacts with the resting enzyme resulting in its reduction to water and the oxidation of the protein by two electrons to form a high oxidation state intermediate Compound I. One of these oxidising equivalents is located at the iron as an oxy-ferric [Fe (IV) =O] and the other on the porphyrin as a π cation radical species. Compound I is then reduced by a substrate to give a substrate radical and a second intermediate, Compound II

which has lost its porphyrin π cation radical. Compound II is further reduced by a second substrate molecule back to the resting iron (III) state.

(a) E (Fe (III), Porph)) + H_2O_2 → E (Fe (IV=O, $Porph^{\bullet+}$)) + H_2O

Resting-state Compound I

(b) E (Fe (IV=O, $Porph^{\bullet+}$)) + S_{red} → E (Fe (IV=O, Porph)) + S_{ox}

Compound I Compound II

(c) E (Fe (IV=O, Porph)) + S_{red} + $2H^+$ → E (Fe (III), Porph)) + S_{ox} + H_2O

Compound II Resting-state

Figure 1.12 Reaction sequence in catalytic cycle of haem peroxidases.

E represents the enzyme, Porph**,** the haem porphyrin ring, S_{red} the reducing substrate and S_{ox} the oxidized product.

The above figure 1.12 is applicable to most, but not all, reactions catalyzed by the haem peroxidases, irrespective of the specific enzyme involved; the oxidation of iodide (Roman and Dumbord, 1972) bisulphite ions (Araiso *et al.*, 1976) and stabe amino acid radical of compound ES of CcP Trp •+) (Sivaraja *et al*., 1989), which involve a single-two electron reduction step, are exceptions. The resting-state enzyme and catalytic intermediates Compounds I and II are kinetically and spectrally distinct and their relative abundance and rate of conversion between them can be measured directly by UV-visible absorption techniques (Dunford, 1999c).

In most peroxidases, directly adjacent to proximal His is Phe but C*c*P has a Tryptophan at this location, which is essential for activity (Mauro *et al*., 1988). During the peroxidase catalytic cycle, the enzyme is first oxidised by hydrogen peroxide to give

compound I containing 2 oxidising equivalents. While the haem lost one electron to five Fe^{4+}=O centre, the second electron is removed from an active site group of most haem peroxidases as porphyrin π cation radical (Dolphin *etal*., 1971). In *Cc*P compound I contains unusual free-radical species (Yonetani, 1965). Trp191 has been identified as the radical in the Compound I-like state (ES) (Sivaraja, 1989; Huyett *et al*., 1995). The ES state of C*c*P is one of only four known instances in which an enzyme makes use of a stable amino acid radical particularly Tyr π-radical. In ES one of the oxidising equivalents exists as a reversibly oxidized amino acid residue.

Two peroxidases have been identified that operate through a slightly different mechanism for compound I formation. The Class I yeast C*c*P contains an intermediate equivalent to HRPC-C Compound I in terms of oxidation state, but the second electron required to form the iron-oxygen is provided by the nearby Trp 191 rather than the porphyrin ring. The second oxidising equivalent is located at the Trp 191 as an amino acid radical in C*c*P, as opposed to a porphyrin π cation radical in HRP-C (Sivaraja *et al*., 1989). The site of the radical located on the residue Trp 191 was confirmed by mutational studies (Mauro *et al*., 1988; Erman and Vitello *et al*., 1989). Additional evidence that supports the presence of an amino acid cation radical is the similarity of the UV-Vis absorption spectra of C*c*P compound I and HRP-C Compound II, which are both oxy-ferryl haem group but without a porphyrin π cation radical (Dunford, 1991). The rational for the difference in Compound I structure is not understood. Even the closeness of the tryptophan to the haem group does not seem to be the major reason for the formation of a protein-based radical.

Class I pea ascorbate peroxidase (APX) also contains a tryptophan positioned at a similar location to that of C*c*P, but this is like other peroxidases. APX forms a porphyrin

radical (Pappa *et al*., 1996). Despite the different sources of the second electron to form the oxy-ferryl bond, in formal terms of oxidation state, the intermediates generated are two oxidising equivalents above the Fe (III) resting state and require two-single-electron transfers from substrate molecules to reduce Compound I, first to Compound II and then to the resting state.

1.13 Aims of this project

Delignification of lignocellulosic materials by *Phlebia radiata* is of potential interest commercially as it is one of the most potent wood degrading fungi in Scandinavian forest eco system. The possible application of this enzyme type has stimulated much research into structure and function. The current study has been particularly stimulated by the biotechnological interest in ligninolytic enzymes as industrial biocatalysts for the biotransformation of recalcitrant aromatic compounds including lignin and environmental pollutants such as the polycyclic aromatic compounds.

P. radiata is known to secrete several ligninolytic enzymes, *i.e.* lignin peroxidases, manganese peroxidases and laccases. These native enzymes of *P. radiata* have been studied in liquid medium (Niku-Paavola *et al*., 1988; Lundell, 1993; Lundell and Hatakka, 1994) and solid-state fermentation cultures (Vares, *et al.*, 1995). However, individual enzymes have not been expressed in recombinant form to allow individual study. Genes encoding different MnP isozymes of *P. radiata* have been isolated (Hilden *et al*., 2005) and MnP3 proteins predicted to be more like a versatile peroxidase having a shorter C-terminal tail. MnP3 of this type have not been studied in detail.

The main aims of this work:

1. To manipulate the MnP3 gene of *P. radiata* to allow high-level expression in *E.coli.*
2. To refold and purify wild-type and mutant MnP3 variants into active enzymes.
3. To generate MnP3 mutants by site directed mutagenesis that will allow the specificity of the Mn (II) binding site to be modulated with respect to both Mn^{2+} and other metals.
4. To evaluate the stability of MnP3 and the linkage between stability and Ca^{2+} addition.

Chapter Two

Materials and Methods

All molecular biology methods used were those described by Sambrook *et al*., (1989) unless otherwise stated. Fisher or Sigma Aldrich supplied all chemicals used, unless otherwise stated. All restriction enzymes and their appropriate buffers were supplied by NEB (UK) Ltd, unless other here stated. All Spectroscopic measurements were carried out using a Shimazdu-UV-2401 spectrophotometer. The synthesis of oligonucleotide primers and DNA sequencing was performed by MWG-biotech.

2.1 Cloning of the MnP 3 gene of *Phlebia radiata* in *E.coli* expression vector

2.1.1 Oligonucleotide primer design

Method

The primers for the cloning of the *P. radiata* MnP3 gene into the *E. coli* expression vector, pFLAG1 were designed based on the already published (Hilden *et al*., 2005) *P. radiata* MnP3 gene sequence. Two primers, for the N- terminal and C- terminal ends of MnP3 were designed to amplify the full length coding sequence. The primer design involved the removal of signal sequence and prosequences, the introduction of the first three residues (Methionine, Leucine and Threonine, MLT) from start synthetic CIP gene and codon usage and GC content optimisation. Also, the N-terminal primer had an *Nde* I site introduced and the C- terminal primer a *Bam*H I site. This was to facilitate in-frame clonining, into expression vector, pFLAG1. The primers also have stop codons to ensure that translation is efficiently terminated.

2.1.2 Polymerase Chain Reaction (PCR)

Table 2.1: Materials for PCR reaction

Materials	**Volume**	**Final amount**
Pfu polymerase buffer (10X) (Promega)	5µl	1 X
dNTPs (1mM each)	5µl	10µM each
Primer X 2 (10µM)	5µl + 5µl	1µM
DNA template (5µg/µl)	1µl	5ng
Pfu polymerase (Promega)	1µl	2.5 U
ddH_2O	28µl	
Total	50µl	

Method

The primers were supplied lyophilised. They were dissolved with 10mM Tris, pH 8.5 to a concentration of 100µM for each primer. The volume of the buffer used depended on the MWG specification for the amount of each primer. These remained the main primer stock, and were stored in - 20°C freezer. For each primer 1: 10 solution in water was made to a final volume of 100µl (10µM).

The PCR reaction mixtures were prepared as above but excluding the polymerase. It should be noted that all ingredients were added to PCR tubes and placed in the PCR machine (Perkin Elmer GeneAmp PCR System 9600) for 10 minutes at 95°C (hot start). The 1µl of *Pfu* DNA polymerase was then added and the reaction cycles followed.

Thermal cycling parameters

Hot start	95°C for 10 minutes

Addition of *Pfu* DNA polymerase followed by 25 cycles of:

Denaturation	95°C for 1 minute
Annealing	60°C for 1 minute
Extension	72°C for 5 minutes
then	4°C Indefinite

On completion of the reaction, the PCR products were analysed using 1% agarose gel electrophoresis.

2.1.3 Agarose gel electrophoresis

Materials

Agarose electrophoresis grade powder (Invitrogen)

1x TBE (Tris/Borate /EDTA) solution

Gel box (70ml)

Ficoll loading solution (0.25% (w/v) Bromophenol blue, 15 %(w/v) Ficoll, 0.25% (w/v) Xylene FF)

1 kb DNA ladder marker (Promega)

Ethidium bromide solution (10mg/ml)

Method

Agarose gel electrophoresis is the standard method for separating DNA molecules of different lengths and was conducted to confirm the presence and size of the PCR products. Agarose gel electrophoresis was performed using a 1% (w/v) agarose gel throughout these studies.

The gel was made by addition of 0.7g of electrophoresis-grade agarose powder to 70 ml of 1 x TBE buffer. The agarose in solution was heated in a microwave oven until fully dissolved. Some of it was used to seal the edges of the gel box and the molten gel was then poured into a 70ml gel box. A comb was placed in the gel to form 16 wells for the samples. The gel was allowed to set for about 30 – 60 minutes and 1 X TBE was added to cover the gel surface. Prior to loading, 5µl of PCR product was mixed with 2µl of the loading buffer (Ficoll). 10µl of 1 kb DNA ladder marker was also loaded in a separate well, and then the gel was electrophoresed at a constant voltage of 60 volts until the dye had reached the end of the gel.

Following electrophoresis, the gel was transferred into a staining box containing ddH_2O and 20µl of 10mg/ml ethidium bromide solution and was agitated for about 15 minutes. Ethidium bromide binds strongly to DNA by intercalating between the bases that are stacked in the centre of the DNA helix causing the helix to unwind to accommodate the strain from the dye. The bands were examined by transillumination with UV light and photographed using a digital camera.

2.1.4 TOPO cloning of the PCR product

Materials

PCR product

Taq polymerase

dNTPs (1ml)

X-gal (1ml)

IPTG (1ml)

pCR2.1TOPO TA cloning kit (Invitrogen)

Luria-Bertani-Broth / Agar (L-Broth/Agar)

Chemically competent TOP10 *E. coli* cells (Invitrogen)

Method

Direct cloning of the correctly sized PCR product amplified using *Pfu* polymerase into the pCR2.1TA cloning vector was facilitated by treating the PCR product with *Taq* polymerase. *Taq* polymerase has a non- template dependent terminal transferase activity that adds a single deoxyadenosine (A) termini overhang to 3' ends of PCR fragments. To ensure the presence of 3' A – overhangs on the PCR product, 1µl of *Taq* polymerase and 5 µl of dNTPs were added to the PCR tube and mixed. The tube was then incubated at 72°C for 30 minutes.

TOPO TA cloning provides a highly efficient, one step cloning strategy for the direct insertion of *Taq* treated PCR products into a TA plasmid vector. This cloning approach does not require ligase, restriction enzymes or complex post-PCR procedures and is more efficient than traditional blunt-ended cloning. The plasmid vector supplied is in a linearised form with a single 3' deoxythymidine (T) residue overhang. With A-overhang at the 3' ends of the PCR inserts, efficient cloning will be facilitated. The vector is topoisomerase I activated and contains ampicillin and kanamycin resistance marker

2.1.5 Transformation of chemically competent *E. coli*

Once the PCR product had been cloned into the pCR2.1 vector, the sample was transformed into chemically competent *E. coli* TOP10 thus: 2µl reaction solution was added to the chemically competent cells and allowed to incubate on ice for 15 minutes. This was then "heat shocked" for 30 seconds at 42°C and placed on ice for 2 minutes to recover. 250µl of L-Broth was added and incubated with shaking at 170 rpm and 37°C

for 1 hour for the cells to grow and to allow antibiotic resistance protein expression. This was then centrifuged at 6000 rpm using a micro centrifuge for 2 minutes and most of the supernatant was discarded leaving approximately 100µl medium. The pellet was resuspended and the chemically transformed cells were spread onto an L-agar plate containing suitable selection antibiotic (kanamycin 25µg/µl), 100µl of 20µg/ml of X-gal and 1 ml of 0.2mg/ml of IPTG. Kanamycin was used instead of ampicillin because the PCR template plasmid was ampicillin resistant and this can be used to select against it. The plates were incubated upside down at 37°C overnight.

pCR2.1 contains the TA cloning site within the *lac*Z gene, under the control of a *lac* promoter. This allows for the selection of clones that contain insert by "blue/white" colony selection. Colonies appearing blue shows that no additional DNA is inserted and so the lacZ gene remains intact, enabling the induction of galactosidase by IPTG and the production of blue colour by the action of the galactosidase on the added X-gal. Colonies appearing white implies that DNA inserts have disrupted the *Lac* reading frame, hence, no active β-galactosidase is produced, and therefore only white colonies should contain the desired insert.

2.1.6 Isolation of plasmid DNA

Two methods were used to purify plasmid DNA from *E. coli* cultures. The small-scale purifications, known as "minipreps", were used to purify DNA from 5ml overnight cultures of *E.coli* whereas "midipreps" were used for processing larger culture volumes of 50 to 100ml (see section 2.1.8).

2.1.6.1 Small-scale plasmid DNA preparation (Miniprep)

Materials

L-Broth

10mg/ml of Kanamycin

QIAprep Spin Miniprep Kit (Qiagen)

10mM Tris-HCl, pH 8.5

Methods

Mini-Prep is an easy way to screen single colonies for positive transformants. Colonies of *E.coli* transformants were used to inoculate 5 ml of LB containing 25mgml kanamycin. Cultures were incubated with shaking overnight at 37°C. The plasmid DNA from the resultant overnight cultures was purified using QIAprep Spin Miniprep Kit protocol (QIAGEN), except two 1.5ml aliquots of bacterial culture were used instead of one. In this way, double the amount of DNA from each column was purified. The resultant DNA was collected in 10mM Tris-HCl, pH 8.5 and stored at – 20ºC.

2.1.7 Diagnostic restriction enzyme digestion of pCR 2.1-MnP3 clones

All the restriction enzymes were supplied by New England Biolabs. The manufacturer's recommended assay conditions and restriction enzyme buffer were used with the enzyme.

Materials

Restriction enzyme (*Eco*RI)

Restriction enzyme buffer (10 X)

BSA (1mg/ml)

Miniprep DNA

ddH_2O to make up the required final volume.

Method

Restriction enzyme analysis was used to screen the putative pCR 2.1-MnP3 DNA colonies, to check if the right PCR product had been cloned. The miniprep samples of each colony were digested in a reaction mixture which consisted of 10µl of miniprep DNA, 1µl *Eco*RI, 1µl of BSA, 2µl of *Eco*RI buffer and 6µl of ddH_2O. The reaction mixture was incubated for 4 hours at 37ºC. The digest was evaluated by 1% agarose gel electrolysis (section 2.1.3) and staining with ethidium bromide. Positives were selected for large- scale DNA preparation.

2.1.8 Medium- scale plasmid DNA Isolation (midiprep)

Materials

L- Broth

Kanamycin 10mg/ml

Wizard^{TM} Midi-prep DNA Purification System (Promega)

10mM Tris-HCl, pH 8.5

Method

Upon identifying positive clones, 50µl of overnight culture containing positive transformants was put into 50ml of L-broth with 25mg/ml of kanamycin and was grown overnight at 37ºC, shaking at 170rpm. The resultant bacterial culture was centrifuged, and the DNA was extracted using the Promega Wizard® Plus Midipreps DNA purification system kit. The protocol was followed as described in the accompanying handbook. The resultant DNA was resuspended in 10mM Tris, pH 8.5 and stored at –20ºC.

2.1.9 Spectroscopic determination of DNA concentration

Materials

Quartz cuvettes

10mM Tris-HCl, pH8.5

Midiprep DNA

Method

The purity and concentration of Midiprepped plasmid DNA was determined spectrophotometrically. The samples were diluted 1:50 in 10mM Tris, pH8.5 to a final volume of 500µl. The spectrophotometer was baselined using 10mM Tris, pH8.5. The diluted samples were put in a quartz cuvette and its spectra measured from 350nm to 220nm. The values of absorbances (As) at 260 and 280 determined. The purity of the sample is given by the ratio of A_{260}/ A_{280}; whereby a value of 1.8 – 2 indicated that the sample was pure. The concentrations of the samples were determined by multiplying the A_{260} by the dilution factor (50) and by a conversion factor of 50. (a solution of double stranded DNA of 50µg/ml has absorption of 1 OD unit at 260nm).

2.1.10 Preparation and submission of DNA for automated sequencing

Materials

Midiprep DNA

10mM Tris-HCl, pH 8.5

Universal primers: M13F and M13 R

Method

The cloned MnP3 gene was sequenced to confirm that there were no errors introduced during the PCR or cloning procedures. With the known concentration of DNA, two samples of DNA were produced of 1µg DNA/ 10µl Tris buffer.

Universal primers M13F and M13 R were used. Two samples of DNA were prepared to permit sequencing on both DNA strands as well as to span the full coding region of the MnP3. The DNA samples were sent to MWG -Biotech for sequencing and the results sent back as computer files. The MnP3 sequence files were aligned against the designed gene construct. Sequence assembly and editing of sequence data were performed using the modules SeqManII and EditSeq of the Lasergene99 software suite (v. 4.06) (DNASTAR, Inc., Madison, Wisconsin, USA).

2.1.11 Digestion of pCR2.1-MnP3 for cloning into pFLAG1 and purification by Geneclean.

Materials

Restriction enzyme buffer (10 x NEB4)

BSA (1mg/ml)

Restriction enzymes (*Nde*I and *Bam*HI)

Midiprep DNA

Geneclean III kit (BIO 101)

Low melting point agarose (Gibco).

Method

The expected total volume of the digest was 70µl. The reaction mixture consisted of 49µl of DNA, 1/10 of the volume of 10 X restriction enzyme buffer No. 4, 1/10 of volume of 10 X BSA and 1/10 of the restriction enzymes in the proportion of 4µl of *Nde*1 and 3µl of *Bam*H1. The mixture was incubated for 1 hour at 37ºC and the digestion efficiency was evaluated on a 1% agarose gel (section 2.1.3) except low melting point agarose was used. A significant amount of the MnP3 gene fragment was

apparent on the low melting point agarose gel, and then the Geneclean III (BIO 101) method was used to repurify the DNA from the gel according to the manufacturer's instruction. The MnP3 gene fragment was finally resuspended in 10µl ddH_2O. 3µl were used on another 1% agarose gel to check the procedure had been successful.

2.1.12 Restriction digestion of pFLAG1

Materials

pFLAG1 plasmid (600ng/µl)

Restriction enzyme buffer (10 x, NEB 2)

BSA

Restriction enzymes (*Nde*I and *Bgl* II)

ddH_2O

Method

20µl reaction mixture contained: pFLAG1 at a concentration of 30ng/µl, 2µl of BSA, 2µl of restriction enzyme buffer, 0.5µl of *Nde*I, 0.5µl of *Bgl* II and 13µl of ddH_2O. Control digestion mixtures with just *Nde*I or just *Bam*HI or neither enzyme were also prepared. The mixtures were incubated at 37ºC for 1 hour and the efficiency of the digests was evaluated by agarose gel electrophoresis (section 2.1.3). If the single enzyme digest had reacted fully, then the double digest was assumed to be complete also.

2.1.13 Ligation of MnP3 gene DNA into pFLAG1 and transformation into *E.coli*

Materials

T4 DNA ligase (New England Biolabs)

Ligation buffer (10 x) (0.5M Tris-HCl, PH 7.8, 100mM $MgCl_2$, 100mM DTT, 10M ATP)

1mg/ml BSA (1mg/ml)

pFLAG1 *Nde*I/*Bgl* II digested (30ng/µl)

Genecleaned MnP3 gene fragment

ddH_2O

Method

Ligation was achieved using T4 DNA ligase. The linear pFLAG1 DNA and the MnP3 gene fragment were mixed in an eppendorf tube in a 1: 5 molar ratio respectively. One tenth of the final volume of the mixture was added as 10 x concentrated ligation buffer as well as BSA (0.1mg/ml) to a total volume of 20µl. 1µl of T4 DNA ligase was used. Two control mixtures were included: Control I contained every component except the MnP3 gene. Control II contained no MnP3 gene and no ligase. The mixtures were incubated overnight at 4ºC.

10µl of all ligation mixes were transformed into chemically competent DH5α *E.coli* and plated on L-agar plates with 100µg ampicilin (as section 2.1.5).

2.1.14 Identification of pFLAG1-MnP3 clones.

12 colonies from the experimental transformation were inoculated into 5 ml LB containing 100 µg/ml ampicillin, and shaken overnight in an incubator at 37°C. Small-scale plasmid preparation from each colony was then performed as in section 2.1.6.1. The final DNA solution was extracted using 50 µl of 10 mM Tris-HCl, pH 8.5.

To check if any of the colonies contained correctly ligated pFLAG1-MnP3 plasmid DNA, restriction digestion (section 2.1.7) was carried out on miniprep DNA using *Nde*I and *Xho*I together with NEB buffer 4. This will release the full length MnP 3 gene so that its presence and size can be confirmed after electrophoresis (section 2.1.3).

Once positive colonies had been identified, 2 were selected and more DNA was prepared by midiprep (section 2.1.8). The DNA concentration was measured for both

(section 2.1.9) and samples sent for sequencing (2.1.10) using custom primers SEQ 1 (forward) and SEQ 5 (reverse).

2.1.15 Glycerol stocks

pFLAG1-MnP3 clones, which were correct on sequencing, were stored as glycerol stocks for future use. A colony was inoculated into 50 ml L-broth containing 100µg/ml ampicillin and incubated overnight at 37°C with shaking. 1ml of each of the cultures was added to a Nunc cryovial using sterile technique. Then 0.5 ml of sterile 50% glycerol was added and the tube was inverted to mix and placed at – 80°C. When needed, the glycerol stock was thawed slightly and a streak was made onto an L-agar plate to generate single colonies.

2.2 Generation of mutant MnP3 genes

Mutagenesis of the MnP3 gene was carried out by the whole plasmid amplification method (Doyle *et al*., 1998) (See Figure 2.1). PCR-based Whole Plasmid Amplification Mutagenesis using 'back-to-back' primers and *Pfu* DNA polymerase results in the production of a linear 6.3kb double- stranded DNA fragment. The template DNA is then digested away using *Dpn*I and the linear DNA PCR fragment is circularised by T4 polynucleotide kinase phosphorylation and ligation using T4 DNA ligase. The ligation mixture is then transformed into *E. coli* strain DH5α. Clones are tested for the presence of intended nucleotide changes and the fidelity of the ligation junction by new restriction enzyme site digest.

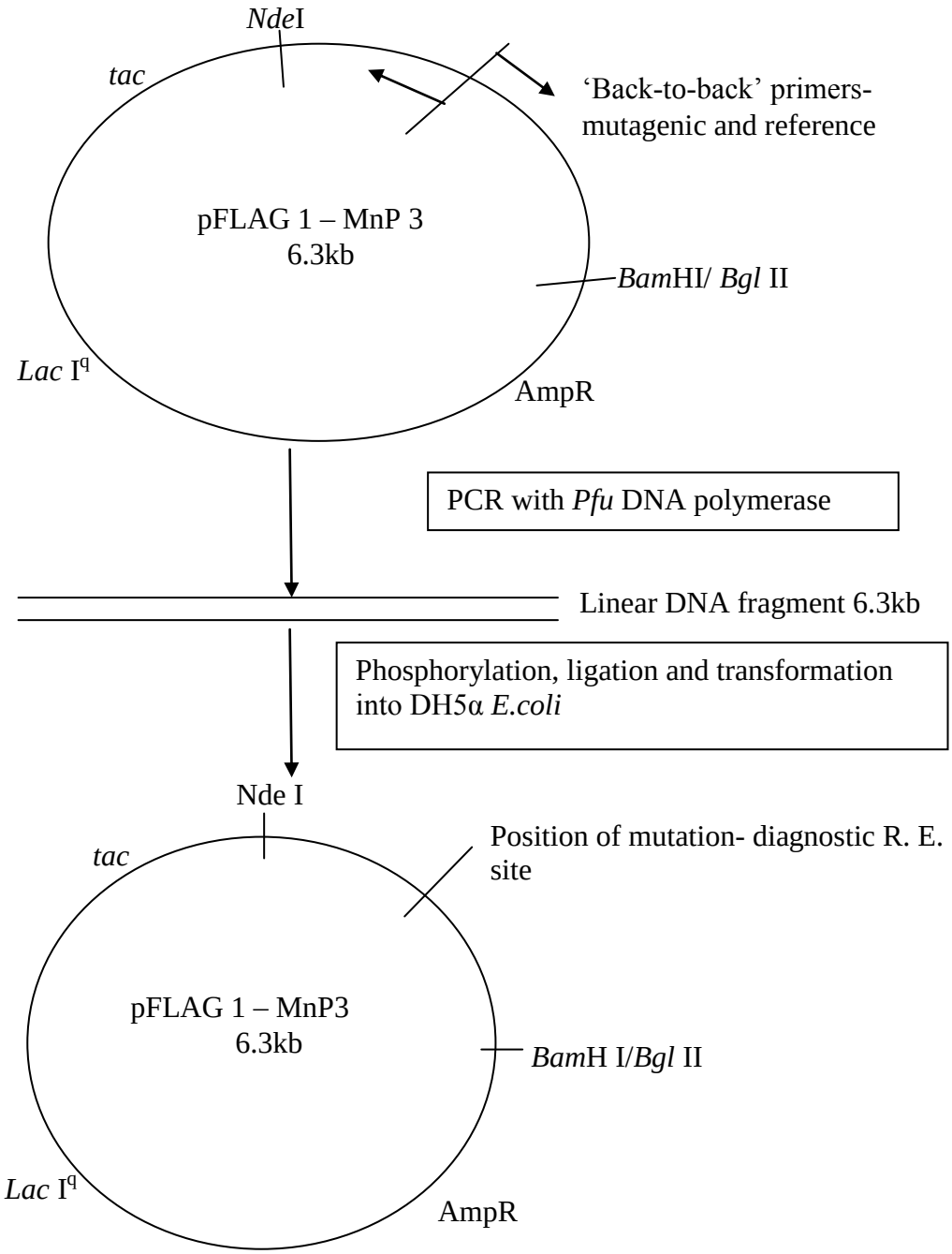

Figure 2.1: PCR-based whole plasmid amplification method (WPAM) of site-directed mutagenesis.

2.2.1 Oligonucleotide primer design for mutagenesis

Primers were designed in collaboration with Dr. Wendy Doyle and synthesised by MWG-Biotech Ltd. The alignment of the MnP3 protein sequence with the sequence of *P.chrysosporium* MnP had identified the residues responsible for manganese binding. These were E40, E44 and D186 (as for engineered MnP3 numbering). For each mutant gene to be engineered two primers were designed: one (the mutagenic primer) overlapped the area to be mutated and contained the intended base change(s). The other (reference) was designed to anneal exactly back to back on the opposite strand of the DNA template (pFLAG1-MnP3). Silent mutations were also incorporated so that a new restriction enzyme site was introduced to be used and for identification of mutant clones. Mutant genes to be made included E40H, E44H, E40H/E44H, D186H and D186N.

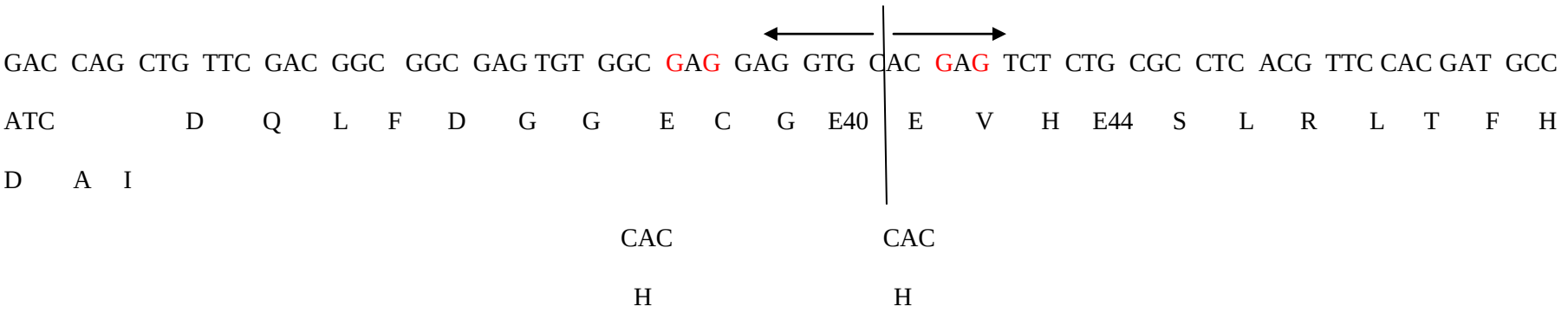

The *Apa*L I site is already present between the two binding sites, (GTGCAC)

wt1	CAC CTC CTC GCC ACA CTC GCC	Tm = 72°C	**Primers:**
wt 2	CAC GAG TCT CTG CGC CTC ACG TTC	Tm = 78°C	E40H : wt2 and H1
			E44H : wt1 and H2
			E40H/E44H: H1 and H 2
H1	CAC CTC G*TG* GCC ACA CTC GCC GC	Tm = 62°C	
H2	CAC C*AC* TCT CTG CGC CTC ACG TTC	Tm = 58°C	

Figure 2.2: Primer design for *P. radiata* MnP 3 mutants, E40H, E44H and E40H/E44H showing the mutations to the wild type gene and the restriction enzyme site used for screening, *Apa*LI, which is already present between the two mutating residues.

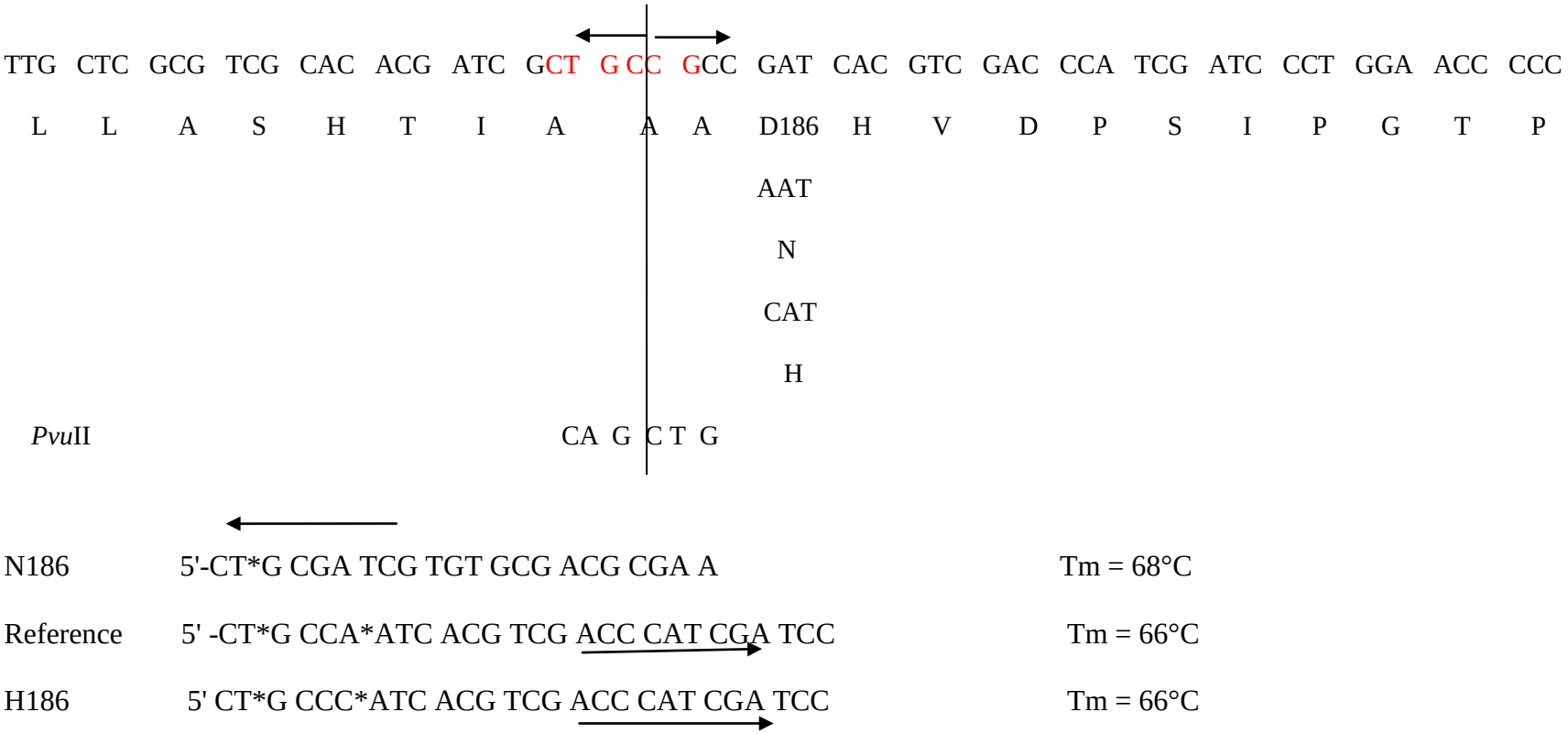

Figure 2.3: Primer design for *P. radiata* MnP3 mutants, D186N and D186H.

The mutations to the wild-type to introduce the D183N and D183H mutants are shown as well and the silent mutations required to form new *Pvu* II site.

2.2.2 Polymerase chain reaction (PCR)

Materials

pFLAG1-MnP3 (5ng/µl)-6.3kb

Mutagenic /reference primers (10µM)

Pfu polymerase (10) buffer (Promega).

dNTP mix (1mM each)

Pfu DNA polymerase (Promega)

ddH_2O

50% glycerol

Methods

The PCR reactions (50 µl final volume) were set up as in section 2.1.2 except that 50% glycerol was also added. Glycerol enhances DNA denaturation by decreasing the primer-template complex thereby lowering the annealing temperature. The thermal cycling parameters used are listed below; the long extension time is needed for the product size of 6.3kb.

Hot start	95°C for 10 min
Addition of *Pfu* DNA polymerase followed by 25 cycles of:	
Denaturation	95°C for 1 min
Annealing	50°C for 1 min
Extension	72°C for 16 min
then	4°C forever (∞)

The success of the PCR was verified by running 5µl of each mutagenic reaction on 1% agarose gel (section 2.1.3).

2.2.3 Purification of the mutagenic PCR products

Materials

Dpn I restriction enzyme

Phenol chloroform: Isoamyl alcohol 25:24:1

3M sodium acetate solution, pH 5.2

100% Ice-cold ethanol

70% Ice-cold ethanol

Methods

To cleave the methylated wild-type template from the final PCR mixture, 1 µl of *Dpn* I was added and incubated for 1 hour at 37°C. The *Dpn* I endonuclease (target sequence: 5'- Gm ATC - 3') is specific for methylated and hemimethylated DNA (Nelson and McClelland 1992). The mutated DNA, made by PCR, is not methylated and therefore stable to *Dpn*I. The PCR mixture was then transferred to an eppendorf tube and ddH_2O was added up to 150 µl. Proteins (*Pfu* and *Dpn* I) were then removed by the addition of 150µl a 25: 24: 1 mixture of phenol, chloroform and isoamyl alcohol, mixing and centrifugation at 13,000 rpm for 30 seconds. The proteins precipitate at the interface between the aqueous top and the organic bottom layers, leaving the DNA in the aqueous solution. This layer was transferred into a new eppendorf tube with care taken not to disturb the interface. The organic layer was discarded. The same process as above was repeated with the addition of 150 µl of chloroform to remove traces of phenol.

Ethanol precipitation was then employed to optimise the DNA concentration. The concentration of Na^+ was adjusted to 0.3 M in the PCR mixture. 11% of 3M sodium acetate solutions was added, the samples thoroughly mixed and the 2 volumes of ice-cold ethanol added. The samples were allowed to stand for 15 min at a temperature of -20°C to effectively precipitate DNA. The samples were then centrifuged at 13,000 rpm

for 10 minutes. The supernatant was carefully removed with care taken not to disturb the precipitated DNA pellet. 500µl of 70% ethanol was added and spun at 13,000 rpm for 5 minutes. The supernatant was carefully removed and the tubes were placed in a filter hood to dry. 8µl of ddH_2O was then added to the tubes to resuspend the DNA; the recovery was checked by running 2 µl of the DNA sample on a 1% agarose gel (section 2.13).

2.2.4 Recircularisation of the PCR products and transformation into *E.coli*

Materials

T4 DNA ligase buffer (10 x)

T4 polynucleotide kinase

T4 DNA ligase

Methods

A phosphorylation reaction was conducted to add 5' phosphate groups to the ends of the purified linear PCR product. This was achieved by mixing 8µl of the DNA solution, 1 µl of 10 x T4 DNA ligase buffer and 1 µl of T4 polynucleotide kinase making a total volume of 10µl. The ligase buffer used is suitable for the phosphorylation reaction. The reaction was incubated at 37°C for 1 hour.

A ligation reaction was then carried out by adding recircularised DNA. To the phosphorylated DNA, 8 µl of ddH_2O, 1 µl of 10 x T4DNA ligase buffer and 1 µl of T4 polynuceotide kinase, giving a total volume of 20 µl. The reaction mixture was incubated at 4°C overnight. Using the transformation protocol described in section 2.1.5 the MnP3 mutant plasmids were transformed into chemically competent DH5α cells. Transformants were selected on L-agar plates containing 100µg /ml ampicillin.

2.2.5 Identification of correct MnP3 mutant gene colonies

LB containing 100µg/ml ampicillin

Methods

To check that the desired mutations had been included and the DNA had correctly ligated, 12 colonies of *E. coli* DH5α transformants for each mutant were selected and grown with shaking at 37°C overnight in 5 ml L-broth containing 100µg/ml ampicillin. Minipreps were used to prepare plasmid DNA (section 2.1.6.1), which were then digested with the relevant restriction enzyme depending on the new site introduced (see sections 2.1.7 and 2.2.1). For mutants E40H, E44H and E40H/E44H the restriction enzyme used was *Apa*LI, whilst for D186N and D186H it was *Pvu*II (Caroline Santivale, unpublished work).

Once possible colonies had been identified for each mutant, 2 were selected, more DNA was prepared by midiprep (section 2.1.8), the DNA concentration was measured (section 2.1.9) and sample were sent for DNA sequencing (section 2.1.10) using primers SEQ 1 and SEQ 5 (section 2.1.13).

2.3 Expression, refolding and purification of MnP3 protein

2.3.1 Transformation of pFLAG1-MnP3 wild-type and mutants into W3110 *E. coli* cells

pFLAG1-MnP3 wild-type and mutant DNAs were transformed into chemically competent *E.coli* W3110 cells (a robust fermentor strain) (section 2.1.5). The transformants were plated on L-agar containing 100µg/ml ampicillin and incubated overnight at 37ºC.

2.3.2 Small-scale manganese peroxidase 3 expression

Expression of the MnP3 gene, as cloned in the expression vector pFLAG1, is under the control of the *tac* promoter. This is quite a strong promoter formed by the hybridisation of two different regions of the *trp* and *lac* promoters. Induction was with a non-hydrolysable lactose analogue, isopropyl-β-D-thiogalactoside (IPTG).

Materials

L-broth with 100µg/ml ampicillin

200 mM IPTG

20mM Tris-HCl, pH 8.0

1mM EDTA

1mM DTT,

6 M urea

50 mM Tris-HCl, pH 8.0

1mM EDTA

30 mM DTT

10 M urea

Method

The W3110 pFLAG1-MnP 3 wild-type and mutant colonies were inoculated into 5ml of L-broth containing 100µg/ml ampicillin and shaken at 37ºC overnight. A glycerol stock was prepared in the morning for each culture as described in section 2.1.15 above.

200µl from each 5ml overnight was inoculated into 20ml L-broth in a 100ml conical flask containing 100µg/ml ampicillin and the flask shaken at 37°C. The growth of the cultures was monitored at regular intervals by measurement of the absorbance at 500nm (A_{500}) using a Shimadzu UV-1601 PC UV-Vis spectrophotometer. Growth continued

until the A_{500} reached a value of 0.8. The expression of MnP 3 protein was then induced by the addition of freshly prepared IPTG to a final concentration of 1mM. The cultures were then grown for a further 3 hours.

An inoculated but un-induced culture was grown for the same time (negative control). The growth of a colony containing pFLAG1-HRP plasmid (known to express well) was also included as a positive control. Note peroxidase protein is usually expressed into inclusion bodies. 3ml of each culture was spun at 6,000 rpm for 2 min. The cells were resuspended in 500µl of 20 mM Tris-HCl, pH 8.0, 1 mM EDTA, 1 mM DTT and 6 M urea by vortexing. The resuspended cells were sonicated (MSE 150W Ultrasonic Disintegrator MK2, Crawley, UK) on ice for 30 seconds, centrifuged for 15 min at 13,000 rpm and the resulting supernatant discarded. The protein containing inclusion body pellets obtained were resuspended in a further 500µl of the buffer and sonicated to redissolve the pellet. An equal volume of the above buffer supplemented with 3% Triton (final Triton concentration of 1%) was added. The solution was left to stand at room temperature for 10 min and was then centrifuged for 15 min at 13,000 rpm. The supernatant was discarded. The resulting pellets were resuspended in 30µl 50mM Tris-HCl, pH 8.0, 1mM EDTA, 30mM DTT, 10M urea by vigorous vortexing and then centrifuged at 13,000rpm for 10 minutes. The presumed MnP3 containing supernatant was removed from the small, rather thin pellet carefully and stored in the freezer (-20ºC), before being run on an SDS-PAGE gel.

2.3.3 Sodium Dodecyl Sulphate Polyacrylamide Gel Electrophoresis (SDS-PAGE)

Materials

12 % Resolving gel, 10ml **for two gels**

1.25l of 3M Tris-HCl, pH8.5

4.3ml of 28 % Acrylamide (28g acrylamide, 0.735 g bis acrylamide/100ml)

0.05 ml 20% SDS

1.9 ml of ddH_2O

2.5 ml of 0.14% ammonium persulphate

5 µl TEMED

Stacking gel (7% acrylamide w/v), total volume 12 ml

1.5 ml of 1 M Tris/ SDS (4.8 ml 1 M Tris-HCl, pH 7.0 + 0.2 ml 20% SDS)

1.5 ml of 28 % acrylamide

3.0 ml of ddH_2O

6.0 ml of ammonium persulfate

15 µl of TEMED

Staining solution

10 % acetic acid

10 % methanol

0.1% Coomassie blue

Destain solution

10 % acetic acid

10 % methanol

10 X reservoir buffer (100 ml**)**

3 g Tris-HCl, pH 8.3

14.4g glycine

5 ml of 20 % SDS

Sample buffer (1:1 ratio)

1 g SDS

2 ml glycerol

2 ml Bromophenol blue

1.25 ml of 1 M Tris, pH 7.0

2 ml of 2-mercaptoethanol

2.75 ml of ddH_2O

Total volume of 10 ml

Method

A 12% resolving gel was prepared as above. The gel was poured between the two glass plates and allowed to set for about 30 minutes. Similarly, the stacking gel was prepared as above and was poured over the resolving gel and allowed to set for about 30 minutes with comb in place. The plates were assembled on the BioRad Protein electrophoresis apparatus. Protein samples were prepared by mixing in a 1:1 ratio with sample buffer. A volume of 15µl of sample was loaded onto the stacking gel using a Hamilton syringe and run at a constant current of 20 mA in 1 x Running Buffer. When the samples had moved through the stacking gel, the current was increased to 40 mA until the dye reached the bottom of the gel. Gels were stained with Coomasie Blue stain overnight at room temperature and then destained using destain solution on a rocking table until the protein bands became visible. The cultures of the best protein-expressing clones were used to make glycerol stocks (section 2.1.14).

2.3.4 Large-scale expression of manganese peroxidase 3

Materials

Terrific Broth (TB)

For each 2 litre baffled flask:

6g Tryptone

12g Yeast extract

4 ml glycerol

450ml ddH_2O

Phosphate Buffer (10x)

For each 50ml:

6.27g anhydrous K_2HPO_4

1.17g KH_2PO_4

N/B: 50ml of Phosphate buffer was added to each 450ml of Terrific Broth, when cultures were set up for growth.

Both solutions were then autoclaved.

1 mM IPTG

Methods

Small-scale expression tests provided evidence of successful expression of MnP3. A large-scale growth was therefore undertaken using Terrific Broth as growth medium. This medium is known to be very efficient for *E. coli* growth. 50µl of a glycerol stock were inoculated into 50 ml L-broth culture containing 100µg/ml ampicillin, and shaken overnight at 37°C. 5ml of this 50 ml culture were inoculated into each of 10 2 litre flasks of 500 ml Terrific Broth and 100µg/ml ampicillin. Cultures were grown at 37°C with vigorous shaking at 170rpm.The cells were grown until the absorbance at 500 nm (A_{500}) was 1.0, before induction with sterile IPTG to a final concentration of 1mM, and growth for a further 3.5 hours. Cells were then harvested by centrifugation at 4,000rpm (Beckman Model J- 6B Centrifuge) for 30 min to separate cells from the media. The supernatant was tipped off and cell pellets frozen at – 20°C.

2.3.5 Isolation and solubilisation of unfolded MnP3 inclusion bodies

Materials

Resuspension solution:

50mM Tris-HCl, pH8.0

10mM EDTA

5mM DTT

Lysozyme

Washing solutions

20mM Tris, pH 8.0

1mM EDTA

5mM DTT

+/-3% (v/v) Triton X-100

Solubilisation buffer:

50 mM Tris-HCl, pH8.0

1 mM EDTA

1 mM DTT

6 M Urea

Method

Over-expression of proteins in *E. coli* often leads to the formation of inclusion bodies (Kane and Hartley, 1988), whose mechanism is unclear. Inclusion bodies are insoluble protein aggregates, which consist primarily of the overexpressed protein, and disruption of cells followed by isolation of the inclusion bodies typically results in a greater than 50% pure product (Kane and Hartley, 1988).

The cell pellets were thawed and resuspended in 200ml of resuspension buffer. The final volume of the mixture was approximately 240ml. The cells were lysed using lysozyme (2mg/ml final concentration). The solution was mixed and left on the bench until the extract became very viscous and stringy. The cells were further disrupted by sonication (MSE ultrasonic disintegrator MK2) for 2 x 1 min. After centrifugation at 15,000rpm (Beckman, J2 – 21) for 30 min, each inclusion body protein pellet was resuspended by homogenisation in 20 ml wash buffer with no Triton, which was then supplemented with 10ml of the same buffer containing 3% Triton X-100. This helps to remove membrane components and proteases that may have absorbed onto the hydrophobic inclusion bodies. The solutions were mixed and the inclusion bodies recentrifuged at 15,000rpm for 30 minutes. The pellets were washed two further times. The final washed was carried out without Triton X-100 to remove any traces of detergent that might subsequently affect the efficiency of the folding procedure. The protein pellets were stored at – 20°C. The washed protein pellets were resuspended all together in 30ml solubilisation buffer using a homogeniser. The mixture was allowed to stand at room temperature for 15 minutes and was then centrifuged at 15,000 rpm for 30 min to remove remaining insoluble material which could act as nuclei for protein precipitation during refolding.

2.3.6 Determination of protein concentration

The supernatant containing urea-solubilised MnP3 was retained for protein concentration assay (Biorad); BSA was used as protein standard. Volumes of 2, 4, 6,8,10 and 12 microlitres of a 1mg/ml BSA stock solution were added successively in microcuvettes and filled up to 20µl with the same solubilisation solution as above. These microcuvettes corresponded respectively to protein concentrations of 100, 200, 300, 400, 500, 600 µg/ml. A volume of 20µl of the solubilised MnP3 protein, which

was previously diluted 40 times, was added to another microcuvette. To each microcuvette, 1ml of 5 times diluted Biorad assay reagent was added, mixed and allowed to stand for 5 minutes for the blue colour to develop. The Spectrophotometer was first autozeroed using the solubilisation solution and assay reagent as a blank solution. The BSA standard absorbances were measured at 595nm and a straight line was observed. The concentration of the solubilised MnP3 was then read off and multiplied by the dilution factor.

2.3.7 Folding of MnP3

Materials

Fold solution

5mM $CaCl_2$

0.15M Urea

0.5mM GSSG

0.1mM DTT

50mM Tris-HCl, pH 9.5

200µg /ml MnP3 protein

20µM haemin (15mM = 10.9mg/ml in 0.1M NaOH).

Method

Initial attempts to refold *P.radiata* MnP3 into active protein started with identification and application of successful protocols for refolding of plant peroxidases (Smith *et al*., 1990; Doyle *et al*., 1996; Perez - Boada *et al*., 2002). Finally, large-scale refolding of *P.radiata* MnP3 was performed under the optimal conditions of Perez - Boada *et al*., 2002. To bring the 6M Urea in the solubilised MnP3 protein solution to the required 0.15M Urea in the fold, it needed to be diluted 40 times. Therefore the MnP3 protein

solution was brought to 8mg/ml with solubilisation buffer. The 8mg/ml protein solution in the fold resulted in the required 200µg/ml protein concentration. However, the 40 times dilution would also bring the 1mM DTT concentration in the solubilisation buffer to 0.025mM. Hence, an additional 0.075mM DTT was added to the folding medium to give the required final 0.1mM DTT. The folded MnP3 was therefore obtained from a fold medium of 50mM Tris-HCl, pH 9.5, 5mM $CaCl_2$, 0.5mM GSSG, 0.1mM DTT, 0.15M Urea, 20µM haemin and a protein concentration of 200µg/ml. After addition of protein solution into the folding medium with stirring, the folding solution was divided into 400ml in aliquots in 1000ml beakers and stored in a dark cupboard at room temperature overnight.

2.3.8 Concentration of the folding mixture, dialysis and FPLC

Materials

2l of ddH_2O

2l 0.1M NaOH

Amicon spiral-wound concentrator (10000Da)

Amicon stirred ultrafiltration cell with a PM – 10 membrane10, 000 Da)

4l of 20mM Sodium acetate pH 4.3, 1mM $CaCl_2$.

4l of 10mM Sodium Succinate, pH 6.0, 1mM $CaCl_2$.

500ml 10mM Sodium Succinate, pH 6.0, 1mM $CaCl_2$ and 1M Sodium chloride.

Dialysis membrane (12,000Da cut-off)

500ml 10mM Na Succinate, pH 6.0, 0.2mM $CaCl_2$.

Mono-Q Column (Pharmacia).

Gel-filtration column (PD 10, Pharmacia).

Method

The Amicon spiral-wound concentrator unit was flushed with 2 litres of 0.1M NaOH and then 2 litre ddH_2O. The folding mixture was then concentrated to a final volume of approximately 250ml. This was in turn concentrated to a volume of approximately 45ml using an Amicon stirred ultrafiltration cell with a PM-10 membrane.

The resultant enzyme solution was then dialysed against 4L 20 mM sodium acetate, pH 4.3, with 1mM $CaCl_2$, in the cold room overnight, and then centrifuged at 15,000 rpm (Beckman J2-21) for 30 minutes to remove aggregates. It was then dialysed against 10mM sodium succinate, pH 6.0, with 1mM $CaCl_2$ again in the cold room overnight and recentrifuged at 15,000 rpm for 30minutes.

The protein solution in 10mM sodium succinate, pH 6.0, with 1mM $CaCl_2$ was syringe-filtered before loading on to a Mono-Q anion exchange column (Pharmacia). The active enzyme was eluted with a gradient of NaCl from 0-0.5 M with MnP3 appearing as a sharp peak at approximately 300 mM NaCl.

The fractions that contained the most MnP 3 were collected and gel-filtered using a PD 10 desalting column (Pharmacia) into 10mM sodium succinate, pH 6.0 buffer with 0.2mM $CaCl_2$. The purified MnP3 obtained was frozen beaded in liquid nitrogen before storing at – 80°C.

2.4 Characterisation of MnP3 enzymes

2.4.1 Resting-state UV-visible spectrum for MnP3

Standard spectroscopic operations were performed on a Shimadzu UV-2401 PC Spectrophotometer fitted with a Lauda Ecoline 003 Model circulating thermostated water bath and jacketed cuvette holder. The enzyme absorbance spectrum was determined in the presence of 10mM Na succinate buffer, pH 6.0 by scanning a

wavelength range of 250 – 750nm, using 1cm transmission matched quartz cuvettes (Hellma Ltd).

2.4.2 Determination of the Soret extinction coefficient (ε_{Soret}) for MnP3 wild-type and mutants.

The extinction coefficient of the Soret peak for *P. radiata* wild-type MnP3 and mutant enzymes was determined by the pyridine haemochrome method (Fuhrhop and Smith, 1975), which measures the total haem content of MnP3 by forming pyridine-haem complexes from extracted haem produced on treating MnP3 enzymes with alkali. Three independent determinations were carried out in 10mM Na succinate, pH 6.0. Enzyme solution (800µl of approximately 2µM) was prepared with the same buffer and the resting-state Soret peak absorption recorded. The enzyme solution was then treated with 88µl of 1M NaOH and 175 µl of pyridine. The mixture was divided equally between two matched quartz cuvettes, and a baseline taken. Then the solution in the sample cuvette was reduced by the addition of a few sodium dithionite crystals and the difference in absorbance values of A_{555} and A_{542} of the difference spectrum was recorded. The extinction coefficient (ε_{Soret}) for each MnP 3 enzyme was then calculated using the published extinction coefficient for the reduced – oxidised haem ($A_{555} - A_{542}$) = 20.7mM $^{-1}$cm^{-1}(Fuhrhop and Smith, 1975) and the known absorbance of the resting state enzyme Soret peak.

2.4.3 Molecular mass determination by SDS-PAGE and MALDI-TOF- MS

The molecular mass of *P. radiata* MnP3 was approximated using SDS-PAGE with a 12% gel with marker proteins (Sigma wide-range) as described in section 2.3.3. It was also accurately determined by matrix-assisted laser desorption/ ionization time–of-flight

mass spectrometry (MALDI-TOF- MS) at the Mass Spectrometry Centre, University of Sussex.

For MALDI-TOF MS analysis of intact MnP3 proteins, 1µl protein sample of 200µM was mixed with an equal volume of a saturated solution of α-cyano-4-hydroxycinnamic acid matrix in 1:1 acetonitrile and water. An aliquot (1µl) of the final solution was applied to the sample target and allowed to dry and crystallise prior to insertion into the high vacuum of the Micromass MALDI LR-TOF machine from Waters. The sample was allowed to load, the laser was fired (the energy of the laser was at 60%) and the detector placed in linear mode. The data were accumulated until a m/z spectrum of reasonable intensity was achieved.

2.4.4 Determination of hydrogen peroxide concentration

Method

A 1 in 100 dilution of bought 30% H_2O_2 stock solution in ddH_2O was first prepared (approximately 100 mM). This stock solution was further diluted 10 times and a UV/Vis spectrum recorded by scanning over the range of 220 to 320 nm. The absorbance was measured at 240 nm and the extinction coefficient (ϵ) at 240 nm of $39.4 M^{-1} cm^{-1}$ (Nelson and Kiesow, 1972) used to calculate the concentration of the diluted sample and hence the 10 x stronger stock. To get a working solution, the stock solution was further diluted to a desired concentration if necessary.

2.4.5 Determination of the pH optima for Mn (II) and ABTS oxidation by *P. radiata* MnP3 enzymes.

The optimum pH values for the oxidation of Manganese (II) and 2, 2'-azino-bis (3-ethylbenz-thiazoline-6-sulfonic acid) (ABTS) by wild-type *P. radiata* MnP3 were

determined by assaying enzyme activity in 100mM tartrate buffers of varying pH. For Mn (II) oxidation, assay mixtures contained 1mM $MnSO_4$, 0.1mM H_2O_2, and 0.023µM enzyme and a pH range from 3.5 to 10.0 was used. For ABTS oxidation, the assay mixtures contained 1.6mM ABTS, 0.1mM H_2O_2, and 0.006 µM enzyme and a pH range of 3.0 to 5.5 was used.

Similarly, the pH optima for all MnP3 mutants were also determined for Mn (II) and ABTS as substrates. For Mn (II) oxidation, the assay mixtures contained enzyme concentration of 0. 4µM E40H/E44H, 0.34µM E44H, 0.3µM E40H, 0.3µM D186H and 0.21µM D186N, 0.1mM hydrogen peroxide, and 25mM $MnSO_4$, pH range 3.5 to 12.0. For ABTS oxidation by MnP3 mutants, the assay mixtures contained 0.0022µM E40H/E44H, 0.0094µM E44H, 0.0015µM E40H, 0.0096µM D186H and 0.0086µM D186N, 1.6mM ABTS and 0.1mM H_2O_2, pH range 2.5 to 5.5. The total volume of all assay mixtures was 1 ml and the assays were performed at 25°C. The reaction was initiated by the addition of hydrogen peroxide and the increase in absorbance at 238 nm or 414 nm, for Mn (II) and ABTS, respectively, was measured using a UV/Vis spectrophotometer (Shimadzu UV- 2401 PC). All the assays were performed in triplicate. To determine a *pKa* for Mn (II) oxidation, the mean rates for the various pHs were calculated; from this, log K (observed) was calculated and plotted against pH

2.4.6 Steady-state kinetic analysis of MnP3 activity with manganese (II)

Mn (II) is assumed to be the *in vivo* substrate for manganese peroxidase. A set of apparent steady-state kinetic constants for Mn (II) to Mn (III) oxidation for each of the *P. radiata* MnP3 enzymes was obtained by measuring the initial rates of assays at 238 nm for varying $MnSO_4$ concentrations: 0.02 - 1.0mM for wild-type, D186H and D186N mutants and 1 – 35mM for E40H, E44H, and E40H/E44H mutants. Enzyme

concentrations of 0.8nM and 0.2µM were used for wild-type and mutants, respectively, while the buffer was 100mM Na tartrate, pH 5.0 and hydrogen peroxide was fixed at 0.1mM. All assays were performed at 25°C. Note that the product being detected is actually a Mn (III)-tartrate complex with $\varepsilon_{238} = 6.5 mM^{-1} cm^{-1}$ (Wariishi *et al*., 1992).

A set of hydrogen peroxide apparent steady state constant for wild-type MnP3 was also determined using hydrogen peroxide in the range of 0.02 – 0.1mM, at fixed MnSO4 of 1.0mM in 100 Na tartrate, pH 5.0. Initial rates for each assay (µmol $mins^{-1}ml^{-1}$ = U), determined in triplicate for each substrate concentration, and then to turnover numbers. Data analysis, plotting and manipulations were carried out using the solver tools of Microsoft Excel and the statistic analysis software, SigmaPlot for Windows V4.01 (SPSS UK Ltd, Woking, UK). From the K_m (Michaelis-Menten constant) and k_{cat} obtained, specificity constants (k_{cat}/K_m) were calculated. In addition, an activity assay was further conducted at pH 8.0 using the above steady-state conditions to see how *P. radiata* MnP3 will behave catalytically at alkaline pH.

2.4.7 Steady-state kinetic analysis of MnP3 activity with ABTS

2, 2'-azino-bis (2-ethylbenzthiozoline-6-sulphonic acid) (ABTS), is a commonly used peroxidase substrate with very high levels of activity shown by plant peroxidases (Moreira *et al*., 2006).

Wild-type MnP3 ABTS assays were carried out in 100mM Na tartrate buffer, pH 3.0, with an ABTS concentration of fixed 0.1mM H_2O_2 and about 0.01µM enzyme.

Similarly, ABTS assays conducted for all mutant MnP3 enzymes with enzyme concentrations: 0.01µM for E40H, E44H, D186N and D186H and 0.02µM for

E40H/E44H while ABTS ranges were: 0.02 – 3.6mM for E40H and D186N, 0.02 – 2.8mM for E44H, 0.02 – 3.2 mM for D186H and 0.01 – 6.5mM for E40H/E44H.

Formation of the radical product as a function of time was measured, at 25°C, by monitoring the increase in absorbance at 414nm. Assays were made in triplicate. Initial rates were determined using ε_{414} = 36.8 $mM^{-1}cm^{-1}$ (Childs and Bardsley, 1975) and were then converted to turnover numbers.

2.4.8 Effect of different organic acid buffers on the kinetic parameters of Mn (II) oxidation by *P. radiata* MnP3.

Activity assays were conducted using each of the organic acid buffers, tartrate, malonate and lactate to determine which buffer gave the highest activity with MnP3. The steady-state kinetics of Mn (II) oxidation were assayed at 238 nm, and at 25°C in 100 mM of appropriate Na buffer (tartrate, malonate or lactate) at pH 5.0. Reaction mixtures contained Mn (II) ($MnSO_4$) ranging from 0.2 – 1.2 mM for wild-type enzyme, and 1 – 45 mM for all the mutant enzymes, with fixed 0.1 mM H_2O_2 and enzyme concentrations approximately 0.2 µM for the mutant enzymes and 8.0 nM for wild-type enzyme. The MnP activity was followed as either the formation of the Mn (III)-tartrate complex (ε_{238} = 6500M^{-1} cm^{-1}) (Wariishi *et al*., 1992), Mn (III)-malonate complex (ε_{238} = 8500$M^{-1}cm^{-1}$) (Kuan *et al*., 1993) and Mn (III)-lactate complex (ε_{238} = 3500$M^{-1}cm^{-1}$) (Kuan *et al*., 1993). All assays were done in triplicate. Data analysis, plotting and manipulations were carried out using the solver tools of Microsoft Excel and the statistic analysis software, SigmaPlot for Windows V4.01 (SPSS UK Ltd, Woking, UK). From the K_m (Michaelis-Menten constant) and k_{cat} values obtained, specificity constants (k_{cat}/K_m) were calculated.

2.4.9 Steady-state kinetics of the inhibition/activation of *P. radiata* MnP3 by different metal ions

The effects of different metal ions on the activity of wild-type and mutant variants of *P. radiata* MnP3 were determined by the addition of the metal ion at a fixed concentration to an assay reaction mixture either Mn (II) activity or ABTS activity (sections 2.4.6, 2.4.7). Assays were carried out in the presence of 0.8mM Zn (II), 0.8mM Co (II) or 0.2mM Cu (II), as well as 0.8mM Na (I) as control. Concentrations were 0.02 – 1.0mM Mn (II) for wild-type enzyme (7.5nM) and 1 – 35mM Mn (II) for the mutant enzymes (0.15µM) or 0.06 – 2.8mM ABTS for all MnP3 enzymes at fixed 0.1mM H_2O_2. The K_m and the apparent k_{cat} parameters were obtained using SigmaPlot (SPSS, Inc.) software. Inhibition constants (K_i) for the different metal ions were calculated from the kinetic parameters using the equations thus:

$K_i = Km\,[I]/K_mI - K_m$ for competitive and $Ki = Vmax^i[I]/Vmax\text{-}Vmax^i$ non-competitive inhibition.

2.4.10 Formation and reduction of MnP3 compounds I and II

A 10µM enzyme solution was prepared in 10mM Na succinate, pH 6.0. To produce MnP3 Compound I, a 1 molar equivalent (10µM) of H_2O_2 was added and the spectrum for Compound I was taken. MnP3 Compound I was then allowed to undergo spontaneous decay to resting enzyme state in the absence of any reductant. The decay process was monitored spectroscopically for the region of 750 – 250 nm and spectra were recorded every 2 minutes. Similarly, MnP3 Compound two was produced directly by adding 2 molar equivalents (20µM) of H_2O_2 to the resting state enzyme and the spectrum recorded immediately.

To attempt to reduce the Compound II enzyme back to the resting state, three methods were used. In the first, 1 molar equivalent concentration (10µM) of $MnSO_4$ was added and a spectrum taken immediately, and then followed by every 2 minutes. Secondly, to see if other divalent metal ions could reduce Compound II to resting state enzyme, 1 molar equivalent (10µM) of $CoSO_4$ was added to the enzyme intermediate and spectra recorded every 2 minutes until most of Compound II was reduced to resting enzyme. Thirdly, a control experiment was conducted with no metal added; the Compound II was allowed to undergo self-reduction with the spectra recorded every 2 minutes.

2.4.11 Binding of Mn (II) and other divalent metal ions to MnP3 from *P. radiata*

Materials

2mM $MnSO_4$

2mM $CoSO_4$

2 mM $CuSO_4$

2mM $ZnSO_4$

10mM K phosphate buffer, pH 6.0

2ml of 0.5mg MnP3 (wild-type)

2ml of 0.5mg of each MnP3 mutant (E44H, E40H/E44H, DI89H and D189N).

0.5mg Myoglobin (purity 95-100%, source: horse heart)

0.5mg recombinant Horseradish peroxidase

0.5mg native plant (HRP)

0.5mg recombinant *Coprinus cinereus* peroxidase

Method

All samples (enzymes and metals) were prepared using syringe filtered buffer, 10mM potassium phosphate, pH 6.0. Three groups of protein samples were used in this

experiment: metal-treated, non-treated and calcium deficient samples (i.e. no calcium in FPLC purification buffer, see section 2.3.8). The metal-treated enzymes samples were prepared by incubating 0.5mg of each protein with 2mM of each metal (Mn, Co, Zn, Cu) at room temperature for 1 hour. The Fe content of the samples was added during protein folding, while Ca was added during protein folding and purification (except for the samples with no Ca in the FPLC buffer). Separation of metalloproteins from adventitiously bound inorganic impurities was performed through gel-filtration using PD-10 Desalting Columns packed with Sephadex^{TM} G-25 medium (GE Healthcare Bio-Sciences Uppsala, Sweden), and dialysis against 4 litres of 10 mM K phosphate, pH 6.0 for 20 hours at 4°C. A first dialysis was for 12 hours, followed by a second dialysis in freshly prepared buffer for 8 hours. To prepare the 0.5mg/ml of each protein sample, spectrum was taken with 10 mM Potassium phosphate, pH 6.0 used as blank using a Shimadzu UV-2401 PC spectrophotometer fitted with a Lauda Ecoline 003 Model circulating thermostated water bath and jacketed cuvette holders. The absorbances obtained and the molar absorption coefficient of each protein was used to estimate the protein concentration. For each protein, 2ml of 0.5mg/ml was prepared for the first dialysis. After first dialysis, 1ml of each protein sample was taken and frozen in liquid nitrogen and stored at – 80°C until ready for use. Non-treated and non-dialysed protein samples that served as control were gel filtered in the same buffer in the day of the experiment. The metal content of each protein sample and their buffers were determined by inductively coupled plasma mass spectrometry (ICP-MS) at the University of Sussex Mass Spectrometry Centre. The values obtained represent average and standard deviation of at least three readings.

The measured amount of Ca, Fe, Mn, Co, Cu and Zn metal ions in the samples was quantified in ppb (parts per billion), which was converted to nanomoles. The number of measured metal molecules was determined using atomic mass numbers (Fe: 55.84, Ca: 40.08, Mn: 54.94, Co: 58.93, zinc: 65.37, Cu: 63.54) g/mol and a ratio between divalent metal molecules and iron molecules was calculated. The potential significance of these findings with respect to binding of divalent metals to MnP3 proteins is discussed.

2.4.11.1 Principles of ICP-MS

A schematic diagram showing the main components of an ICP-MS, i.e. nebulizer, spray chamber, plasma torch, interface, and detector is presented in Figure 2.4.

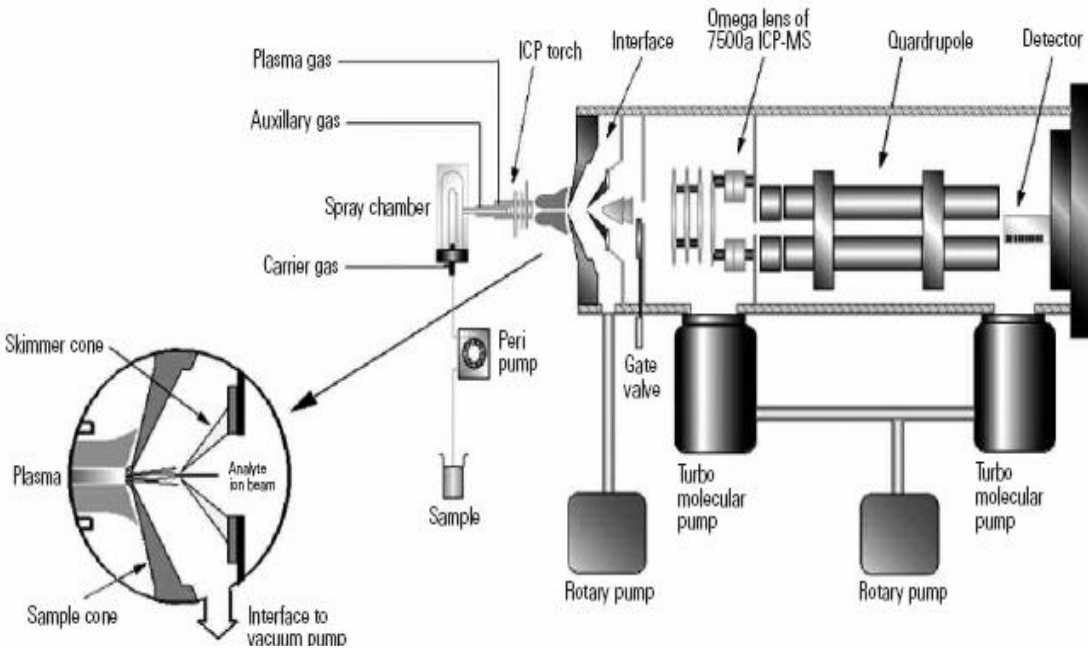

Figure 2.4: Schematic diagram of Agilent 7500 Series ICP-MS instrument (taken from Agilent 7500 Series ICP-MS instrument manual)

ICP-MS is a technique that couples two well established technologies, namely inductively coupled plasma (ICP) and a mass spectrometer (MS). The following description of the principles of operation of an ICP-MS applies to the analysis of

aqueous solutions using pneumatic nebulisation although other methods of sample introduction such as laser ablation or graphite furnace vapourisation can be used.

The operational principles of ICP-MS can be subdivided into three sections, ion production, ion extraction and mass analysis. This is shown diagrammatically in Figure 2.5

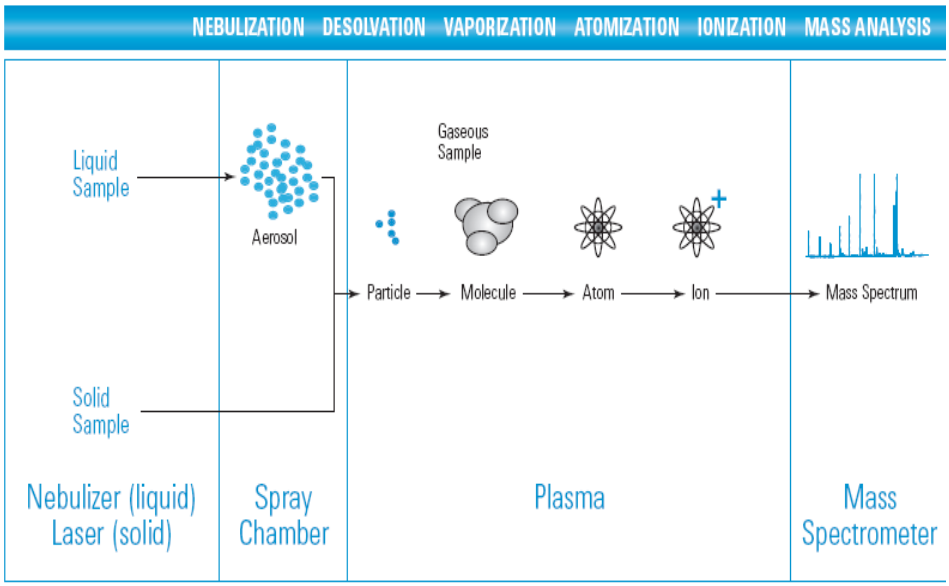

Figure 2.5: Schematic diagram showing the operational principles of an ICP-MS (taken from Agilent instrument manual).

Ion production

The metal-containing sample is introduced in liquid form into a nebulizer at a rate of 1 ml/min. In the spray chamber, the analyte is converted into a fine aerosol with argon gas. The particles are carried through the plasma by argon gas and emerge from the mouth of the plasma torch through a sample injector as a mixture of ions, atoms and residual molecular fragments. With the very high temperature of the plasma approximately 6,000°C to 10,000°C (Nelms, 2005), the analyte is volatilized, desolvated, atomized and ionised and positively charged ions formed from the argon

carrier gas (e.g. Ar^{+}, ArO^{+}, ArH^{+} and $Ar^{2+)}$ can ultimately cause isobaric interferences with some isotopic masses (Houk, 1986).

Ion extraction

The interface region is one of the crucial areas of ICP mass spectrometer, through which the ions are efficiently transported with electrical integrity from the plasma, which operates at atmospheric pressure of $3.7x10^{-6}$ mbar, to the mass spectrometer. The interface region consists of a sampling cone with a central orifice of 1.0 mm, at a distance of 10 mm from the plasma torch. The second cone, the skimmer cone with an orifice of 0.75 is located behind the sampling cone and is positioned to transmit as much of the sample beam as possible. These two cones are usually made of titanium nitride-coated nickel. The pressure behind the sampling cone is maintained at 2.7 mbar by a rotary pump vacuum pump. The mean free path in the region between the two cones is increased by expansion of gas in the zone, leading to stopping reactions between species and maintaining the composition of the extracted gas. With the removal of most of the gas by rotary pump, only a small fraction passes via the skimmer cone.

Mass analysis

On extracting the ions from the interface region, the electrostatic ion analyser collects and directs them into the quadrupole mass analyser. The amount of photons reaching the detector of the quadrupole mass analyser is minimised since they have the potential to increase signal noise. An oscillating electric field is produced within the analyser by applying radio frequency and direct current voltages across alternate diagonal pairs of four rods of quadrupole mass analyser. Altering the relative magnitudes of the radio frequency and direct current voltages applied across the rods of the mass analyser helps in the selection of particular masses for detection (Delves, 1988). The ions are detected

by an electron multiplier and the data are collected in a multichannel analyser. It is the production and detection of large quantities of ions that gives ICP-MS its characteristic ultra trace detection capability. By acquiring the mass of the plasma, data can be obtained for almost the entire periodic table in just minutes with detection limits typically less than picograms per milliter (pg/ml) or micrograms per litre (µg/l) for most elements.

2.4.12 The pH cycle of *P.radiata* wild-type MnP3 and mutants, E40H/E44H, D186H, D186N.

The UV-vis spectra were recorded on a Shimadzu UV-2401 spectrophotometer using 1 cm path-length quartz cuvette. A high enzyme concentration (117µM) was used in this experiment to enable sufficient absorbance at wavelengths greater than 450nm. A mixed buffer containing 10mM MOPS and 10mM Bicine pH 6.7 was used to record a spectrum of an initial low pH enzyme sample (form AH, see section 6.2.1). This sample was then diluted with an equal volume of 50mM MOPS and 50mM Bicine pH 9.05, resulting in a final pH of 8.6. The sample was scanned within 1 min of adjusting the pH and the spectrum of an initial high pH form of the enzyme (form A^-) was recorded. The sample was then incubated for one hour at 25°C and a spectrum of the final high pH form of the enzyme (form I^-) taken. Next, the sample was further diluted with an equal volume of buffer containing 170mM MOPS and 170 mM Bicine, pH 5.95 resulting in a final pH of 6.7. The sample was scanned within 1 min of pH adjustment and the spectrum of the initial product (form X) of this downward pH jump recorded. The sample was then further incubated for 24 hours at 25°C and a spectrum for the recovered form (AH'), similar to the initial low pH form of the enzyme produced. Finally, after 24 hours of incubation at pH 6.7, 0.4mM $CaCl_2$ was added to the protein sample in the cuvette to see if the extent of recovery could be enhanced. Small samples

of each enzyme form were taken and frozen immediately in liquid nitrogen for activity assays later.

A control experiment using wild-type MnP3 was also setup as described above. After raising the pH to 8.6, a spectrum of the initial high pH form of the enzyme (form A^-) was taken, then 5mM $CaCl_2$ was added to enzymes form A^-. Rapid scans were then taken at two minutes interval for one hour. Then the same protocol as before was followed.

2.4.13 Thermal stability of wild-type MnP3 from *P. radiata* and mutant E40H/E44H

To determine the effect of temperature on the stability of *P. radiata* MnP3, the temperature-induced inactivation of MnP3 was monitored as follows: Enzyme solutions, 2.5 µM for wild-type MnP3 and 10 µM for E40H/E44H were incubated in 10 mM Sodium succinate at pH 6.0 in the presence of the calcium chelator, EDTA (0.5mM), in a water bath at either 25°C, 40°C or 50°C. The kinetics of inactivation was measured directly by following the time-dependent fall in peroxidase activity using the Mn (II) → Mn (III) assay. At time intervals, three 20 µl aliquots of heat-treated enzyme mixture were taken and assayed for activity at 25°C, both in the presence and absence of 0.4mM $CaCl_2$. The activity assay contained 100mM Na tartrate buffer, pH5.0 or pH 8.0 1mM $MnSO_4$ and 0.1mM H_2O_2 (section 2.4.6). Wild-type MnP3 was assayed at pH 5.0, except for the 40°C incubation where activity was also measured at pH 8.0. All assays for the mutant E40H/E44H were carried out at pH 8.0 (optimum pH). The activity was expressed as a percentage (%) of remaining activity. The data of these remaining activities plotted against time and fitted to a double exponential decay plot.

Thermal inactivation of MnP3 was then also monitored with the enzyme incubated in the presence or absence of 5mM $CaCl_2$ instead of 0.5mM EDTA.

2.4.14 Determination of melting point for *P. radiata* wild-type and mutant MnP3 enzymes.

Thermal denaturation of MnP3 was also monitored by using circular dichroism (CD) employing a JASCO J-715 spectropolarimeter fitted with a peltier temperature control. Dry nitrogen was purged continuously into the instrument before and during the experiment.

Three sets (non-treated, 5mM $CaCl_2$- treated, and 0.5mM EDTA treated) wild-type MnP3 and a mutant E40H/E44H enzymes were used for this study. The MnP3 solutions of (1.6 µM in 10 mM Sodium acetate, pH 6.0) were placed in a 1mm quartz cuvette and valves recorded at 222 nm as the temperature was raised from 5 to 90°C, at a constant rate of 1°C/min, with 16 of equilibration at each temperature. The temperature value at the midpoint of the denaturation curve (Tm where formally 50% of the protein molecules are native and the 50% are unfolded) was determined assuming that during transition, two distinct and populated states were present, the native (N) and the unfolded state (U). Noise in the data was smoothed using the JASCO J -715 software. The ellipticity values were obtained in millidegrees directly from the instrument and converted to ASCII files using the instrument software from where the values were plotted against temperature using SigmaPlot 8.0 software.

2.4.15 Reactivation of thermally inactivated EDTA-treated wild-type MnP3

Material and Method

An EDTA-treated wild-type enzyme mixture (2.5µM) in 10mM Na succinate, pH 6.0 that had been incubated at 50ºC for 5 hours lost approximately 98% of the initial activity. Its activity was measured in the Mn (II) assay and recorded as zero time. 5mM $CaCl_2$ was added to this enzyme mixture, and the activity of the enzyme assayed again correcting for dilution. The remaining sample was incubated at 4°C and assayed for activity at 30 minutes intervals.

Chapter Three

Cloning and expression of manganese peroxidase 3 (MnP3) of *Phlebia radiata* in *E.coli* and production of MnP3 mutant genes.

3.1 Introduction

The study of structure-function relationships of peroxidases requires an efficient and flexible economical protein production system. Genes encoding these enzymes from different organisms have already been cloned and homologously or heterologously expressed in different hosts. Expression systems that have so far been used to produce peroxidases include *P. chrysosporium*, baculovirus, Aspergillus, *E.coli*, yeast, mammalian cell and insect cell. Choosing the best expression system for the present study requires evaluating the options, from yield to glycosylation, to ease of purification to economics of scale-up.

3.1.1 Homologous expression systems for peroxidases

An homologous expression system has been used for LiP and MnP genes from *P. chysosporium* in which the genes are recombined into the *P. chrysosporium* genome under the control of the constitutive glyceraldehyde-3-phosphate dehydrogenase promoter (Kishi *et al*., 1994; Mayfield *et al*., 1994). As the expression organism used is the same as the origin of the gene, the enzyme was fully processed and secreted, and was as similar to the native enzyme as possible (Mayfield *et al*., 1994; Sollewijn Gelpke *et al.,* 1999; Gold *et al.,* 2000). This system did yield large quantities of active enzyme (Mayfield *et al*., 1994), but required extensive screening of transformants to isolate highly productive clones. A disadvantage of this system is that structure/function studies involving site-directed mutants would be compromised by the continuing presence of the wild-type enzyme.

3.1.2 Heterologous expression systems for peroxidases

A number of alternative hosts have been developed used for expression of peroxidases with various outcomes thus:

Over-expression of peroxidases

E.coli is by far the most widely employed recombinant protein expression host (Casadaban *et al*., 1983; Shatzman and Rosenberg, 1987). Its popularity is due to its ease of handling and transformation and high growth rates and ability to express high levels of protein. Some strains producing up to 30% of their total protein as recombinant material.

The first active peroxidase to be over-expressed heterologously in bacteria was cytochrome *c* peroxidase (C*c*P) (Fishel *et al*., 1987), a cytosolic enzyme from *Saccharomyces cerevisiae*. Up to 10% of the bacterially produced C*c*P polypeptide had its haem group properly inserted and was active. However, denaturation and refolding in the presence of added haem resulted in the recovery of active recombinant C*c*P to almost 100% (Fishel *et al.,* 1987). Since C*c*P expression, *E.coli* has been used to expression many different peroxidases. HRP C (Smith *et al*., 1990), LiPH8 (Doyle and Smith, 1996; Whitwam and Tien, 1996), CiP (Kim *et al*., 2009), VP (Perez-Boada *et al.,* 2002), MnP (Whitwam *et al*., 1995), etc. all produce insoluble inclusion body protein on expression that has to be refolded in the presence of haem to produce fully active enzyme. The recovery of active enzyme can be low (only 1% for LiPH8) but is compensated for by the ease of production and expression of site-directed enzyme mutants.

The baculovirus expression system has also been tried for the over-expression of peroxidase, (LiP H8 (Jonsson and Li, 1991) and LiP H2 (Johnson *et al*., 1992), and MnP (Pease *et al*., 1991). Although active heterologous expression has been achieved, only a low activity of peroxidase was detected in each case. Expression of HRP in mammalian cells also gave low levels of expression (Chriswell, 1988). The HRP mutants discovered in *S.cerevisiae* have been expressed in yeast, *Pichia pastoris* (Cregg *et al*., 1993; Morawski *et al*., 2000; Gu *et al*., 2003; Jiang *et al*., 2008). As many studied peroxidase enzymes are of fungal origin, fungal and other species have been tried as heterologous recombinant host, e.g. Aspergillus (Aifa *et al*., 1999), *S. cerevisiae* (Gazaryan, 1994), *Pichia pastoris* (Daly and Hearn, 2005; Macauley *et al*., 2005) and insect cells (Hartmann and Ortiz de Mantellano, 1992; Ozaki and Ortiz de Montellano, 1995).

In this study, MnP3 from *Phlebia radiata* was expressed in *E.coli* strain W3110. The driving force to using the *E.coli* heterologous expression system was the previous experience and success recorded in our laboratory for the expression of wild-type and mutant HPR C, LiP H8, CiP (Smith *et al*., 1990; Doyle and Smith, 1996). Also, the closet homolog to *P. radiata* MnP3, VP from *Pleurotus eryngii* was successfully expressed in *E.coli* (Perez-Boada *et al.*, 2002). Although refolding of inclusion body material is to be expected, the levels of protein obtained should be sufficient for a detailed characterisation of enzymes obtained.

Yeast, a food organism has been used as alternative host for expression of peroxidase enzymes (Sawai-Hatanaka *et al*., 1995). This is based on the many advantages of the yeast: ease of genetic manipulation, high levels of protein expression, the ability to perform higher eukaryotic protein modifications, easy scale-up of fermentation, and

simple purification of secreted recombinant proteins (Daly and Hearn, 2005; Macauley *et al*., 2005). Added advantages are the availability of complete genomic sequence, the nuclear stable high copy plasmids and ability to secrete the target protein (Hitzeman *et al*., 1990). However, hypermannosylation is a common feature in yeast, hindering proper folding and therefore the activity of the protein.

Another expression system developed is that with *Aspergillus* (Stewart *et al*., 1996). This system has the advantage of yielding high-level expression of active enzymes without the possibility of cross contamination.

Saccharomyces cerevisiae (Sawai-Hatanaka *et al*., 1995), *Aspergillus oryzae* (Petersen *et al*., 1993), and *Aspergillus awamori* (Lokman *et al*., 2003) have been examined as heterologous expression systems for *Coprinus cinereus* peroxidase (CiP) production. Methylotrophic yeast, *Pichia pastoris* has been developed as an expression system of choice for foreign protein production on an industrial scale and has been successfully used to express CiP (Daly and Hearn, 2005; Macauley *et al*., 2005).

Also, significant LiP transcript but weak extracellular activity was found upon expression of a LiPH8 cDNA clone in a Tunisian *Aspergillus niger* strain (Aifa *et al*., 1999). In *E.coli*, LiP H8 was expressed as inactive inclusion bodies although activation was obtained *in vitro* (Doyle and Smith, 1996; Whitwam and Tien, 1996). Also, significant LiP transcript was found upon expression of a LiPH8 cDNA clone in *Aspergillus niger* strain under the control of plant nopaline synthase promoter and terminator but extracellular lignin peroxidase activity in this construct was weak (Aifa *et al*., 1999). A number of filamentous fungal species are capable of secreting large amounts of proteins into the medium and are therefore exploited for the production of homologous and heterologous proteins. Expression of recombinant proteins of fungal

origin is usually very efficient, and production levels of grams per litre are within reach (van den Hondel *et al*., 1991). However, the reports presented so far on the expression of fungal peroxidases in filamentous fungi indicate that their overproduction is difficult to accomplish. The expression of the lignin peroxidase gene of *Phlebia radiata* in *Trichoderma reesei*, although resulting in detectable mRNA levels, failed to produce any extracellular LiP (Saloheimo *et al*., 1989).

All previous attempts to over-express MnP genes in either *P.chrysosporium* or alternative hosts have resulted in low enzyme yields (Andrawis *et al*., 1990; Kersten *et al*., 1995; Stewart *et al*., 1996; Gelpke *et al*., 1999). In addition, recombinant expression systems: heterologous expression systems (*E.coli*, insect cell, yeasts, and ascomycetous fungi) (Pease *et al*., 1989; Conesa *et al*., 2002; Punt *et al*., 2002) for MnP have been established (Stewart *et al.*, 1996; Whitwam *et al.*, 1996), allowing structure-function studies of mutant MnPs (Kishi *et al*., 1996; Kishi *et al*., 1997; Whitwam *et al*., 1997). Also, most resulted in no active enzyme or very low yields. Exceptions include expression systems with *Aspergillus* spp. which exhibited 1–5 mg/l production of active enzyme (Aifa *et al*., 1999; Ruiz-Duenas *et al*., 1999c; Lu-Chau *et al*., 2004), while the best result was obtained in an *Aspergillus niger* expression system where up to 100 mg/l of *P. chrysosporium* MnP was produced (Conesa *et al.*, 2000).

The other system utilized *Aspergillus* (*Emericella*) spp. as the host organism, but the production yield of active protein was low: 1 mg/l under conventional culture conditions for *A. niger* (Ruiz-Duenas *et al*., 1999c) or 2 mg/l even under the optimized conditions for *A. nidulans* using a bioreactor (Lu-Chau *et al*., 2004).

3.1.3 Mutagenesis

The crystal structure of *P.chrysosporium* MnP has been reported (Sundaramoorthy *et al*., 1994). The structure revealed the putative Mn (II) with binding site. The ligands to the ion being Glu 35, Glu39, Asp 179, a haem propionate, (Kishi *et al*., 1996; Kusters-van Someren *et al*., 1995; Sundaramoorthy *et al*., 1997), and two water molecules (Sundaramoothy *et al*., 1994). The 3 residues of recombinant *P. radiata* MnP3, Glu40, Glu44, Asp 186 involved in the mutagenesis (current work) are those that, by sequence alignment with *P. chrysosporium* MnP, have been determined to be the putative amino acid ligands of the Mn (II) binding site of this enzyme (Note that the equivalent database numbering for fungal *P. radiata* MnP3 would be Glu37, Glu41 and Asp183), as the recombinant protein has 3 residues added to the N-terminus for expression purposes. Site-directed mutants E35Q, E39Q and E35Q/D179N of *P. chrysosporium* MnP have been made and characterised.

Steady-state kinetic analyses of the mutants, E35Q and E39Q yielded K_m values for Mn (II) in Mn(II) oxidation approximately 50-fold greater than the corresponding K_m value for the wild-type enzyme. Similarly, the k_{cat} values for Mn (II) in Mn (II) oxidation by these mutants was approximately 300-fold lower than that for the wild-type MnP. With the E35Q-D179N double mutant, the K_m value for Mn (II) oxidation was approximately 120-fold greater and the k_{cat} value approximately 100-fold less, that for the wild-type MnP enzyme. In contrast, the K_m values for H_2O_2 and the rates of Compound I formation were similar for the mutant and wild-type MnPs.

The aim of current study was to introduce different amino acids into the Mn (II) binding site, i.e. E40H, E44H, E40H/E44H, D186H and D186N of the *P. radiata* MnP3 enzyme. Recently, X-ray crystal studies of MnP (Smith, A. T. / Klaus - personal

communication) have raised doubts as to exact nature of the metal, Mn^{2+} or Zn^{2+} in the metal-binding site. Therefore it is important to probe the precise geometry of the Mn ligands within the binding site of MnP3 and also the flexibility of the Mn (II)-binding site, with regard to the incorporation of other metal ion.

3.2 Cloning wild-type (MnP3) gene into pFLAG1

3.2.1 Primer design

This research work started with the design of primers for the recloning of wild-type *P. radiata* MnP3 into an *E.coli* expression vector, pFLAG1 (see Figure.3.1). Two primers, one 5' and one 3' to the MnP3 gene reading frame were made to engineer the N-terminus of the MnP3 protein and to incorporate a restriction site at each end of the gene for in-frame cloning. These primers therefore allowed the amplification of a full length gene fragment, encoding the mature MnP3 protein sequence without the signal sequence, and also adding to the 5' end codons for an additional 3 amino acid residues, for M, L and T respectively. It had previously been shown that for *E.coli in vitro* expression of *Coprinus cinereus* peroxidase, these N-terminal residues gave much increased protein expression (W. Doyle, unpublished work). The two restriction enzyme sites incorporated were *Nde*I at the 5' end of the gene and *Bam*HI at the 3' end of the gene. It was checked that both enzymes did not cut internally to the MnP3 gene. These sites allowed cloning, the correct way around, into the *Nde*I and *Bam*HI sites of pFLAG1. Finally, in designing the 5' primer, codon usage and GC content were optimised to ensure maxiumum expression. The properties of the primers are listed in Table 3.1 below.

a) N – Terminal primer for MnP3

5' GTT GCC TGC CCC GAT GGT GTC AAC ACT GCT 3' - Mature DNA sequence
V A C P D G V N T A - Mature protein sequence
. ** . * **. *** *** **. *** *** **

*Eco*RI *Nde*I
5' GAATTC CAT ATG TTA ACT GTG GCT TGC CCA GAT GGT GTG AAC ACT GC 3' – Engineered DNA sequence – UU1 primer-47 mer

M L T V A C P D G V N T - Wanted protein sequence

25 matches in 29 for the homologous region of the sequence but total oligo is 47mer

b) C – Terminal primer for MnP3

5'- TCT GTT GCG CCT GTC CCC CCG TCG- 3' - mature DNA sequence

*Bam*HI *Eco*RI

5' - TCT GTT GCG CCT GTC CCC CCG TCG TAA **GGATCC GAA TTC-**3' – engineered DNA sequence

S V A P V P P S STOP

*Eco*RI *Bam*HI

5'- **GAATTC GGATCC** TTA CGA CGG GGG GAC AGG CGC AAC AGA- 3'- reverse complement – UU2 primer-39 mer

Figure 3.1: **Oligonucleotide primer design for cloning MnP3 gene of *P. radiata* into pFLAG1.**

The added bases forming restriction enzyme sites are shown in blue and the three codons for the introduced methionine, leucine and threonine (MLT) residues are indicated in red.

Table 3.1: Properties of the designed primers for engineering the N- and C-terminii of *P. radiata* MnP 3 for *E.coli* expression

Primer Designation	Length	GC Content (%)	Tm (ºC)
UU1 - N-Terminal	47	46.8	74.7
UU2- C-Terminal	39	59	> 75

Tm is the thermal midpoint of denaturation of each primer. It is calculated according to the following equation:

$$Tm = 4(G + C) + 2(A + T)$$

where G, C, A, and T represent the number of times each base is present in the primer sequence. Determination of Tm is necessary to find the annealing temperature for PCR amplification.

3.2.2 Amplification of the modified wild-type MnP3 gene by PCR

The complete MnP3 gene of *Phlebia radiata* strain 79 (ATCC 64658) was obtained from our collaborators Kritiina Hilden and colleagues, University of Helsinki, Finland. The GeneBank accession number for MnP3 cDNA/pCR 2.1.TOPO is AJ566200.

Analysis of the MnP3 gene revealed a shorter C-terminal and that it is structurally more related to lignin peroxidase (*Phanerochaete chrysosporium* LiPH8/H2). It has also been found that in MnP3 gene, alanine replaces the exposed tryptophan present in LiP and versatile peroxidases. This gene is described in detail in Hilden *et al*., 2005. Our designed primers were used to amplify and modify the gene. The PCR method used is

described in section 2.1.2 and utilised high-fidelity *Pfu* DNA polymerase to minimise errors. The expected DNA fragment was confirmed by 1% agarose gel electrophoresis as just over 1 kb (see Figure 3.2)

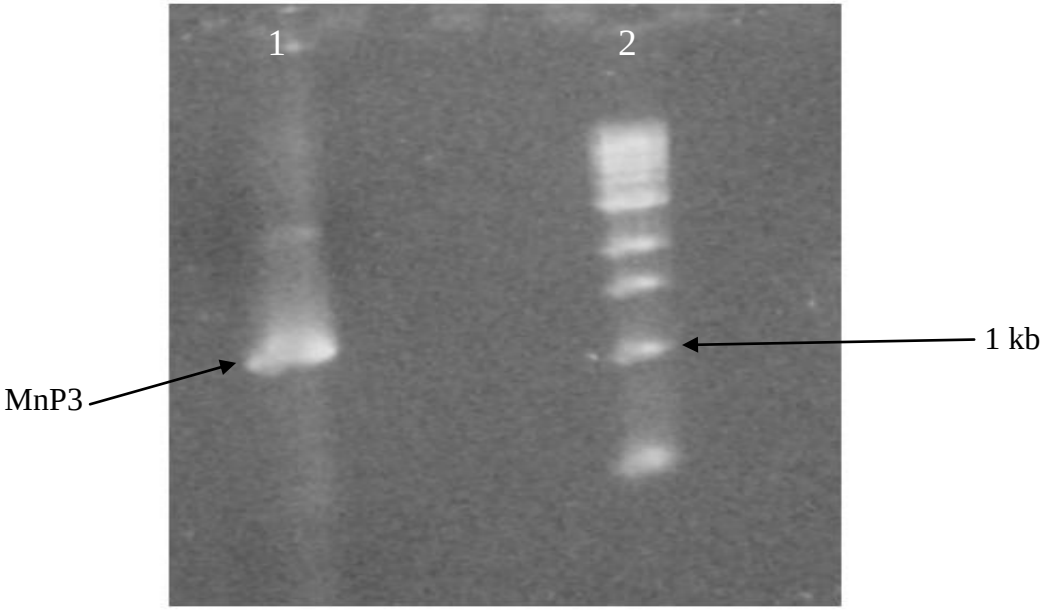

Figure 3.2: 1% agarose gel of PCR product showing engineered MnP3 gene (lane 1) and molecular weight marker (lane 2).

3.2.3 TOPO TA cloning of engineered MnP3 gene.

Initial attempts were made to subclone the engineered MnP3 gene directly into the *E.coli* expression vector pFLAG1; however this was not successful. Hence, it was decided to first of all subclone into the pCR2.1 vector using TOPO TA cloning and then reclone into pFLAG1.

The TOPO TA cloning method as described in the manufacturer's manual and section 2.1.4 was employed. Since *Pfu* polymerase was used to amplify the engineered MnP3 gene, addition of single deoxyadenosine overhangs was necessary for cloning into the

pCR2.1 vector. A short incubation with *Taq* polymerase was used to do this. The products of the TOPO TA cloning were then transformed into chemically competent TOP 10 cells and positive transformants were selected by "blue/white" colony selection, *i.e.* white colonies should contain the MnP3 gene insert.

Selected white colonies were therefore inoculated into 5ml L-broth and grown overnight. Plasmid DNA was isolated by miniprep and then digested with *Eco*RI enzyme (section 2.1.7). For a positive colony digestion with this enzyme should result in two fragments, the MnP3 gene of approximately 1 kb and the pCR2.1 vector of 3.9kb. A positive colony was confirmed by 1% agarose gel electrophoresis (see Figure 3.3), and more DNA was midipreped (section 2.1.8).

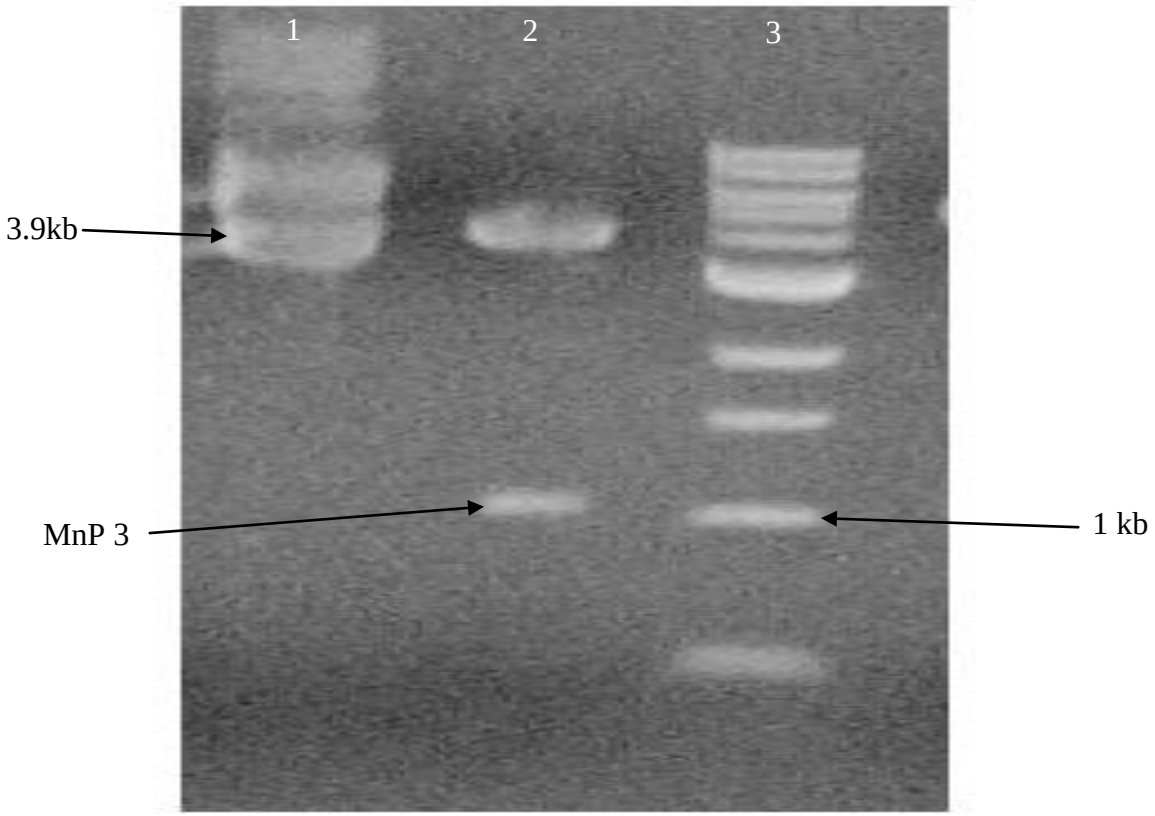

Figure 3.3: 1% agarose gel showing the engineered MnP3 gene fragment released from pCR 2.1 after digestion with *Eco*R1 i.e. a positive clone. Lane 1 is undigested clone DNA, lane 2 is digested clone DNA and lane 3 is molecular weight marker.

DNA sequencing (section 2.1.10) of both strands of the pCR2.1-MnP3 clone confirmed that the PCR process had generated the correct engineered gene with no extra errors. The sequencing results were analysed using the Seqman module of the DNASTAR program.

3.2.4 Cloning the engineered MnP3 gene from pCR2.1-MnP3 into the *E.coli* expression vector pFLAG1.

The commercially available, ampicillin-resistant, *E.coli* expression vector pFLAG1 contains the isopropyl thiogalactoside (IPTG) inducible *tac* promoter for protein expression, with an *Nde*I restriction site situated adjacent for cloning purposes. The *tac*

promoter is an extremely strong synthetic promoter, formed from different regions of the *trp* and *lac* promoters. The pFLAG1 vector also contains a *Bgl*II restriction site 3' to the *Nde*I site, which when digested is compatible with a *Bam*HI cut overhang. Therefore pFLAG1 was digested with *Nde*I and *Bgl*II (Figure. 3.4) and the pCR2 .1-MnP3 was digested with *Nde*I and *Bam*HI to release the MnP3 gene (Figure 3.5 and section 2.1.12).

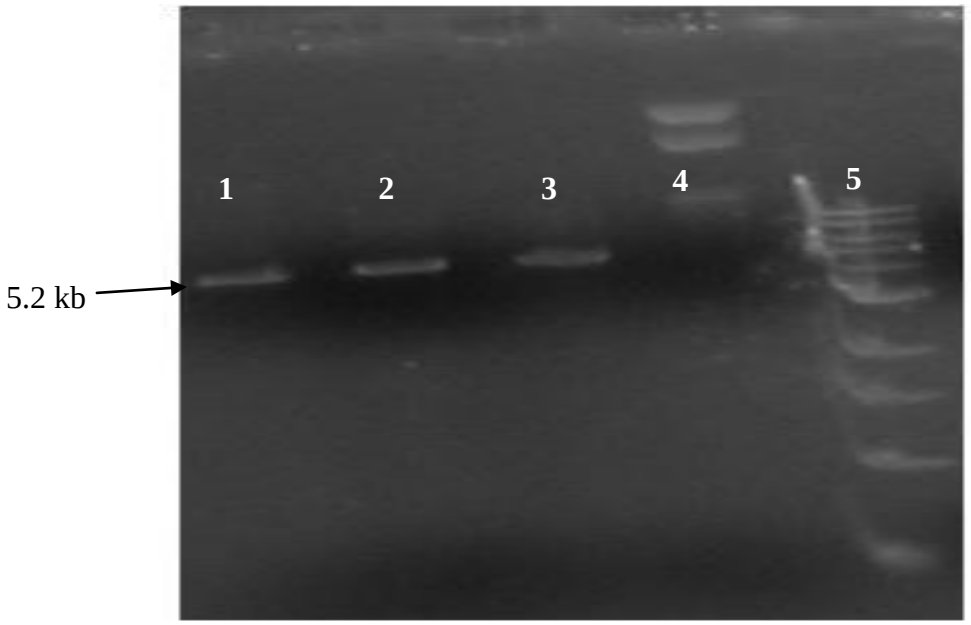

Figure 3.4: 1% agarose gel of digestion of pFLAG1 with *Nde*I and *Bgl* II. Lane 1 is the double digest with both enzymes; lanes 2 and 3 are single digests with *Nde*I only or *Bgl* II only, while lane 4 is undigested plasmid and lane 5 is molecular weight marker.

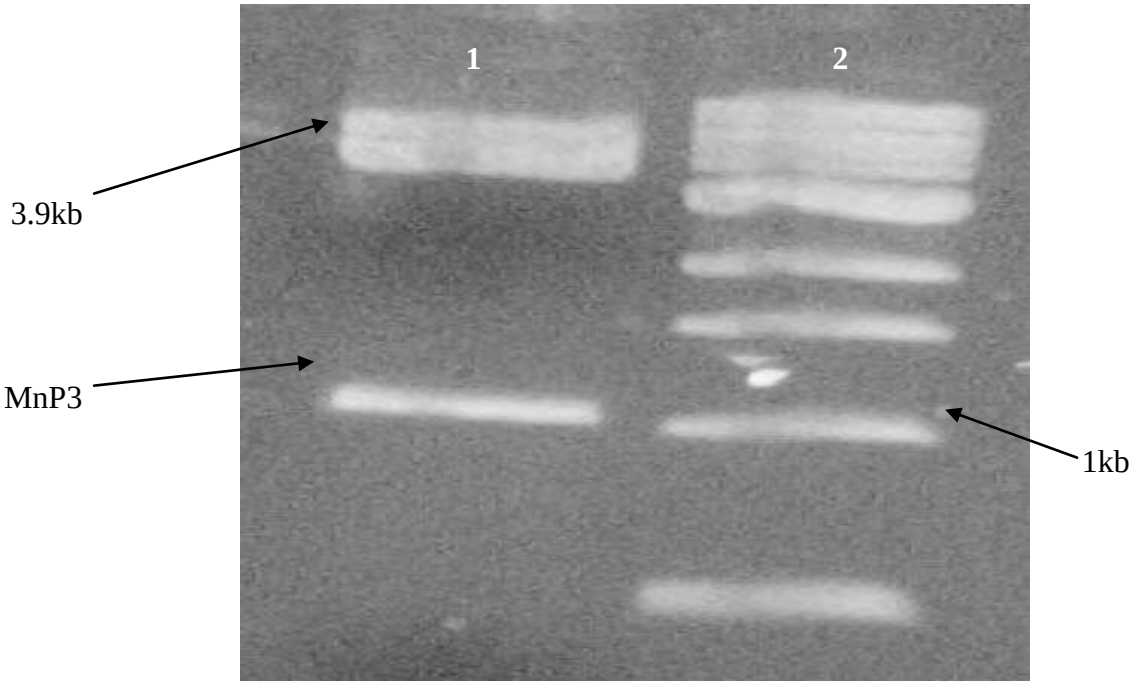

Figure 3.5: 1% agarose gel of *Nde*I and *Bam*HI digested pCR2.1-MnP3.

Lane 1 is the MnP3 gene. Lane 2 is molecular marker**.**

After digesting a large quantity of pCR2.1-MnP3 with *Nde*I and *Bam*HI the entire digest was loaded onto a 1% agarose gel so that the MnP3 fragment could be excised and purified by the geneclean method (section 2.1.11). Ligation of the genecleaned engineered MnP3 gene into digested pFLAG1 was then carried out with a molar ratio of 5:1 (section 2.1.13). Two ligation controls were also set up, one with no DNA and the other with no DNA and no ligase. All were then transformed into library efficiency, chemically competent DH5α *E.coli* cells (section 2.1.5).

3.2.5 Screening for pFLAG1-MnP3 constructs

After 5ml overnight cultures were miniprepped, 12 colony DNAs were screened for the presence of the MnP3 gene insert by restriction digestion using *Nde*I and *Xho*I enzymes (section 2.1.14). Colonies were compared on a 1% agarose gel electrophoresis (Figure 3.6). The enzyme *Xho*I was used to digest after the 3' end of the gene as the ligation had involved the ligating together of *Bgl*II and *Bam*HI overhangs. This means that the ligated DNA is not now digestible by either enzyme; *Xho*I however is present in pFLAG1 just after *Bgl*II. However, *Xho*I is also present in the MnP3 gene at 753 bp position. This means that a positive colony will give a main insert DNA fragment of approximately 750 bp, rather than 1kb. The other 300 bp fragment is too small to be seen on the gel in Figure. 3.6.

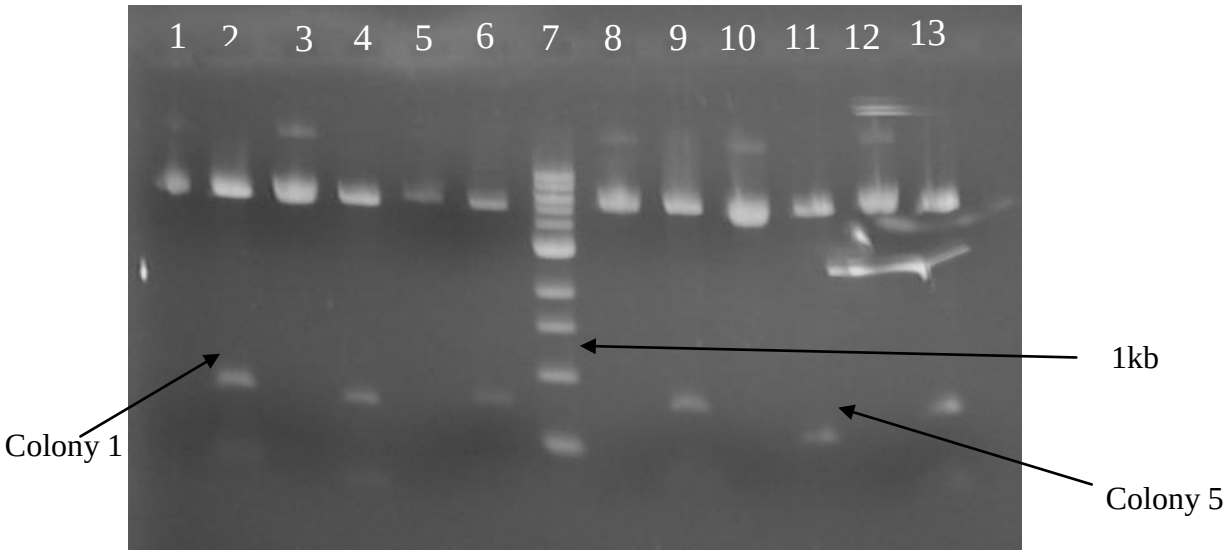

Figure 3.6: 1% agarose gel showing *Nde*I/*Xho*I analysis of potential pFLAG1-MnP3 colones. Positive clones show an insert size of approximately 750 bp i.e. colonies 1, 2, 3, 4 and 6. Lanes 1, 3, 5, 8, 10 and 12 are undigested samples; lanes 2, 4, 6, 9, 11 and 13 are digested samples. Lane 7 is molecular weight marker.

Of the 6 transformants characterised, 5 contained an approximate 750kb insert size, while the insert of colony 5 was of a smaller size, about 600 bp, as can be seen in Figure 3.6. Although 750 bp was the size expected both colonies 1 and 5 were midiprepped to obtain more DNA and sent for sequencing (section 2.1.10). The sequences from these two colonies were aligned and compared with the expected sequence. The MnP3 insert from colony 1 was found to be the engineered MnP3 gene that had been correctly inserted into pFLAG1. However, the smaller insert size of colony 5 arose from the loss of 438 bases at the 3' end of the gene. This could have occurred due to nuclease activity during cloning or more likely a low level of *Bam*HI star activity in the pCR2.1-MnP3 digest that yielded this fragment for cloning. The resulting correct construct pFLAG1-MnP3 was transformed into *E.coli* W3110 chemically competent cells.

3.2.6 Expression of wild-type *P.radiata* MnP3 protein in *E.coli*

Expression of MnP3 protein from the engineered gene was demonstrated in *E.coli* W3110 cells, where it was found to be inducible by the addition of IPTG to the medium. 5ml samples of W3110 cells containing pFLAG1-MnP3 were grown in L-broth until absorbance at 500nm was approximately 0.8 before adding IPTG. After 31/2 hours the cells were harvested by centrifugation, lysed and the insoluble protein partially purified (section 2.3.2). A negative control, *i.e.* no induction, was also grown along with a positive control of W3110 cells containing pFLAG1-HRP which was induced. Like other recombinant peroxidases previously expressed in *E.coli* e.g. HRP (Smith *et al*., 1990; Doyle and Smith, 1996), *P. radiata* MnP3 was found to be sequestered into insoluble inclusion bodies; no MnP3 protein could be detected in the soluble protein fraction (data not shown). An SDS-PAGE gel of resolubilised inclusion body protein is shown below (Figure. 3.7)

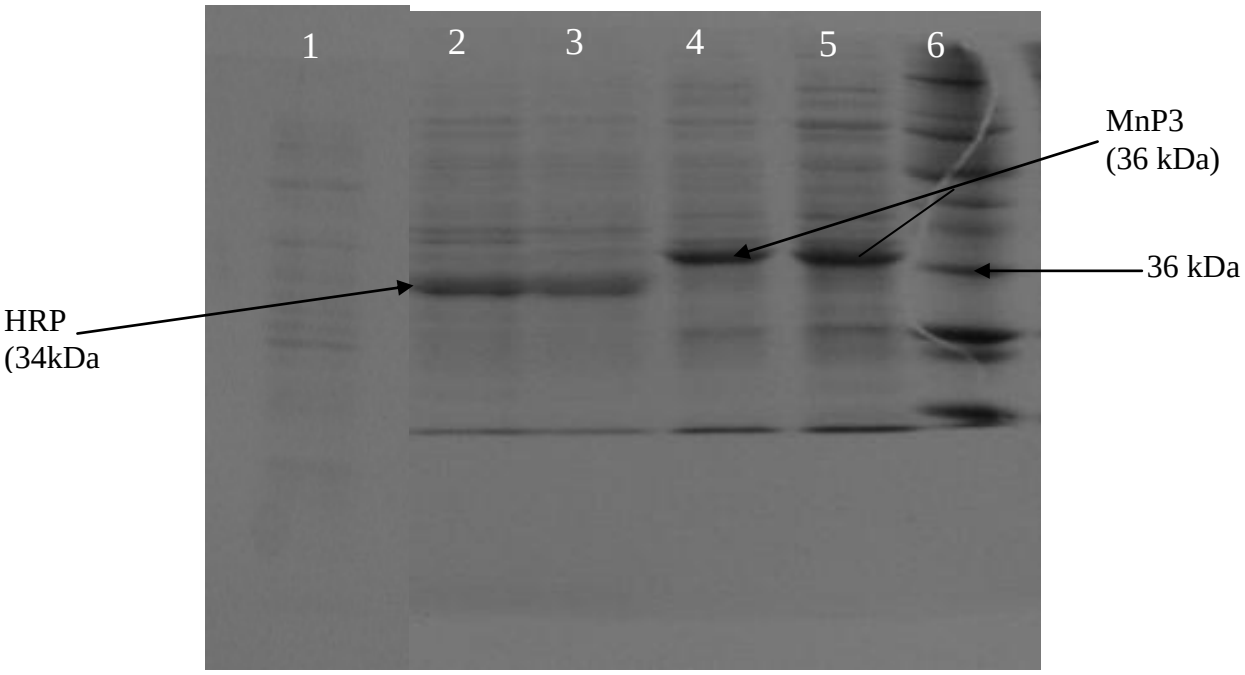

Figure 3.7: SDS-PAGE analysis of insoluble inclusion bodies after small-scale expression of MnP3. Inclusion body protein pellets were solubilised in 6M urea and loaded on a 12% resolving SDS-PAGE protein gel. Lane 1 is the negative control-MnP3 no induction. Lanes 2 and 3 are positive controls- HRP and lanes 4 and 5 are induced MnP3 samples. Lane 6 is the molecular weight marker (full-range Rainbow (Biorad laboratories)). Gel was stained with Comassie Blue. SDS-PAGE was conducted as described in section 2.3.3.

As predicted from the engineered gene sequence, the SDS-PAGE gel showed a clearly visible band of expressed MnP3 with a molecular mass of about 36 kDa.

3.2.7 Refolding and purification of active wild-type MnP3 enzyme

The success in expressing MnP3 at the small-scale level led to the large-scale expression, as described in section 2.3.4. The inclusion bodies obtained which were

approximately 80% MnP3 protein (Figure 3.7) were partially purified by use of 1% Triton, a detergent. To obtain active MnP3 enzyme, the inclusion body protein was then solubilised using a large amount of denaturant, in this case 6M urea, and then refolded.

Initial attempts to refold *P.radiata* MnP 3 in *vitro*, involved protocols previously used for the refolding of other plant and fungal peroxidases. These 3 different methods were: Smith *et al*., 1990 for HRP (50 mM Tris, pH 8.0, 1 mM EDTA, 2 M urea, 5 mM $CaCl_2$, 5µM bovine hemin, 0.7 mM oxidized glutathione, 100µM DTT and 200µg/ml enzyme), Doyle *et al*., 1996 for LiP H8 from *P. chrysosporium* (50 mM Tris, pH 9.5, 0.1mM EDTA, 2.1 M urea, 5 mM $CaCl_2$, 10µM bovine haemin, 0.7 mM GSSG and 200µg/ml enzyme); and Perez - Boada *et al*., 2002 for VP from *Pleurotus eryngii* (50mM Tris-HCl, 9.5, 5mM $CaCl_2$, 0.5mM GSSG, 0.1 mM, DTT, 0.15M urea, 20µM haemin and 0.1mg/ml protein at pH 9.5 were employed).

Of the methods tried, only the versatile peroxidase refolding conditions gave a significant level of activity with ABTS from refolding mixture. This was therefore used throughout for refolding of both the wild-type and the mutant MnP3 enzymes.

Following refolding of the protein, using the versatile peroxidase conditions, the resultant solution was concentrated and dialysed as described in section 2.3.7 before a final purification step, using ion exchange on a FPLC system. A gradient of 0 -1M NaCl over 30 ml was run through a Mono Q cation exchange column, and a large protein peak was eluted at approximately 300 mM NaCl. This peak was coloured and in assays showed high levels of ABTS activity. Therefore the active fractions were pooled, gel-filtered into 10mM Na succinate, pH 6.0 containing 0.2mM $CaCl_2$ and frozen in liquid N_2. Figure 3.8 shows a typical elution profile obtained for *P.radiata* recombinant MnP3 enzymes.

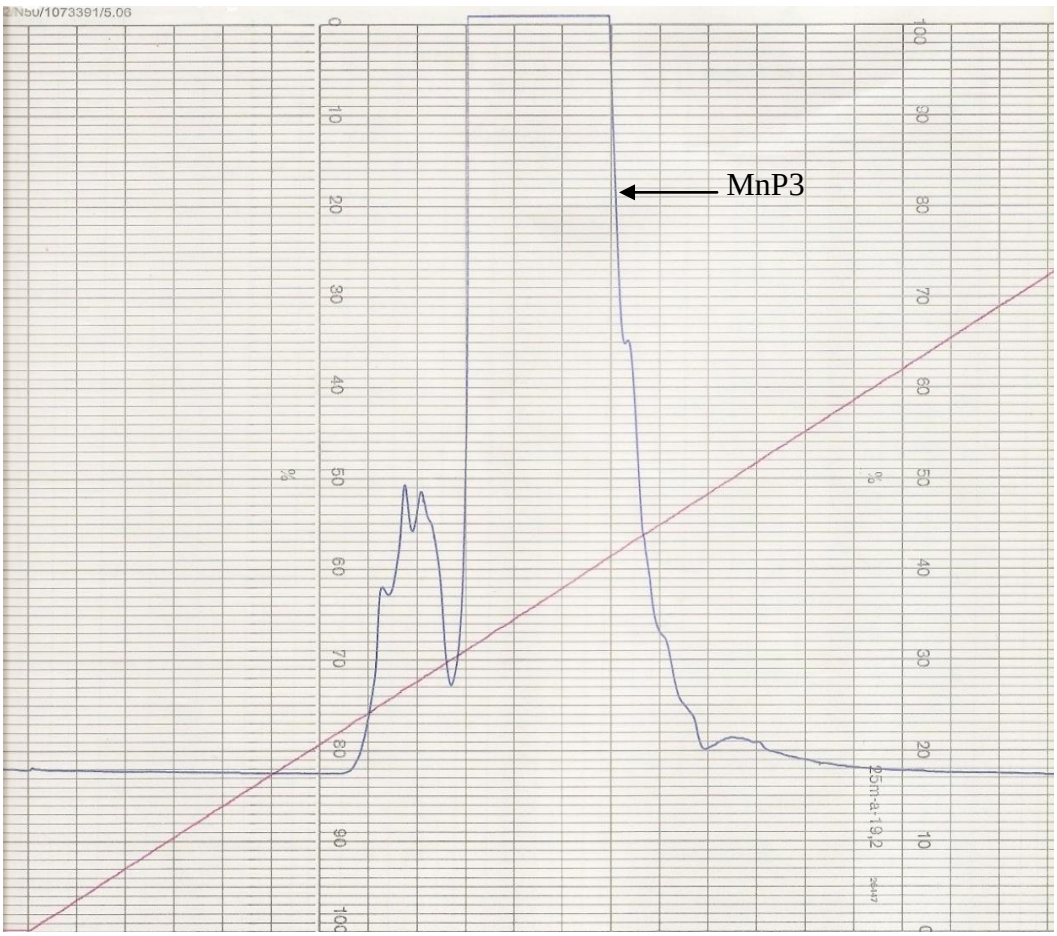

Figure 3.8: Typical cation exchange chromatogram for *P. radiata* wild-type MnP3. Active MnP3 enzyme was purified using the FPLC with a Mono-Q anion exchange column in 10mM Na succinate buffer, pH 6.0, 1mM $CaCl_2$ with a linear NaCl gradient of 0 -1M as indicated by (—). The MnP3 enzyme eluted, as indicated by A_{280} (—) peak, at approximately 300mM NaCl.

Approximately 7 mg of active MnP3 was purified from a 5 litre *E.coli* expression, after refolding and purification. Therefore, the recovery of enzyme is at a rate of 1.4 mg / litre culture, and refolding efficiency was 6 -7%. This is similar to both HRP and CiP levels after refolding (Smith *et al.*, 1990; W. Doyle, personal communication).

A typical wild-type MnP3 spectrum is shown below:

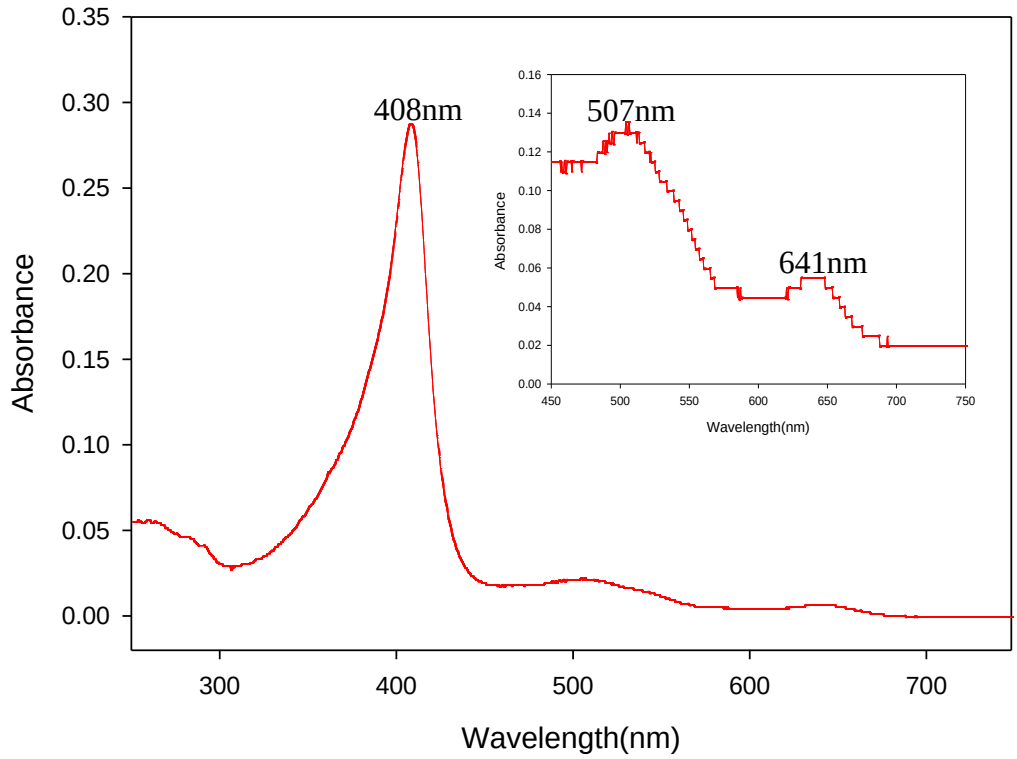

Figure 3.9: Resting state UV/Visible absorption spectrum for purified *P. radiata* wild-type MnP3. The spectrum was recorded in 10 mM Na succinate, pH 6.0 at 25ºC. The Soret is at 408nm, while the insert is the magnified region of 450 – 750nm showing the charge transfer bands at 641 and 507nm. Refer to section 4.2 for more detail.

The spectral characteristics of the engineered MnP3, Soret (408nm), CTI (641nm) and CTII (507nm) are very similar to those of fungal (*P. radiata*) MnP3 enzyme (Karhunen *et al*., 1990) and MnP, Soret (406nm), CTI (632nm) and CTII (502nm) from *Phanerochaete chrysosporium* (Glenn and Gold, 1985; Glenn, *et al.*, 1986), suggesting that the enzyme is correctly folded, with the haem in the correct environment.

3.3 Mass characterization

Figure 3.10 shows MALDI data for wild-type MnP3. The additional peaks are due to the internal standards (and impurities in them), which are necessary for accurate

MALDI-TOF mass determinations of above 20kDa (Teske *et al*., 2000). The MnP3 peak is at 36.065 kDa, compared to a calculated molecular mass of 35.703 kDa.

Table 3.2 Actual and predicted mass of wild-type and mutant MnP3 enzymes. The predicted masses were determined by calculation using the translated protein sequence and dnaStar Software. The Actual masses were determined by MALDI-TOF-MS.

Enzymes	**Actual mass (Da)**	**Predicted mass (Da)**
Wild-type	36065	35704
E40H	36224	35709
E44H	36033	35709
E40H/E44H	36086	35714
D186H	36057	35726
D186N	36051	35703

These data indicate that the enzyme is monomeric, similar to those described for other fungal MnPs (Matsubara *et al*., 1996; Schneega β *et al*., 1997; Palma *et al*., 2000; Wang *et al*., 2002).

As shown in Figure 3.10 and Table 3.2, the predicted and the actual masses were not consistent. The error observed between the predicted mass and the actual mass is due to Mass spectrometer calibration error as the machine is only calibrated for small masses.

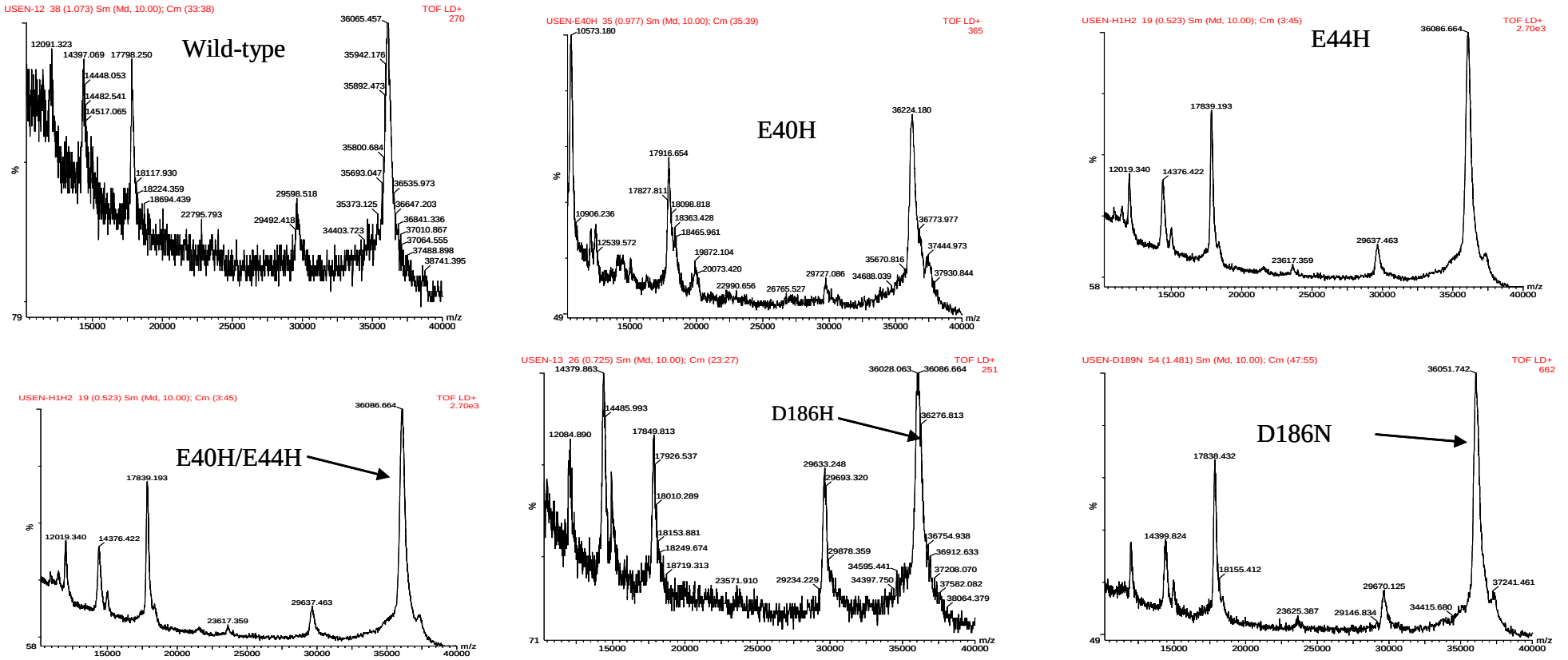

Figure 3.10: MALDI-TOF mass spectrum of the engineered wild-type MnP3 from *P. radiata.* See Table 3.2 for the predicted and actual mass of the wild-type and mutant MnP3 enzymes.

3.4 Generation of MnP3 mutant genes

The technique employed to generate mutant MnP3 genes was a previously established site-directed mutagenesis protocol, which utilises the Polymerase Chain Reaction (PCR) (Doyle *et al*., 1998) (see Section 2.2.1). This method has the advantage of not requiring the presence of a nearby unique restriction enzyme site for recloning purposes.

The template for the PCR was pFLAG1-MnP3, which contains the engineered wild-type MnP3 from *P. radiata*. For each mutagenesis, two back-to-back primers (mutagenic and reference) were designed which would anneal to opposite strands of the template DNA, with their 5' termini adjacent in sequence. Mutagenic primers were designed to introduce the site-specific mutation(s) required, while either or both primers also contained silent mutation(s), resulting in a new restriction enzyme site to be present in the mutated DNA. Part of the new restriction site was present in each primer so digestion also selected for the integrity of the ligation site. Proof reading *Pfu* DNA polymerase was used to extend the primers to produce linear copies of the whole plasmid containing the mutated bases.

The presence of PCR product corresponding in size to the template DNA (6.3kb) was shown using agarose gel electrophoresis. The PCR product mix then underwent *Dpn*I digestion to remove the methylated template, phenol/chloroform extraction, and ethanol precipitation, followed by phosphorylation with T4 polynucleotide kinase and ligation with T4 ligase, before the mixture was transformed into chemically competent *E.coli* DH5α cells.

The mutant MnP3 genes generated were E40H, E44H, E40H/E44H, D186H, and D186N. As earlier stated (section 3.1), the numbering is for our modified wild-type MnP3 protein that has 3 additional residues at the N-terminus, M, L, and T, to ensure

good protein expression (section 3.2.1). The equivalent database numbering for *Phlebia radiata* wild-type MnP3 would then be E37, E41 and D183. The 3 residues involved in the mutagenesis are those that by sequence alignment with *P.chrysosporium* MnP have been determined to be the ligands of the Mn (II) binding site of the MnP3 enzyme.

A summary diagram for the E40H, E44H and E40H/E44H mutation method is shown in Figure 2.2, whilst a summary for D186N and D186H mutations is shown in Figure 2.3. Whilst, for clarity, the method of the D186N and D186H mutations is discussed here, the author is grateful to Miss Caroline Santivale for the actual production of the mutant genes (Santivale, C. 3rd year project), and her results will not be shown here.

3.4.1 PCR mutagenesis

The whole plasmid amplification method PCR conditions (section 2.2.1) were used initially for all mutations. A 6.3kb PCR product was obtained for E40H and E40H/E44H (see Figure 3.11), however, the band for E44H was faint, and hence the PCR was repeated with the addition of either 5% DMSO or 5% glycerol; to see if the yield could be increased. The DMSO slightly improved the yield (see Figure 3.12), whilst glycerol had no effect at all.

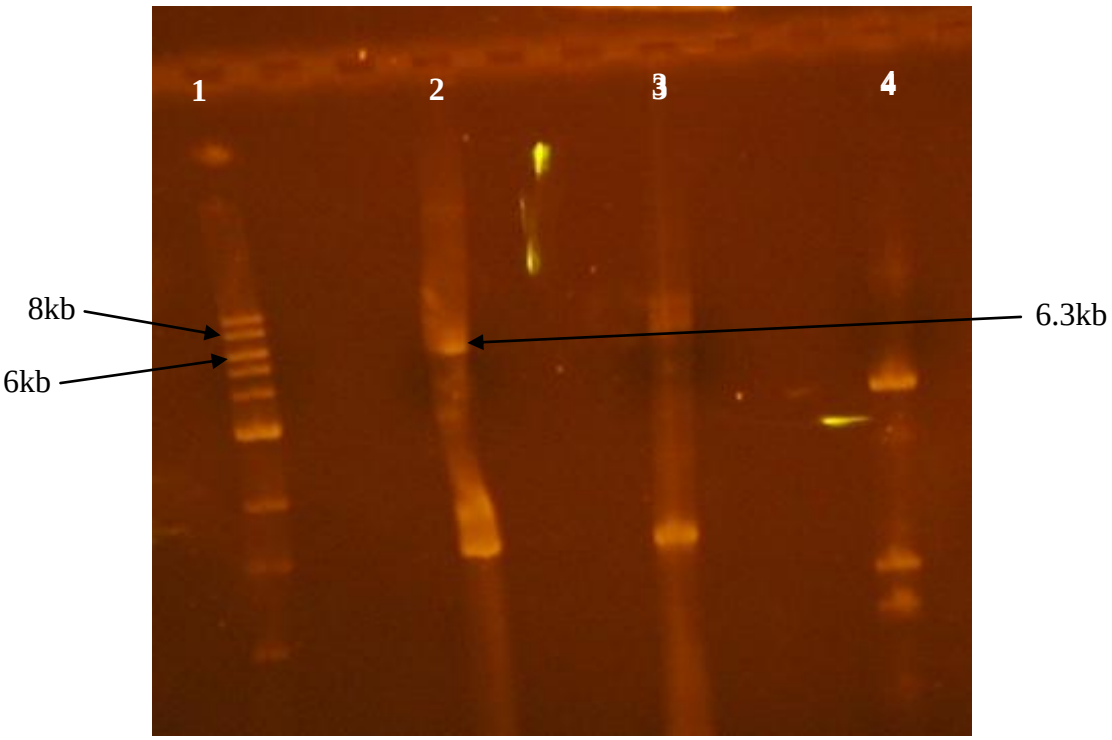

Figure 3.11: 1% agarose gel electrophoresis of mutant MnP3 gene PCR products. Lane 1 molecular weight marker, lane 2 (E40H/E44H), lane 3 E40H, lane 4 E44H. The band for at 6.3kDa for lane 4 E44H is present but faint.

Note that for all mutants one or more additional PCR products were also present. As these other DNA fragments were small (1.5 kb or less) it was hoped that they would either not be competent for transformation or would be easily screened for.

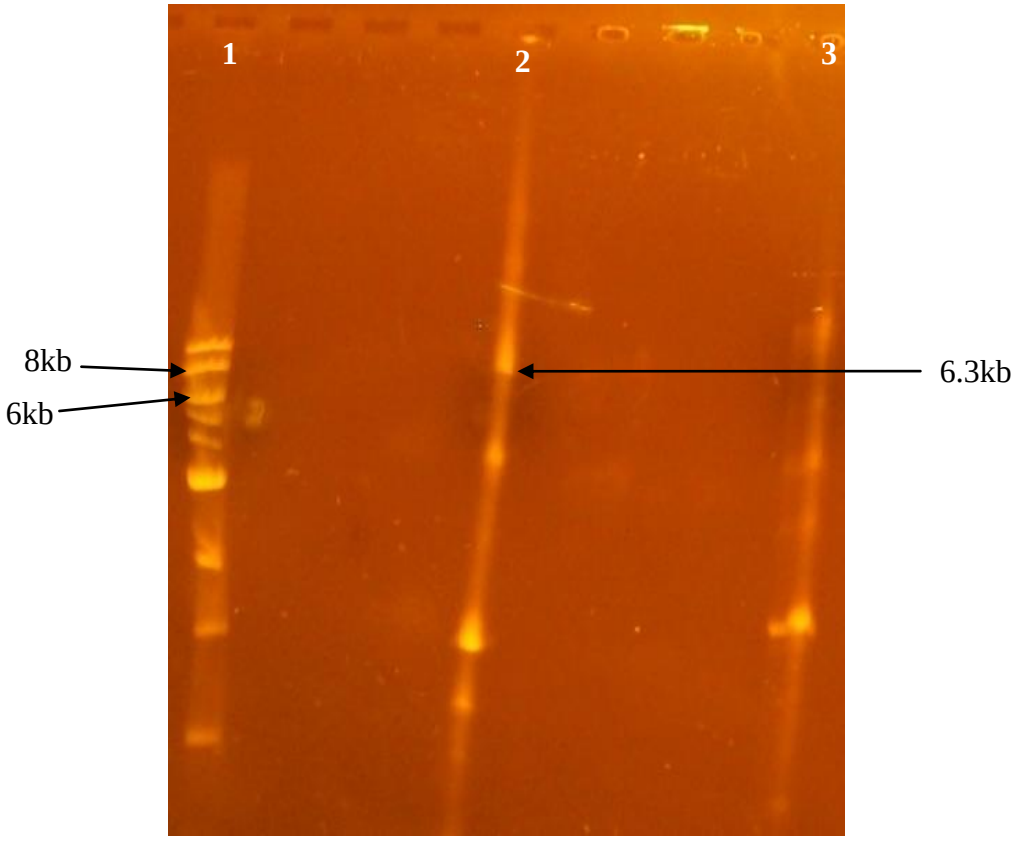

Figure 3.12: 1% agarose gel electrophoresis of mutant MnP gene PCR product for E44H with DMSO. Lane 1 molecular weight marker, lane 2 E44H with 5% DMSO and lane 3 E44H with 5% glycerol. The band at 6.3kDa for sample with 5% glycerol is present but faint.

3.4.2 Screening for positive mutant clones by diagnostic restriction enzyme digest.

After the PCR, DNA was purified, recircularised and transformed. Miniprep DNA from 12 colonies for each mutant was screened by restriction enzyme *Apa*L I digest for the presence of the restriction site present in the gene between the E40 and E44 codons. Correctly religated plasmid should give a DNA fragment pattern similar to the wild-type MnP3 plasmid. A 1% agarose gel for the E40H mutation is shown below with a wild-type MnP3 plasmid digestion present as a control. It can be seen that only colonies

2 and 6 give the complicated pattern of digestion, which is the same as for the wild-type. Therefore, the percentage recovery of correct mutant for these ones is approximately 20%.

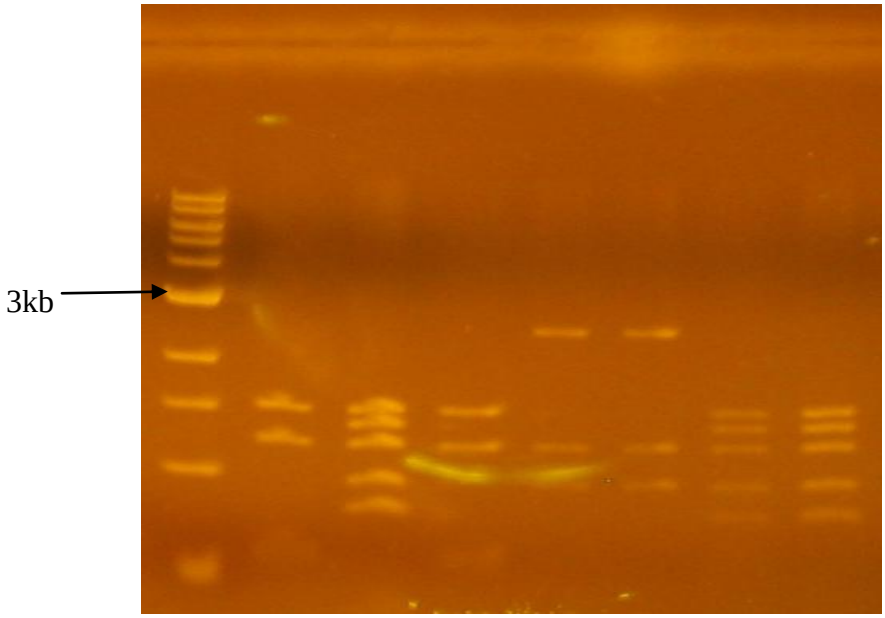

Figure 3.13: 1% agarose gel electrophoresis of *Apa*LI diagnostic digest for pFLAG1-E40H MnP3. Lane 1 molecular weight marker, lanes 2, 4, 5, 6 incorrect clones1,3,4,5, lanes 3 and 7 positive clones 2 and 6, showing DNA bands of 960, 1245, 1402 and 1656 bp, compare to wild-type in lane 8.

For the other two mutants the percentage recovery of correct mutant genes was similar to that of E40H (approximately 20% each)

3.4.3 DNA sequencing

DNA from one positive colony for each mutant MnP3 gene was sequenced (MWG Biotech) and the results analysed using the Seqman module of the DNASTAR program. All three mutant genes were found to have the intended mutations at the designated positions, and no other mutations mistakenly produced during the PCR procedure.

3.4.4 Protein expression of the new MnP3 mutant variants, E40H, E44H and E40H/E44H, D186H and D186H.

Each of the mutant MnP3 gene plasmids were transformed into W3110 *E.coli* cells for protein expression. Analysis by SDS-PAGE of extracts from cultures induced with IPTG, showed that all mutant genes expressed a protein of the correct size, approximately 36kDa; present in inclusion pellets (Figure 3.14). Similar levels of expression were seen for all mutants: note the wild-type protein was from a purified sample.

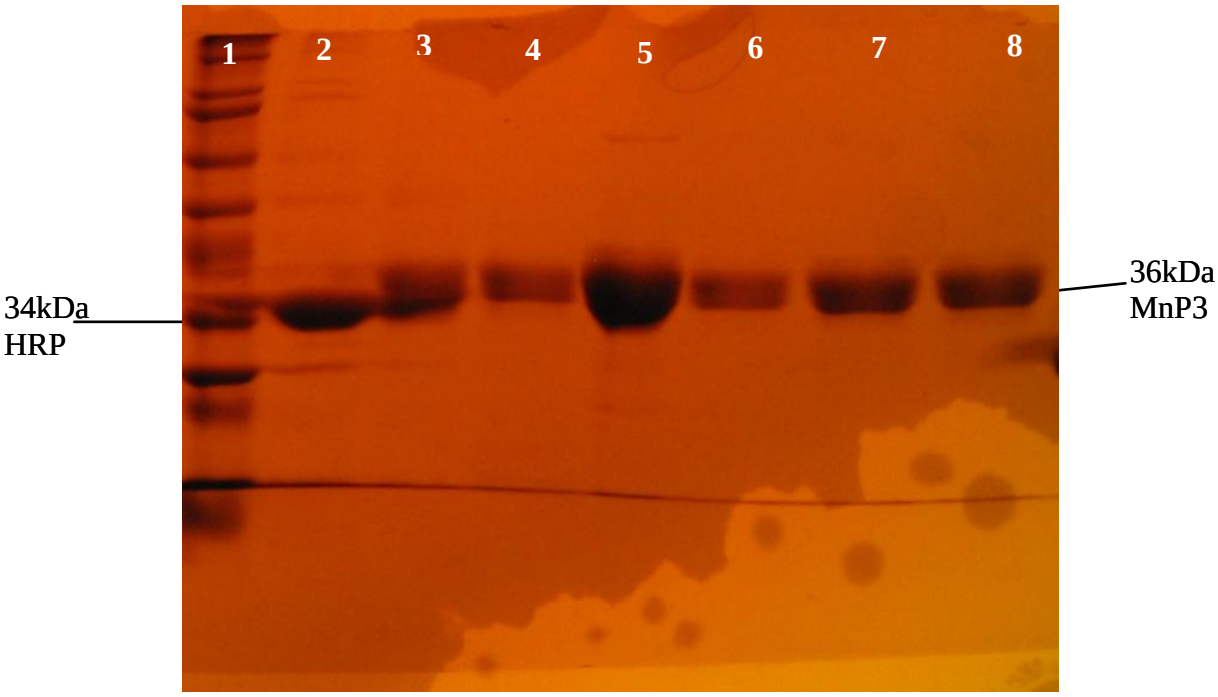

Figure 3.14: SDS-PAGE of *P. radiata* purified wild-type MnP3 protein and mutant variants isolated from inclusion bodies. Protein extracts were loaded on a 12% resolving SDS-PAGE protein gel. Lane 1 Molecular weight marker, lane 2 HRP, lane 3 D186H, lane 4 D186N, lane 5 wild-type, lane 6 E40H/E44H, lane 7 E40H and lane 8 E44H. Bands visualised using Comassie Blue staining. Note that the wild-type MnP3 and HRP proteins were from purified samples.

Large-scale expression of each of the mutant MnP3 proteins was then performed. Inclusion bodies were purified and the mutant proteins folded using the same conditions as those previously found to be successful for the wild-type enzymes (section 3.2.6). Active mutant enzyme was then purified using Mono Q anion exchange chromatography during which all behaved similarly to the wild-type protein. A total of 5-7mg active enzyme was obtained for each mutant from a 5 litre *E.coli* expression. This is equivalent to amounts recovered for wild-type MnP3 and suggests a similar recovery rate during the refolding process.

3.5 Conclusion

The wild-type MnP3 of *P.radiata* has been successfully cloned in to pFLAG1 and mutant genes E40H, E44H and E40H/E44H, D186N and D186H generated using the PCR based, whole plasmid amplification method of site-directed mutagenesis. The presence of the intended nucleotide changes and absence of any unwanted changes in the mutant genes was confirmed first by restriction enzyme screening and then by DNA sequencing. Both the wild-type and mutant proteins have been expressed in *E.coli.* The resulting inclusion body proteins have been refolded into active enzyme and purified. Mass characterisations by SDS-PAGE and MALDI-TOF have shown that both the wild-type and mutant MnP3 enzymes were approximately 36 kDa in weight.

Chapter Four

General characterisation of *P. radiata* wild-type MnP3 and mutants

4.1 Introduction and background

There has been considerable interest in the nature of the iron porphyrin prosthetic groups of peroxidases, their intermediates, and relevance to protein function. Comparative UV-vis spectral analysis of peroxidases can provide instructive insights into the electronic characteristics of these enzymes and constitutes an initial starting point for further work (Dunford, 1999). The coordination and spin state of the haem group can be characterised by the presence, intensity and position of key absorption peaks, which are in turn influenced by the surrounding distal haem environment (Dunford, 1999). The participation of haem proteins (e.g. peroxidases) in oxygen transport, peroxide reduction and disproportionation, the mitochondrial electron transport chain, and drug metabolism (cytochrome P450) stresses the biological importance and diversity of functional roles of the iron porphyrins (Dolphin, 1978).

Peroxidases, like other haem proteins, have intense visible absorption bands that arise predominantly from transitions of electrons of the porphyrin ring but also have contributions from the iron and its ligands (Gouterman, 1961). In many respects MnP resembles other fungal and plant peroxidases (Dunford, and Stillman, 1976; Hewson and Hager, 1979). Previous studies using electronic absorption (Glenn and Gold, 1985), EPR and resonance Raman spectroscopies (Mino *et al*., 1998) indicate that the iron in the native MnP protein is in the high-spin, ferric state, with histidine coordinated as a fifth ligand. Peroxidase absorption bands in the visible and near ultraviolet region are of two types, they are due either to $\pi \rightarrow \pi^*$ or charge-transfer transitions. The former involve the π electrons of the porphyrin, while the latter involve the transition of d

electrons in the ferric iron (Smith and Williams, 1970; Dunford, 1999). There is enhancement of the charge – transfer absorption bands when the symmetry of the haem is broken, such that electron density at the metal and porphyrin changes (Makinen and Churg, 1983). Packing forces from the polypeptide chain can distort the haem from planarity (Jentzen *et al*., 1998). Local electric fields and ring substituents also reduce the symmetry of the haem (Manas *et al*., 1999; Manas *et al*., 2000; Kaposi *et al*., 2001; Prabhu *et al*., 2002). This reduction of symmetry can change the interactions of the d_π orbitals of the metal with the π orbitals of the pyrrole rings. The metal d_π electrons can also be raised in energy by interaction with the axial ligands. Due to the sensitivity of the charge-transfer (CT) transitions to various influences from the protein, the CT absorption bands can be used to study subtle properties of the haem site (Srajer and Champion, 1991; Leone *et al*., 1992; Stavrov, 2001).

An intense absorption band exists in the near ultraviolet region (400-425 nm), which is referred to as the Soret peak. High-spin complexes have a Soret maximum in the range of 400 – 410 nm, while low-spin complexes have a Soret maximum between 415 nm and 425 nm. In the high spin system, a CT I band is in the range of 620 - 640 nm, whereas the CT II band is located at approximately 500 nm (Brill and Williams, 1961). As the population of the low spin form increases, the CT I and the CT II often decrease in intensity and are replaced by absorption bands at ~560 nm and ~530 nm, referred to as low spin α and β bands, respectively.

The optimal conditions for catalysis by different peroxidases are not identical (Abelskov *et al*., 1995). pH is a determining factor in enzymatic activity as it alters the ionization states within the enzyme and the substrate (Voet and Voet, 2003). The active site of enzymes is frequently composed of ionisable groups (prototropic groups) that must be

in the proper ionic form in order to maintain the conformation of the active site, enzyme-substrate binding, or reaction catalysis. The behaviour of the enzyme activity at different pH values can therefore provide information concerning the identities of the ionisable groups at the active site (Whitaker, 1994).

Scheme 4.1

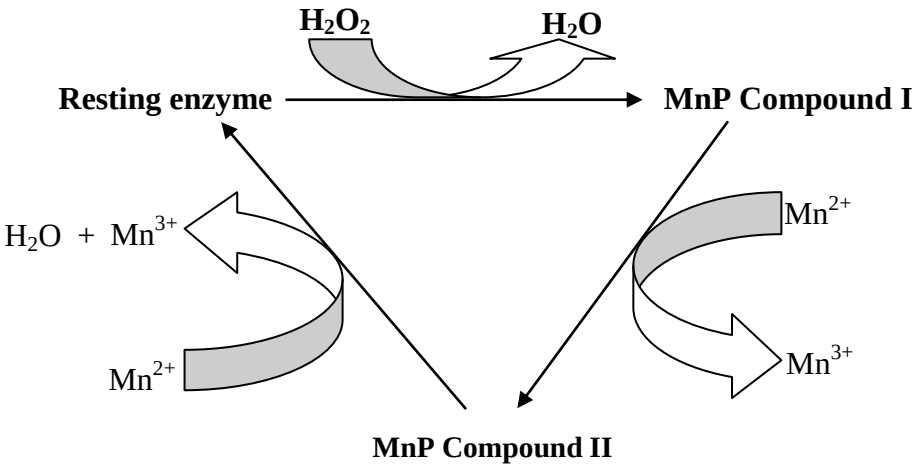

$$MnP + H_2O_2 \longrightarrow MnP\ I + H_2O$$

$$MnP\ I + Mn^{2+} \longrightarrow MnP\ II + Mn^{3+}$$

$$MnP\ II + Mn^{2+} \longrightarrow MnP + Mn^{3+} + H_2O$$

$$Mn^{3+} + AH \longrightarrow Mn^{2+} + A^{\bullet}H$$

AH – Phenolic compounds including lignin

Catalytic cycle of manganese peroxidase (MnP) and associated partial reactions (Modified from Wariishi *et al*., 1989; Ikehata *et al*., 2005; Perez-Boada *et al*., 2005).

4.1.1 The role of Mn in MnP activity

MnP has a similar catalytic cycle to other plant and fungal peroxidases (Dunford & Stillman, 1976; Wariishi *et al*., 1988, 1989a; Gold and Alic, 1993). However, unlike other peroxidases, MnP functions in a rather indirect way. It is unique in its ability to efficiently oxidize Mn(II) to Mn(III) (see Scheme 4.1) by electron transfer to the hypervalent haem of the oxidized enzyme (Glenn *et al*., 1986; Wariishi *et al*., 1992).

The Mn (III) is believed to dissociate from the enzyme and form a diffusible oxidant complex with dicarboxylic acid chelators such as pyrophosphate (Glenn and Gold, 1985), tartrate (Pasczynski *et al*., 1986), oxalate (Glenn and Gold, 1985; Kuan *et al*., 1993) or lactate (Glenn *et al*., 1986). The catalytic activity of MnP is strictly dependent on chelating organic acids and it has been proposed that these acids complex Mn (III) thus stabilising its redox potential (Pasczynski *et al*., 1986; Aitken and Irvine, 1990; Mielgo, 2003) and stimulating the enzyme activity (Wariishi *et al*., 1989). Previous studies have shown that the chelators affect not only the reaction of divalent Mn (II) with Mn peroxidase (Glenn *et al*., 1986) but also the reaction of Mn (III) with its organic substrates (Forrester *et al*., 1988).

The Mn (III) complexes formed enzymatically have been shown to further oxidize several aromatic substrates of MnP (Pasczynski *et al*., 1986; Glenn *et al*., 1986), while electrochemical studies have demonstrated that several organic acid complexes of Mn (III) are able to oxidize lignin model compounds (Cui and Dolphin, 1990). This makes it possible to deliver the oxidising potential of the haem active site to distant sterically bulky substrates, which are unable to access the active site of the MnP (Wariishi *et al*., 1988). This scheme is similar to the way in which veratryl alcohol (VA, 3, 4-dimethoxybenzyl alcohol), as the cation radical ($VA^{\bullet+}$), is known to act as a mediator, or diffusible oxidant, for the oxidation of lignin by LiP (Harvey *et al*., 1986) and is attractive as it explains how oxidizing power from the enzyme could be made available to large insoluble substrates such as lignin.

The rate of catalysis is also dependent on the nature of the dicarboxylic acid Mn (III) chelator (Kuwahara *et al*., 1984; Glenn *et al*., 1986; Forrester *et al*., 1988). Due to the importance of these chelators to Mn peroxidase action (Wariishi *et al*., 1991),

experiments to observe the effect of different organic acid chelators on the activity of MnP3 from *Phlebia radiata* were conducted using Na - tartrate, lactate and malonate as chelators at pH 5.0.

A distinctive characteristic of MnP is that the best reducing substrate for Compounds I and II is Mn (II), a metal ion naturally present in wood. However, Compound II of MnP exhibits an absolute requirement for Mn (II) as an exclusive reductant essential for the completion of the catalytic cycle of the enzyme (Glenn *et al*., 1986; Wariishi *et al*., 1989; Wariishi *et al*., 1998). Indeed, not only is Mn essential for the activity of MnP (Wariishi, 1991), but it also regulates the production of MnP (Bonnarme and Jeffries, 1990; Brown *et al*., 1990), laccase, and LiP in *P. chrysosporium* and in other white rot fungi (Perez and Jeffries, 1990).

Enzymatic oxidation of Mn (II) to Mn (III) has also been reported to occur in prokaryotic catalase-peroxidase (Magliozzo and Marcinkeviciene, 1997), while enzyme-mediated oxidation of Mn (II) can be achieved indirectly via the superoxide anion radical (Munoz *et al*., 1997). Manganese can also be involved in several reactions catalyzed by LiP. Popp *et al*., (1990) reported the oxidation of Mn (II) to Mn (III) by LiP in the presence of veratryl alcohol and oxalic acid, both of which are natural metabolites of *P. chrysosporium*. The oxidation of veratryl alcohol by LiP is enhanced by Mn (II), but only in the presence of an organic acid, as a potential chelator of Mn (III) (Bono *et al*., 1990). Although other donors can reduce Compound I of LiP to Compound II, only Mn (II) is capable of very rapidly reducing MnP compound II to its original state, thereby allowing the enzyme to initiate new substrate oxidations (Wariishi *et al*., 1988; Wariishi *et al*., 1989).

ABTS (Scheme 4.2) is a well-known substrate for peroxidases (Childs and Bardsley, 1975) and has been shown to be rapidly oxidised by MnPs (Paice *et al*., 1993; Martinez *et al.,* 1996; Hofrichter *et al*., 1999). The chemical properties of ABTS and its oxidation by peroxidases, particularly HRPC, have been intensively studied (Aliaga and Lissi, 1998; Campos and Lissi, 1997; Childs and Bardsley, 1975; Scott *et al*., 1993). ABTS undergoes a single electron oxidation in the presence of peroxidase and hydrogen peroxide to produce a long-lived cation radical. This radical product has an intense blue/green colour and thus its accumulation can be measured spectroscopically (Childs and Bardsley, 1975). Note that MnP does not require a functional Mn (II) oxidation site for ABTS to be a good substrate as its oxidation is more 'non-specific in nature.

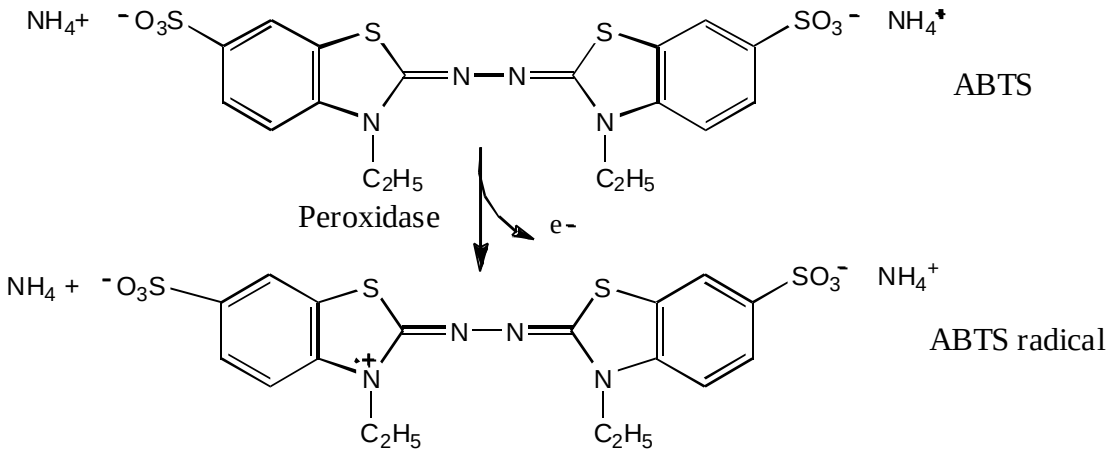

Scheme 4.2: Structure of 2, 2'—azino -di- (3-ethylbenzoline-6-sulfonic acid) (ABTS) (Childs and Bardsley, 1975)

4.1.2 Effects of other metals on MnP activity

Manganese (II) oxidation by MnP has been found to be inhibited by cobalt Co (II), copper Cu (II), iron Fe(II), and Fe (III) (Glenn and Gold, 1985; Pasczynski *et al*., 1986; Aitken and Irvine, 1990). Cu (II) effectively inhibited MnP by catalyzing the decomposition of the Mn (III) - tartrate complex in the presence of hydrogen peroxide (Aitken and Irvine, 1990). It is possible that other metal ions act to inhibit MnP activity

in the same way. Co (II), which is slowly oxidized to Co (III) by MnP (Glenn *et al*., 1986) at low concentration, has been found to inactivate the enzyme in a time-dependent manner (Harris *et al*., 1991; Youngs *et al*., 2000).

Molecular modelling and kinetic studies have indicated that Mn (II) -binding and oxidation are sensitive to subtle changes in protein ligand geometry (Kusters-van Someren *et al*., 1995; Kishi *et al*., 1996; Sollewijn *et al*., 1999; Young *et al*., 2001). Competition using, metals other than Mn, has been used as a method for studying Mn (II) the binding site. Indeed, the flexibility of the Mn-binding site in MnP allows a wide variety of metal ions to bind (Sundaramoorthy *et al*., 2005). However, only Cd (II) seems to exhibit a dissociation constant similar to that of Mn (II) (Youngs *et al*., 2000), indicating that these metals bind at the same site and in reversible competition. Other divalent cations, such as Co (II) (Harris *et al*., 1991), Fe (II), and Zn (II) showed relatively poor binding (Youngs *et al*., 2000). Trivalent cations such as the lanthanides Sm (III) and Eu (III), have been found to competitively inhibit Mn (II) oxidation (Youngs *et al*., 2000), and NMR studies have shown binding of Ce (III) and Gd (III) to the MnP active site (Banci *et al*., 1998). The stable lanthanides, therefore, have been proposed to mimic the binding of Mn (III) (Banci *et al*., 1998). While it is attractive to use these metals in functional studies of MnP, the lanthanides have a much larger mass-to-charge ratio, larger ionic radii, tend to accept more ligands, and adopt a much wider variety of ligation geometries than Mn (III) (Cotton and Wikinson, 1988). Therefore, it is necessary to use transition metals with ligation geometries close to Mn.

In this chapter, results showing the general properties of wild-type *P. radiata* MnP3 enzyme will be discussed and compared with those of the MnP3 mutant enzymes. Comparison will also be made with the classical MnPs from other organisms described

in the literature. Particular emphasis will be on spectral characteristics, optimal pH conditions for activity during Mn (II) and ABTS oxidation, steady-state kinetic parameters for Mn (II) and ABTS oxidation, effects of organic acid buffers on kinetic parameters for Mn (II) oxidation, sensitivity of the Mn-binding site to other metal ions with respect to Mn (II) oxidation and the formation and stability of MnP3 catalytic intermediates.

4.2 Resting-state UV-visible spectrum for MnP3

Experiments to determine the resting-state UV-visible spectra for *P. radiata* wild –type and mutant MnP3 enzymes were conducted as described in section 2.4.1 of this thesis. The resting state UV-visible spectrum for wild-type MnP3 is shown in section 3.2.7. The key spectral characteristics of *P. radiata* wild-type MnP3 and associated mutants are listed in Table 4.1, while Figure 4.1 shows an overlay of the resting state UV/Vis absorption spectra for these enzymes.

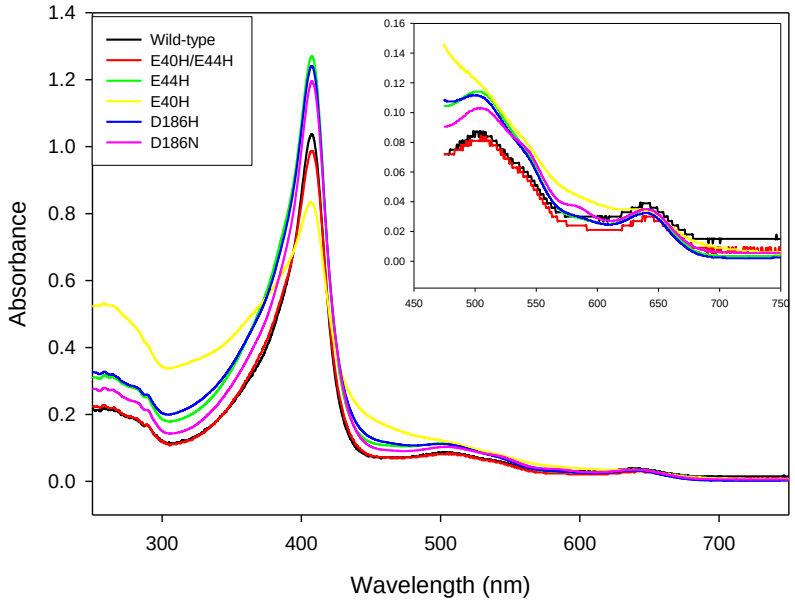

Figure 4.1: Overlay of the resting state UV/Visible absorption spectra for *P.radiata* wild-type MnP3 and mutant variants. The spectra were recorded in 10mM sodium succinate, pH 6.0. (—) wild-type, (—) E40H/E44H, (—) E44H, (—) E40H, (—) D186H and (—) D186N. The insert to the figure on the upper right corner is a magnification of the 450 to 750 nm region.

Table 4.1: Summary of the spectroscopic characteristics of resting state *P. radiata* wild-type and mutant MnP3 enzymes. Spectra were recorded in 10 mM sodium succinate, pH 6.0.

MnP3	**Soret (nm)**	**CTI (nm)**	**CTII (nm)**	**ε_{Soret} (mM^{-1} cm^{-1})**	**RZ**
Wild-type	408	641	507	173 ± 9	5.6
E40H	408	629	–	164 ± 17	2.1
E44H	408	642	503	160 ± 17	4.5
E40H/E44H	408	641	505	169 ± 9	5.2
D186H	408	640	506	170 ± 12	4.4
D186N	408	640	506	168 ± 6	5.0
[a]MnP3 (fungal)	407	640	508	–	5.0
[b]MnP	406	632	502	–	4.5
[c]LiP	407	632	500	–	5.0

Rz, the ratio of A_{Soret} / A_{280nm}, is a measure of the purity of the enzyme preparation.

The ε_{Soret} value is the mean of 3 readings with standard deviation.

[a]Karhunen *et al.*, 1990; [b]Mayfield *et al.*, 1994; [c]Gold *et al.*, 1984.

The electronic absorption spectrum of wild-type recombinant MnP3 from *P. radiata* contains the sharp Soret band at around 408 nm, and charge transfer bands at 507 and 641nm are present. This is essentially identical to the characteristics of the native fungal *P. radiata* MnP3 with Soret maximum at 407 nm, and charge transfer bands at 508 and 640 nm (Karhunen *et al*., 1990). Figure 4.1 and Table 4.1 show that the spectral characteristics of the wild-type MnP3 and Mn site mutant enzymes except E40H, are very similar, all being substantially high spin haem enzymes. This means that mutations at the Mn-binding site appear to cause minimal perturbation to the haem environment. A small but significant effect in the visible region of the E40H was observed relative to the other MnP3 enzymes; CT I appeared at 629 nm and the Soret at 408 nm, while CT II was not as pronounced. As can be seen from the spectrum, (yellow spectrum, Figure 4.1) significant light scattering was evident, indicating some aggregation of the protein. To remove the aggregates, the enzyme was centrifuged at 13,000rpm for 15 minutes in the cold room followed by filtering through a 0.22 nm filter. All attempts to remove the scattering, however, did not yield any change in the spectrum. Hence, aggregation was believed to be a peculiar property of this mutant as it was observed on numerous occasions with different enzyme batches.

These spectral characteristics of MnP3 are very similar to those of MnP, 406, 632 and 502 nm for Soret, CT I and CT II respectively, from *P. chrysosporium* (Mayfield *et al.*, 1994) and to those of *P. chrysosporium* LiP, with Soret at 407nm, CT I at 632 nm and CT II at 500nm (Gold *et al*., 1984) and show that MnP3 from *P. radiata* is typically a high-spin haem peroxidase, probably a little more 6-coordinate like LiP, but clearly distinct from the more 5-coordinate classical high spin peroxidases such as HRP.

The resting–state spectrum of peroxidases can also provide information about the purity of a particular enzyme sample. The Reinheitszahl number (R_Z) gives a convenient

measure of purity and is the ratio of the absorbance at the Soret peak and at 280nm (A_{Soret}/ A_{280}). The R_Z is thus in principle a measure of haem content relative to the aromatic amino acid content of a sample. In the case of HRP, high purity samples have R_Z values in the range 3.0-3.5 (Dunford, 1982; Dunford, 1991; Dunford, 1999). However, HRP is a 5-coordinate haem protein. For 6-coordinate haem enzymes like MnP3 and LiP, previous R_Z values of 5.1 and 5.9 for LiP and MnP, respectively, have been found (Johjima *et al*., 1994). The wild-type and four mutant MnP3 enzymes, E44H, E40H/E44H, D186H and D186N in this study have R_Z values greater than 4 (see Table 4.1), indicative of high purity enzyme. However, the E40H R_Z of 2.1 is the result of the aggregation mentioned earlier. Since all the enzymes in this study were treated in the same way for folding and purification, it is unlikely that this enzyme is less pure than the others. Note that an SDS Page gel of wild-type recombinant MnP3 and E40H showed that they both appear equally pure (data not shown)

4.3: **Measurement of Soret extinction coefficients (ε_{Soret}) of recombinant wild-type and mutant MnP3 enzymes.**

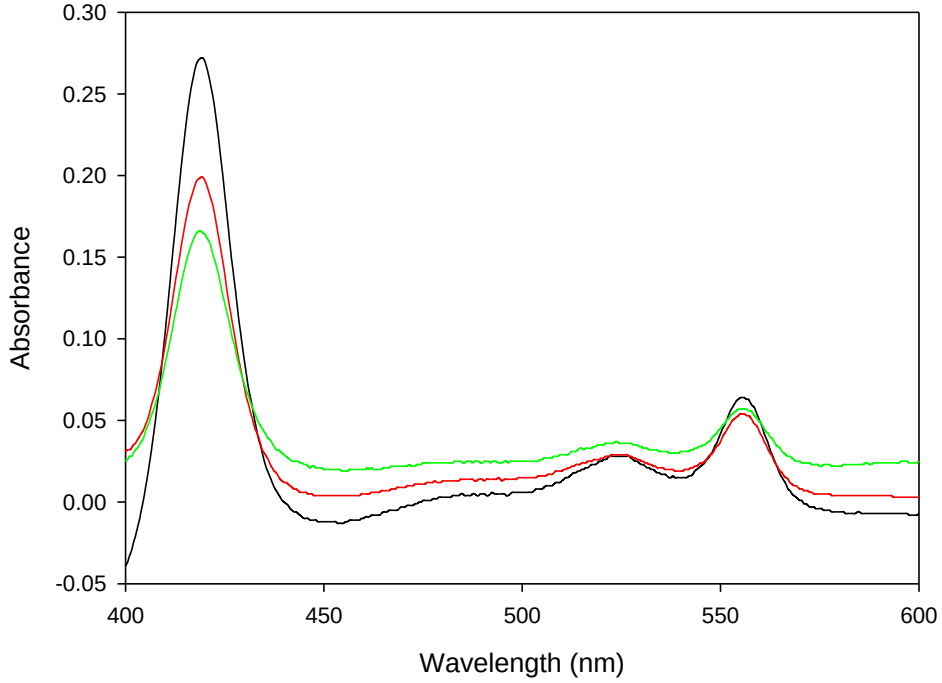

Figure 4.2: UV-visible spectra of pyridine haemochrome experiment (reduced minus oxidised haem-pyridine complex), overlayed for wild-type (WT), E40H/E44H and D186N mutant MnP3. (—) WT, (—) E40H/E44H, (—) D186N. 2µM of each of the enzymes was treated with 88µl of 1M NaOH and 175 µl of pyridine and was further reduced by sodium dithionite. The reduced haem-pyridine peak is at 556nm.

The extinction coefficient of the Soret peak, which gives a measure of the absorption strength of the haem in the context of the protein environment, was determined by the pyridine haemochrome method (Fuhrhop and Smith, 1975 see section 2.4.2, in triplicate). Figure 4.2 shows the pyridine hemochrome spectra of wild-type MnP3 and representative mutants, E40H/E44H and D179N. In this present study, the recombinant wild-type MnP3 Soret extinction coefficient value was calculated to be 173 ± 9 $mM^{-1}cm^{-1}$. The mutant enzymes gave absorption coefficients that were all within error of

the wild-type (Table 4.1) and similar to other fungal peroxidases with an established six-coordinate haem iron (Tien and Kirk, 1988). However, the extinction coefficient of fungal MnP3 enzyme has been previously calculated at 202 $mM^{-1}cm^{-1}$ at 408 nm (Karhunen *et al*., 1990). This value may therefore be in error.

4.4 Determination of pH optimum and apparent *pKa* for Mn (II) and ABTS oxidation by *P. radiata* wild-type and mutant MnP3 enzymes.

The aim of this study was to ascertain the optimum pH for *P. radiata* MnP3 enzyme activity. The optimum pH values for enzyme catalysed reactions with Mn (II) or ABTS were therefore determined by assaying enzyme activity in 100 mM tartrate buffers of varying pH ranges, from 3.5 to 12.0 and 2.5 to 5.5 for Mn (II) oxidation, and ABTS

4.4.1 Mn (II) oxidation activity

Figure 4.3 and Table 4.2 show the pH optima data for Mn (II) substrate oxidation by MnP3. A sharp acidic pH optimum for wild-type MnP3 activity was observed. In this study, the highest wild-type MnP3 turnover number was found to be at pH 5.0, while the enzyme was very active at the pH range from 4.5 to 5.5. Though the enzyme has it pH optimum in the acidic region, it was observed to be moderately active at alkaline pH, showing similar activity of approximately 18 % of the maximum in the pH range of 6.5 to 8.5 with a sharp decrease towards no activity at pH 10.0. *P.radiata* wild-type MnP3 with a pH optimum at 5.0 is consistent with the literature (Bonnen *et al*., 1994; Hinder *et al*., 2002). The optimum pH for Mn (II) oxidation by MnP from *P. chrysosporium* is reported to be 4.5 (Johnson *et al*., 1994) while those of other MnPs, *P. sordid* (Kishi *et al*., 1994), *D. squaleus* (Perie *et al*., 1996), and *L. edodes* (Forrester *et al*., 1990) are also in the acidic range.

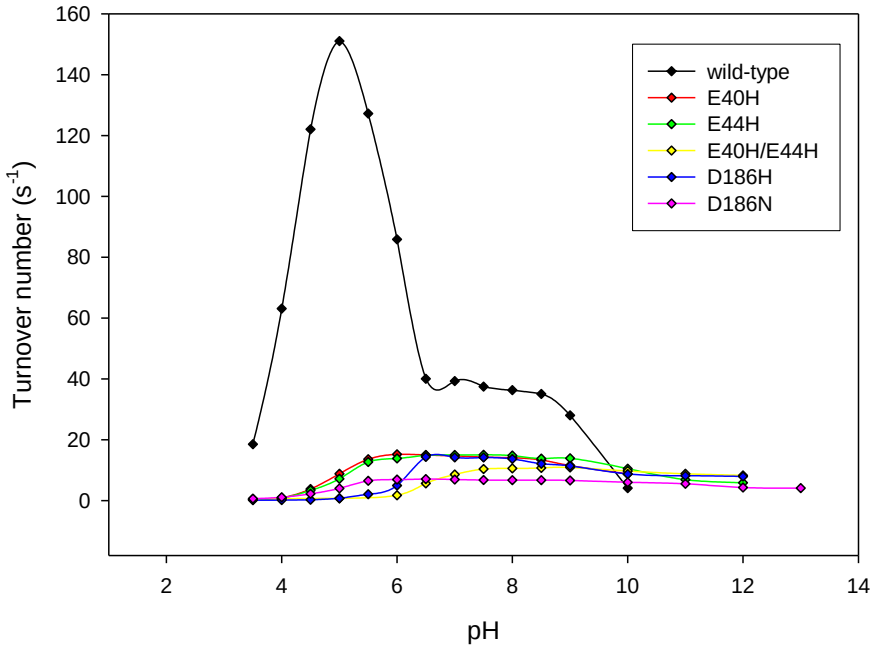

Figure 4.3: pH optima for Mn (II) oxidation by *P. radiata* wild-type and mutant MnP3 enzymes. (—) WT, (—) E40H, (—) E44H, (—) E40H/44H, (—) 186H and (—) D186N. The reactions were performed in 100 mM sodium tartrate buffer at different pHs , using 0.1 mM H_2O_2, and 1mM $MnSO_4$ for wild-type and 25mM $MnSO_4$ for the mutant enzymes, as well as enzyme concentrations 0.023 µM (wild-type), 0.34µM (E40H), 0.34µM (E44H), 0.4µM (E40H/E44H), 0.3µM (D186H), and 0.21µM (D186N). All assays were conducted at 25°C (section 2.4.5).

Table 4.2: pH optima and apparent *pKa*'s for Mn (II) oxidation by wild-type and mutant *P. radiata* MnP3 enzymes. Assays to determine the optimum pH for activity during Mn (II) oxidation were performed in 100 mM sodium tartrate buffer at different pHs, using 0.1 mM H_2O_2, and 1.0 mM $MnSO_4$ for wild-type and 25mM $MnSO_4$ for the mutant enzymes, as well as enzyme concentrations 0.023 µM (wild-type), 0.34µM (E40H), 0.34µM (E44H), 0.4µM (E40H/E44H), 0.3µM (D186H), and 0.21µM (D186N). The assays were conducted at 25°C.

Enzyme	**pH optima**	**Apparent *pKa***
Wild-type	~ 5.0/8.0	~ 4.5; 5.5; 6.5; ~ 9.0
E40H	6.0 - 8.0	~ 5.5
E44H	6.0 - 8.0	~ 5.5
E40H/E44H	7.5 – 10.0	~ 7.0
D186H	6.5 - 8.0	~ 6.5
D186N	5.5 - 12	~ 5.5

All variants had substantially decreased activity at low pH, consistent with the loss of one or more Mn ligands at the interaction site, but all retained significant residual activity at pH values > 5.5 (up to 35% of wild-type). The variants broadly fell unto three groups (Figure 4.3): those that were maximally active at pH 6.0 (E40H, E44H, E40H/E44H), those requiring pH values ≥ 6.5 (D186H) and those requiring pH values > 7.5 (D186N). It is important to note that several variants actually have a higher activity than wild-type at pH ~ 10.0 and approximately 40 % of the wild-type activity in the mid alkaline range.

A plot of log k (observed) against pH (Figure 4.4) was used to determine the apparent *pKa* for Mn (II) dependent oxidation. From Figure 4.3, it can be seen that wild-type enzyme behaviour is complex and may involve as many as four critical ionizations, labelled 1,2,3,4 on Figure 4.4a.

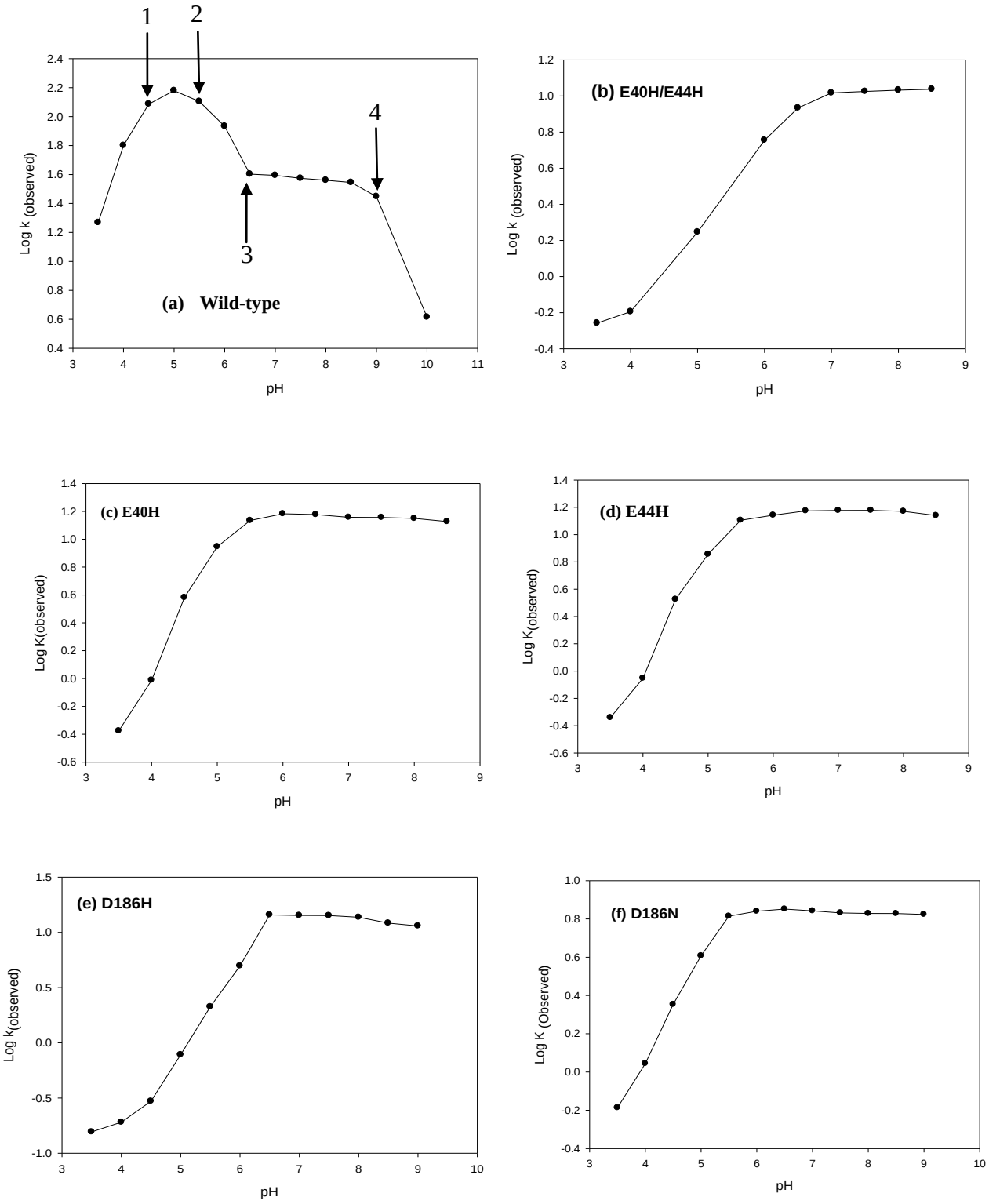

Figures 4. 4: Plots of log k (observed) against pH for the Mn (II) oxidation assay, for determination of *pKa*'s for *P. radiata* wild-type and mutant MnP3 enzymes. Apparent *pKa*'s were determined from the intersection of the idealised slopes from the graphs. Assays were performed as for Figure 4.3 (section 2.4.5)

These presumably reflect deprotonation of one or more carboxylate ligands at the Mn site, starting at *pKa* ~ 4.5, followed at higher pH by *pKa*'s at ~ 5.5, ~ 6.5 and ~ 9.0. The origins of these are unclear at present, although the complex dissociation and ionization equilibrium of the Mn tartrate complexes relevant as substrates should be considered. An acidic *pKa* at ~ 5.5 is preserved in the E40H, E44H and D186N mutants, but is shifted to 6.5 in the D186H mutant implying that for this variant deprotonation of the new H186 residue is essential to allow Mn oxidation at higher pH. Similarly the apparent *pKa* for the E40H/E44H double variant is shifted to ~ 7.0 perhaps because both His residues must be deprotonated to allow activity. Mn oxidation in mid-alkaline range with up to two of the classical carboxylate ligands replaced is still quite significant (~ 40% of wild-type). Moreover, the results for D186N and D186H variants imply that histidine is better tolerated in this respect than asparagine. The loss of carboxylate ligands clearly impacts the low pH end of the activity profile far more than the alkaline end. It would appear that at higher pH Mn oxidation is less dependent on the precise ionization of the Mn binding site, particularly if histidine is the substituting residue.

This discovery that *P. radiata* wild-type recombinant MnP3 enzyme is able to oxidise Mn (II) under both acidic (faster) and alkaline (slower) conditions, and the relatively good performance of the E40H/E44H and D186H variants at alkaline pH values, is particularly interesting in the light of potential industrial applicability. Pulping and pulp bleaching are routinely performed under alkaline conditions and thus any enzyme used in the pulp and paper industry is required to react under alkaline conditions. Most MnP's from wood-colonizing white-rot fungi have been found to have highly acidic pH optima (Hatakka, 1994), so in previous studies on lignin degrading enzymes (Johnson *et al*., 1994; Perez and Jefferies, 1992; Sarkar *et al*., 1997), the enzymes tried were active

only under acidic pH conditions. *P. radiata* wild-type MnP3 enzyme being moderately active at alkaline pH range therefore makes it unique in comparison with other MnP's of white- rot fungi studied to date. The ability of MnP3 enzymes from *P. radiata* to be active under alkaline conditions might make them useful in the pulp and paper industry for treatment of alkaline black liquor and bleaching effluent and / or to bleach the pulp previously cooked under alkaline conditions.

4.4.2 pH dependence of Mn (II) oxidation Michaelis-Menten kinetic parameters

Given earlier results (Figure 4.3) showing significant Mn (II) oxidation activity at both high and low pH for wild-type MnP3, Mn (II) oxidation activity was measured at pH 5.0 and pH 8.0 in the presence of 100 mM tartrate. The aim was to ascertain the effectiveness of the mutant enzymes at high and low pH in comparison to the wild-type. The results are presented in Figure 4.5 and Table 4.3.

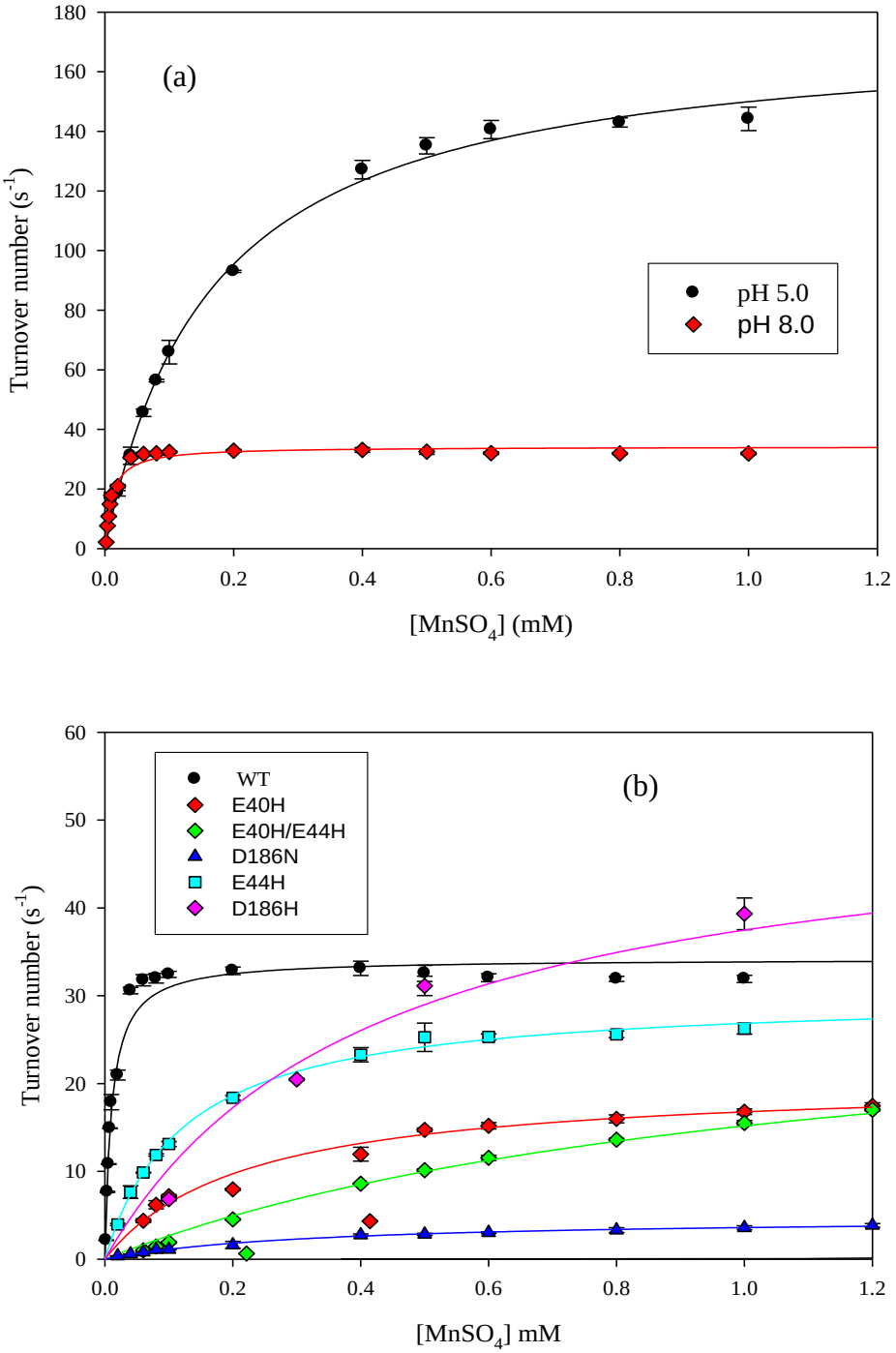

Figure 4.5 (a): pH dependence of Mn (II) oxidation kinetic parameters, (b) Mn (II) oxidation by MnP3 enzymes at pH 8.0. (a) Wild-type MnP3 pH 5.0 (—) and (b) 8.0 (—), (—) WT, (—) E40H, (—) E44H, (—) E40H/E44H, (—) D186H, (—) D186N at pH 8.0. A data point represents the mean of three independent determinations with standard errors indicated. Assays were carried out using the standard protocol as described in section 2.4.6. Data were fitted to the Michaelis equation using SigmaPlot. The kinetic parameters are presented in Table 4.3.

Table 4.3: Kinetic parameters for Mn (II) oxidation by *P. radiata* wild-type MnP3 and mutant variants at pH 5.0 and 8.0. A data point represents the mean of three independent determinations with standard errors indicated. Assays were carried out using standard protocol as described in section 2.4.6. Data were fitted to the Michaelis equation using SigmaPlot.

MnP3	pH	K_m (mM)	k_{cat} (s^{-1})	k_{cat}/K_m (mM^{-1} s^{-1})	pH	K_m (mM)	k_{cat} (s^{-1})	k_{cat}/K_m (mM^{-1} s^{-1})
Wild-type	5.0	0.17 ± 10	175 ± 3.0	1029	8.0	0.01 ± 0.0001	34 ± 0.8	3109
E40H	5.0	11 ± 0.4	12 ± 0.2	1.01	8.0	0.22 ± 0.03	21 ± 0.7	92
E44H	5.0	9 ± 0.5	12 ± 0.3	1.5	8.0	0.12 ± 0.01	30 ± 0.4	244
E40H/E44H	5.0	20 ± 3	2.0 ± 0.1	0.08	8.0	1.09 ± 0.10	32 ± 2	29
D189H	5.0	23 ± 4	0.8 ± 0.1	0.04	8.0	0.42 ± 0.05	53 ± 1	128
D189N	5.0	30 ± 4	8.0 ± 0.5	0.30	8.0	0.33 ± 0.02	5.0 ± 0.1	15

For all enzymes the apparent K_m values for Mn (II) decreased as the pH was increased. For wild-type MnP3 the K_m value for Mn (II) decreased from 0.17 mM at pH 5.0 to 0.011 mM, at pH 8.0. However, the corresponding k_{cat} is decreased 5-fold, so that the effectiveness ratio (k_{cat}/K_m) showed a significant increase by about approximately 3 – fold. This result means that at pH 8.0 all *P. radiata* MnP3 enzymes have enhanced affinity for Mn (II), showing that deprotonation of the Mn site results in progressively higher affinity. The ability of *P. radiata* MnP3 to have a high catalytic efficiency over a wide pH range makes this enzyme unique. As some industry activities, such as pulping and bleaching, are mainly performed under highly alkaline conditions and the waste generated is also alkaline, this is an exciting finding. No comparative data for *P. chrysosporium* MnP at high pH can be found, so whether this property has simply been overlooked or not is unclear.

In contrast to the wild-type enzyme, the k_{cat} values at pH 8.0 for the five MnP3 mutant enzymes, E40H, E44H, E40H/E44H, D186H, and D186N are significantly higher than at pH 5.0 (Table 4.3). This, along with the already mentioned dramatic decreases in K_m leads to an increase effectiveness ratio for all variants of between 50 and 3200-fold. However, none of the mutant enzymes reach the efficiency of the wild-type enzyme, even at pH 8.0.

4.5 ABTS oxidation

Figure 4.6 illustrates the pH dependence of ABTS turnover for the wild-type and MnP3 variant enzymes. All the enzymes examined showed a strong acidic pH preference. The activity for ABTS oxidation by wild-type MnP3 was highest at pH 3.0 and decreased to zero at pH 5.5. All the MnP3 mutant enzymes exhibited a similar profile with pH optimum at pH 3.0. A non-specific interaction site for ABTS in the general region of the Mn (II) binding site cannot be excluded since there are significant effects for all

variants. It implies that protonation events are required for ABTS oxidation. The general effect is probably related to charge neutralisation of sulphonate groups on ABTS.

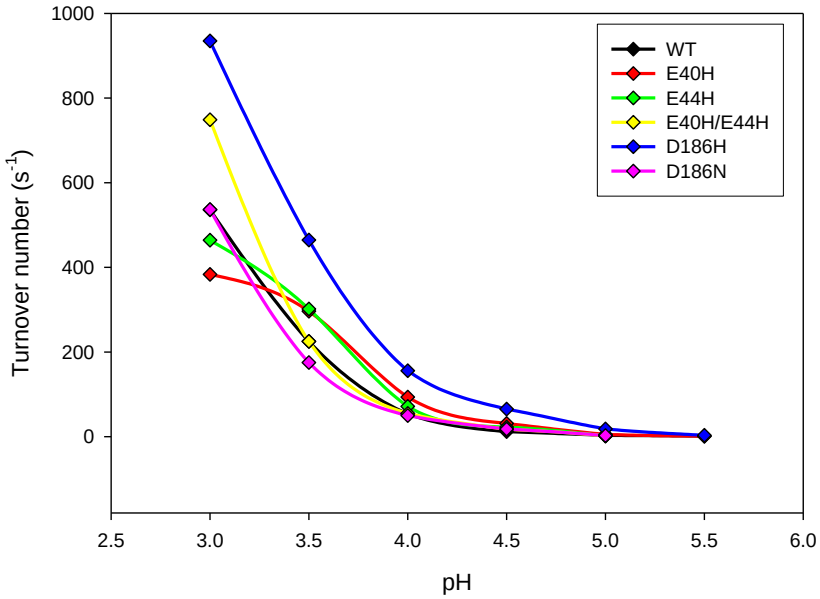

Figure 4.6: pH profiles for ABTS oxidation by *P. radiata* wild-type MnP3 enzyme and mutants, E40H, E44H, E40H/E44H, D186H and D186N. The reactions were performed in 100 mM sodium tartrate buffer, using 0.1 mM H_2O_2, 1.6 mM ABTS and enzymes of concentrations: 0.006µM (WT)(—), 0.0015µM (E40H)(—), 0.0094µM (E44H)(—), 0.0022µM (E40H/E44H)(—), 0.0096µM (D186H)(—), and 0.0086µM (D186N)(—) (section 2.4.5). Temperature was 25ºC.

4.6 Steady-state kinetic analysis of Mn (II) oxidation by wild-type and mutants MnP3 from *P. radiata*

In this section, the steady-state kinetic parameters for Mn (II) oxidation by *P. radiata* MnP3 enzymes were determined as a function of Mn (II) concentration. Data were obtained by measuring the initial rates of Mn (II) oxidation assays for varying $MnSO_4$ concentrations in the range 0.02 - 1.0 mM with a fixed H_2O_2 concentration of 0.1 mM and in the presence of 100 mM Na tartrate, pH 5.0 (see section 2.4.6). For all enzymes, results followed apparent Michaelis-Menten kinetics (Figure 4.7) and after iterative

fitting to the Michaelis equation in SigmaPlot, the kinetic parameters for Mn (II) oxidation were determined and are listed in Table 4.4

The K_m value for Mn (II) of wild-type MnP3 was found to be 0.17 ± 0.01mM, while the apparent k_{cat} value was 175 ± 0.3 s^{-1} (Table 4.3). MnP3 variants had K_m values, 65-fold (E40H), 50-fold (E44H), 117-fold (E40H/E44H), 139-fold (D186H) and 178 - fold (D186N) higher than wild-type MnP3, where as, the k_{cat} values for E40H, E44H, E40H/E44H, D186H and D186N mutant enzymes were ~ 93 % lower compared to that of the wild-type enzyme at pH 5.0. The corresponding catalytic efficiencies (K_{Mn}^{2+}) for the mutant enzymes for Mn (II) oxidation are therefore drastically decreased compared to the wild-type MnP3. The dramatic loss of catalytic efficiency by the MnP3 mutants clearly shows the importance at lower pH of native and protonation states of the amino acid residues forming the Mn (II) binding site in catalysis. These findings are consistent with the findings of Kishi *et al*., (1996).

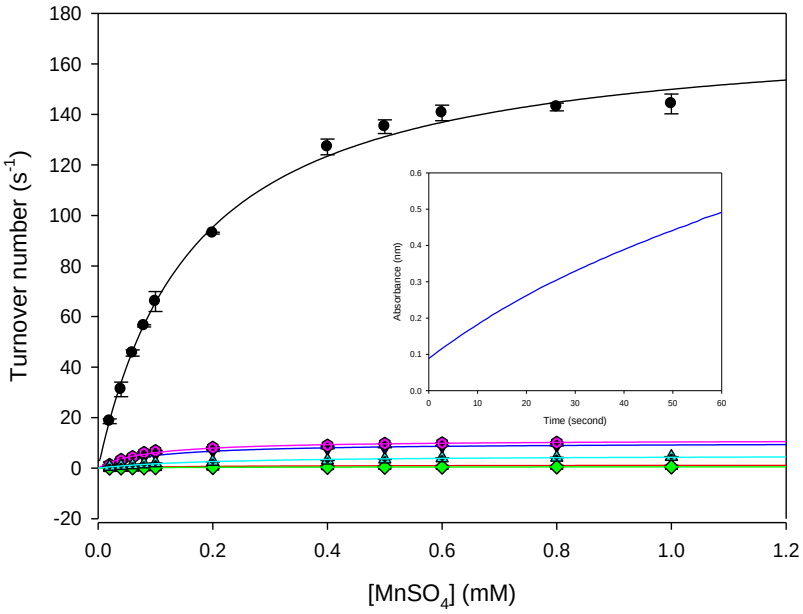

Figure 4.7: The dependence of Mn (II) oxidation on Mn (II) concentration by wild-type MnP3 and E40H, E44H, E40H/E44H, D186H and D186N mutant variants. (—) WT, (—) E40H, (—) E44H, (—) E40H/E44H, (—) D186H, (—) D186N. A data point represents the mean of three independent determinations with standard errors indicated. Assays were carried out as described in section 2.4.6, with a fixed H_2O_2 of 0.1 mM and the data fitted to the Michaelis equation using SigmaPlot. The kinetic parameters extracted from the plots are presented in Table 4.3. The insert is a typical Absorbance Vs Time plot of MnP3 activity assay.

Table 4.4: Steady-state kinetic parameters for Mn (II) oxidation by wild-type and mutant MnP3 enzymes from *P. radiata*. Assays were carried out in 100mM Na tartrate, pH 5.0, using a range of Mn (II) concentrations (0.02 – 1.0 mM) and fixed 0.1 mM H_2O_2, at 25°C. The concentration of wild-type protein in the assay mixtures was 8.0 nM, while that of the mutant variants was 0.15 µM. Three independent determinations were carried out for each $MnSO_4$ concentration.

Enzymes	K_m **(mM)**	k_{cat} **(s^{-1})**	k_{cat}/K_m **(mM^{-1} s^{-1})**
MnP3	0.17 ± 0.01	175 ± 0.3	1029
E40H	11 ± 0.4	12 ± 0.2	1.0
E44H	8.5 ± 0.5	12 ± 0.3	1.5
E40H/E44H	20 ± 3	1.7 ± 0.1	0.08
D186H	23 ± 4	0.84 ± 0.1	0.04
D186N	30 ± 4	8.0 ± 0.5	0.30

The steady-state kinetics of Mn (II) activity were also evaluated as a function of hydrogen peroxide concentration, in the presence of a fixed Mn (II) concentration (1.0 mM) for wild-type MnP3 (see Figure 4.8). A K_m of 16 ± 2 µM was determined with an apparent k_{cat} of 227 ± 11 s^{-1} (Figure 4.8). This K_m value for peroxide is significantly lower than the value of 140µM reported by Glenn *et al.*, (1986) for MnP from *P. chrysosporium* at pH 4.5. This result is indicative of a very high affinity of MnP3 for H_2O_2, with a catalytic efficiency calculated to be 1.4 X 10^7 mM^{-1} s^{-1}.

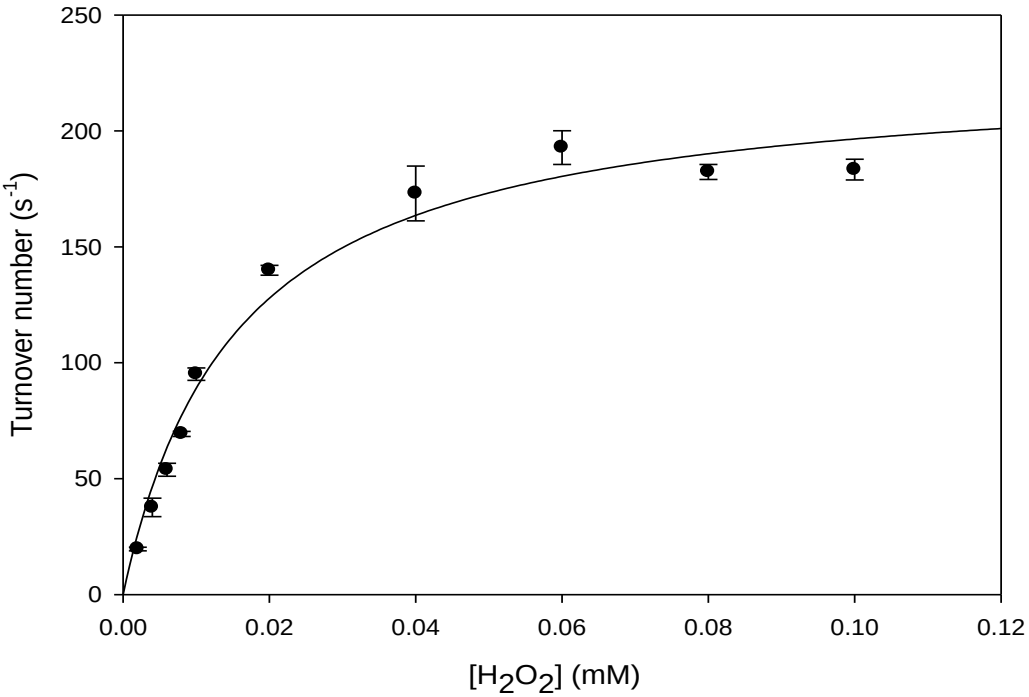

Figure 4.8: The dependence of Mn (II) oxidation on H_2O_2 concentration by wild-type MnP3. Assays were carried out as described in section 2.4.6, with fixed $MnSO_4$ of 1.0 mM and the data fitted to the Michaelis equation using SigmaPlot. Each data point represents the mean of three independent determinations with standard error.

4.7 Steady-state kinetic analysis of ABTS oxidation by wild-type and mutant MnP3 from *P. radiata*.

Initial steady-state kinetic parameters for ABTS oxidation by wild-type MnP3 and mutant enzymes were determined in 100 mM Na tartrate, pH 3.0 (Section 2.4.7). Data were obtained over a range of ABTS concentrations (depending on enzymes), with a fixed H_2O_2 concentration of 0.1 mM. All enzymes followed apparent Michaelis-Menten kinetics (Figure 4.9) and after fitting to the Michaelis equation in SigmaPlot, the kinetic parameters were determined and are shown in Table 4.5.

Table 4.5: Steady-state parameters for the oxidation of ABTS by wild-type and mutant MnP3 enzymes from *P. radiata*. Assays were carried out in 100 mM Na tartrate buffer, pH 3.0 using 0.1 mM H_2O_2 and at 25°C. The concentration of wild-type protein in the assays 0.01 µM, while that of the mutant variants range from 0.1 – 6.5 mM (see section 2.4.7). Three independent determinations carried out for each ABTS concentration.

Variant	K_m **(mM)**	k_{cat} **(s^{-1})**	k_{cat}/K_m **(mM^{-1} s^{-1})**
Wild-type	1.4 ± 0.1	912 ± 41	651.4
E40H	0.5 ± 0.1	369 ± 13	738
E44H	0.3 ± 0.1	491 ± 24	1637
E40H/E44H	4.2 ± 0.4	615 ± 28	146.4
D186H	0.24 ± 0.03	1007 ± 27	4196
D186N	1.3 ± 0.1	762 ± 28	586

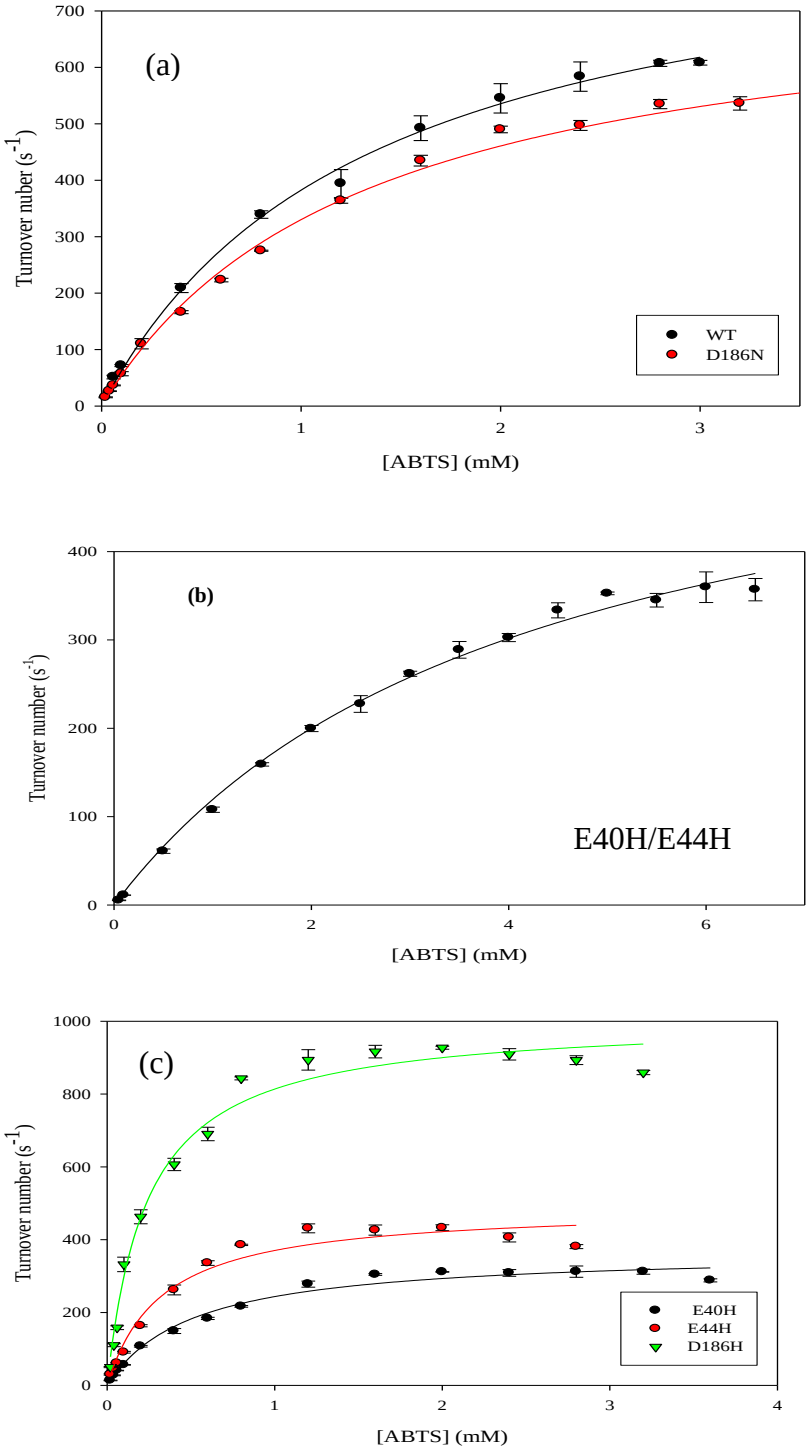

Figure 4.9: The dependence of ABTS oxidation on ABTS concentration by MnP3 enzymes. (a) (—) WT**,** (—) D186N, (b) (—) E40H/E44H, (c) **(**—) E40H, (—) E44H, (—) D186H. A data point represents the mean of three independent determinations with standard errors indicated. Assay mixtures contained 0.01µM enzyme, 0.02 – 3.6mM ABTS and 0.1mM H_2O_2 in 100mM tartrate buffer, pH 3.0 at 25°C. Data were fitted to Michaelis equation using SigmaPlot. The kinetic parameters are presented in Table 4.5.

The apparent K_m value for ABTS of wild-type MnP3 was found to be 1.4 ± 0.1mM, while the apparent k_{cat} value was 912 ± 41 s^{-1}(Table 4.5). The apparent K_m values for E40H, E44H and D186H were 2.7- fold, 4.3-fold and 5.8-fold lower, respectively while D186N was equivalent to the wild-type enzyme. In contrast, the apparent K_m value for ABTS of the double mutant, E40H/E44H, was approximately 3-fold higher than the wild-type. Results also show that the apparent k_{cat} values for ABTS oxidation of E40H, E44H, E40H/E44H and D186N mutant proteins were 40%, 54%, 67% and 84% of the value of the wild-type enzyme, whereas, D186H was approximately equivalent to the wild-type MnP3. The apparent K_m and k_{cat} values obtained were used to estimate apparent catalytic efficiencies (k_{cat}/K_m), as a comparative measure of enzyme effectiveness. These were found to be equivalent to wild-type for E40H and D186N, approximately 2-fold and 6-fold higher for E44H and D186H, respectively and approximately 4-fold lower for E40H/E44H MnP3.

For the five mutant variants studied, two E40H/E44H and D186N, strictly obeyed standard Michaelis-Menten kinetics, as does wild-type MnP3 (Figure 4.9). However, three other mutants E40H, E44H, and D186H show some evidence of substrate inhibition effects. This behaviour is complex and it would be inappropriate to draw any firm conclusions based on this limited data knowing that MnP3 appear sensitive to mechanistic inhibition at higher peroxide concentrations e.g. formation of Compound III. However, the reduction in K_m of E40H, E44H and D186H means that the amino acid substitutions have created enzymes with a higher affinity towards ABTS, with a resultant higher effectiveness ratio with respect to ABTS for E44H and D186H. In contrast, the double mutant, E40H/E44H with higher K_m for ABTS than the wild type enzyme has a reduced affinity for ABTS resulting in a reduced catalytic efficiency compared to wild-type. These results confirm that for MnP3 the Mn oxidation site is

also the site for ABTS oxidation, although the effects of the mutations on the ABTS oxidation are less severe than for Mn (II) oxidation.

4.8 Effect of different organic acid buffers on the kinetic parameters of Mn (II) oxidation for *P. radiata* wild-type MnP3 and mutant variants.

MnP activity is also known to be stimulated by simple organic acids, which chelate the Mn (III) ion product of catalytic activity. The relative stabilities of the Mn (III)-lactate complex and Mn (III)-malonate complex have been documented (Wariishi *et al*., 1992).

The structures of organic acids used in this experiment are as follows:

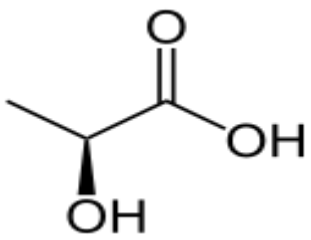

Lactic acid

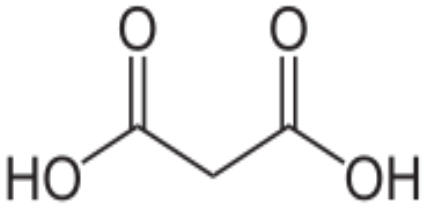

Malonic acid

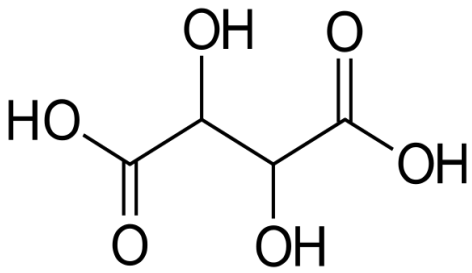

Tartaric acid

Figure 4.10a: Structures of organic acids, lactic acid, malonic acid and tartaric acids.

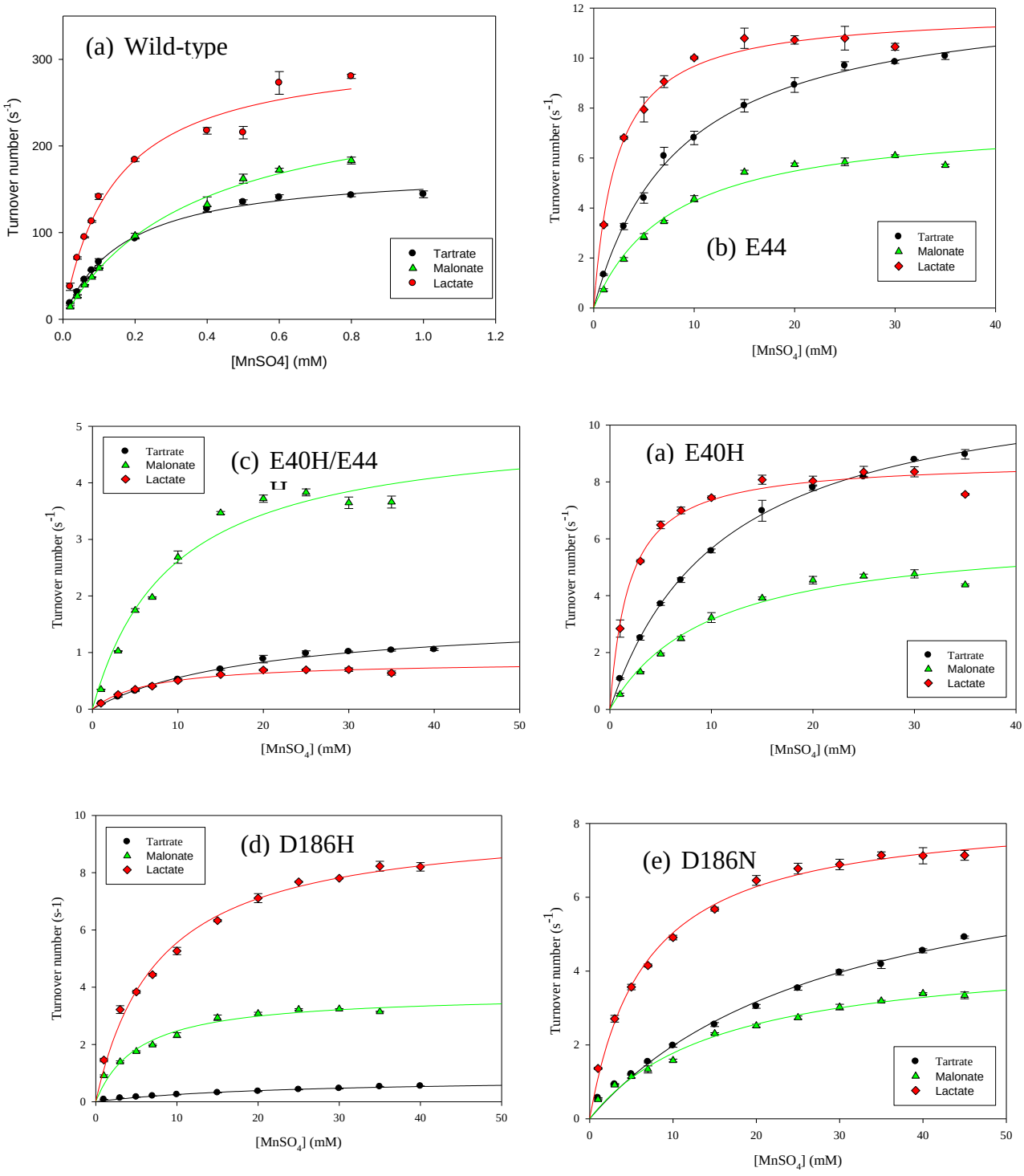

Figure 4.10b: Effect of organic acid Mn (III) chelators on kinetic parameters of MnP3 mutant variants during Mn (II) oxidation. (—) tartrate, (—) malonate, (—) lactate. The reactions were carried out in 100 mM Na tartrate, pH 50 as described in section 2.4.8. A data point represents the mean of three independent determinations with standard errors indicated. Data were fitted to the Michaelis equation using SigmaPlot. The kinetic parameters are summarized in Table 4.6.

Table 4.6: Kinetic parameters for Mn (II) oxidation by wild-type and mutant MnP3, with different organic acid Mn (III) chelators. As described in section 2.4.8. Oxidations of Mn (II) was carried out using 100mM of appropriate buffer (sodium tartrate, sodium malonate or sodium lactate) pH 5.0. Reaction mixtures contained 0.03 – 0.2µM MnP3, 0.1mM H_2O_2 and 0.2 -1.2 mM $MnSO_4$ for wild-type and 1 – 45mM $MnSO_4$ for mutants enzymes. Results are the average of three determinations with the standard errors indicated.

	Tartrate			**Malonate**			**Lactate**		
MnP3	K_m **(mM)**	k_{cat} **(s^{-1})**	k_{cat}/K_m **(mM^{-1} s^{-1})**	K_m **(mM)**	k_{cat} **(s^{-1})**	k_{cat}/K_m **(mM^{-1} s^{-1})**	K_m **(mM)**	k_{cat} **(s^{-1})**	k_{cat}/K_m **(mM^{-1} s^{-1})**
Wild-type	0.17 ± 0.01	175 ± 3.0	1029.4	0.31 ± 0.01	240 ± 3.0	774	0.13 ± 0.02	300 ± 11	2308
E40H	11 ± 0.4	12.0 ± 0.2	1.0	10 ± 2	6.3 ± 0.4	0.63	2.0 ± 0.2	9 ± 0.20	4.50
E44H	8.5 ± 0.5	12 ± 0.3	1.4	8.0 ± 1	8.0 ± 0.4	1.00	2.3 ± 0.2	12 ± 0.30	5.20
E40H/E44H	20 ± 3	1.7 ± 0.1	0.09	9.2 ± 2	5.0 ± 0.4	0.54	7.0 ± 1.1	0.9 ± 0.04	0.13
D186H	23 ± 4	0.84 ± 0.1	0.04	5.3 ± 0.8	4.0 ± 0.2	0.75	8.0 ± 0.7	10 ± 0.30	1.25
D186N	30 ± 4	8.0 ± 0.5	0.30	16.0 ± 2	5.0 ± 0.2	0.31	7 .0 ± 0.4	8.4 ± 0.13	1.20
MnP[a]		176[b]			220[c]			211[d]	

a *P.chrysosporium* MnP

b Boe *et al*. (1993) 50mM sodium tartrate, pH 4.5, 0.02µM MnP, 0.1mM H_2O_2 and 0.2mM $MnSO_4$.

c Kuan *et al*. (1993), 40mM sodium malonate, pH 4.5 0.1µM MnP, 50µM H_2O_2 and 0.2mM $MnSO_4$.

d Kuan *et al*. (1993) 40mM sodium lactate, pH 4.5 0.1µM MnP, 50µM H_2O_2 and 0.2mM $MnSO_4$

In this section, the effect of different organic acid chelators on the Mn (II) oxidation activity of *P. radiata* MnP3 has been characterised. The study was conducted in the presence of organic acids with reported ability to act as Mn (III) chelators (Warrishi *et al*., 1997), i.e. tartrate, malonate, lactate and oxalate. The results obtained from these experiments are summarized in Figure 4.10b and Table 4.6. Worthy of note is that oxalate, earlier proposed to be the physiological chelator for Mn (III) in *P. chrysosporium* at least (Kuan and Tien, 1993) was used in this study, but negligible activity at pH 5.0 was found, meaning that no data could be obtained. Note also, that the data in Table 4.6 for tartrate buffer are the same as those presented in Table 4.4 and have already been discussed in section 4.5. In this section the data on tartrate will be revisited with the aim of comparing it to the other organic acid chelators.

The Mn (II) K_m values obtained for wild-type MnP3 for Mn (II) oxidation using tartrate, malonate and lactate at pH 5.0 were found to be 0.17 ± 0.01 mM, 0.31 ± 0.01 mM and 0.13 ± 0.02 mM, respectively. These results show that out of the three buffers investigated, wild-type MnP3 has the highest affinity for Mn (II) in the presence of either tartrate or lactate. The k_{cat} value obtained when the reactions were conducted in tartrate buffer was however lower than either in malonate buffer or lactate buffer. Consequently, the results show that MnP3 has the highest catalytic efficiency in oxidizing Mn (II), 2308 $mM^{-1}s^{-1}$ when the reaction takes place in lactate buffer, followed by tartrate and then malonate.

These results seem to confirm that organic acid chelators are involved in the catalytic cycle of MnPs. Comparing the k_{cat} values of *P. radiata* MnP3 with MnP of *P. chrysosporium* (Table 4.6), shows that for these two enzymes tartrate and malonate values are very similar but that for lactate, MnP3 is 142% that of *P. chrysosporium*

MnP. These results are also different from those observed for MnP from *A. terreus* LD-1 where lactate inhibited the MnP activity completely (Kanayama *et al*., 2002). However, the observed K_m values for MnP3 with the three buffer systems are all relatively high, compared to the values previously reported for *P.chrysosporium* (Kuan *et al*., 1993; Aitken and Irvine, 1989).

Similarly, steady-state kinetic parameters for Mn (II) oxidation were also determined for the five MnP3 mutant enzymes with the three organic acids as described in the methods section 2.4.8. The results in Figure 4.10b and Table 4.6 show K_m values for all the MnP3 mutant enzymes were relatively higher and k_{cat} relatively lower compared to the wild-type values when reactions occurred in tartrate, malonate or lactate. The increase in *Km* of all the MnP3 mutant enzymes implies that mutations of the Mn (II)-binding site have generated enzymes with less affinity for Mn (II) as evident in gross decrease in their catalytic efficiencies relative to the wild-type MnP3. E40H and E44H MnP3 mutant variants behaved similarly to wild-type when activity assays were conducted in tartrate, malonate and lactate buffers with these two enzymes being most effective in lactate buffer with catalytic efficiencies of 4.5 and 5.2 $mM^{-1}s^{-1}$ respectively, and showing least effectiveness in malonate buffer (Figure 4.10 (a and b) and Table 4.6).

The double mutant, E40H/E44H behaved differently from the wild-type in these organic acid buffers by being most effective in malonate buffer with catalytic efficiency of 0.54 $mM^{-1}s^{-1}$ and least effective in tartrate buffer, having k_{cat}/K_m ratio of 0.09 $mM^{-1}s^{-1}$. Hence, the replacement of Glu 40 and Glu 44 with histidines at the manganese–binding site of MnP3 created a farless active enzyme, thereby showing the importance of Glu 40 and Glu 44 in the binding and oxidation of Mn (II) by MnP3 of *P. radiata.*

The D186H and D186N MnP3 mutant variants also behaved differently from the wild-type MnP3 enzyme in the organic acid buffers used. While the D186H was most efficient in lactate and least efficient in tartrate buffer, the D186N also showed the most effectiveness in lactate and equivalent catalytic efficiencies in both malonate (0.31 mM^{-1} s^{-1}) and tartrate (0.30 mM^{-1} s^{-1}) buffers. However, D186N had the largest increase in the K_m value among the five MnP3 mutant enzymes studied, with much lower k_{cat} values in the buffers used. This resulted in the catalytic efficiency of D186N being reduced by 3400, 2500 and 1920 – fold in tartrate, malonate and lactate respectively, compared to the wild-type. The implication is that the D186N mutation was least favoured with histidine being a somewhat better alternative, the D186N variant also showed the lowest Mn (II) specificity constant in malonate buffer. Clearly mutation specific preferences for organic acid chelating buffers have been created and histidine remained a better alternative to asparagine in terms of retaining significant Mn peroxidase activity.

4.9 The formation and reduction of MnP3 Compounds I and II

MnP has the same basic catalytic cycle as other plant and fungal peroxidases. Since *Phlebia radiata* MnP3 is a new MnP enzyme an attempt was made to investigate the intermediates of the catalytic cycle and their stability. The aim was also to see if other divalent metals other than Mn, most notably Co, could reduce Compound I or II to the resting state enzyme (See section 2.4.10 for full experimental method). Table 4.7 lists the characteristics of several peroxidase Compound I and Compound II species, along with MnP3 from *P. radiata* (see later sections).

4.9.1 Formation of *P.radiata* MnP3 Compound I, and its auto-reduction to resting state enzyme.

The redox states of MnP3 were studied during the catalytic cycle. The absorption spectrum of wild-type *P. radiata* MnP3 enzyme has maxima at 408 nm (Soret band), 507 nm (CT II) and 641 nm (CT I), in 10 mM Na succinate, pH 6.0. Attempts were made to convert the resting state enzyme to Compound I, by titrating an enzyme solution with one molar equivalent of H_2O_2 (section 2.4.9). A scan after 2 minutes gave a spectrum with some of the properties of Compound I (reduced Soret extinction) but also some of the properties of Compound II (Figure 4.12a). Comparison between this spectrum and *P. chrysosporium* MnP Compound I (Wariishi *et al*., 1988 and 1989), *P. chrysosporium* LiP Compound I (Renganathan and Gold, 1986), HRP Compound I (Dunford and Stillman, 1976), Chloroperoxidase Compound I (Palcic *et al*., 1980) and Lactoperoxidase Compound I (Kimura and Yamazaki, 1979) suggests that *P. radiata* MnP3 Compound I is relatively unstable and is very similar to that observed for native (fungal) MnP (Karhunen *et al*., 1990).

MnP3 Compound I show a characteristic reduction of the Soret intensity, and move to 410 nm, of 37 %. This observation is consistent with that of Tuisel *et al*., (1990), where 48% Soret reduction was observed during the formation of LiP Compound I, with apparent shift in the Soret wavelength also to 410 nm (Table 4.7). The reduced Soret intensity suggests the π-cation radical nature of the MnP Compound I porphyrin ring (Dunford, 1982).

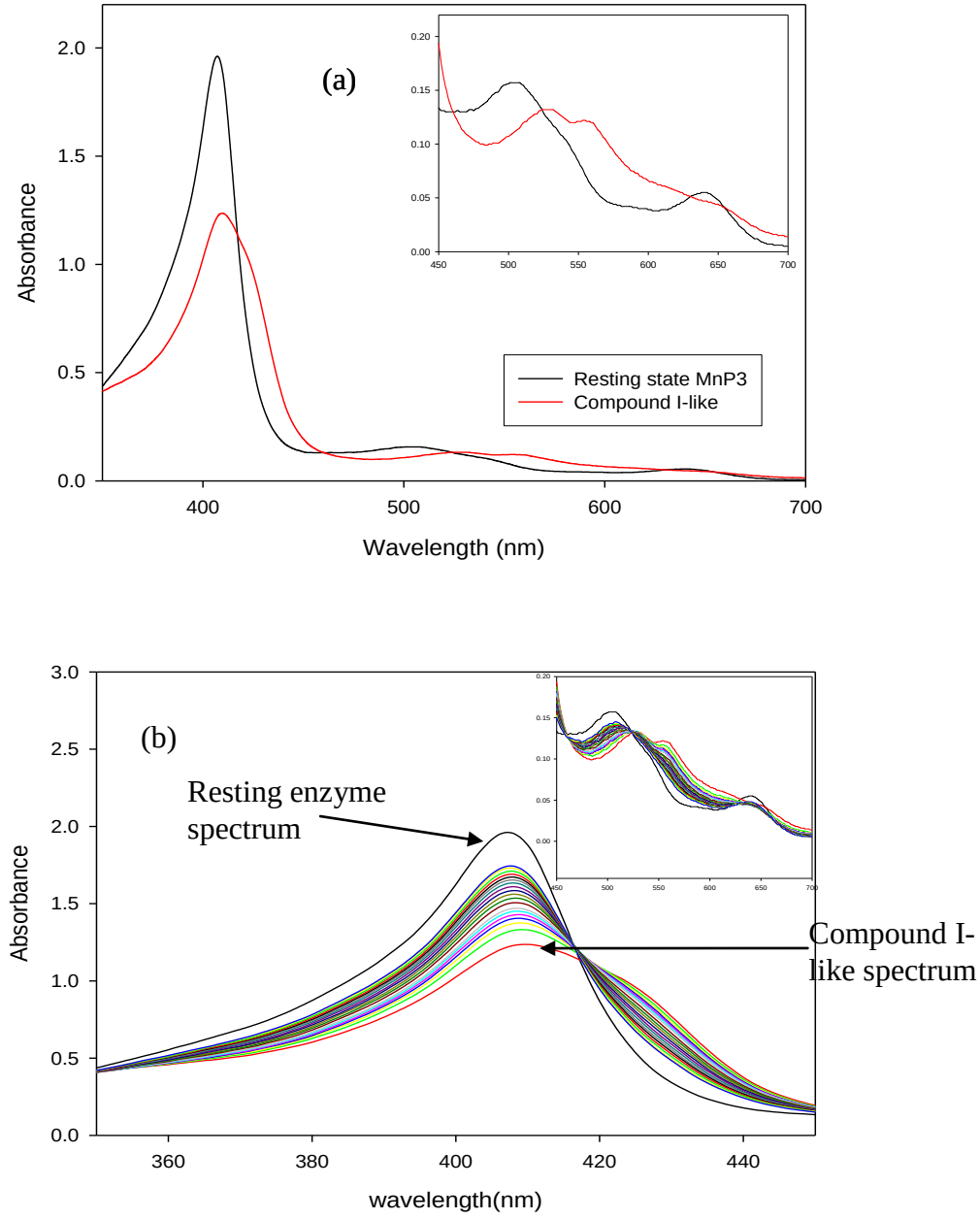

Figure 4.11: (a) UV-visible spectrum of *P. radiata* wild-type MnP3 Compound I. (b) Auto recovery of MnP3 Compound I back to resting state enzyme.

Spectra were recorded in 10mM succinate buffer, pH 6.0. To produce the Compound I-like spectrum, 1 molar equivalent of H_2O_2 was added to resting state enzyme. Spontaneous decay of *P. radiata* MnP3 Compound I to resting enzyme in the absence of reductant. Spectral scans recorded every 2 minutes. The spectra show the occurrence of an isosbestic point at 418 nm. The insert shows the enlarged 450-700 nm region.

Table 4.7: Absorption maxima of oxidized intermediates of several peroxidases.

	Compound I				**Compound II**			
Peroxidase	**Absorption maximum (nm)**				**Absorption maximum (nm)**			**Ref.**
MnP3	410	—	—	—	420	533	557	This work
MnP (*P.chrysosporium*)	407	558	605	650	420	528	555	a
LiP (*P.chrysosporium*)	408	550	608	650	420	525	556	b
HRP	400	557	622	650	420	527	554	c
Chloroperoxidase	367	545	610	688	438	542	571	d
Lactoperoxidase	410	562	600	662	433	537	568	e

[a]Wariishi *et al*. 1988 and 1989. [b]Renganathan and Gold (1986). [c]Dunford and Stillman (1976). [d]Palcic *et al*., (1980); Nakajima *et al*. (1985). [e]Kimura and Yamazaki (1979).

Compound I slowly converted (auto-recovery) back to the unoxidized resting state within 38 minutes, displaying a single isosbestic point at 418 nm (see Figure 4.11b). This is evidence that Compound I is unstable and is being auto-reduced back to the resting state; note, the absorbance of the Soret band has increased and the maximum changed back to 408 nm. The time-scale is slow with a decay rate constant of 0.032 ± 0.001, and a half-life ~ 22 min.

4.9.2 Formation of MnP3 Compound II and reduction back to the resting enzyme.

Compound II has a formal iron oxidation state of IV. Mossbauer (Schultz *et al*., 1984) and resonance Raman (Rakhit *et al*., 1976; Felton *et al*., 1976; Termer and Reed, 1984) spectroscopies indicate a Fe^{IV} =O structure for HRP Compound II and the Resonance Raman evidence of Andersson *et al*., (1987) also suggests a Fe^{IV}=O structure for LiP Compound II. As with HRP, LiP compound II and *P.chrysosporium* MnP, Compound

II's the Soret maximum of *P. radiata* MnP3 Compound II was found to be less intense and red-shifted to 420 nm and the other maxima were at 533 and 557 nm (Figure 4.12a, Table 4.7).

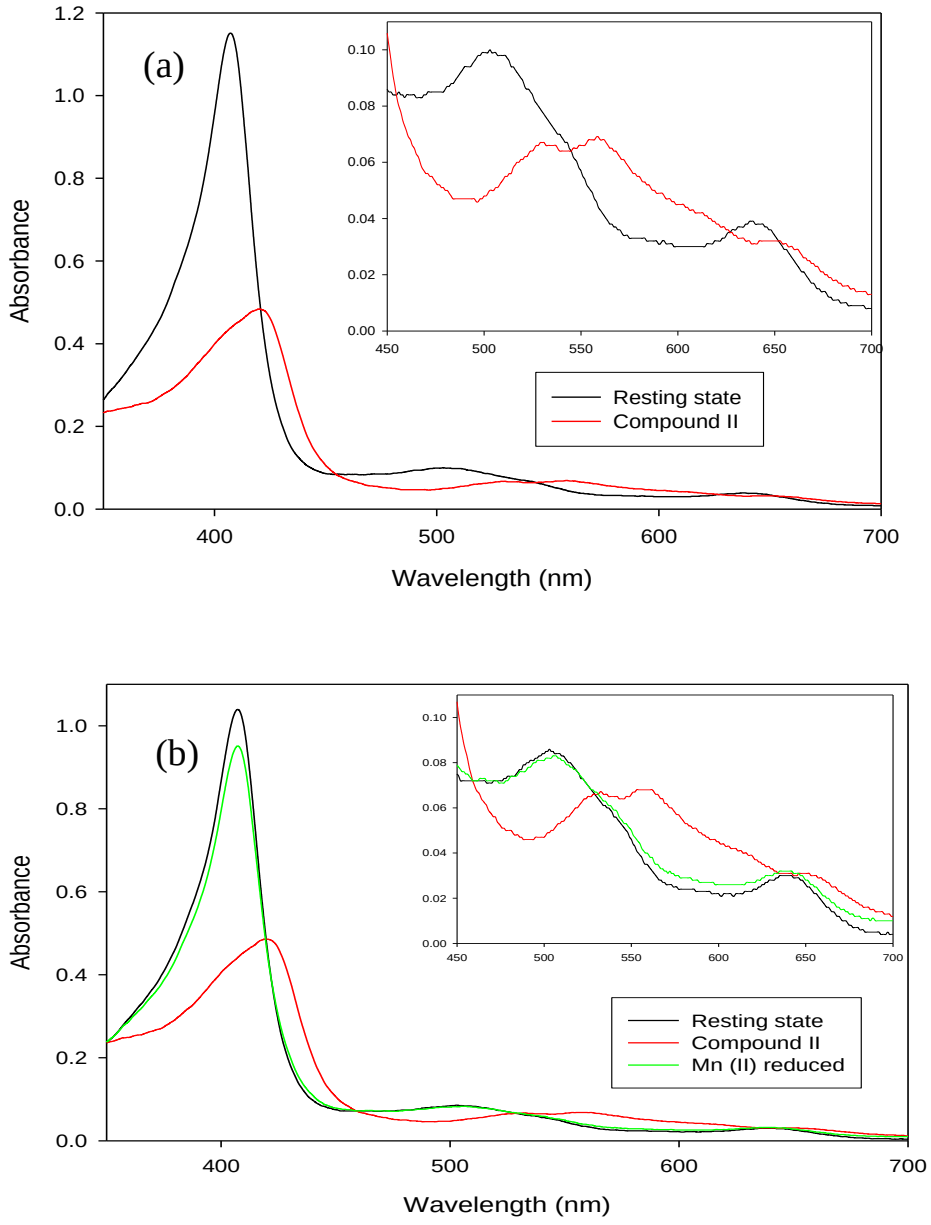

Figure 4.12 (a) UV-visible spectrum of *P. radiata* of wild-type MnP3 Compound II. (b) Reduction of Compound II of MnP3 to resting state on the addition of Mn (II). Spectra were recorded in 10 mM sodium succinate, pH 6.0 at 25°C. To produce MnP3 Compound II, 2 moles equivalents of H_2O_2 were added to resting state enzyme. Mn (II) reduction was achieved by the addition of 1 mole equivalent of MnSO4, and the spectrum recorded immediately.

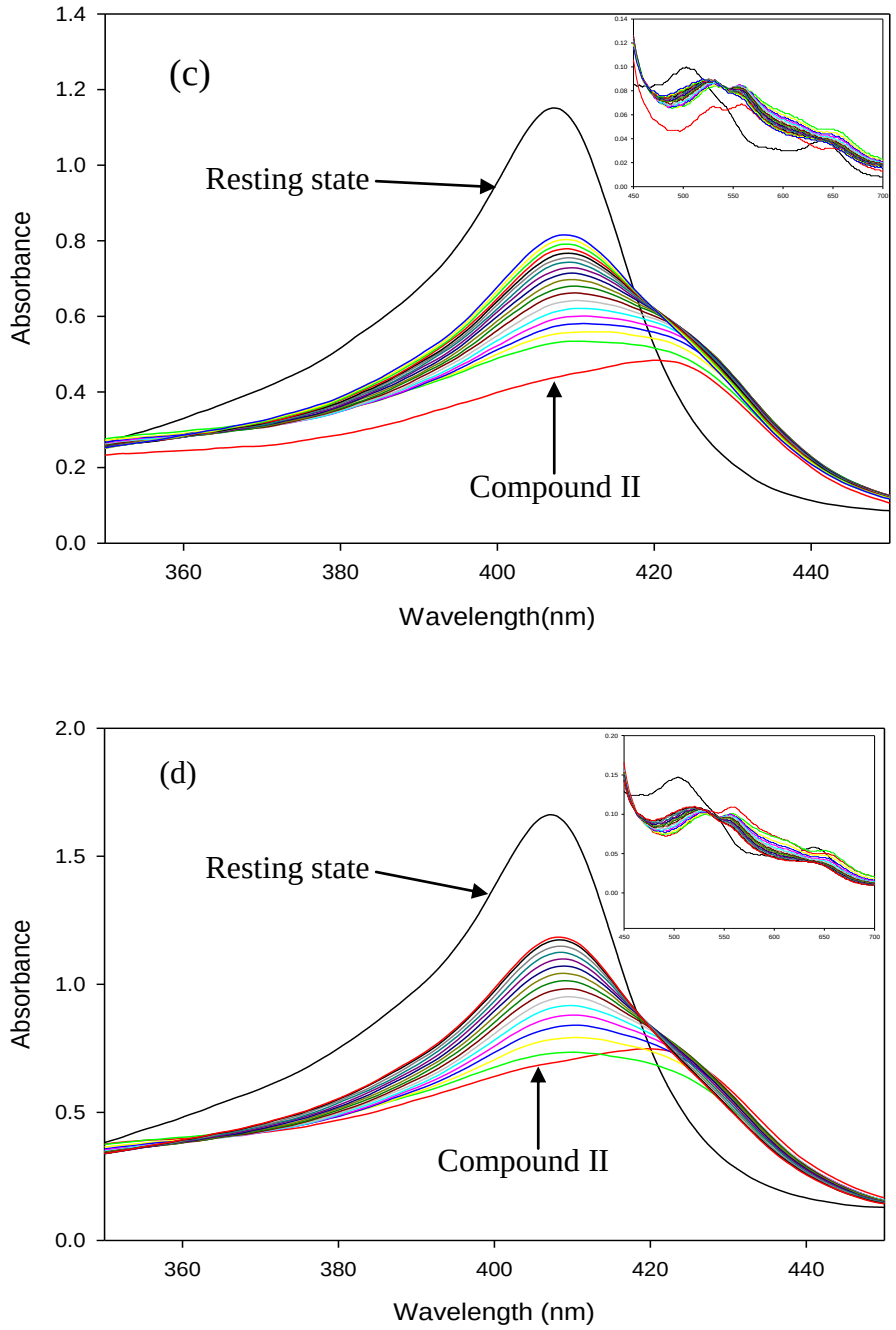

Figure 4.12: (c) Reduction of Compound II of MnP3 to resting state wild-type in the presence of $CoSO_4$. (d) Auto-reduction of MnP3 Compound II to the resting state enzyme. Spectra were recorded in 10 mM sodium succinate, pH 6.0. To produce MnP3 Compound II, 2 molar equivalents of H_2O_2 were added to resting state enzyme. After addition of 1 molar equivalent of $CoSO_4$ spectrum were recorded every 2 minutes. Spontaneous decay of *P. radiata* MnP3 Compound II to resting enzyme in the absence of reductant. The insert shows the enlarged 450 – 700 nm region.

In contrast to HRP compound II, and consistent with *P. chrysosporium* MnP Compound II, the intensity of the Soret of *P. radiata* MnP3 Compound II is reduced to approximately 70% that of the resting enzyme.

To confirm the specific role of Mn (II) in the mechanism of the enzyme, the ability of Mn (II), and also Co (II), to reduce Compound II of MnP3 was examined. As shown in Figure 4.12b, the addition of 1 molar equivalent of Mn (II) in the form of $MnSO_4$ to MnP3 Compound II immediately reduced this intermediate back to the resting state enzyme. Unfortunately, very rapid reduction precluded the determination of the decay rate constant, which would have required stopped flow measurements. In contrast, the addition of 1 molar equivalent of $CoSO_4$ had only a little effect on the rate of decay of Compound II to the resting state enzyme. It took about 32 minutes for Co (II) to reduce about 71% of MnP3 Compound II with a decay rate constant of $0.0247 \pm 0.0002\ s^{-1}$ and a half-life of ~ 28 min compared to the control experiment, where Compound II was allowed to undergo auto-reduction to the resting state in the absence of any reductant, which took about 38 minutes to recover approximately 71% of absorbance value, with rate constant of $0.0171 \pm 0.0003\ s^{-1}$ and a half-life of ~ 41 min.

P. radiata MnP3 therefore appears to be a conventional H_2O_2-requiring, Mn (II) oxidising peroxidase with a conventional Mn^{2+}-binding site, which is sensitive to competitive inhibition by Cu^{2+} ions. However, it has a more alkaline range for catalysis than that reported for other MnP enzymes.

4.10 Effect of metal ions on the steady-state kinetics of *P. radiata* MnP3

Studies were conducted to probe the specificity of interaction of the Mn-binding site with other divalent metal ions. Experiments were carried out by the addition of another metal ion, at a fixed concentration to an assay reaction mixture either for Mn (II) activity or ABTS activity (sections 2.4.6 and 2.4.7). The full detail of the experimental method is described in section 2.4.9. The metal ions used were 0.8 mM Zn (II), 0.8mM Co (II) or 0.2 mM Cu (II), as well as 0.8mM Na as control. Both the sulphate (SO_4^{2-}) and chloride (Cl^-) forms of these metal ions were used, to distinguish between anion and cation effects.

4.10.1 Sensitivity of Mn (II) oxidation by *P. radiata* wild-type MnP3 to other metal ions.

Figure 4.13 and Table 4.8 show the effects of Na, Zn, Cu and Co as sulphates on the kinetic parameters of *P. radiata* wild-type MnP3 Mn (II) oxidation. The previous results for wild-type MnP3 gave the apparent Mn (II) K_m value for Mn oxidation as 0.17 ± 0.01mM and apparent k_{cat} as 175 ± 3 s^{-1}, in the absence of any added metal ion. Na and Co were found to have little effect on K_m while k_{cat} is increased slightly. In contrast, a significant 65 % increase in K_m and a slight increase in k_{cat} was observed in the presence of 0.8mM $ZnSO_4$, indicating a strong competitive effect on MnP3 activity with an inhibition constant (K_i) of 2.0 mM. $CuSO_4$ also affected both the K_m and apparent k_{cat}, increasing the K_m by 29% but decreasing the k_{cat} by 23%, suggesting a more mixed type of inhibition and giving ki values of 0.7 mM (competitive) and 0.7 mM (non-competitive).

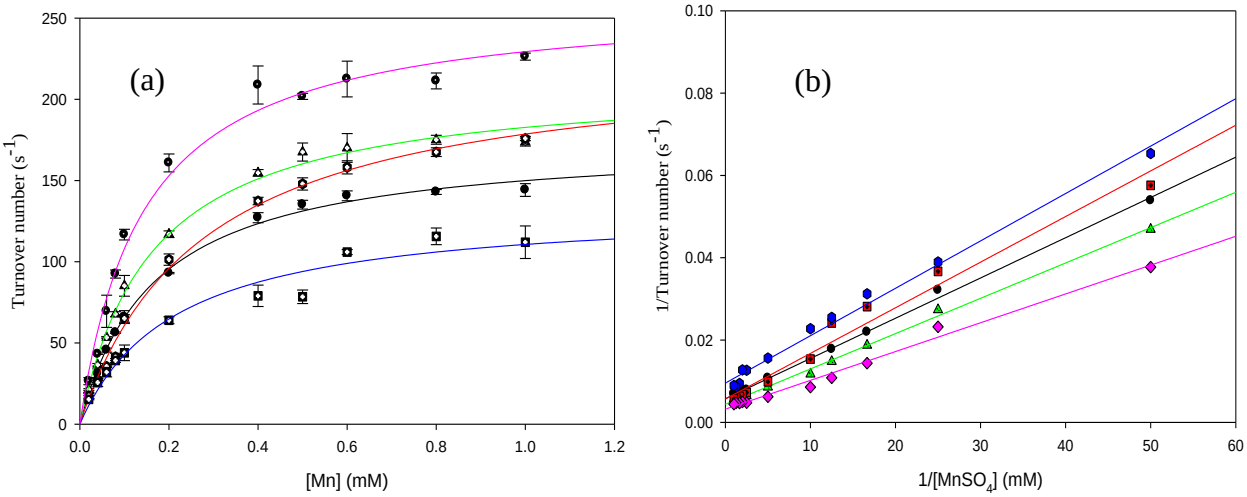

Figure 4.13: (a & b) Effect of metal ion addition as sulphates on Mn (II) oxidation by wild-type MnP3.

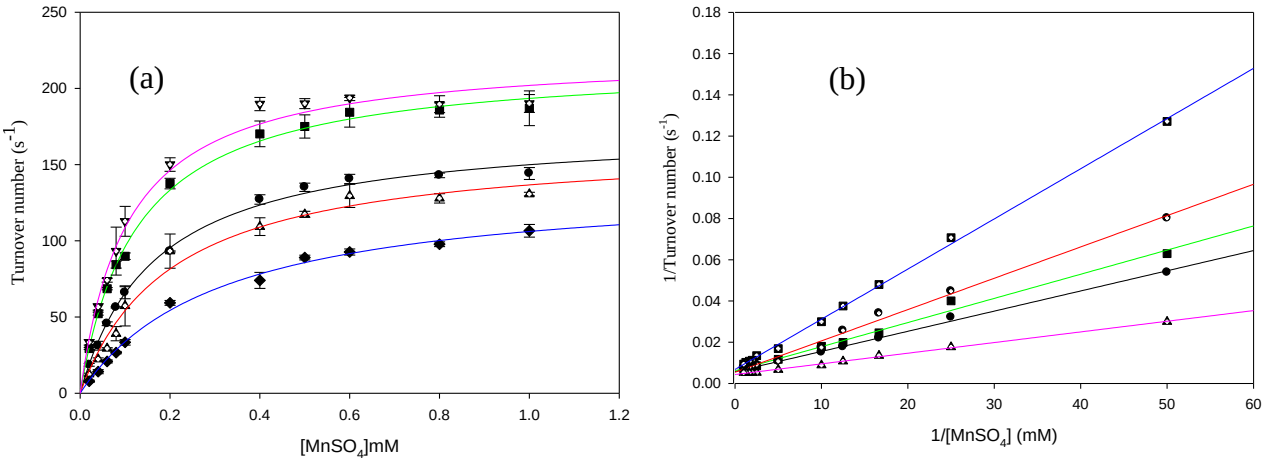

Figure 4.14: (c & d) Effect of metal ion addition as chloride on Mn (II) oxidation by wild-type MnP3.

(a). Turnover number against Mn (II) concentration. **(b)** Double – reciprocal plot of 1/ Turnover against 1/ [$MnSO_4$]. (—) $MnSO_4$ only, (—) 0.8m $NaSO_4$, (—) 0.8mM $ZnSO_4$, (—) 0.2mM $CuSO_4$, (—) 0.8mM $CoSO_4$. Reaction mixtures contained 100mM Na tartrate buffer , pH 5.0 at 25°C, fixed H_2O_2 concentration (0.1mM), varying $MnSO_4$ concentrations (0.02 – 1.0). (see sections 2.4.6 and 2.4.8).

Table 4.8: Kinetic parameters for Mn (II) oxidation by *P. radiata* wild-type MnP3 in the presence or absence of metal ions. Metals, 0.8mM Zn (II), 0.2mM Cu (II), and 0.8mM Co (II) in the form of sulphate ($SO_4 2^-$) or chloride (Cl^-) were used. 0.8Mm Sodium (Na_2SO_4 or NaCl) as control. Activity assays were performed in 100mM Na tartrate, pH 5.0 at 25°C using varying concentrations $MnSO_4$ and fixed 0.1mM H_2O_2 (see sections 2.4.6.and 2.4.9)

Metals added	K_m **(µM)**	k_{cat} **(s^{-1})**	k_{cat}/K_m **(mM^{-1} s^{-1})**	K_i **(mM)**	**Metals added**	K_m **(µM)**	k_{cat} **(s^{-1})**	k_{cat}/K_m **(mM^{-1} s^{-1})**	K_i **(mM)**
$MnSO_4$ only	167 ± 10	175 ± 3	1.0 x 10^6		**$MnSO_4$ only**	167 ± 10	175 ± 3	1.0 x 10^6	
0.8 mM Na_2SO_4	163 ± 12	212 ± 5	1.3 x 10^6	−	**0.8 mM NaCl**	127 ± 7	218 ± 3	1.7 x 10^6	−
0.8 mM $ZnSO_4$	275 ± 23	228 ± 7	8.3 x 10^5	2.0	**0.8 mM $ZnCl_2$**	204 ± 29	165 ± 8	8.1 x 10^5	3.6 13
0.2 mM $CuSO_4$	215 ± 44	135 ± 9	6.3 x 10^5	0.7 0.7	**0.2 mM $CuCl_2$**	313 ± 27	139 ± 5	4.4 x 10^5	0.2 0.8
0.8 mM $CoSO_4$	143 ± 16	262 ± 9	1.8 x 10^6	−	**0.8 mM $CoCl_2$**	106 ± 10	223 ± 6	2.1 x 10^6	−

Apparent kinetic parameters are estimated from the best fit to the Michaelis-Menten equation. K_i - inhibition constant. Two K_i (competitive and non competitive) are presented in the case of mixed inhibition.

Figure 4.14 (a & b) and Table 4.8 shows the summary of results in the presence of Na, Zn, Cu and Co as the chloride. NaCl and $CoCl_2$ were observed to behave like their sulphate counterparts, with small decrease in K_m and increase in apparent k_{cat} respectively. $ZnCl_2$ and $CuCl_2$ increased K_m by 22 % and 87 % respectively. A similar effect was observed for the sulphates counterpart. However, $ZnCl_2$ did not k_{cat} but $CuCl_2$ decreased k_{cat} by 21 %. It is important to note that the SO_4^{2-} and Cl^- salts of Cu behave differently; SO_4^{2-} is mildly stimulatory to activity, with a small effect on k_{cat}.

Chloride on its own has been found to have no strong effect on the activity of MnP3. However, chloride ions have been identified to be the cause of reduced activity in laccase (Bonomo *et al*., 2001). The inhibition of approximately 70% of veratryl alcohol oxidase activity by Cl^- (Tuisel *et al*., 1990). $CuCl_2$ and $ZnCl_2$ function as mixed inhibitors of MnP3 with K_i values of ~ 0.2 mM (competitive) and ~ 0.8 mM (non-competitive) for $CuCl_2$ while $ZnCl_2$ with K_i value of ~ 4 mM is more of a competitive inhibitor like the sulphate counterpart. In this context, mixed inhibition encompasses a broad range of behaviour and for simplicity is reported as having competitive and non-competitive components. Cu was by far the strongest competitive inhibitor.

4.10.2 Effect of metals ions on ABTS oxidation by *P. radiata* wild-type MnP3.

The effect of metal ions on the activity of wild-type MnP3 was also examined for ABTS oxidation. The apparent kinetic parameters (K_m and k_{cat}) obtained from the Michaelis-Menten plots (Figure 4.15) are presented in Table 4.9 together with the calculated inhibition constants (K_i) where discernable.

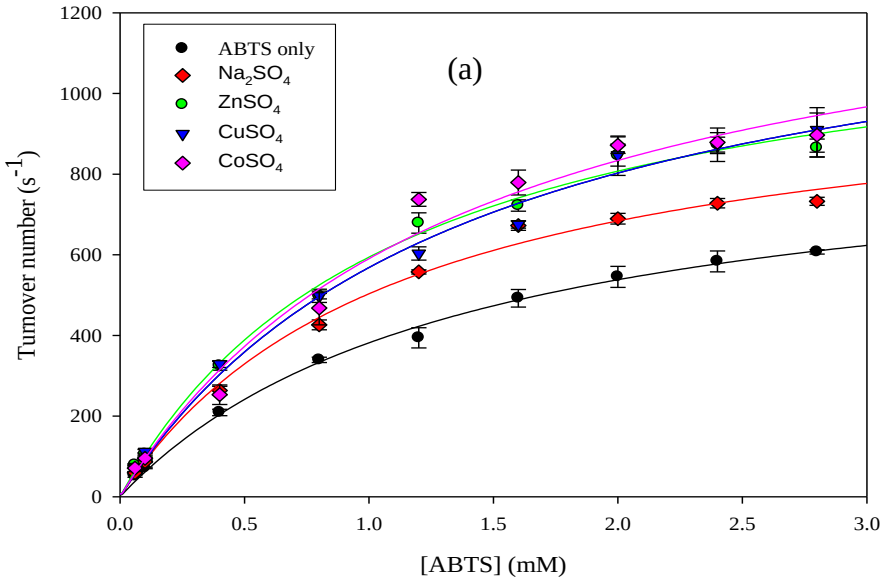

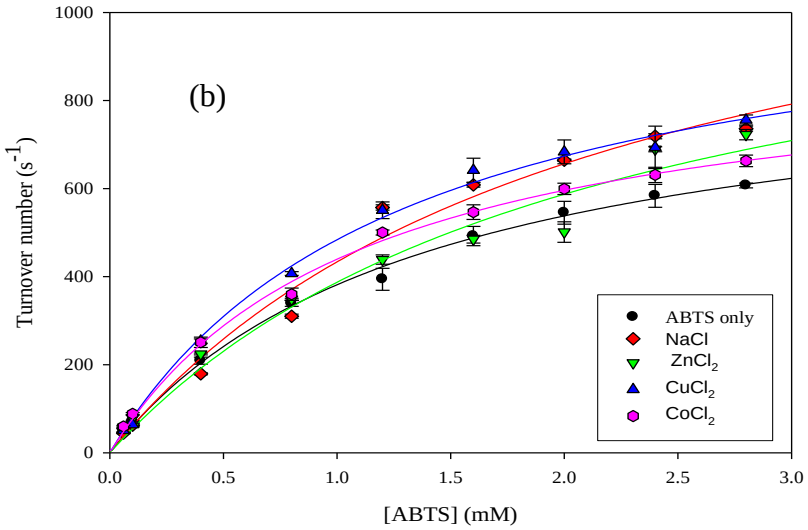

Figure 4.15 (a & b): Effect of metal ion addition on ABTS oxidation of wild-type MnP3 (a) (—) (0.06 – 2.8mM) ABTS, (—) 0.8mM Na_2SO_4, (—) 0.2mM $CuSO_4$, (—) 0.8mM $CoSO_4$, (—) ZnSO4 and (b) (—) (0.06 – 2.8mM) ABTS, (—) 0.08Mm NaCl, (—) 0.8mM $ZnCl_2$, (—) 0.2mM $CuCl_2$, (—) 0.8mM $CoCl_2$. Reaction mixtures contained 100mM Na tartrate buffer, pH 5.0, at 25°C fixed H_2O_2 concentration (0.1mM) and varying ABTS concentration (see section 2.4.7 and 2.4.8). (a) Metals as $SO4^{2-}$. (b) Metals as Cl^-.

Table 4.9: Kinetic parameters for ABTS oxidation by *P. radiata* wild-type MnP3 in the presence or absence of metal ions. Metals, 0.8mM Zn, 0.2mM Cu, and 0.8mM Co in the form of sulphate (SO_4^{2-}) or Chloride (Cl^-) were used. 0.8mM Sodium (Na_2SO_4 or NaCl) as control. Activity assays were performed in 100mM Na tartrate, pH 5.0 at 25°C using varying concentrations $MnSO_4$ and fixed 0.1mM H_2O_2 (see sections 2.4.7 and 2.4.9).

Metals added	K_m **(µM)**	k_{cat} **(s^{-1})**	k_{cat}/K_m **($mM^{-1}\ s^{-1}$)**	K_i **(mM)**	**Metals added**	K_m **(µM)**	k_{cat} **(s^{-1})**	k_{cat}/K_m **($mM^{-1}\ s^{-1}$)**	K_i **(mM)**
$MnSO_4$ only	1390 ± 139	912 ± 41	6.6 X 10^5		**$MnSO_4$ only**	1390 ± 139	912 ± 41	6.6 X 10^5	
0.8 mM Na_2SO_4	1120 ± 142	1067 ± 55	9.5 X 10^5	—	**0.8 mM NaCl**	2112 ± 580	1350 ± 197	6.4 X 10^5	1.5
0.8mM $ZnSO_4$	1121 ± 141	1260 ± 153	1.1 X 10^6	—	**0.8 mM $ZnCl_2$**	2131 ± 737	1213 ± 35	5.7 X 10^5	1.5
0.2 mM $CuSO_4$	1404 ± 337	1419 ± 153	1.0 X 10^6	—	**0.2 mM $CuCl_2$**	1105 ± 103	926 ± 35	8.4 X 10^5	−
0.8 mM $CoSO_4$	1402 ± 220	1365 ± 96	9.7 X 10^5	—	**0.8 mM $CoCl_2$**	1291 ± 143	1109 ± 53	8.6 X 10^5	−

Apparent kinetic parameters are estimated from the best fits to the Michaelis-Menten equation. K_i, inhibition constant. Two K_i (competitive and non competitive) are presented in the case of mixed inhibition.

The K_m value for ABTS oxidation in the absence of any metal ion was found to be 1.4 ± 0.1 mM and the apparent k_{cat} 912 ± 41 s^{-1}. Na_2SO_4 and $ZnSO_4$ were observed to have a similar weak effect on *Km*, decreasing it by ~ 20%. Both salts had a stimulatory effect on apparent k_{cat} increasing it by approximately 17% and 38% respectively. $CuSO_4$ and $CoSO_4$ separately had no significant effect on K_m but their apparent k_{cat} values were significantly increased by ~ 50 % each.

Similarly, Table 4.9 also shows a summary of apparent kinetic parameters for ABTS oxidation in the presence of $ZnCl_2$, $CoCl_2$ and $CuCl_2$ as effectors. NaCl was used as control. The results show a significant increase in the both the K_m and k_{cat} values in the presence NaCl and $ZnCl_2$. NaCl and $ZnCl_2$ increased the K_m by 52% and 53% respectively, while the apparent k_{cat} was also increased by 48 % and 33 % respectively. This type of behaviour is not simple but has a competitive component (Table 4.9) with K_i values of ~ 1.5 mM for both NaCl and $ZnCl_2$ respectively. It is difficult to disentangle general ionic strength effects. $CuCl_2$ appears to have a slight stimulatory effect on apparent k_{cat}, ~ 22 %, while K_m is decreased slightly. It appears that chloride on it own has a significant effect on the K_m of the enzyme for ABTS oxidation. As observed, Na, Zn, Co and Cu appear to be weakly stimulatory. However, there are generalised ionic strength effects. A number of metals are mildly stimulatory of ABTS activity including Na suggesting that a general cation effect possibly a charge neutralisation effect may be involved. The affect of Zn and Cu are however specific to Mn (II) oxidation.

4.10.3 Sensitivity of Mn (II) oxidation by MnP3 mutant, E40H to other metal ions.

It was of interest to see whether the change of ligand set at the Mn oxidation site resulted in changes to metal ion specificity. Michaelis-Menten parameters for the enzymatic reaction in the presence and absence of metal ions were determined using E40H MnP3 (Figure 4. 16a,

Table 4.10). The K_m value for Mn^{2+} of the E40H enzyme was 11.1 ± 0.4 mM, whereas k_{cat} value was 12.0 ± 0.2 s^{-1}, with no metal ion added.

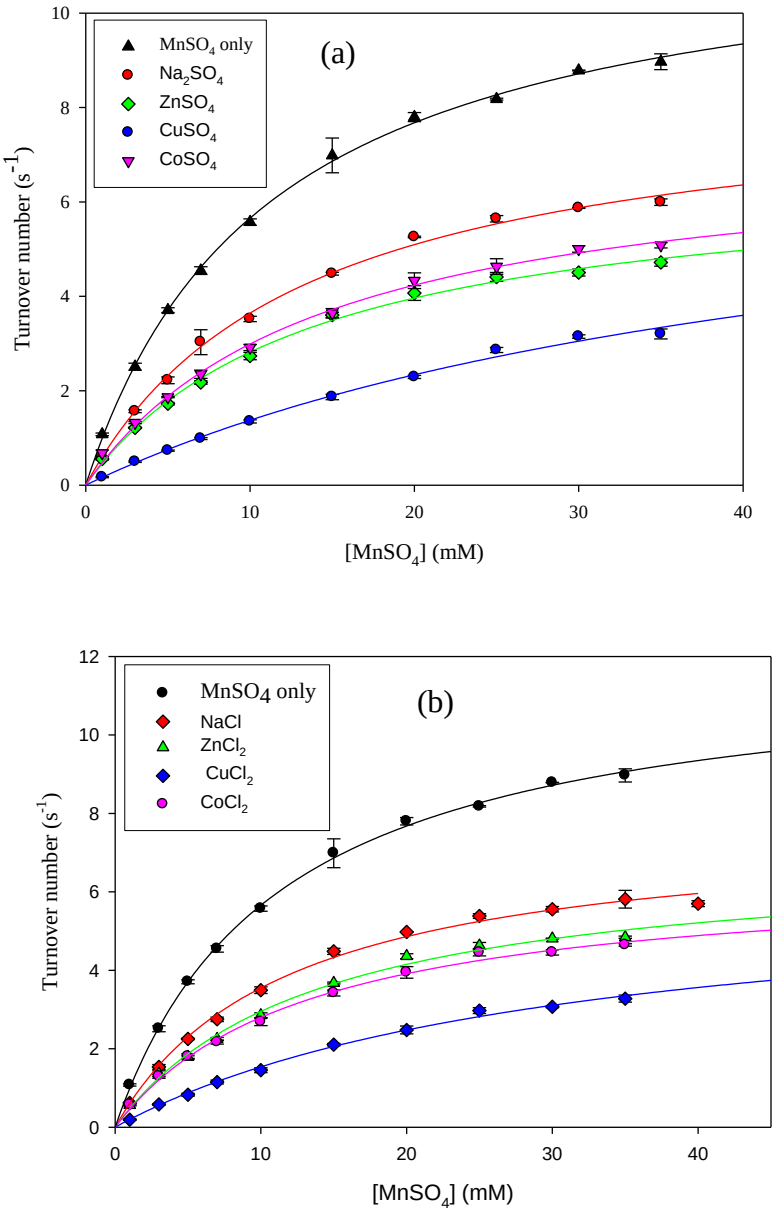

Figure 4.16 (a & b): Effect of metal ion addition on Mn (II) oxidation of MnP3 mutant, E40H. **(a)** 0.8mM $ZnSO_4$ (—), 0.2mM $CuSO_4$ (—), 0.8mM $CoSO_4$ (—) as 0.8Mm $NaSO_4$ (—). **(b)** 0.8mM $ZnCl_2$ (—), 0.2mM $CuCl_2$ (—), 0.8mM $CoCl_2$ (—) and 0.8Mm NaCl (—). The activity assay performed in 100mM Na tartrate buffer, pH 5.0 at 25°C using fixed H_2O_2 and varying concentrations MnSO4 (—) (see section 2.4.7 and 2.4.8). (a) Metals as SO_4^{2-} , (b) Metals as Cl^-.

Table 4.10: Kinetic parameters for manganese (II) oxidation by *P. radiata* MnP3 mutant, E40H in the presence or absence of metal ions Metals, 0.8mM Zn, 0.2mM Cu, and 0.8mM Co in the form of sulphate (SO_4^{2-}) or Chloride (Cl^-) were used. 0.8Mm Sodium (Na_2SO_4 or NaCl) as control. Activity assays were performed in 100mM Na tartrate, pH 5.0 at 25°C using varying concentrations $MnSO_4$ and fixed concentrations 0.1mM H_2O_2. (see sections 2.4.6 and 2.4.9).

Metals added	K_m **(mM)**	k_{cat} **(s^{-1})**	k_{cat}/K_m **(mM^{-1} s^{-1})**	K_i **(mM)**	**Metals added**	K_m **(mM)**	k_{cat} **(s^{-1})**	k_{cat}/K_m **(mM^{-1} s^{-1})**	K_i **(mM)**
$MnSO_4$ only	11 ± 0.4	12 ± 0.2	1.01		**$MnSO_4$ only**	11 ± 0.4	12.0 ± 0.2	1.08	
0.8 mM Na_2SO_4	13.2 ± 0.8	8.5 ± 0.2	0.63	4.4 2.0	**0.8 mM NaCl**	12.0 ± 0.8	8.0 ± 0.2	0.7	10 1.6
0.8 mM $ZnSO_4$	14.0 ± 1	7.0 ± 0.2	0.5	3.0 1.1	**0.8 mM $ZnCl_2$**	14.0 ± 1.3	7.0 ± 0.3	0.5	3.0 1.1
0.2 mM $CuSO_4$	47.0 ± 7	8.0 ± 0.8	0.2	0.06 0.40	**0.2 mM $CuCl_2$**	31.2 ± 3.3	6.3 ± 0.4	0.2	0.1 0.2
0.8 mM $CoSO_4$	14.3 ± 1	7.3 ± 0.2	0.5	2.8 1.2	**0.8 mM $CoCl_2$**	13.2 ± 1.1	6.5 ± 0.2	0.5	4.2 1

Apparent kinetic parameters are estimated from the best fits to the Michaelis-Menten equation. Two K_i (competitive and non competitive) are presented in the case of mixed inhibition.

Figure 4.16 and Table 4.10 show the effect of Na, Zn, Cu and Co on activity of MnP3 mutant variant E40H in the form of sulphates during Mn (II) oxidation. In the presence of Na, Zn and Co the values of apparent K_m slightly increased while apparent k_{cat} values decreased. The inhibition of Mn (II) oxidation by these metals was more non-competitive in nature. Cu was found to significantly increase apparent K_m by ~ 300%, and decrease apparent k_{cat} by 36% , indicating a mixed type of inhibition with K_i values of 0.06 mM (strongly competitive) and 0.4 mM (non-competitive).

Similarly, Figure 4.16b and Table 4.10 presents the kinetic parameters of Mn (II) oxidation in the presence of Na, Zn and Co as chlorides. These results follow a similar trend observed for the sulphate counterpart with The K_i values for a more non-competitive inhibition ranging from 0.2 – 1 mM. $CuCl_2$ also behaved similarly to its sulphate counterpart. This behaviour implies a decrease in the apparent affinity of the enzyme for the substrate. The K_i values for the competitive component of ~ 10 mM, ~ 3 mM, ~ 0.1 mM, and ~ 4.0 mM for NaCl, $ZnCl_2$, $CuCl_2$ and $CoCl_2$ respectively.

It can be seen that Cu (II) gave the largest decrease on the reaction rate with corresponding strongest inhibition due to the smallest K_i (see Table 4.10).

This effect of Cu ions on the activity of MnP3 mutant enzyme, E40H is consistent with that observed for the wild-type MnP3 enzyme, where Cu was by far the strongest competitive inhibitor of the enzyme.

4.10.4 Sensitivity to metal ions of Mn (II) oxidation by MnP3 mutant, E44H.

Steady-state kinetics was measured for manganese (II) oxidation by MnP3 mutant, E44H in the presence and absence of Na, Zn, Cu and Co as described previously, all followed apparent Michaelis-Menten kinetics and kinetic parameters, catalytic efficiency and the inhibition constant (K_i) are shown in Table 4.11, Figure 4.17a.

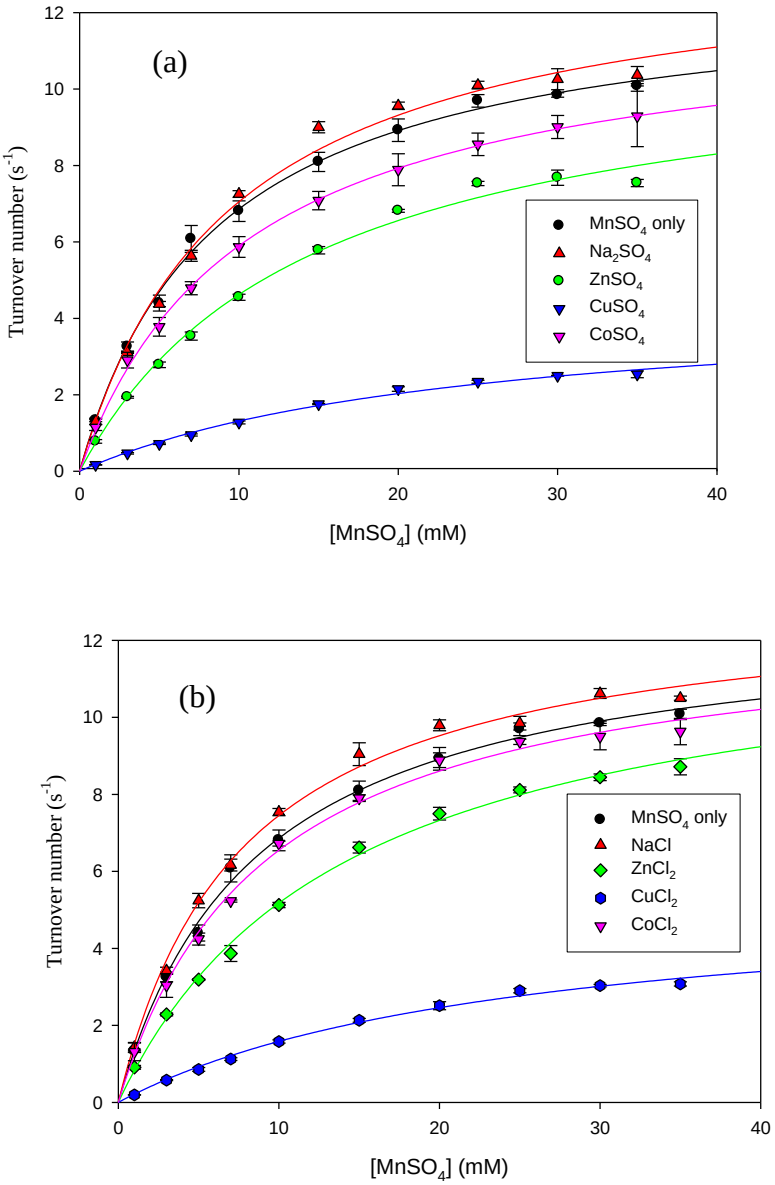

Figure 4.17 (a & b): Effect of metal ion addition on Mn (II) oxidation of MnP3 mutant enzyme, E44H. (a) (—) 0.8mM $ZnSO_4$, (—) 0.2mM $CuSO_4$, (—) 0.8mM $CoSO_4$ (—) 0.8mM $NaSO_4$. **(b)** 0.8mM $ZnCl_2$ (—), 0.2mM CuC_2 (—), 0.8mM $CoCl_2$ (—) and 0.8Mm $NaSO_4$ (—). Reaction mixture contained 100mM Na tartrate buffer, pH 5.0, fixed H_2O_2 concentration (0.1mM), and varying $MnSO_4$ concentration(see sections 2.4.7 and 2.4.8). (a) Metals as SO_4^{2-} ; (b) Metals as Cl^-

Table 4.11: Kinetic parameters for manganese (II) oxidation by *P. radiata* MnP3 mutant, E44H in the presence or absence of metal ions. Metals, 0.8 mM Zn, 0.2 mM Cu, and 0.8 mM Co in the form of sulphate (SO_4^{2-}) or Chloride (Cl^-) were used. 0.8 mM Sodium (Na_2SO_4 or NaCl) as control. The activity assay performed in 100 mM Na tartrate, pH 5.0 at 25°C using varying concentrations $MnSO_4$ and fixed concentration 0.1 mM H_2O_2. (see sections 2.4.6 and 2.4.9).

Metals added	K_m **(mM)**	k_{cat} **(s^{-1})**	k_{cat}/K_m **(mM^{-1} s^{-1})**	K_i **(mM)**	**Metals added**	K_m **(mM)**	k_{cat} **(s^{-1})**	k_{cat}/K_m **(mM^{-1} s^{-1})**	K_i **(mM)**
$MnSO_4$ only	9 ± 0.5	13 ± 0.3	1.5		**$MnSO_4$ only**	9 ± 0.5	13 ± 0.3	1.5	
0.8 mM $NaSO_4$	10 ± 1	14 ± 0.5	1.5	6.8	**0.8 mM NaCl**	7.7 ± 0.5	13 ± 0.3	1.7	−
0.8 mM $ZnSO_4$	15 ± 1.4	11 ± 0.5	0.8	1.1 6.5	**0.8 mM $ZnCl_2$**	14 ± 1	13 ± 0.4	0.9	1.2
0.2 mM $CuSO_4$	24 ± 3	5 ± 0.3	0.2	0.1 0.1	**0.2 mM $CuCl_2$**	25 ± 3	6 ± 0.3	0.2	0.1 0.2
0.8 mM $CoSO_4$	1 ± 0.4	12 ± 0.2	1.2	3.4 16.0	**0.8 mM $CoCl_2$**	9 ± 0.6	13 ± 0.3	1.4	−

Apparent kinetic parameters are estimated from the best fits to the Michaelis-Menten equation. Two K_i (competitive and non competitive) are presented in the case of mixed inhibition.

In the absence of any metal ions, the K_m during Mn (II) oxidation was 8.5 ± 0.5 mM and the *kcat* was 12.7 ± 0.3 s^{-1}. Na_2SO_4, had little effect on K_m and the apparent $k_{cat.}$

$ZnSO_4$, $CuSO_4$ and $CoSO_4$ were found to significantly increase K_m by ~ 71 %, ~ 185 % and ~ 24 % respectively. $CuSO_4$ again significantly decreased apparent k_{cat} by 65% relative to the control. Thus, $ZnSO_4$, $CuSO_4$ inhibited the activity of E44H with a mixed inhibition effect in both K_m and k_{cat} with K_i values of ~ 1.0 mM (strongly competitive) and ~ 6 mM (non-competitive) for Zn; and ~ 0.1 mM (competitive) and ~ 0.1 mM (non-competitive) for Cu. Cu had the strongest inhibitory effect on E44H MnP3 mutant variant.

Similarly, the effect of metal ions on the activity of E44H was also studied using Na, Zn, Cu and Co in the chloride form. NaCl showed little effect on K_m. $ZnCl_2$ significantly increased K_m by 67% with no detectable effect on k_{cat}. The Plot in Figure 4.17b shows a pure competitive inhibition with a calculated K_i value of ~ 1.2 mM. $CuCl_2$ strongly increased the K_m by a factor of 2 and also significantly decreased the apparent k_{cat} by 54% compared to control. Therefore, Cu remains the strongest inhibitor of E44H with an extremely mixed effect in both K_m and apparent k_{cat} with inhibition constants of ~ 0.1 mM (competitive) and ~ 0.2 mM (non-competitive). It is note worthy that the $SO4^{2-}$ and Cl^- salt of all the metal ions behave very similarly with E44H mutant.

4.10.5 Sensitivity of Mn (II) oxidation by MnP3 mutant, E40H/E44H to metals ions.

In the absence of any metal ion effector, the K_m and the k_{cat} for Mn (II) oxidation by E40H/E44H was 20 ± 2 and 2 ± 0.1 s^{-1} respectively. The results of kinetic experiments on oxidation of Mn (II) by E40H/E44H in the presence of metal ions are presented in Figure 4.18a and Table 4.12.

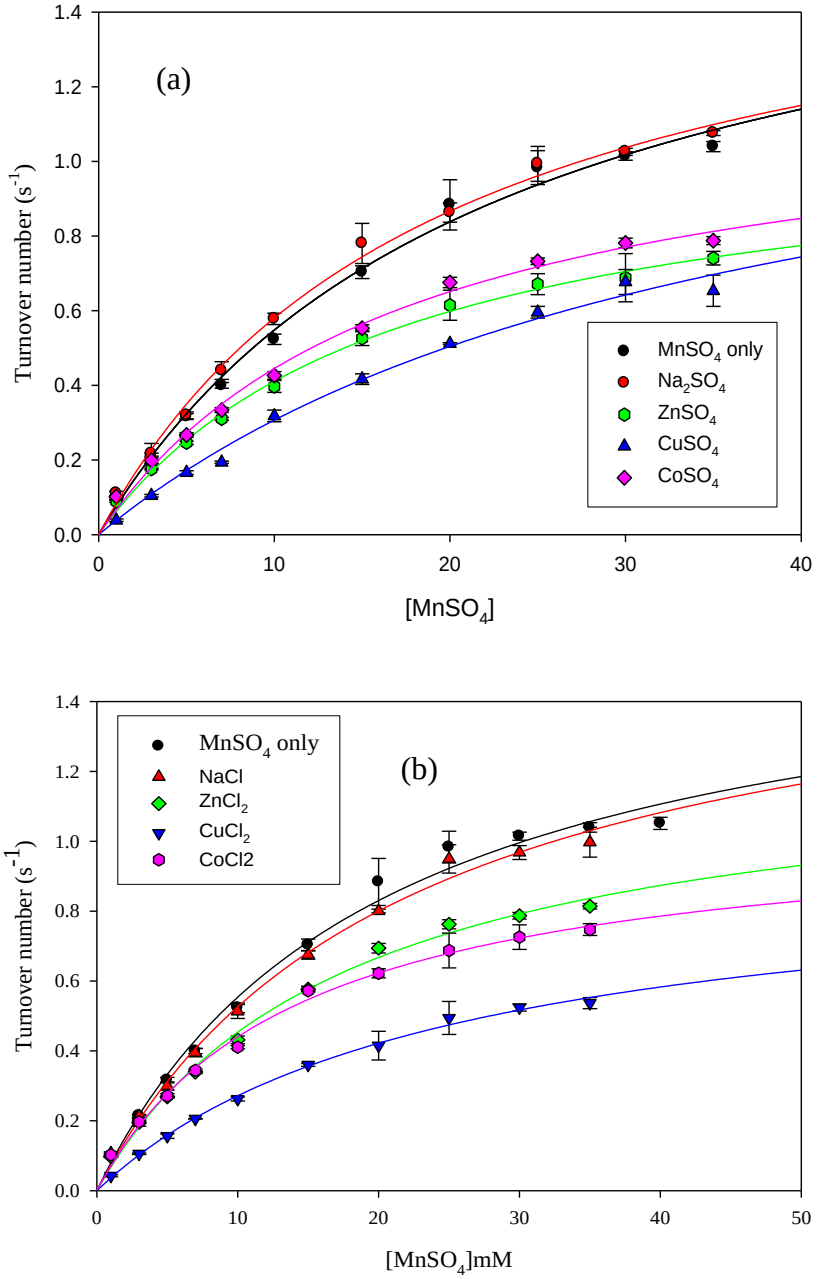

Figure 4.18 (a & b): Effect of metal ion addition on Mn (II) oxidation of MnP3 mutant enzyme, E40H/E44H. (a) (—) 0.8mM $ZnSO_4$, (—) 0.2mM $CuSO_4$, and (—) 0.8mM $CoSO_4$, and (—) 0.8mM $NaSO_4$. (b) (—) 0.8mM $ZnCl_2$, (—) 0.2mM $CuCl_2$, and (—) 0.8mM $CoCl_2$ and (—) 0.8mM NaCl. Activity assays were performed in 100mM Na tartrate, pH 5.0 at 25°C using varying concentrations (—) $MnSO_4$ and fixed concentration (0.1mM) H_2O_2. (a) Metals as SO_4^{2-} ; (b) Metals as Cl^-.

Table 4.12: Kinetic parameters for manganese (II) oxidation by *P. radiata* MnP3 mutant, E40H/E44H in the presence or absence of metal ions. Metals, 0.8mM Zn, 0.2mM Cu, and 0.8mM Co in the form of sulphate (SO_4^{2-}) or Chloride (Cl^-) were used. 0.8Mm Sodium (Na_2SO_4 or NaCl) as control. The activity assay performed in 100mM Na tartrate, pH 5.0 at 25 °C using varying concentrations $MnSO_4$ and fixed concentration 0.1mM H_2O_2. (see sections 2.4.6 and 2.4.9).

Metals added	K_m **(mM)**	k_{cat} **(s^{-1})**	k_{cat}/K_m **(mM^{-1} s^{-1})**	K_i **(mM)**	**Metals added**	K_m **(mM)**	k_{cat} **(s^{-1})**	k_{cat}/K_m **(mM^{-1} s^{-1})**	K_i **(mM)**
$MnSO_4$ only	20 ± 2	1.7 ± 0.1	0.08		**$MnSO_4$ only**	20 ± 3	1.7 ± 0.09	0.08	
0.8 mM Na_2SO_4	19 ± 2	1.7 ± 0.07	0.09	–	**0.8 mM NaCl**	22 ± 2	1.7 ± 0.09	0.08	8.9
0.8 mM $ZnSO_4$	17 ± 1	1.1 ± 0.04	0.07	1.6	**0.8 mM $ZnCl_2$**	18 ± 2	1.3 ± 0.06	0.07	2.5
0.2 mM $CuSO_4$	36 ± 2	1.4 ± 0.2	0.04	0.2 1.8	**0.2 mM $CuCl_2$**	25 ± 2	0.9 ± 0.04	0.04	0.8 0.3
0.8 mM $CoSO_4$	17 ± 2	1.2 ± 0.06	0.07	2.1	**0.8 mM $CoCl_2$**	14 ± 1	1.1 ± 0.04	0.07	0.4

Apparent kinetic parameters are estimated from the best fits to the Michaelis-Menten equation. Two K_i (competitive and non competitive) are presented in the case of mixed inhibition.

$ZnSO_4$ and $CoSO_4$ had only small effect on K_m but $ZnSO_4$ and $CoSO_4$ appear more non-competitive with Mn (II) with inhibition constants of ~ 1.6 and 2.1 mM respectively. On the other hand, $CuSO_4$ significantly increased K_m by 82%, and slightly decreased the apparent k_{cat} by ~ 15 %. This effect of Cu on kinetic parameters of E40H/E44H shows that $CuSO_4$ is a more competitive inhibitor with K_i ~ 0.2 mM. The investigation on the effect of Na, Zn, Cu and Co as the chloride was also conducted and the results presented in Table 4.12. $CoSO_4$ had a decreasing effect on both K_m and apparent k_{cat}. Thus, decreasing them by 29% and 36% respectively.

The steady-state kinetic results in the presence of $CuCl_2$ and $CoCl_2$ (Figure 4.18b and Table 4.12), showed that $CoCl_2$ was strongly non-competitive, with inhibition constants of 0.4 mM. This implies that Co does not compete with Mn (II) for the Mn-binding site. It is noteworthy that the chloride salt of Co behaved differently during Mn (II) oxidation as chloride salt was more inhibitory. $CuCl_2$ was observed to increase the K_m by about 25 % and reduced the apparent k_{cat} by ~ 43 %, again showing a mixed type of inhibition with K_i ~ 0.8 mM (competitive) and ~ 0.3 mM (non-competitive). The effect of Cu on the activity of E40H/E44H was consistent with the results obtained for wild-type MnP3 and the mutants, E40H and E44H.

4.10.6 Sensitivity of Mn (II) oxidation by MnP3 mutant, D186H to metal ions.

In the absence of any added metal ion the K_m and the k_{cat} for Mn (II) oxidation were 23 ± 4 mM and 0.84 ± 0.07 s^{-1} respectively, while the catalytic efficiency was 0.036 $mM^{-1}\mathbf{s^{-1}}$. Figure 4.19 (a and b) and Table 4.13 shows the effect of addition of Na, Zn (II), Cu (II) and Co (II) as sulphates or chlorides on activity of *P. radiata* MnP3 mutant, D186H.

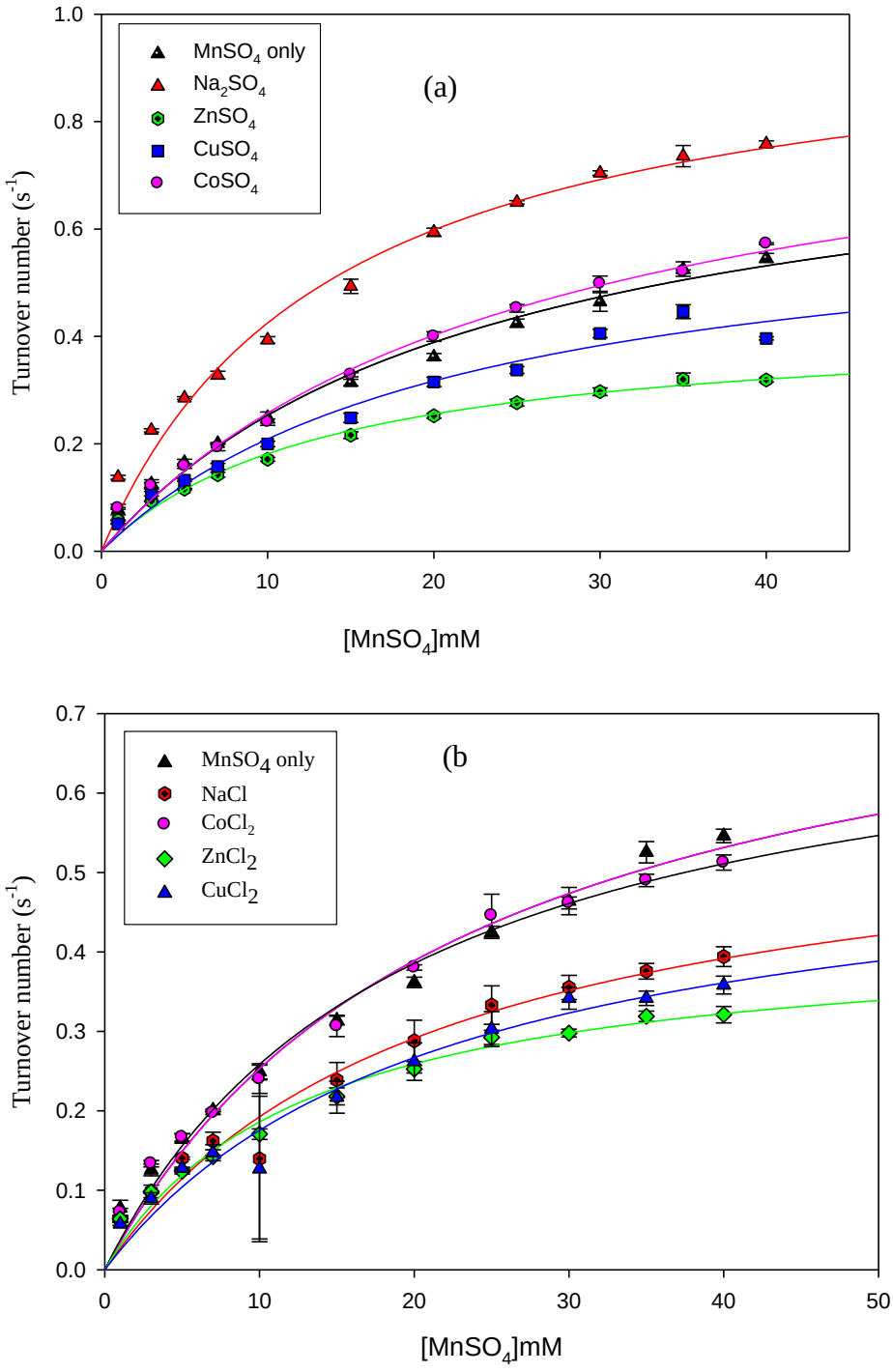

Figure 4.19 (a & b): Plots showing effect of metal ion effectors Mn (II) oxidation by MnP3 mutant enzyme, D186H. (a) (—) 0.8 mM $ZnSO_4$, (—) 0.2 mM $CuSO_4$, and (—) 0.8 mM $CoSO_4$, and (—) 0.8 mM $NaSO_4$. (b) (—) 0.8 mM $ZnCl_2$, (—) 0.2 mM $CuCl_2$, and (—) 0.8 mM $CoCl_2$ and (—) 0.8mM NaCl. Activity assays performed in 100 mM Na tartrate, pH 5.0 at 25°C using varying concentrations (—) $MnSO_4$ and fixed H_2O_2 concentration (0.1mM). (a) Metals as SO_4^{2-} ; (b) Metals as Cl^-.

Table 4.13: Kinetic parameters for manganese (II) oxidation by *P. radiata* MnP3 mutant, D186H in the presence or absence of metals Metal ion, 0.8 mM Zn, 0.2 mM Cu, and 0.8 mM Co in the form of sulphate (SO_4^{2-}) or Chloride (Cl^-) were used. 0.8 mM Sodium (Na_2SO_4 or NaCl) as control. Activity assays performed in 100mM Na tartrate, pH 5.0 at 25°C using varying concentrations $MnSO_4$ and fixed concentration (0.1mM) H_2O_2. (see sections 2.4.6 and 2.4.9).

Metals added	K_m **(mM)**	k_{cat} **(s^{-1})**	k_{cat}/K_m **(mM^{-1} s^{-1})**	K_i **(mM)**	**Metals added**	K_m **(mM)**	k_{cat} **(s^{-1})**	k_{cat}/K_m **(mM^{-1} s^{-1})**	K_i **(mM)**
$MnSO_4$ only	23 ± 4	0.84 ± 0.1	0.04		**$MnSO_4$ only**	23 ± 4	0.8 ± 0.07	0.04	
0.8 mM Na_2SO_4	14 ± 2	1.0 ± 0.1	0.07		**0.8 mM NaCl**	21 ± 5	0.6 ± 0.07	0.03	2.1
0.8 Zn SO_4	14 ± 2	0.4 ± 0.2	0.03	0.8	**0.8 mM $ZnCl_2$**	13 ± 2	0.4 ± 0.3	0.03	0.8
0.2 mM $CuSO_4$	22 ± 5	0.7 ± 0.1	0.03	0.7	**0.2 mM $CuCl_2$**	22 ± 6	0. 6 ± 0.07	0.03	0.4
0.8 mM $CoSO_4$	26 ± 4	0.9 ± 0.1	0.04	7.1	**0.8 mM $CoCl_2$**	19 ± 3	0.8 ± 0.05	0.04	7.6

Apparent kinetic parameters are estimated from the best fits to the Michaelis-Menten equation. Two K_i (competitive and non competitive) are presented in the case of mixed inhibition.

The results show Na_2SO_4 as having stimulatory effect on MnP3 activity, as K_m decreased by approximately ~ 41% while apparent k_{cat} increased by 20 %. In contrast, $ZnSO_4$ competitively inhibited D186H decreasing K_m by 41% and decreased the apparent k_{cat} by approximately 49 %. $CoSO_4$ had little effect on D186H activity. $ZnSO_4$ and $ZnCl_2$ behaved similarly with a decreasing effect on both K_m and k_{cat}, indicating non-competitive inhibition effect with K_i ~ 0.8 mM. $CuSO_4$ and $CuCl_2$ behaved in a similar way to D186H mutant, with non-competitive inhibition having K_i approximately 0.7 mM and 0.4 mM respectively. What is notable is that the strong competitive effect of Cu^{2+} is largely removed in the D186H variant. Cu behaves very similarly to Zn^{2+} unlike the wild-type and previous variants.

4.10.7 Sensitivity of MnP3 mutant, D186N to metal ion addition.

Mn (II) oxidation catalyzed by a *P. radiata* MnP3 mutant, D186N in the presence and absence of Na_2SO_4, $ZnSO_4$, $CuSO_4$, and $CoSO_4$ follow apparent Michaelis-Menten kinetics and the kinetic parameters are shown in Table 4.14.

Table 4.14: Kinetic parameters for manganese (II) oxidation by *P. radiata* MnP3 mutant, D186N in the presence or absence of metal ions. Metals, 0.8 mM Zn, 0.2 mM Cu, and 0.8 mM Co in the form of sulphate (SO_4^{2-}) or Chloride (Cl^-) were used. 0.8 mM Sodium (Na_2SO_4 or NaCl) as control. Activity assay performed in 100 mM Na tartrate, pH 5.0 at 25 °C using varying concentrations $MnSO_4$ and fixed concentration 0.1 mM H_2O_2. (see sections 2.4.6 and 2.4.9).

Metals added	K_m **(mM)**	k_{cat} **(s^{-1})**	k_{cat}/K_m **(mM^{-1} s^{-1})**	K_i **(mM)**	**Metals added**	K_m **(mM)**	k_{cat} **(s^{-1})**	k_{cat}/K_m **(mM^{-1} s^{-1})**	K_i **(mM)**
$MnSO_4$ only	30.0 ± 4	8.0 ± 0.5	0.3		**$MnSO_4$ only**	30 ± 4	8.0 ± 0.5	0.26	
0.8 mM Na_2SO_4	24 .0 ± 3	7.3 ± 0.5	0.3		**0.8 mM NaCl**	26.4 ± 3	8.0 ± 0.5	0.30	
0.8 Zn SO_4	26.0 ± 3	6.2 ± 0.4	0.2	2.8	**0.8 mM $ZnCl_2$**	26.0 ± 4	6.2 ± 0.4	0.24	2.7
0.2 mM $CuSO_4$	34.0 ± 3	7.1 ± 0.3	0.2	1.6 1.6	**0.2 mM $CuCl_2$**	36.0 ± 5	7.3 ± 0.5	0.20	1.06 2.09
0.8 mM $CoSO_4$	23.0 ± 3	7.0 ± 0.4	0.3	5.6	**0.8 mM $CoCl_2$**	24.0 ± 3	7.0 ± 0.4	0.30	4.1

Apparent kinetic parameters are estimated from the best fits to the Michaelis-Menten equation. Two K_i (competitive and non competitive) are presented in the case of mixed inhibition.

The K_m and k_{cat} values for Mn (II) oxidation conducted in the absence of any metal ion effector were 30.3 ± 4 mM and 8.0 ± 0.5 s^{-1} respectively. $NaSO_4$ and $CoSO_4$ were found to slightly decrease the K_m and k_{cat} by ~ 22 and ~ 23 % respectively, whereas $ZnSO_4$ and $CuSO_4$ did not have any strong effects and the variants were generally very sensitive to inhibition by any metal ion. The metal binding site is presumably largely non functional regardless of metal present. The results for the effects of metal ions as chlorides on the activity of D186N showed a very similar trend to that observed for the sulphate counterparts (Table 4.14). NaCl had little effect. Like the sulphate counterparts, $ZnCl_2$, $CoCl_2$ and $CuCl_2$ gave only weak effects.

It was generally observed that inhibition by metal ions was not in itself in some cases a highly stringent process, as ions, which inhibited the enzyme activity, also had a concomitant stimulatory effect on activity in some cases. The degree of inhibition or stimulation was different for each metal ion relative to enzyme. The dual effects of metals to enzyme activity could also be due to a differential affinity of the metal ion for various states of the enzyme (Arnold and Zhang, 1994). Even sodium, the univalent ion that was used as control was occasionally observed to influence the activity of the *P. radiata* enzymes either by stimulation or inhibition.

The ionic radii, ligand preference and co-ordination numbers of the ions involved in this study are crucial. Ionic radii of 0.072 nm (0.72Å) for Co^{2+} and Cu^{2+}, 0.074 nm (0.74 Å) for Zn^{2+} , and 0.08 nm (0.80 Å) for Mn (II) (Coolbear *et al*., 1992). Ionic radius partially determines an ion's ability to occupy a metal-binding site at the active centre (whether to promote or inhibit enzyme activity). The importance of ionic radii and stereochemical requirements in determining the suitability of a metal ion for substitution was demonstrated by Arnone *et al*., (1971). Ions with ionic radii close to the native ion occupying the specific metal-binding site exhibit good stimulation of the enzyme.

The metal ions, Mn (II), Co (II), Zn (II), and Cu (II) belong to the first transition series in the periodic table of elements. Manganese (II) ions have some preference for octahedral coordination; while copper (II) ions tend to form tetragonal or square-planar complexes. Both zinc and cobalt (II) ions prefer lower coordination numbers (tetrahedral coordination), although cobalt (II) ions do not form a number of octahedral complexes. With regard to ligand preferences for these metal ions, the manganese (II) ion accepts ligands with either oxygen or nitrogen donor atoms, but the bivalent metal ions to the right of the transitions series show an increasing preference for ligands with nitrogen donor atoms. Generally, the Co (II), Cu (II) and Zn (II) are known to show an increasing preference for ligands with nitrogen or sulphur ligands. This suggests that inhibition of MnP3 by metal ions is dependent on the preferred ligand types and the co-ordination number of the ion, the former perhaps being the dominant factor. The strongest inhibition of the enzyme by Cu (II) compared to Zn (II) and Co (II) may be a consequence of its tetragonal coordination preference. The inhibition may also reflect increase in the number of bonding interactions or effective binding of the inhibitors to the enzyme as a result of the shorter and stronger bonds. The strongest inhibition by copper (II) ions may also be that they have fewer constraints on the co-ordination geometries they adopt and can easily occupy sites of low symmetry. Also, their complexes may be labile, allowing an easy exchange of ligands.

4.11 Conclusion

Wild-type MnP3 and mutant enzymes exhibited essentially identical spectral features and that UV/visible spectra of all MnP3 enzymes were found to be typical of a 6-coordinate high spin haem protein. Wild-type MnP3 enzyme showed optimal activity with Mn (II) at pH 5.0 and remained moderately active (approximately 27%) in the pH range 6.0-8.5. The MnP3 mutants maximum activity ranged between 5.5 and 8.0. Wild-type and mutants MnP3 enzymes

exhibited a similar pH profile with optimum at pH 3.0, for ABTS oxidation. Mutation has severely decreased the catalytic efficiency for Mn (II) oxidation at pH 5.0. MnP3 showed enhanced affinity for Mn (II) at alkaline pH and a more alkaline range for catalysis than ever reported for any MnP. At higher pH MnP3 can function with alternative ligands in the Mn (II) site and does not have an absolutely obligate requirement for an all carboxylate ligand set. These results further strongly confirm that Mn^{2+} binding site is the only productive catalytic site for Mn^{2+} oxidation.

For the wild-type MnP3, Na and Co behaved similarly as they were stimulatory to activity. Cu and Zn affected both K_m and k_{cat} with a mixed inhibitory effect. Cu was by far the strongest competitive inhibitor. E40H/E44H and D186H were strongly inhibited by Co (II), non-competitively. E40H, E44H and E40H/E44H were inhibited (mixed) by Cu and Zn. Cu having by far the strongest competitive effect like the wild-type. D186H was strongly inhibited by Zn and Cu, non-competitively. Strong competitive inhibitory effect of Cu observed in other MnP3 enzymes is largely removed in this variant. D186N was not strongly affected by any of the metal ions. Meaning that the binding site is presumably largely non functional regardless of metal present. It has generally been observed that histidine substitutions retained a strong selectivity for Cu (II) as competitive inhibitor and that Zn being generally non-competitive suggests involvement of sites other than the Mn (II) site.

The results suggest that MnP3 mutant variants have been created in which the metal binding functionality has been largely lost e.g. D186N and E40H/E44H. However, single histidine substitutions retain both the higher pH activity and a strong selectivity for Cu (II) as a competitive inhibitor. The binding of Zn is generally always more non-competitive suggesting that sites other than the Mn (II) site are involved.

Chapter Five

Binding of manganese (II) and other divalent metals to MnP3 from *Phlebia radiata*

5.1 Introduction and background

The structure, fold and function of a protein are dependent on its amino acid sequence, and in some instances, on interacting cofactors (Gregory *et al*., 1993). Metal ions play a key role for the function of many proteins (Jensen, 2007). The interaction of the metal ion with the protein and its involvement in the function of the protein vary widely. Amino acid residues provide the functional groups in a protein, which are the potential ligands for a metal cation (Sarkar, 1987). Metals affect variously protein structure and may bring about overall structural stability. Metals in protein structures also influence other processes such as catalysis, substrate binding and activation, transportation and storage (Kennedy and Gibney, 2001; Liu & Xu, 2002). Proteins often interact weakly with monovalent ions, such as K^+ and Na^+, while divalent ions, such as Ca^{2+} and Mg^{2+}, interact more strongly (Garcia *et al*., 2006). However, transition metal ions, such as Cu^{2+}, Zn^{2+}, Fe^{3+}, Fe^{2+}, Mn^{2+} and Co^{2+}, due to their features (density, small atomic radius and interaction via electromagnetic and electrostatic forces) have the strongest coordinating interactions, and thus occur in metalloproteins (Garcia *et al*., 2006).

Manganese has attracted much attention for its role as an important cofactor of several electron-transfer metalloproteins (Pecoraro & Hsieh, 2000; Maneiro *et al*., 2003; Puglisi *et al*., 2004). Adequate knowledge of the mechanism by which Mn (II) binds to MnP during catalytic turnover is critical to the detailed characterisation of *P. radiata* MnP3 function. The binding site for Mn (II) in *P. chrysosporium* MnP has been identified by X-ray crystallography (Sundaramoorthy *et al*., 1994; 1997). The relative importance of the ligands

forming this site has been demonstrated by the kinetic characterisation of mutants of these residues (Kishi *et al*., 1996). Based on the three-dimensional structure of the protein, a single binding site for Mn (II) has been proposed to exist on the surface of the protein near the meso edge of the haem prosthetic group (Sundaramoorthy *et al*., 1994) (Figure 1.5). This binding site is acidic in character and is comprised of three carboxylate ligands, provided by residues Glu35, Glu39, Asp179, a haem propionate oxygen, and by Wat520 and Wat441 (Sundaramoorthy *et al*., 1994). The interaction with one of these water molecules is stabilized through hydrogen bonding to the second haem propionate group. Although this structure addresses many critical issues concerning the mechanism of Mn (II) binding, it does not provide information concerning the stability of the Mn (II) protein interaction or the manner in which binding is affected by solution conditions and the presence of carboxylic chelators such as those examined in chapter 4. No information on the possibility of replacement of Mn (II) by alternative divalent metal ions at the Mn (II) binding site is available.

For MnP3 from *P. radiata*, there is no X-ray crystallographic data yet available. However, the Mn (II) binding site can be modeled by comparison with the homologous *P.chrysosporium* structure. *Phlebia radiata* MnP3 can therefore be used to study how other divalent metal cations interact with MnP enzymes. During the structure solution of the versatile peroxidase (also an MnP) (Ruiz-Duenas *et al*., 2007) key confusion was whether Zn^{2+} or Mn^{2+} was present at the Mn site, since the enzyme had been crystallised in the presence of excess Zn^{2+} and no exogenous Mn had been added. The Mn^{2+} site appeared open and the C-terminal tail disordered – perhaps indicative that Zn^{2+} was present.

5.2 Methods used in studying metal-protein interaction

Several approaches have been used in studying metal binding to proteins. The earliest methods involved equilibration of the metal ion with a solution of isolated protein, and the separation of the free metal ion from that bound to the protein by equilibrium dialysis (Rao

and Lal, 1958; Ryall, 1974) or ultra filtration (Girous and Schoun, 1981). These methods are still being used extensively to determine the binding strength and the number of metals ions bound per protein molecule. The drawback of these methods includes the requirement for relatively large quantities of protein, the difficulty of automating and the time required. Other techniques include electron spin resonance (ESR) (Rakhit, 1985), UV and visible spectroscopy (Appleton and Sarkar, 1971), nuclear magnetic resonance (NMR) (Laussac and Sarkar, 1980), circular dichroism (CD) (Laurie and Pratt, 1986; Bal *et al*., 1998), resonance Raman (Sarkar, 1987), X-ray crystallography, X-ray absorption near edge structure (XANES), and extended X-ray absorption fine structure (XAFS) (Sarkar, 1987).

These methods have contributed immensely to the understanding of the interaction between metal ions and proteins at the molecular level. However, these techniques according to Sarkar (1987) also have some disadvantages, including: the difficulty in studying the interaction of multi-metal ions with proteins, experiments are restricted to observable spectral changes; special probe with a single electron is required in some cases (e.g. ESR), resulting spectrum complex, and detection sensitivity by some spectroscopic methods is relatively low. In the present study metal interaction to MnP3 has been investigated using Inductively Coupled Plasma Mass Spectrometry (ICP-MS).

5.2.1 Inductively coupled plasma mass spectrometry (ICP- MS)

ICP-MS, since it development as an analytical method in 1980 (Houk, 1980), has been used to determine trace, minor and major chemical elements in almost every analytical field (Nelms, 2005; Beauchemin, 2006; Ammann, 2007). ICP-MS holds a unique position by virtue of its high analytical throughput, excellent detections limits (pg g^{-1} to ng g^{-1}) for most elements, minimal matrix effects, specific responses to most metal elements, semimetals or metalloid,

the capability of up to 8 magnitudes of linear dynamic range, and its simple coupling to another method (Wang *et al*., 2009).

ICP-MS can measure a full suite of elements in a single, multi-element acquisition, accepts almost any sample type and also provides isotopic information. One of the fastest growing areas of ICP-MS is in speciation measurement, which involves the combination of a chromatographic technique with ICP-MS as detector to determine the chemical form of the element in the sample. These capabilities help to explain the widespread acceptance of ICP-MS across all industry types, and confirm the status of ICP-MS as the premier technique for metal measurement (Ammann, 2007; Zoorob *et al*., 1998).

5.3 Determination of the stoichiometry of metal/protein interactions

Quantifying metals in proteins is challenging. Since metals are ubiquitous, their presence will obviously interfere with experiments such as metal ion content determination and substitution. Conventionally, the molecular metal content of proteins is assessed by determination of the total metal concentration in protein solutions. The protein concentration of this investigated solution is obtained by photometry. The accuracy of this approach is compromised by poor precision of the protein quantification and by the fact that the measurement solution might contain metal impurities as a result of the protein preparation procedure. So in studying metal-protein interactions, care is taken to avoid any contamination by metals from external sources. Ultra-pure water and reagents of the highest purity available are used and plasticware as opposed to glassware. It is also essential to have an accurate protein molecular weight. In the case of recombinant proteins the sequence will generally be known allowing calculation of the molecular weight.

An absolute protein concentration determination is required for a reliable metal content determination. Accurate measurement of absolute protein concentration is challenging, since

every protein quantification method is subject to idiosyncrasies. The usual strategy is to perform an absolute determination on a sample, and this will then be a reference for subsequent determinations of the proteins. The usual methods for absolute protein determination are measurement of dry mass and absolute amino acid analysis. Measurement of dry mass involves evaporating away the solvent from a protein sample in an oven at low pressure and directly measuring the mass of the remaining protein with an analytical balance (review by Kupke and Dorrier, 1978). The process usually requires a large amount of protein (typically 10 – 100mg) for accurately weighing. However, due to the amounts of MnP3 protein available in this study, it was not possible to determine an absolute protein concentration.

Therefore the method used in this work to measure protein concentration was to calculate the molar extinction coefficient at 280 nm for the MnP3 protein. This allowed rapid and non-destructive protein concentration determinations, without the need for a standard curve, simply by measuring an absorbance at 280 nm. Usually, the initial measurement to make when investigating the interaction of metal with protein is the concentration of protein and in order to calculate metal/protein stoichiometry, normally the molar concentration of protein in a sample is required. In this case the ion content of the haem can be used as an internal standard to establish an accurate ratio.

5.4 Results and discussion

The aim of this study was to investigate the concentration of metals, Fe, Ca, Mn, Co, Zn, and Cu in samples of MnP3, and other peroxidase proteins using the ICP-MS technique. These proteins were recombinant wild-type and four mutants of *P. radiata* MnP3, recombinant Horseradish peroxidase (HRP), native Horseradish peroxidase (nHRP), recombinant *Coprinus cinerus* peroxidase (CiP) and Myoglobin, the latter as a control.

All protein samples were first prepared by gel-filtration into ultra pure 10mM potassium phosphate buffer, pH 6.0. Four types of protein sample, non-treated with no dialysis, non-treated dialysed, metal-treated dialysed and calcium-depleted no dialysis were used in this study. The metal-treated sample, and a control non-treated, was prepared by incubating 0.5 mg of protein with 2 mM of each metal, as a divalent cation, in 10mM potassium phosphate, pH 6.0. These samples were then dialysed twice, first for 12 hours and then for 8 hours against 10,000-fold excess of the buffers with ICPMS measurements taken after both dialyses. It should be noted that the proteins were not treated with Fe or Ca, as excess Ca^{2+} is added during the folding process and haem is present stoichiometrically. The calcium-depleted samples were prepared by the normal protein folding method except that Ca^{2+} was later omitted from FPLC buffers. The values quoted are the average of at least 3 readings.

The analysis conditions were set for simultaneous Fe, Ca, Mn, Co, Zn and Cu detections. The calibration used was a simple 2-point calibration at 0 and 1000ng/ml of each of the elements measured; the 0ng/ml (blank) solution was TraceSelectUltra grade water from Fluka, while the 1000ng/ml calibration solution was made by diluting a 10,000ng/ml multi-element calibration solution supplied by Alfa Aesar (Johnson Matthey), with TraceSelectUltra grade water. The instrumental detection limits presented in Table 5.1 were based on three measurements of the blank buffer solutions.

Instrumental detection limits of ICP-MS were calculated from 11 replicate analyses of the calibration blank solution using Germanium as internal standard for all analytes except calcium, where Scandium was used.

Table 5.1: Instrumental detection limits of ICP-MS

Elements	Instrumental detection limits (ng/ml)
Fe	0.49
Ca	7.62
Mn	0.029
Co	0.003
Cu	0.36
Zn	2.04

Concentrations of metals in ICP-MS are conventionally expressed in parts per billion (ppb), defined as one nanogram of metal dissolved in one millilitre of solvent. Thus, 1 ppb represents different ion concentrations for different metals depending on atomic weight of the element in question. The amount in ng/ml was therefore converted to nmol by dividing by the molecular weight of the element concerned. The nmol amount of each metal was then used to find the stoichiometric ratio relative to that of the iron. It was also assumed that one atom of iron is present per protein molecule.

5.4 .1 Determination of Fe, Ca, Mn, Co, Cu and Zn content in wild-type MnP3.

Table 5.2 shows Fe: Ca stoichiometric ratios for wild-type MnP3 samples obtained after the first and second dialyses.

The stoichiometric values for Ca to Fe after second dialysis were between 1.7 and 2.3 for all samples, confirming the theoretical value of 2 indicating Ca binding to the proximal or distal sites. These values in turn were between 5 and 16 % lower than the values after the first dialysis indicating some slight instability or loss of Ca ions from one or both, of the Ca sites. This is in part confirmed by the Ca-deficient sample which gives a value at the lower end of

the range, 1.7, even after no dialysis, indicating some loss of Ca from one, or both, of the Ca sites during purification.

For the Mn-treated sample (Table 5.2) the Mn to Fe stoichiometric value of 0.82 after the first dialysis indicates that wild-type MnP3 has the potential to bind Mn^{2+}. However, further dialysis resulted in a reduction to 0.13, 84 % Mn^{2+} loss. This indicates that the interaction between Mn (II) and MnP3 is relatively loose. The Co to Fe stoichiometric value for wild-type MnP3 after the first dialysis was 0.3; the enzyme retained 0.2 atoms (67%) of the cobalt ions after the second dialysis. It therefore appears that the enzyme has better affinity for Co than it does for Mn.

Table 5.2 Determination of iron, calcium, manganese cobalt, copper and zinc content of wild-type MnP3 by ICP-MS.

Calculated values of metals showing the amount of metals bound to protein in part per billion (ppb) and in nanomole (nmol) in parentheses and the stoichiometric values compared to iron (Fe).

Samples	**Iron, ppb ±SD (nmol ±SD)**	**Calcium, ppb ±SD (nmol ±SD)**	**Manganese, ppb ±SD (nmol ±SD)**	**Cobalt ,ppb ±SD (nmol ±SD)**	**Copper, ppb ±SD (nmol ±SD)**	**Zinc, ppb ±SD (nmol ±SD)**	**Stoichiometric ratios**				
							Fe : Ca	**Fe : Mn**	**Fe : Co**	**Fe: Cu**	**Fe: Zn**
MnP 3 (Non-treated) 1st dialysis	664 ± 1.2 (12 ± 0.02)	960 ± 7.3 (24 ± 0.2)	7.3 ± 10 (0.13 ± 0.2)	0.6 ± 3 (0.01 ± 0.1)	ND	ND	1 : 2	1 : 0.011	1 : 0.0008	ND	ND
MnP3 (Non-treated) 2nd dialysis	637 ± 0.6 (11 ± 0.01)	839 ± 3.4 (21 ± 0.1)	6 ± 3 (0.1 ± 0.1)	0.412 ± 2 (0.01± 0.03)	ND	ND	1 : 1.8	1: 0.009	1: 0.0006	ND	ND
MnP3 (Mn treated) 1st dialysis	843 ± 0.8 (15 ± 0.02)	1125 ± 3.4 (28 ± 0.1)	684 ± 15 (13 ± 0.3)	2.4 ± 8 (0.04 ± 0.1)	ND	ND	1: 1.9	1: 0.82	1: 0.003	ND	ND
MnP3 (Mn treated) 2nd dialysis	834 ± 2.2 (15 ± 0.04)	1075 ± 3 (27 ± 0.1)	104 ± 8 (2 ± 0.2)	0.14 ± 4 (0.0024 ± 0.1)	ND	ND	1: 1.8	1: 0.13	1: 0.0002	ND	ND
MnP3 (Co treated) 1st dialysis	757 ± 2 (14 ± 0.04)	1056 ± 4.3 (26 ± 0.11)	14 ± 10 (0.3± 0.2)	217 ± 18 (4 ± 0.3)	ND	ND	1: 1.9	1: 0.02	1: 0.3	ND	ND
MnP 3 (Co treated) 2nd dialysis	685 ± 0.8 (12 ± 0.02)	828.3 ± 2 (20 ± 0.1)	8.2 ± 8 (0.2 ± 0.1)	12 ± 3.3 (0.2 ± 0.1)	ND	ND	1: 1.7	1: 0.012	1: 0.2	ND	ND
MnP 3 (Zn treated) 1st dialysis	635 ± 3 (11 ± 0.1)	1117 ± 4 (28 ± 0.1)	ND	ND	20 ± 2.4 (0.32 ± 0.04)	4841 ± 3.4 (74 ± 0.1)	1: 2.5	ND	ND	1: 0.03	1: 7
MnP 3 (Zn treated) 2nd dialysis	570 ± 4 (10.2 ± 0.1)	957 ± 3 (24 ± 0.1)	ND	ND	24.2 ± 2.4 (0.4 ± 0.04)	4656 ± 4 (71 ± 0.1)	1: 2.3	ND	ND	1: 04	1: 7
MnP 3 (Cu treated) 1st dialysis	728 ± 5.2 (12 ± 0.1)	1168 ± 1.4 (29.2 ± 0.03)	ND	ND	45100 ± 4 (710 ± 0.1)	31 ± 3.2 (0.5 ± 0.1)	1: 2.5	ND	ND	1: 62	1: 0.04
MnP 3 (Cu treated) 2nd dialysis	709 ± 5 (13 ± 0.1)	1057± 4 (26.4 ± 0.1)	ND	ND	8937 ± 0.08 (141 ± 0.001)	23 ± 3.4 (0.4 ± 0.1)	1: 2.1	ND	ND	1: 11.1	1: 0.03
MnP3 (No treatment) No dialysis	649.6 ± 3.1 (12 ± 0.1)	1159 ± 9 (29 ± 0.23)	15 ± 8 (0.3 ± 0.14)	1.32 ± 9 (0.03 ± 0.2)	ND	ND	1: 2.5	1 : 0.023	1 : 0.002	ND	ND
MnP 3 (No Ca^{2+} in FPLC buffer) No treatment, No dialysis	785 ± 2.2 (14 ± 0.04)	982 ± 4 (25 ± 0.1)	3 ± 10 (0.1 ± 0.2)	0.6 ± 7 (0.01 ± 0.1)	ND	ND	1: 1.7	1 : 0.004	1: 0.0007	ND	ND

ND (Not determined)

For the Cu-treated sample, for every one atom of Fe, 62 atoms of Cu were observed to bind to MnP3 after the first dialysis, while after the second dialysis, the Cu to Fe stoichiometric value had reduced to 11, indicating strong adventitious binding of Cu to wild-type MnP3. For the Zn-treated sample, the stoichiometric Zn to Fe ratio after the first dialysis was 1:7, which remained unchanged after the second dialysis indicating a more specific and tighter binding of Zn^{2+} ions to MnP3 enzyme. However, the level of both Zn and Cu in the protein after the second dialysis is higher than that obtained even for Ca. The ability of MnP3 to retain these metals was unexpected.

5.4.2 Determination of Fe, Ca, Mn, Co, Cu and Zn content of MnP3 mutant, E44H.

The metal contents of MnP3 mutant enzymes were also determined to see if mutation of the enzyme's putative Mn (II)-binding site had affected ability to retain divalent metal ions. The data on binding of Mn and other metal divalent cations to MnP3 mutant E44H, is presented in Tables 5.3. As before the relative concentration of calcium to iron was found to be about the expected 2 (1.9-2.3) for all E44H samples analysed.

However, for the Mn-treated sample, the stoichiometric Mn to Fe ratio of 0.33 after first dialysis was grossly reduced to 0.037 on second dialysis. These values suggest that the binding affinity of the putative Mn (II) site has been dramatically reduced compared to the wild-type enzyme, due to the removal of one of the metal-binding ligands. Similarly, data on the Co-treated E44H sample show a reduction in Co^{2+} binding; from the 0.31 ratio of Co bound to the enzyme after first dialysis, only 0.043 (14%) remained bound to the enzyme after second dialysis.

The stoichiometric Zn to Fe value for E44H after first dialysis was measured as 4.5, which was observed to reduce to 4.0 on further dialysis. The E44H mutant Cu to Fe ratio on the

other hand was 38 on first dialysis, reduced to 28 with a second dialysis. Again, this figures are high even after the second dialysis, when compared to the Ca, Mn and Co values.

On comparison, this mutant behaved with Zn similarly to the wild-type enzyme. However, this enzyme behaved differently with Cu (II). From the wild-type data (Table 5.2), a massive loss of 82% of bound Cu (II) was observed between treatments, whereas, E44H mutant recorded only 26% Cu (II) loss, suggesting that E44H has the ability to retain Cu^{2+} better than the wild-type enzyme once bound. Some simpler explanation e. g. partial Cu^{2+} contamination of a later sample cannot be entirely ruled out.

Table 5.3 Determination of iron, calcium, manganese and cobalt content of E44H MnP3 by ICP-MS.

Calculated values of metals showing the amount of metals bound to protein in part per billion (ppb) and in nanomole (nmol) in parentheses and the stoichiometric values compared to iron (Fe). Error represent standard deviation (SD)

Samples	**Iron, ppb ±SD (nmol ±SD)**	**Calcium, ppb ±SD (nmol ±SD)**	**Manganese, ppb ±SD (nmol ±SD)**	**Cobalt, ppb ±SD (nmol ±SD)**	**Copper , ppb ±SD (nmol ±SD)**	**Zinc, ppb ±SD (nmol ±SD)**	**Stoichiometric ratios**				
							Fe : Ca	**Fe : Mn**	**Fe : Co**	**Fe: Cu**	**Fe: Zn**
E44H (Non-treated) 1st dialysis	381 ± 1.1 (7 ± 0.02)	521 ± 5 (13 ± 0.123)	1.2 ± 7 (0.033 ± 0.12)	0.27 ± 2.4 (0.005 ± 0.04)	ND	ND	1: 1.91	1: 0.005	1 : 0.0007	ND	ND
E44H (Non-treated) 2nd dialysis	379 ± 4 (7 ± 0.1)	515 ± 6.2 (13 ± 0.2)	1.2 ± 5.95 (0.022 ± 0.11)	0.21 ± 1.9 (0.004 ± 0.0003)	ND	ND	1: 1.91	1: 0.003	1: 0.0006	ND	ND
E44H (Mn treated) 1st dialysis	536 ± 1.3 (10 ± 0.02)	731 ± 7 (18.3 ± 0.2)	173 ± 23 (3.2 ± 0.41)	0.80 ± 7 (0.014 ± 0.11)	ND	ND	1: 1.9	1: 0.33	1: 0.002	ND	ND
E44H (Mn treated) 2nd dialysis	528 ± 3 (10 ± 0.1)	717 ± 2 (18 ± 0.04)	20 ± 4 (0.35 ± 0.1)	0.22 ± 0.9 (0.004 ± 0.1)	ND	ND	1: 1.9	1: 0.04	1: 0.0004	ND	ND
E44H (Co treated) 1st dialysis	614 ± 2 (11 ± 0.04)	899 ± 4 (22.4 ± 0.10)	2.1 ± 21.13 (0.038 ± 0.4)	197 ± 12.3 (3.4 ± 0.21)	ND	ND	1: 2	1: 0.004	1: 0.31	ND	ND
E44H (Co treated) 2nd dialysis	538 ± 2 (10 ± 0.04)	762 ± 2 (19 ± 0.04)	1.6 ± 14 (0.028 ± 0.3)	24.3 ± 0.6 (0.41 ± 0.01)	ND	ND	1: 2	1: 0.003	1: 0.043	ND	ND
E44H (Zn treated) 1st dialysis	809 ± 0.9 (15 ±0.02)	1256 ± 3.1 (31.3 ± 0.1)	ND	ND	26.3 ± 0.9 (0.41 ± 0.02)	4228 ± 2 (65 ± 0.03)	1: 2.2	ND	ND	1: 0.03	1: 4.5
E44H (Zn treated) 2nd dialysis	785 ± 3 (14 ± 0.1)	1066 ± 4.1 (27 ± 0.1)	ND	ND	20.2 ± 3 (0.32 ± 0.043)	3444 ± 4 (53 ± 0.06)	1: 1.9	ND	ND	1 : 0.023	1: 4
E44H (Cu treated) 1st dialysis	838 ± 4.51 (15 ± 0.01)	1294 ± 4.03 (33 ± 0.1)	ND	ND	36240 ± 6 (571 ± 0.09)	18 ± 7.2 (0.27 ± 0.11)	1: 2.2	ND	ND	1: 38	1: 0.02
E44H (Cu treated) 2nd dialysis	789 ± 2.2 (14 ± 0.04)	1093 ± 3.52 27.3 ± 0.1)	ND	ND	24870 ± 1.3 (391 ± 0.02)	15 ± 7.2 (0.23 ± 0.11)	1: 1.9	ND	ND	1 : 28	1: 0.02
E44H (No treatment) No dialysis	789.3 ± 0.5 (14 ± 0.01	1284 ± 3.4 (32 ± 0.1)	ND	ND	ND	ND	1: 2.3	ND	ND	ND	ND

ND (Not determined)

5.4.3 Determination of Fe, Ca, Mn, Co, Cu and Zn content of MnP3 mutant, E40H/E44H by ICP-MS

Table 5.4 shows the result of ICP-MS analysis for MnP3 mutant, E40H/E44H. For all the samples the stoichiometric value of calcium to iron was approximately 2, consistent with the expected calcium content for MnP3.

For the Mn-treated sample, the Mn to Fe stoichiometric value was 0.18 (100%) after the first dialysis, with the amount of bound manganese ions reduced to 0.03 (16.7%) after the second dialysis. These results show less Mn retention than for the wild-type enzyme and also lower than the single E44H mutant suggesting that the double Mn-site ligand mutation have had a larger effect than the single mutant. Similarly, the Co to Fe stoichiometry was 0.32 after the first dialysis but was reduced to 0.094 after the second dialysis. E40H/E44 retained 3 times more cobalt than manganese, unlike the wild-type and E44H mutant that retained approximately the same levels of each. This observation is in agreement with the natural order of stability for divalent metal complexes (Irving and Williams, 1948), with Co-E40H/E44H MnP3 complex being more stable than the Mn-E40H/E44H MnP3 complex.

The data in Table 5.4 also shows the interaction of Zn and Cu with E40H/E44H MnP3. The result showed a Zn to Fe stoichiometric ratio of 6:1 after the first dialysis and 5.1:1 after the second dialysis. Out of 46.2 ions of Cu attached to E40H/E44 after the first dialysis, only 11.8 (25.5%) atoms remained bound to the enzyme after the second dialysis. Comparing the amount of Zn and Cu retained by the enzyme after second dialysis relative to the amount bound after the first dialysis, it is evident that the enzyme binds Zn^{2+} more tightly than Cu^{2+}.

Table 5.4 Determination of iron, calcium, manganese cobalt, copper and zinc content of MnP3 mutant, E40H/E44H by ICP-MS. Calculated values of metals showing the amount of metals bound to protein in part per billion (ppb) and in nanomole (nmol) in parentheses and the stoichiometric values compared to iron (Fe). Error represent standard deviation (SD)

Samples	**Iron, ppb ±SD (nmol ±SD)**	**Calcium, ppb ±SD (nmol ±SD)**	**Manganese, ppb ±SD (nmol ±SD)**	**Cobalt, ppb ±SD (nmol ±SD)**	**Copper, ppb ±SD (nmol ±SD)**	**Zinc, ppb ±SD (nmol ±SD)**	**Stoichiometric ratios**				
							Fe : Ca	**Fe : Mn**	**Fe : Co**	**Fe: Cu**	**Fe: Zn**
E40H/E44H (Non-reated) 1st dialysis	550 ± 2 (10 ± 0.03)	791 ± 5 (20 ± 0.14)	0.31 ± 8 (0.006 ± 0.2)	0.66 ± 1 (0.011± 0.02)	ND	ND	1: 2	1: 0.001	1: 0.0011	ND	ND
E40H/ E44H (Non-reated) 2nd dialysis	535 ± 1.1 (10 ± 0.02)	736 ± 3 (18.4 ± 0.1)	0.28 ± 10 (0.005 ± 0.2)	0.22 ± 2 (0.004 ± 0.03)	ND	ND	1: 1.9	1: 0005	1: 0.00042	ND	ND
E40H/E44H (Mn treated) 1st dialysis	715 ± 2 (13 ± 0.03)	1049 ± 4.2 (26 ± 0.1)	123 ± 26 (2.24 ± 0.5)	0.52 ± 7 (0.009 ± 0.11)	ND	ND	1: 2	1: 0.18	1: 0.001	ND	ND
E40H/E44H (Mn treated) 2nd dialysis	629 ± 0.4 (11.3 ± 0.01)	873 ± 0.8 (22 ± 0.02)	17.3 ± 1.3 (0.32± 0.024)	0.122 ± 4 (0.002 ± 0.06)	ND	ND	1: 1.9	1: 0.03	1: 0.0002	ND	ND
E40H/E44H (Co treated) 1st dialysis	708 ± 2.02 (13 ± 0.04)	1026 ± 2 (26 ± 0.05)	1.15 ± 2.1 (0.021 ± 0.4)	239 ± 13 (4.1 ± 0.22)	ND	ND	1: 2	1: 0.002	1: 0.32	ND	ND
E40H/E44H (Co treated) 2nd dialysis	690 ± 1.3 (12.4 ± 0.02)	921 ± 2 (23 ± 0.1)	0.25 ± 0.6 (0.005 ± 0.11)	69 ± 0.9 (1.2 ± 0.02)	ND	ND	1: 1.9	1: 0.0004	1: 0.094	ND	ND
E40H/E44H (Zn treated) 1st dialysis	742 ± 0.7 (13.3 ± 0.01)	1170 ± 2.3 (29 ± 0.1)	ND	ND	10 ± 1.4 (0.16 ± 0.02)	5055 ± 0.7 (77.3 ± 0.01)	ND	ND	1: 2.2	1: 0.012	1: 6
E40H/E44H (Zn treated) 2nd dialysis	686 ± 3 (12.3 ± 0.04)	1119 ± 3 (28 ± 0.1)	ND	ND	10 ± 2 (0.16 ± 0.024)	4102 ± 4 (63 ± 0.1)	ND	ND	1: 2.3	1: 0.013	1: 5.1
E40H/E44H (Cu treated) 1st dialysis	724 ± 0.6 (13 ± 0.01)	1134 ± 5 (28 ± 0.1)	ND	ND	38180 ± 2.2 (601 ± 0.04)	10 ± 3 (0.15 ± 0.1)	ND	ND	1: 2.2	1: 46.2	1: 0.012
E40H/E44H (Cu treated) 2nd dialysis	662 ± 3 (12 ± 0.1)	1015 ± 2 (25 ± 0.1)	ND	ND	8923 ± 4 (140 ± 0.1)	9 ± 6 (0.132 ± 0.1)	ND	ND	1: 2.1	1: 11.8	1: 0.011
E40H/E44H (Non-reated) No dialysis	731 ± 7 (13 ± 0.1)	1076 ± 2 (27 ± 0.1)	ND	ND	ND	ND	ND	ND	1: 2.1	1: 0.031	1: 0.00034
E40H/E44H (No Ca in FPLC buffer),No treated, No dialysis	632 ± 2 (11.3 ± 0.03)	913 ± 4 (23 ± 0.11)			ND	ND			1: 2	1: 0.0015	1: 0.0012

ND (Not determined)

The insignificant Zn loss by this enzyme shows that this enzyme has less tendency to lose Zn than Cu once complexed. This implies that the Zn-E40H/E44H complex is more stable than Cu-E40H/E44H complex. This observation is consistent with that observed for the wild-type and E44H mutant MnP3 and also consistent with metalloproteins universal order of preference for essential divalent metals (Irving & Williams, 1948).

5.4.4 Determination of Fe, Ca, Mn, Co, Cu and Zn content of MnP3 mutant, D186H by ICP-MS

The interaction of Mn (II) and other divalent metals (Co, Zn, and Cu) with MnP3 mutant, D186H using the ICP-MS technique and the results are presented in Table 5.5.

Of the stoichiometric amount of Mn, 0.18 (100%) contained in D186H mutant after the first dialysis, only 0.0184 (10%) was retained by this enzyme after the second dialysis. There was a huge loss of 0.16 (90%) of bound Mn^{2+} during the second dialysis. Similarly of the 0.18 (100%) cobalt cations complexed with D186H after the first dialysis, the enzyme was observed to lose 0.15 (83%) of the remaining Co^{2+} during the second dialysis, leaving 0.03 (17%) cobalt cations bound to the protein. This result clearly demonstrates that D186H had slightly more affinity for Co than Mn. The retention trend of Mn and Co by this MnP3 mutant was similar to that observed for the wild-type enzyme.

The D186H MnP3 contained 8.44 (100%) atoms of Zinc cations after the first dialysis, which reduced to 7.1(84%) during the second dialysis, with a loss of 1.34 (16%) of bound Zn^{2+}. The stoichiometric Cu/Fe value was 65 (100%) after the first dialysis and reduced to 16 (25%) on further dialysis with a loss of 49 (75%) of bound Cu^{2+}. The binding behaviour of Zn^{2+} and Cu^{2+} to D186H was similar to that of the wild-type MnP3 protein. The stoichiometric retention of Cu by this enzyme was as before greater than that of Zn. It has also been observed that the enzyme has less tendency to loose Zn^{2+} than Cu^{2+} once bound.

Comparing this mutant with the wild-type, the results (Table 5.2 and 5.5) showed that the mutant D186H retained more Cu ions than the wild-type while both enzymes retained the equal amount of Zn atoms.

Table 5.5 Determination of iron, calcium, manganese cobalt, copper and zinc content of MnP3 Mutant, D186H by ICP-MS.

Calculated values of metals showing the amount of metals bound to protein in part per billion (ppb) and in nanomole (nmol) in parentheses and the stoichiometric values compared to iron (Fe). Error represent standard deviation (SD)

Samples	**Iron, ppb ±SD (nmol ±SD)**	**Calcium, ppb ±SD (nmol ±SD)**	**Manganese, ppb ±SD (nmol ±SD)**	**Cobalt, ppb ±SD (nmol ±SD)**	**Copper, ppb ±SD (nmol ±SD)**	**Zinc, ppb ±SD (nmol ±SD)**	**Stoichiometric ratios**				
							Fe : Ca	**Fe : Mn**	**Fe : Co**	**Fe: Cu**	**Fe: Zn**
D186H(Non-treated) 1st dialysis	532 ± 1 (10 ± 0.02)	722 ± 3 (18 ± 0.1)	0.79 ± 4 (0.0143 ± 0.1)	0.182 ± 1 (0.0031 ± .023)	ND	ND	1: 1.9	1: 0.002	1: 0.00033	ND	ND
D186H(Non-treated) 2nd dialysis	500 ± 1 9.0 ± 0.02)	718 ± 4 18 ± 0.1)	0.52 ± 3 (0.01 ± 0.1)	0.14 ± 3 (0.0024 ± 0.1)	ND	ND	1: 2	1: 0.0011	1: 0.00027	ND	ND
D186H (Mn treated) 1st dialysis	812 ± 0.8 (15 ± 0.01)	1225 ± 4 31 ± 0.01)	142 ± 24 (2.6 ± 0.4)	11 ± 3 (0.19 ± 0.1)	ND	ND	1: 2.1	1: 0.18	1: 0.013	ND	ND
D186H (Mn treated) 2nd dialysis	710.3 ± 2 (13 ± 0.04)	943 ± 0.4 (24 ± 0.01)	13 ± 5 (0.233 ± 0.1)	0.11 ± 3 (0.0018 ± 0.1)	ND	ND	1: 1.9	1: 0.018	1: 0.00014	ND	ND
D186H (Co treated) 1st dialysis	628 ± 1 (11.2 ± 0.02)	821 ± 3 (21 ± 0.1)	1.43 ± 25 (0.03 ± 0.5)	119 ± 27 (2.02 ± 0.5)	ND	ND	1: 1.8	1: 0.0023	1: 0.18	ND	ND
D186H (Co treated) 2nd dialysis	550 ± 2 (10 ± 0.03)	790 ± 3 (20 ± 0.1)	0.794 ± 3 (0.015 ± 0.1)	15.21 ± 1 (0.26 ± 0.02)	ND	ND	1: 2	1: 0015	10.026	ND	ND
D186H (Zn treated) 1st dialysis	520 ± 1 (9.3 ± 0.02)	875 ± 3.2 (22 ± 0.1)	ND	ND	9.13 ± 2 (0.144 ± 0.06)	5137 ± 5 (79 ± 0.07)	1: 2.3	ND	ND	1:0.015	1: 8.44
D186H (Zn treated) 2nd dialysis	506 ± 3 (9 ± 0.05)	846 ± 3 (21 ± 0.07)	ND	ND	90 ± 5 (0.14 ± 0.1)	4120 ± 4 (63 ± 0.06)	1:2.3	ND	ND	1: 0.016	1: 7.1
D186H (Cu treated) 1st dialysis	6078 ± 2 (11 ± 0.03)	940.2 ± 4.4 (24 ± 0.11)	ND	ND	45010 ± 4 (708 ± 0.07)	22.4 ± 3 (0.34 ± 0.04)	1: 2.2	ND	ND	1: 65	1: 0.032
D186H (Cu treated) 2nd dialysis	564.4 ± 3 (10 ± 0.06)	827 ± 5 (21 ± 0.13)	ND	ND	10270 ± 5 (162 ± 0.08)	6.2 ± 0.6 (0.094 ± 0.1)	1: 2	ND	ND	1: 16	1: 0.0093
D186H (No treatment) No dialysis	681 ± 1.3 (12.2 ± 0.023)	1190 ± 4 (30 ± 0.1)	ND	ND	ND	ND	1:2.4	ND	ND	ND	ND

ND (Not determined)

5.4.5 Determination of Fe, Ca, Mn, Co, Cu and Zn content of MnP3 mutant, D186N by ICP-MS

The amount of Fe, Ca, Mn, Co Zn and Cu in MnP3 mutant, D186N was determined using ICP-MS analytic technique and the results shown in Table 5.6. The Ca stoichiometry for various samples of D186N ranged from 1.8 to 3.0, with the majority being about ~ 2.0. The data (Table 5.6) for manganese-treated samples showed that for every 1 atom of Fe complexed with D186N, only 0.2 (100%) atoms of Mn remained bound to this enzyme after the first dialysis. Further dialysis left the enzyme with 0.012 (6%) specifically bound with a loss of 0.19 (94%). Similarly, the total cobalt content of D186N was 0.14 (100%) after the first dialysis, which reduced to 0.026 (19 %) showing a loss of 0.114 (81%) during the second dialysis. This result clearly showed that the MnP3 mutant, D186N retained more cobalt cations than manganese, indicating that the Co-D186N complex is more stable than Mn-D186N complex.

For the more competitive divalent metal cation zinc, the content of D189N mutant was 8.14 (100%) at the end of the first dialysis, a reduction of 2.94 (36%) in the amount of Zn^{2+}, leaving the enzyme with a 5.2 (64%) stoichiometrically bound zinc cations after the second dialysis. For Cu, 64 (100%) atoms of copper were retained in the D186N enzyme after the initial dialysis. This was observed to reduce to 16 (25%) on further dialysis with the enzyme losing 48 (75%) of bound Cu^{2+}. A similar divalent metal binding trend was observed in the wild-type MnP3 enzyme from *P. radiata*. It is note worthy that this enzyme retained more Cu atoms and less Zn than the wild-type MnP3.

Table 5.6 Determination of iron, calcium, manganese cobalt, copper and zinc content of MnP3 mutant, D186N by ICP-MS.

Calculated values of metals showing the amount of metals bound to protein in part per billion (ppb) and in nanomole (nmol) in parentheses and the stoichiometric values compared to iron (Fe). Error represent standard deviation (SD)

Samples	Iron, ppb ±SD (nmol ±SD)	Calcium, ppb ±SD (nmol ±SD)	Manganese, ppb ±SD (nmol ±SD)	Cobalt, ppb ±SD (nmol ±SD)	Copper, ppb ±SD (nmol ±SD)	Zinc, ppb ±SD (nmol ±SD)	Stoichiometric ratios				
							Fe : Ca	Fe : Mn	Fe : Co	Fe: Cu	Fe: Zn
D186N (Non-treated) 1st dialysis	545 ± 0.7 (10 ± 0.013)	729 ± 4 (18.2 ± 0.1)	0.94 ± 7 (0.02 ± 0.12)	0.183 ± 5 0.003 ± 0.1)	ND	ND	1: 1.9	1: 0.002	1: 00031	ND	ND
D186N (Non-treated) 2nd dialysis	471 ± 2 (8.4 ± 0.04)	676 ± 5 (17 ± 0.13)	0724 ± 4 (0.013 ± 0.1)	0.13 ± 8 (0.0022 ± 0.1)	ND	ND	1: 2	1: 0.002	1: 0.0003	ND	ND
D186N (Mn treated) 1st dialysis	1098 ± 5 (20 ± 0.1)	1553 ± 3 (375 ± 0.1)	219 ± 24 (4 ± 0.44)	0.743 ± 5 (0.013 ± 0.1)	ND	ND	1: 2	1: 0.2	1: 0.0007	ND	ND
D186N (Mn treated) 2nd dialysis	939 ± 0.8 (17 ± 0.02)	1252 ± 3 (31 ± 0.1)	11 ± 4 (0.2 ± 0.1)	0.144 ± 5 (0.0024 ± 0.1)	ND	ND	1: 1.9	1: 0.012	1: 0.00014	ND	ND
D186N (Co treated) 1st dialysis	609 ± 0.4 (11 ± 0.01)	796 ± 2 (20 ± 0.1)	1.18 ± 20 (0.021 ± 0.4)	91.3 ± 19 (1.6 ± 0.33)	ND	ND	1: 1.8	1: 0.002	1: 0.14	ND	ND
D186N (Co treated) 2nd dialysis	579 ± 0.6 (10 ± 0.01)	790 ± 2 (20 ± 01)	0.995 ± 2.6 (0.018 ± 0.1)	16 ± 2 (0.27 ± 0.04)	ND	ND	1: 1.9	0.002	1: 0.026	ND	ND
D186N (Zn treated) 1st dialysis	520 ± 1.0 (9.3 ± 0.02)	824 ± 6 (21 ± 0.14)	ND	ND	8.58 ± 2 (0.14 ± 0.04)	4958 ± 3 (76 ± 0.04)	1: 2.2	ND	ND	1: 0.92	1: 8.14
D186N (Zn treated) 2nd dialysis	446 ± 2 (8 ± 0.1)	729 ± 3 (18 ± 0.1)	ND	ND	8.52 ± 2 (0.134 ± 0.03)	2686 ± 3 (41 ± 0.04)	1: 3	ND	ND	1: 0.012	1: 5.2
D186N (Cu treated) 1st dialysis	656 ± 11 (12 ± 0.03)	978 ± 2 (24.4 ± 0.1)	ND	ND	47370 ± 3 (746 ± 0.1)	16 ± 3.2 (0.244 ± 0.1)	1: 2.1	ND	ND	1: 64	1: 0.02
D186N (Cu treated) 2nd dialysis	564 ± 3 (10 ± 0.1)	786.2 ± 5 (20 ± 0.12)	ND	ND	1027 ± 5 (162 ± 0.1)	6.2 ± 6 (0.094 ± 0.1)	1: 1.94	ND	ND	1: 16	1: 0093
D186N(Non- treated) No dialysis	674 ± 2 (12 ± 0.034)	1117 ± 7 (28 ± 0.1)	8.83 ± 16 (0.16 ± 0.3)	1.32 ± 3 (0.022 ± 0.1)	ND	ND	1: 2.3	1: 0.0133	0.002	ND	ND
D186N(No Ca in FPLC buffer)No treated, No dialysis	690 ± 3 (12.4 ± 0.04)	941 ± 4 (24 ± 0.1)	0.542 ± 12 (0.01 ± 0.2)	0.47 ± 4 (0.001 ± 0.1)	ND	ND	1: 1.9	1: 0.001	1: 0.001	ND	ND

ND (Not determined)

5.5 Interaction of other haem proteins, myoglobin, CiP, recombinant horseradish (HRP) and native horseradish peroxidase (nHRP) with more competitive divalent metals, Cu and Zn

The relative interaction and retention of divalent metals, particularly, manganese, cobalt, zinc and copper with wild-type and mutant *P. radiata* MnP3 enzymes have been investigated. The tight binding and high retention of more competitive divalent metals, Cu^{2+} and Zn^{2+} observed for MnP3 enzymes was particularly interesting, as it aroused curiosity as to the extent that this observation was applicable to other haem proteins. In particular, a comparative study was carried out on other peroxidases (CiP and HRP) and non-peroxidase (myoglobin) metalloproteins. Therefore, 0.5mg of each control enzymes, myoglobin, *Coprinus cinereus* peroxidase (CiP), recombinant horseradish peroxidase (HRP) and native horseradish peroxidase were subjected to the same enzyme preparatory conditions described in the methodology section 2.4.11 followed by ICP-MS analysis. The enzymes used as controls were treated with only copper and zinc. The results of the ICP-MS analysis for the control experiments are presented in Table 5.7.

For the control enzymes, trace amount of calcium was recorded for myoglobin, which was believed to come from a minor contamination, while Ca/Fe stoichiometry for CiP, HRP and nHRP were consistent with that of fungal and plant peroxidases (Barber *et al*., 1995; Yoshida et al., 2000; Veitch, 2004).

Table 5.7 Determination of Iron, calcium, copper and zinc content of Myoglobin, *Coprinus cinereus* peroxidase (CIP), recombinant Horseradish peroxidase (HRP) and non-recombinant Horseradish peroxidase (nHRP) by ICP-MS.

Calculated values of metals showing the amount of metals bound to protein in part per billion (ppb) and in nanomole (nmol) in parentheses and the stoichiometric values compared to iron (Fe). Error represent standard deviation (SD)

Samples	**Iron, ppb ±SD (nmol ±SD)**	**Calcium, ppb ±SD (nmol ±SD)**	**Copper, ppb ±SD (nmol ±SD)**	**Zinc, ppb ±SD (nmol ±SD)**	**Stoichiometric ratios**		
					Fe: Ca	**Fe: Cu**	**Fe: Zn**
Non-treated 1st dialysis							
Myoglobin	963 ± 4 (17 ± 0.1)	56 ± 10 (1.4 ± 0.3)	5 ± 4 (0.08 ± 0.1)	8.7 ± 5 (0.133 ± 0.1)	1: 0.081	1: 0044	1: 0.008
CIP	572 ± 4 (10.2 ± 0.1)	993 ± 4 (25 ± 0.1)	2.2 ± 4 (0.034 ± 0.1)	5.4 ± 4 (0.082 ± 0.1)	1: 2.4	1: 0.0033	1: 0.008
HRP	568 ± 2 (10.2 ± 0.04)	921 ± 6.3 (23 ± 0.2)	3.0 ± 1.5 (0.05 ± 0.02)	10 ± 4 (0.15 ± 0.05)	1: 2.3	1: 0.005	1: 0.02
nHRP	545 ± 2 (10 ± 0.04)	840 ± 2 (21 ± 0.1)	3.44 ± 4 (0.054 ± 0.1)	8.9 ± 7 (0.14 ± 0.11)	1: 2.1	1: 0.006	1: 0.014
Non-treated 2nd dialysis							
Myoglobin	818 ± 4 (15 ± 0.1)	47 ± 9.4 (1.2 ± 0.23)	4.63 ± 4 (0.073 ± 0.1)	8.0 ± 3.3 (0.122 ± 0.1)	1: 0.08	1: 0.005	1: 0.008
CIP	513 ± 2 (9.2 ± 0.04)	894 ± 2 (22.3 ± 0.04)	1.5 ± 4 (0.023 ± 0.1)	1.89 ± 7 (0.03 ± 0.1)	1: 2.4	1: 0.003	1: 0.032
HRP	522 ± 1 (9.4 ± 0.03)	842.4 ± 5 (21 ± 0.13)	1.12 ± 5 (0.018 ± 0.08)	3.8 ± 5.12 (0.06 ± 0.08)	1: 2.24	1: 0.002	1: 0.006
nHRP	522 ± 2 (9.4 ± 0.043)	826± 4 (21 ± 0.1)	0.69 ± 2.2 (0.011 ± 0.04)	-0.271 ± 11 (0.004 ± 0.2)	1: 2.2	1: 0.0014	1: 0.0005
Cu treated 1st dialysis							
Myoglobin	921 ± 3 (17 ± 0.1)	64 ± 18 (1.6 ± 0.5)	3555 ± 2 56 ± 0.04)	4.42 ± 7 (0.07 ± 0.1)	1: 0.1	1: 3.4	1: 0.004
CIP	599 ± 4 (11 ± 0.1)	1000 ± 4 (25 ± 0.1)	23430 ± 4 (369 ± 0.1)	7.95 ± 8 (0.122 ± 0.1)	1: 2.3	1: 34	1: 0.01
HRP	455 ± 3 (8.2 ± 0.06)	692 ± 4.5 (17.3 ± 0.1)	7221 ± 7 (114 ± 0.11)	0.79 ± 9 (0.065 ± 1.6)	1: 2.1	1: 13.9	1:0.00 8
nHRP	553 ± 2 (10 ± 0.4)	856 ± 4.6 (21.4 ± 0.11)	6616 ± 3 (104 ± 0.04)	-0.4622 ± 43 (0.00071 ± 0.7)	1: 2.2	1: 10.5	1: 0.00007

Cu treated 2nd dialysis							
Myoglobin	816 ± 3.6 (15 ± 0.1)	16 ± 21 (0.4 ± 0.5)	3078 ± 3 (48.4 ± 0.04)	3.9 ± 10 (0.06 ± 0.2)	1: 0.03	1: 3.31	1: 0.004
CIP	552 ± 2 (10 ± 0.04)	886 ± 3 (22 ± 0.1)	9812 ± 5 (154 ± 0.1)	1.83 ± 15 (0.03 ± 0.2)	1: 2.21	1: 15.4	1: 0.003
HRP	449 ± 2 (8 ± 0.04)	650.3 ± 2 (16.3 ± 0.1)	2406 ± 0.9 (38 ± 0.01)	0.164 ± 104 (0.012 ± 0.14)	1: 2	1: 4.7	1:0.00 2
nHRP	513 ± 3 (9.2 ± 0.05)	753 ± 5 (19 ± 0.13)	2427 ± 6 (38.2 ± 0.1)	-1.24 ± 12 (0.019 ± 0.2)	1: 2	1: 4.2	1: 0.002
Zn treated 1st dialysis							
Myoglobin	1053 ± 2 (19 ± 0.03)	67 ± 12 1.7 ± 0.3)	5.8 ± 3 (0.09 ± 0.04)	635 ± 6.2 (9.7 ± 0.1)	1: 0.09	1: 0.005	1: 0.5
CIP	594 ± 5 (11 ± 0.1)	1005 ± 6 (25 ± 0.14)	1.3 ± 6 (0.02 ± 0.1)	3467 ± 2 (53 ± 0.034)	1: 2.3	1:0.002	1: 4.8
HRP	495 ± 2 (9 ± 0.04)	804 ± 6.2 (20 ± 0.2)	0.83 ± 2 (0.013 ± 0.03)	2365 ± 1.3 (36 ± 0.02)	1: 2.3	1: 0.002	1: 4.1
nHRP	549 ± 3.5 (9.83 ± 0.01)	850 ± 3.5 (21 ± 0.1)	0.726 ± 4 (0.011 ± 0.1)	1693 ± 6 (26 ± 0.1)	1:2.1	1: 0.0012	1:2.6
Zn treated 1st dialysis							
Myoglobin	897 ± 3.3 (16 ± 0.1)	37 ± 24 (0.92 ± 0.6)	4.9 ±3.4 (0.08 ± 0.1)	331 ± 1.2 (5.1 ± 0.02)	1: 0.06	1: 0.005	1: 0.3
CIP	495 ± 4 (9 ± 0.1)	855 ± 4.5 (21 ± 0.11)	0.97 ± 3 (0.02 ± 0.1)	1100 ± 5 (17 ± 0.1)	1: 2.4	1: 0.0022	1: 1.9
HRP	443 ± 3 (8 ± 0.05)	658 ± 2.3 (16.4 ± 0.1)	0.6793 ± 4 (0.001 ± 0.1)	1879 ± 9.2 (29 ± 0.14)	1: 2.1	1: 0.00013	1: 3.6
nHRP	497 ± 3 (9 ± 0.06)	736 ± 2.4 (18.4 ± 0.1)	0.65 ± 3.4 (0.01 ± 0.054)	1016 ± 11 (16 ± 0.2)	1: 2.1	1: 0.11	1: 1.8
No treatment No dialysis							
Myoglobin	1226 ± 2 (22 ± 0.02)	52 ± 12 (1.3 ± 0.3)	5.03 ± 1 (0.08 ± 0.02)	9.5 ± 3 (0.2 ± 0.1)	1: 0.06	1: 0.004	1: 0.007
CIP	760 ± 3 (14 ± 0.1)	1168 ± 5 (29 ± 0.12)	2.8 ± 3 (0.044 ± 0.1)	11 ± 3 (0.17 ± 0.1)	1: 2.1	1: 0.003	1: 0.03
HRP	580 ± 3 (10.4 ± 0.05)	1014 ± 7 (25.3 ± 0.2)	1.63 ± 4 0.03 ±0.1)	1.26 ± 12 (0.02 ± 0.2)	1: 2.4	1: 0.003	1: 0.002
nHRP	638 ± 3 (11.4 ± 0.05)	1000 ± 7 (25 ± 0.2)	1.75 ± 6 (0.03 ± 0.1)	-1.13 ± 4 (0.02 ± 0.07)	1: 2.2	1: 0.003	1: 0.002

5.5.1 Determination of Fe, Ca, Cu and Zn content of myoglobin by ICP-MS.

The ICP-MS data (Table 5.7) for all the myoglobin samples showed that at the end of the first dialysis, the copper-treated sample was observed to contain 3.4 (100%) atoms of copper. Only a small amount of 0.1 (3%) Cu^{2+} was lost by this enzyme on further dialysis. The zinc-treated samples showed that zinc cation retention by myglobin was quantitatively different from that observed for Cu^{2+}. The stoichiometric content for Zn^{2+} after second second dialysis was 0.3 (60%). Therefore, a higher Cu^{2+} , 3.3 (97%) retention was recorded, when compared to the myoglobin Zn^{2+} content (0.3) after dialyses. These result showed that myoglobin has a higher Cu atom retention potential and formed a stable complex with Cu rather than Zn. It also means that Cu^{2+} binds more tightly to myoglobin than Zn^{2+}.

The retention behaviour of Cu^{2+} versus Zn^{2+} by myoglobin was not similar to what was observed in MnP3 enzymes. This implies that myoglobin has more affinity for Cu than Zn. It would appear that strong retention of Zn^{2+} may be a feature of MnP3.

5.5.2 Determination of Fe, Ca, Cu and Zn content of *Coprinus cinereus* peroxidase (CIP) by ICP-MS.

The ICP-MS analysis data (Table 5.7) for all samples of CiP is presented in Table 5.7. CiP retained 15 (45%) atoms of Cu (II) after second dialysis, while 1.9 (39%) of Zn atoms were recoded after dialyses. The Cu-CiP binding trend was quantitatively similar to that observed for MnP3 enzymes. However, percentage Cu -CiP retention was more than that in MnP3 wild-type. Zn retention by CiP was less than that retained by MnP3 enzymes, meaning that the binding affinity of Zn-CiP is not as strong as that observed in MnP3 enzymes.

5.5.3 Determination of Fe, Ca, Cu and Zn content of recombinant and native Horseradish peroxidase (HRP and nHRPrespectively) by ICP-MS.

The aim of analyzing both the recombinant and native horseradish peroxidases was to see if there could be any difference in the metal binding potential of the two types of HRP enzymes caused by the extensive differences in glycosylation.

The data (Table 5.7) shows the results of the ICP-MS analysis of recombinant and horseradish peroxidase (HRP). 5 (36 %) atoms of Cu remained bound to recombinant HRP after dialysis, native HRP retained 4.2 (40%). Quantatively, both HRP enzymes bound less Cu atoms relative to MnP3 enzymes. On the other hand, out of the stoichiometric 4.1 atoms of Zn bound to HRP, 3.6 (88 %) remained bound after dialyses. This data showed that zinc was tightly bound to HRP very similar to the results obtained with the MnP3 enzymes. The nHRP was observed to retain 1.8 (69%) atoms of Zn at the end of the second dialysis. HRP and nHRP interactions with Cu and Zn were similar with the enzymes Zn binding appearing to be stronger than to Cu.

5.6 Conclusion

In this work, the *in vitro* binding and retention behaviour towards various metal ions of *P. radiata* MnP3 enzymes, horseradish peroxidases (HRP and nHRP), CiP and myoglobin have been observed. Both specific metal-protein and nonspecific metal-protein interactions were involved. It is generally true that for metal ions with nearly the same radii, those with the highest positive charge form the most stable complexes. A careful survey of all the non-metal treated samples in this study has indicated the absence of significant amount of Mn, Co, Zn and Cu in the purified enzymes.

For the metal treated samples, dialysis alters the extent of metal binding of the enzymes under investigation as enzymes unload due to ligand dissociation. The high-affinity metal interactions are not lost even after a second dialysis, seen particularly in the case of copper and zinc. Mn-protein interactions were of lower affinity and are almost completely lost after second dialysis**.** Co was observed to bind although the physiologically relevant metal in MnP3 is Mn, for the E44H mutant it has been observed that Co was better retained than Mn. Cu and Zn were observed to bind tightly with high stoichiometric values. The results obtained where the enzyme binds Cu and Zn more than other metals is consistent with the natural order of stability for divalent metals (often called the Irving-Williams series, Irving and Williams, 1948). Protein flexibility offers an imperfect steric and ligand selection between metals. Hence, affinities for metals have the tendency to a universal order of preference. This order is seen in the results trend with copper and Zn forming the tightest complexes, then nickel and cobalt, followed by ferrous iron and manganese and finally, forming the weakest complexes with calcium and magnesium.

Mg^{2+} and Ca^{2+} (weakest binding) < Mn^{2+} < Fe^{2+} < Co^{2+} < Ni^{2+} < Cu^{2+} < Zn^{2+}

This natural order of stability for divalent metals was observed to be irrespective of the nature of the ligands involved (Mellor and Maley, 1947; 1948). Mellor and Maley, (1947; 1948) also emphasised that this order may be radically changed if the divalency of any of the participants is altered. The stability of complexes formed by any one ligand with a series of metals may be expected to increase with the electronegativity of the metal concerned. In general, electronegativity increases on passing from left to right along a period, and decreases on descending a group in the periodic table. Irving and Williams (1948) did observe that the most stable complexes are always formed by elements terminating the transition series, and that probably the same natural order of stability is preserved throughout each series.

Cu (II) and Zn (II) binding to the proteins studied is not surprising since according to Waldron and Robinson (2009), these metals are highly competitive and are expected to bind tightly to metalloproteins, especially those containing sulphur and nitrogen ligands. Cu and Zn lie at opposite extremes to manganese in the stability series and therefore selectivity by proteins will be especially demanding in terms of the structural requirements of the binding site. In this study, all the protein samples analyzed have been observed to bind more Cu (II) cations than Zn (II). This observation is in agreement with that of Eichhorn, (1973), who noted that the coordinating atom preference of Cu (II) or Zn (II) is S > N > O but for any individual atom, the interaction of Cu (II) is approximately 10-fold stronger than Zn (II). As the divalent species of respective metals become competitive, on moving up the Irving-Williams series, it is anticipated that the number of atoms binding must match the number of correct binding sites with increasing precision to avoid the displacement of metals further down the series. Restricting effective concentration of competitive metals at the top of the Irving-Williams series, weaker metal-binding sites remain available to less-competitive inorganic ions. However, the tight binding of Cu^{2+} and Zn^{2+} to *P. radiata* MnP3 is not in agreement with that observed for *P. chrysosporium* MnP where these metals exhibited poor binding (Harris *et al*., 1991; Sundaramoothy *et al*., 2005).

Experimental evidences (this work) indicate that divalent cations other than Mn are capable of binding to MnP3 from *P. radiata*. It could be observed from the available data that, the wild-type MnP3 contains more Mn atoms than the mutants MnP3 enzymes. Tables 5.2, 5.3, 5.4, 5.5, and 5.6) show that the MnP3 mutant enzymes, E44H, E40H/E44H, D186H and D186N after dialysis retained 93%, 98 %, 86 % and 91 % respectively, less than the wild-type MnP3 enzyme. This is indicative of a higher wild-type Mn affinity than for mutant enzymes. This may be due to structural change(s) in the protein following point substitution of the Mn-

binding residue (s) at the Mn binding site, which suggests that the chemistry of metal (Mn) binding strongly constrains the positions of the ligand residues.

So far, no report exists in the literature of binding between MnP and other divalent metal cations. Available experimental data from this study, which may apply to other MnPs, imply that the Mn-binding site in MnP appear to be rather weakly protected against other divalent metals such as Cu and Zn which has been earlier observed to inhibit enzymatic activity, while the Co effect on this protein was activating (section 4.8.). It may also mean that MnP3 has several separate Cu (II) and Zn (II) – binding sites and / or that these divalent metal cations also bind to the same manganese-binding site. Natural and designed proteins with a single architecture can be adapted to accommodate a variety of metals (Kennedy and Gibney, 2001). The high retention of Cu and Zn showed here by proteins also suggests that these enzymes may have more Cu and Zn motifs with mechanisms to permit greater Cu (II) and Zn (II) retention. In terms of charge-accepting ability, among cations with the same formal charge and similar ionic radii, those that can accept more charge from the bound ligand gain more favourable binding energies. Owing to the hybridization of its 3d and 4s orbitals, Zn^{2+} and Cu^{2+} can accept more charge from a given ligand than Mn^{2+} and Co^{2+}. It could also mean that the charge transfer energy component for a Zn^{2+} and Cu^{2+} complex is more favourable than that for the corresponding Mn^{2+} and Co^{2+} counterparts containing the same set of ligands (Garmer and Gresh, 1994; Dudev and Lim, 2001).

It has also been observed that Zn once bound has the tendency to remain bound to MnP3 enzymes. The HRP interacted with Cu and Zn in a similar way to MnP3 enzymes, whereas, the amounts of Zn and Cu retained by CiP were much less. Myoglobin was observed to behave differently to the MnP3 enzymes it retained more bound Cu than Zn after dialysis, showing a preference for Cu. The tight binding of Cu and Zn to MnP3 is suggestive of

multiple metal-binding sites other than the specific manganese-binding site. The affinity of MnP3 for Cu and Zn is also intriguing in the light of manganese being a specific substrate for this enzyme. While the ligands and site for Zn and Cu binding are not yet certain, the tight binding of these metals to the enzymes makes sulphur-rich cysteine and methionine coordination more likely as possible sites.

Generally, the binding affinity of the Mn-binding site to Mn (II) was grossly reduced by ligand mutation. Mn-MnP3 interactions were of low affinity and are almost completely lost after dialysis. Co (II) retention by MnP3 enzyme was better than Mn (II), particularly, for E40H/E44H. MnP3 enzymes retained more Cu than Zn. Zn bound irreversibly and somewhat non-specifically to MnP3 proteins, this may be a problem in crystallography when Zn is used in the buffer. The high-affinity metal interaction that was not lost even after the second dialysis was observed for Cu and Zn. This is suggestive of multiple tight binding sites for Cu (II) and Zn (II).

Chapter Six

pH stability of wild-type and mutant MnP3 enzymes from *Phlebia radiata*

6.1 Introduction and background

The stability of enzymes in a non-natural environment is a critical issue in biotechnology; *i.e.* their operational stability is of prime importance for any bioprocess. Poor environmental stability remains a major limitation to the large-scale use of peroxidase catalysis (Zamorano *et al*., 2009). In particular, enzyme stability at high pH and temperature is a key feature in evaluating the applicability of lignin degrading peroxidases to any biorefinery type application. The characterisation of MnP3 stability under application-type conditions is therefore important.

The most important factors affecting enzyme activity are pH, temperature and ionic strength. The protein surface is the point of contact with the solvent media, thus the physical and chemical environment are sensed through the surface residues. Polar residues are influenced by pH and depending on their individual *pKa* values changes in their ionization state may interfere with enzymatic activity and / or alter enzyme thermostability (Petersen *et al*., 1998). Studies on barley peroxidase have indicated that the activity of plant peroxidases may be reversibly controlled by pH induced conformational changes (Rasmussen *et al*., 1998).

The peroxidases of Classes II and III share some structural features considered to be important for maintaining protein stability and activity (Howest *et al*., 2001). These structural features, which are absent in Class I peroxidases (Mura *et al*., 2005) include two calcium-binding sites (proximal and distal) and four or five disulfide bridges (Welinder, 1992; Sundaramoorthy *et al*., 1994; Kunishima *et al*., 1996; Schuller *et al*., 1996; Gajhede *et al*., 1997). Note, the disulfide bridges appear in different locations in Class II compared to Class III peroxidases. In general, Class II peroxidases have been found to be more stable thermo-labile and pH sensitive than Class III (Sutherland and Aust, 1996; George *et al*., 1999). Glycosylation of native peroxidases

has also been shown to have a role in stabilizing the protein against inactivation (Nie *et al*., 1999). Recombinant MnP was observed to inactivate at a faster rate than native fungal MnP, this was associated with the lack of glycosylation of the *E.coli* recombinant enzyme (Nie *et al*., 1999).

The relationship between calcium binding and enzyme inactivation has been done primarily by studies on LiP (Nie and Aust, 1997; George *et al*., 1999), MnP (Sutherland *et al*., 1997; Sutherland and Aust, 1997) and HRP (Haschke and Freidhoff, 1978; Shiro *et al*., 1986). Calcium has been proposed to function in the maintenance of the haem microenvironment and hence stabilises enzyme activity (Ogawa *et al*., 1979; Shiro *et al*., 1986; Maranon *et al*., 1993; Sundaramoorthy *et al*., 1994; Iori *et al*., 1995; Howest et al., 2001). It is thought that calcium ions maintain the relative positions of the proximal and distal histidines, respectively, which are involved in the modulation of the peroxidase redox potential and in the acid-base activation of H_2O_2 at the beginning of the catalytic reaction (Sundaramoorthy *et al.*, 1994; Gajhede *et al*., 1997; Choinowski *et al*., 1999).

Numerous studies have been carried out on the stability of *P. chrysosporium* MnP. In *P. chrysosporium* MnP, at the proximal side, there is H-bond between proximal His 173 and the buried side chain of Asp 242, while a H-bond also exists between the distal His and Asn 80 (Sundaramoorthy *et al*., 1994). This H-bonding network is thought to inhibit the transition to the inactive alkaline form of the enzyme. Most haem proteins undergo an acid-alkaline transition from high-spin to low-spin Fe (III) (Smulevich *et al*., 1988). In the acid-alkaline transition, a proton is transferred from H_2O to distal His46 which could result in a H_2O "with hydroxide" character, which in turn changes the Fe (III) to a low–spin state (Smulevich *et al*., 1989). At acidic pH there is restraint, *i.e.* on proton transfer resulting in a high-spin species.

Comparing the alkaline transitions of metmyoglobin, methaemoglobin (Ilgenfritz and Schuster, 1961) and HRP-C (Epstein and Schejter, 1972), the alkaline transition of HRP-C was considered to involve proton dissociation from a water molecule in the six-coordination position of the haem iron. While alkaline transition for metmyoglobin and methaemoglobin occurs rapidly in 1 to 10 micro second, that of HRP-C occurs much more slowly. From the rate constant obtained from a pH jump experiment, alkaline transition for HRP-C occurs two orders of magnitude slower than for metmyoglobin. Using a stopped flow apparatus, rate constants in the range of $6 \times 10^4 - 1.3 \times 10^3\ s^{-1}$ were measured for HRP-C (Epstein and Schejter, 1972), the speed of the alkaline transition of HRP-C was therefore seen as a reflection of a more complex conformational change than a simple deprotonation.

Alkali treatments of LiP H8 (Nie and Aust, 1997a; Nie and Aust, 1997b) and MnP (Sutherland *et al*., 1997) have also been shown to yield low spin species. Research on the mechanism of thermal and alkaline inactivation of Class II peroxidases has revealed a change of the haem iron electronic state, concomitant with structural calcium release (Sutherland *et al*., 1997). MnP exhibits a pH-dependent high- to low-spin transition (*pKa* = 6.67) in the pH range 5.0-8.5 (Kishi *et al*., 1997; Youngs *et al*., 2000). It has also been demonstrated that the apparent inactivation rate at alkaline pH can be decreased by addition of calcium, increased by Ca^{2+} chelators and the inactivated enzyme could be readily recovered upon addition of Ca^{2+}.

Extensive study on the stability of peroxidases from different species has been carried out (Obinger *et al*., 1996; Welinder *et al*., 1993), but so far, no information is available on the stability of *P. radiata* enzymes. In this work, therefore the stability of MnP3 from *P. radiata* has been studied as a function of pH and temperature (Chapter 7) and the involvement of Ca ions in the inactivation of the enzyme investigated.

6.2 The effect of pH on *P. radiata* wild-type and mutant MnP3 enzymes

The aim of the pH cycle experiment was to investigate the effect of different pH conditions (acid and alkaline) on the stability of MnP3 enzymes with respect to spectral properties and activity. This experiment was performed using *P. radiata* wild-type and mutants, E40H/E44H, D186H, D186N MnP3, respectively as described in section 2.4.12.

All UV-vis spectra were recorded spectrophotometerically from 750 nm to 250 nm, while activity assays were conducted using standard Mn (II) oxidation assay conditions (section 2.4.6). Forms that had a distinct UV/Vis profile were designated AH, A^-, I^- and X respectively.

A mixed buffer containing 10 mM MOPS, 10 mM Bicine, pH 6.7, was used to record a spectrum of an initial enzyme sample denoted 'AH'. Form AH was then diluted with an equal volume of a buffer containing 50 mM MOPS, 50 mM Bicine, pH 9.05, to bring the pH to 8.6. The enzyme attained a new form '$A^{-\prime}$ and the spectrum was recorded immediately. With incubation of the enzyme at pH 8.6 and 25°C for about 1 hour, a new enzyme form '$I^{-\prime}$ was obtained and the spectrum recorded. The enzyme was then diluted with another buffer containing 170 mM MOPS, 170 mM Bicine, pH 5.95, taking the pH back to 6.7. This lead to form 'X' of the enzyme, the spectrum was recorded immediately. The enzyme was further incubated for 24 hours at pH 6.7 to recover the original form (AH'), and a spectrum taken. After the 24 hours 0.4mM $CaCl_2$ was added to the protein sample in the cuvette to see if the extent of recovery of AH' could be enhanced. Small samples of each enzyme form were taken and frozen immediately in liquid nitrogen for activity assay at a later point.

The pH cycle is summarised in scheme 6.1 below:

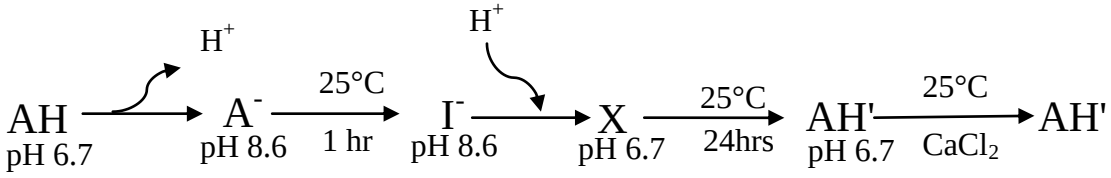

Scheme 6.1: A scheme showing stages in pH cycle of wild-type MnP3

A further experiment for each MnP3 enzyme was also set-up as described above, but with 5mM $CaCl_2$ added to the enzyme at the 'A^{-}' form point. Full details of the experiment are presented in section 2.4.12. For clarity the results are reported in sections detailing changes during the imposed pH cycle.

6.2.1 Wild-type MnP3 spectroscopic and activity changes during the pH transitions.

6.2.1.1 Raising the pH

Figure 6.1 shows the UV/Vis spectra of different forms of wild type MnP3 during the pH cycle described earlier. The starting wild-type MnP3 enzyme in mixed buffer of 10 mM MOPS, 10 mM Bicine, pH 6.7 was designated AH (black spectrum).

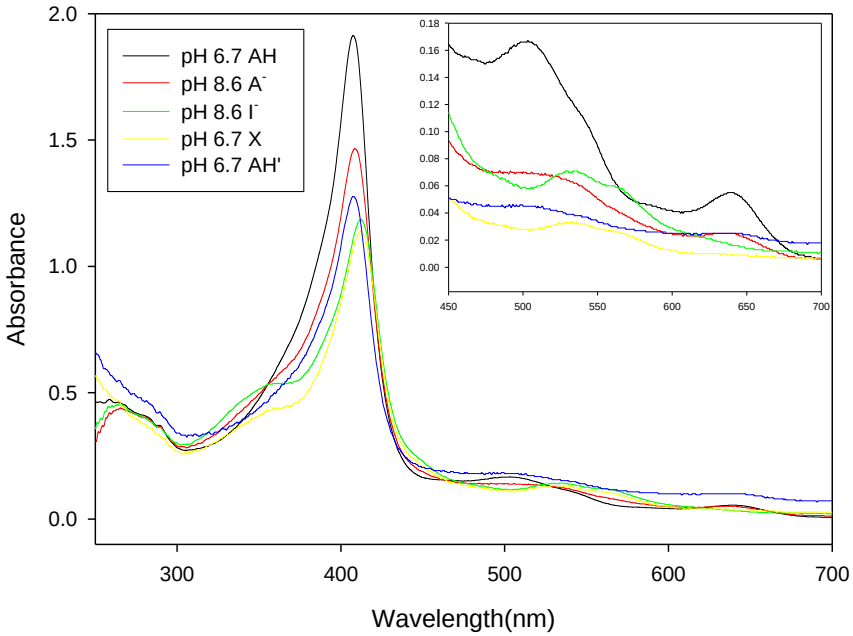

Figure 6.1: UV/visible spectra of the pH cycled forms of wild-type MnP3.
The spectra of A^- , I^- , X and AH' have been corrected for dilution caused by pH adjustment. AH, pH 6.7 (—); A^-, pH 8.6 (—); I^-, pH 8.6 (—) after 1 hour at 25°C; X, pH 6.7(—), AH' pH 6.7 (—) after 24 hours at 25°C and AH' + $CaCl_2$, pH 6.7 (spectrum not shown).

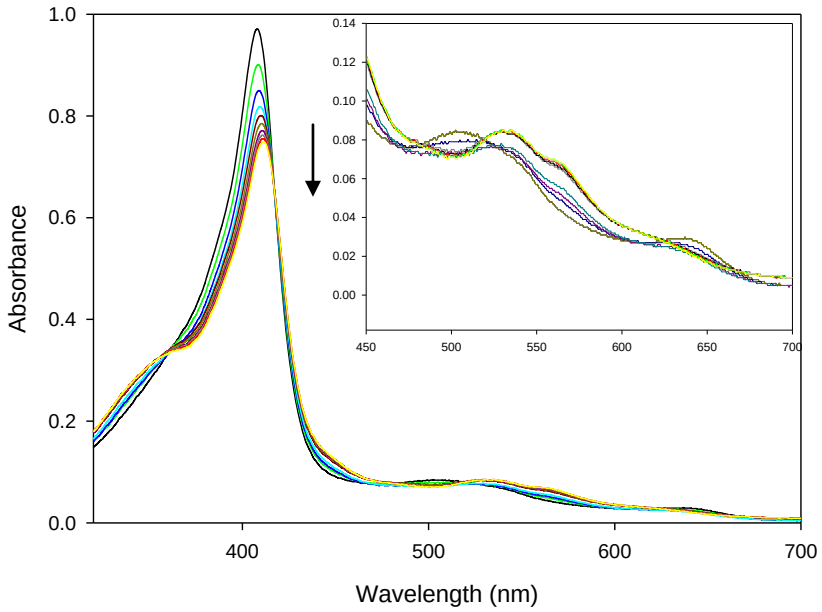

Figure 6.2: UV/visible spectra showing the conversion of wild-type MnP3 form A- to form I-, after pH jump form pH 6.7 to pH 8.6. The enzyme was incubated for 40 mins at 25°C and scans repeated every 2 mins. Spectra show a gradual change from high- spin to low-spin ferric iron in the haem group.

Enzyme dilution with an equal volume of buffer containing 50 mM MOPS, 50mM Bicine, pH 9.05 raised the pH from 6.7 to 8.6. This resulted in the conversion of the enzyme form from AH to A^-, (red spectrum), the spectrum of the initial high pH form of the enzyme (recorded within the first minute of exposure to alkaline conditions). The A^-spectrum showed a decrease in Soret extinction coefficient and activity was reduced to 73%. The Soret position remained unaltered at 408nm while the charge transfer (CT) bands I and II slightly shifted from 638 to 636 nm and 504 to 507 nm, respectively (Table 6.1).

Table 6.1: Spectral characteristics and remaining activities of the different forms of wild-type MnP3 from *P. radiata* with and without 5mM $CaCl_2$ added to A^- form of the enzyme during pH transitions. The experiment was carried out at 25°C. The standard Mn (II) assay conditions as in section 2.4.6 were used. Extinction coefficients were calculated using the concentrations of the various enzyme forms. Characteristics were extracted from spectra depicted in Figures 6.1 and 6.3. Soret, β, α, CT II, CTI, shoulder denote the type of absorption band of the spectra. HS = high spin, LS = low spin. Sample with 5 mM $CaCl_2$ added to A^- form of the enzyme is indicated with 5 mM $CaCl_2$ in bracket.

pH	Predominant form	Percentage remaining activity	Soret (nm)	Extinction coefficient ($mM^{-1}cm^{-1}$)	β (nm)	α (nm)	Soret Shoulder (nm)	CT II (nm)	CT I (nm)	Spin state
6.7	AH	100	408	173	—	—	—	504	638	HS
	AH (5 mM $CaCl_2$)	100	408	173	—	—	—	506	642	HS
8.6	A^-	73	408	148	—	—	—	507	636	HS
	A^- (5 mM $CaCl_2$)	83	408	152	—	—	—	505	640	HS
8.6	I^-	10	412	103	531	559	368	—	—	LS
	I^-(5 mM $CaCl_2$)	60	409	126	—	—	—	508	636	HS
6.7	X	15	412	79	536	559	368	—	—	LS
	X (5 mM $CaCl_2$)	96	407	130	—	—	—	508	641	HS
6.7	AH'	74	409	99	—	—	—	517	638	HS/LS
	AH' (5 mM $CaCl_2$) 12 hours Aggregation	76	408	150	—	—	—	507	640	HS
6.7	AH' 24 hours + 0.4mM $CaCl_2$	81	409	103	—	—	—	503	638	HS
	AH' (5 mM $CaCl_2$) 24 hours Aggregation	73	408	163	—	—	—	501	641	HS

Prolonged incubation of enzyme form A^- at pH 8.6 resulted in more spectral changes as the enzyme slowly converted to form I^- (green spectrum). After one hour of incubation at pH 8.6, the Soret peak had red-shifted to 412 nm, becoming much less intense (54%) and gaining a shoulder at 368 nm, and new peaks corresponding to α and β bands at 559 and 531 nm had appeared. Activity had also decreased to 10% (Table 6.1). These changes suggest that the haem iron of this alkaline inactivated enzyme was now in a low-spin form (Youngs, 2001). Five isosbestic points at 358, 421, 474, 521, and 615 nm, respectively, (Figure 6.2) were observed during this alkali-induced change.

6.2.1.2 Lowering the pH

The pH of the wild-type enzyme solution was then lowered from 8.6 to 6.7. This downward pH jump initiated a reactivation process resulting in enzyme form X (yellow spectrum). The spectrum of form X (recorded within the first minute of return to pH 6.7) showed no change in Soret position at 412 nm, the CT bands I and II did not reappear and the α and β bands at 536, 559 nm and shoulder at 368 nm, respectively were retained, only 5% activity was recovered (Table 6.1).

However, on a more prolonged incubation at pH 6.7, the enzyme slowly returned to a resting-state enzyme form, AH' (blue spectrum), but the return was incomplete. The rate of reactivation and conversion of form X to form AH' was monitored by repeat spectroscopic scans of the sample, and was a very slow process. The AH' spectrum in Figure 6.1 was obtained after 24 hours incubation of the enzyme at 25°C. During the incubation, Soret absorption maximum blue-shifted from 412 to 409nm, the α and β bands at 559, 536 and the shoulder at 368 nm disappeared, while the CT bands reappeared at 638 nm (CT I) and 517 nm (CT II). This indicated a restoration of the high-spin haem state. The pH adjustment from

8.6 to 6.7 and incubation for 24 hours resulted in a recovery of approximately 74 % of the initial activity of the MnP3 enzyme (Table 6.1).

Subsequent treatment of the pH cycled AH' enzyme (form X) with 0.4mM $CaCl_2$ at pH 6.7, did not significantly alter the spectrum after 24 hours incubation but restored an additional 7% of the enzyme's activity (Table 6.1).

The scattering observed in the final AH' spectrum could be caused by irreversible denaturation of some of the enzyme after the long incubation time, consistent with the inability to completely restore the enzyme's activity even with calcium addition.

6.2.2 The effect of addition of 5mM $CaCl_2$ to form A^- during the pH cycle for wild-type MnP3

The response of alkali-treated wild-type MnP3 enzyme to Ca^{2+} addition at an earlier stage in the pH cycle was observed when 5mM $CaCl_2$ was added to form A^- at pH 8.6. The aim was to see if calcium addition would stabilise the enzyme and encourage more reversible behaviour.

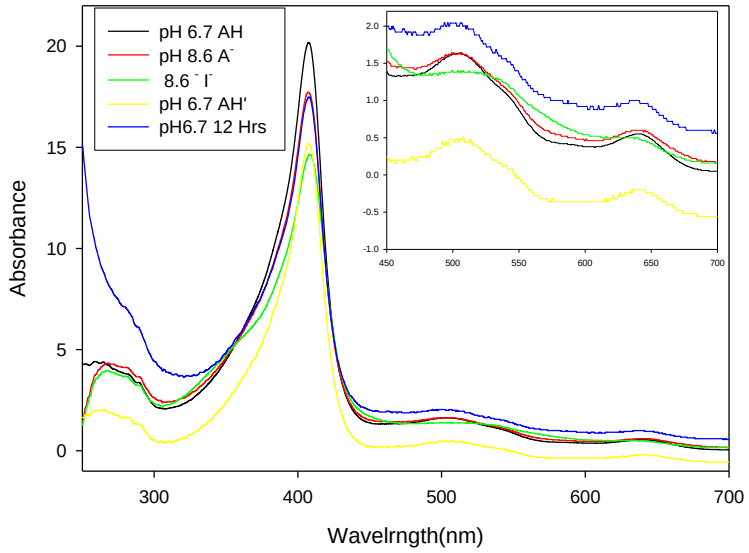

Figure 6.3: UV/visible spectra of pH cycled forms of wild-type MnP3 with 5 mM $CaCl_2$ added. The spectra of A^- , I^- , X and AH' have been corrected for dilution caused by pH adjustment. AH, pH 6.7 (—); A^-, pH 8.6 (—); I^-, pH 8.6 (—) after 1 hour at 25°C; X, pH 6.7(—), AH' pH 6.7 (—) after 12 hours at 25°C pH 6.7.

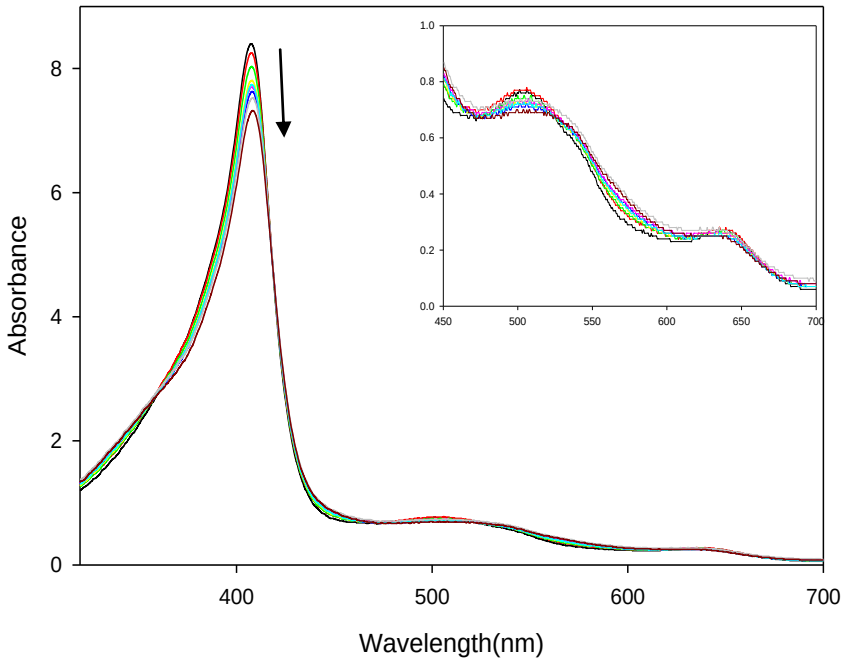

Figure 6. 4: UV/visible spectra of wild-type MnP3 showing the conversion of form A^- to form I^- in the presence of 5mM $CaCl_2$. The enzyme was incubated for 40 mins at 25°C and scans repeated every 2 mins. Spectra show a gradual change from purely high- spin to a mixture of high spin and low spin ferric iron in the haem group.

Form AH was treated with buffer to produce pH 8.6, as above. This resulted in conversion of form AH to form A^- (Figure 6.3, Table 6.1). On addition of 5 mM $CaCl_2$ and incubation of form A^- at pH 8.6 for 1 hr, the enzyme form was partially, and slowly, converted to form I^-, (Figure 6.3). The I^- spectrum had a slight red shift in the Soret peak to 409 nm and a 27% decrease in Soret extinction coefficient. A corresponding 40% decrease in activity was seen. The CT I was also slightly blue shifted to 636 nm, and CTI II was slightly red-shifted to 508nm.

The spectral changes observed are possibly indicative of a mixed population of largely high-spin 6-coordinate enzyme and some low-spin 6-coordinate haem iron. According to the studies of Feis *et al*., (1998) and deRopp *et al*., (1997) using electronic absorption, NMR and resonance Raman spectroscopy at neutral pH, unusual mixed-spin haem states (mixture of high-spin (S = 5/2) and intermediate spin (S = 3/2)) have been observed to be common to three Class III peroxidases, HRP isoenzyme A2, soybean peroxidase, and barley peroxidase at room temperature.

Lowering the pH to 6.7 caused a rapid change in Soret intensity and enzyme activity. The spectrum of the X form of MnP3 (recorded within the first minute of adjusting the pH back to 6.7) showed the Soret peak blue shifted to 407 nm with CT I and CT II bands at 641 and 508 nm, respectively. A restoration to 96% of initial enzyme activity was also observed. The spectrum and activity of the enzyme therefore closely resembled that of resting state, AH.

Interestingly, the activity of the X form was observed to gradually decrease with time (AH' form). Within the first minute of return to pH 6.7, activity was restored to 96 % of the initial activity. After one hour the activity was observed to drop to 85%, while incubation for 24 hours resulted in a decrease to 73%. The gradual activity loss and the inability of the Soret

absorbance to fully return to its initial value may be attributed to enzyme loss through aggregation, a process that apparently the presence of $CaCl_2$ cannot protect against.

Therefore the addition of 5 mM $CaCl_2$ has significantly stabilised the enzymes spectral features and reduced the loss of activity during the alkaline pH change. The transition of enzyme form A^- to I^- is strongly affected by the presence of calcium. Calcium has been observed to prevent the majority of the enzyme changing to the low-spin, largely inactive form. The A- to I- transition therefore involves the loss of one or more Ca^{2+} ions from the enzyme. Calcium was also able to promote the recovery of most of the initial activity (reversible inactivation) but is not able to prevent the final irreversible denaturation and aggregation that is time dependent.

6.2.3 Spectroscopic and activity changes occurring with the MnP3 mutant E40H/E44H, during the pH cycle.

The MnP3 mutant, E40H/E44H was treated in the same way as the wild-type enzyme for the pH cycle experiment. Figure 6.5 shows the UV/visible spectra of E40H/E44H forms during the pH cycle, while Table 6.2 shows the spectral features, activity and extinction coefficients of the different spectroscopic states observed.

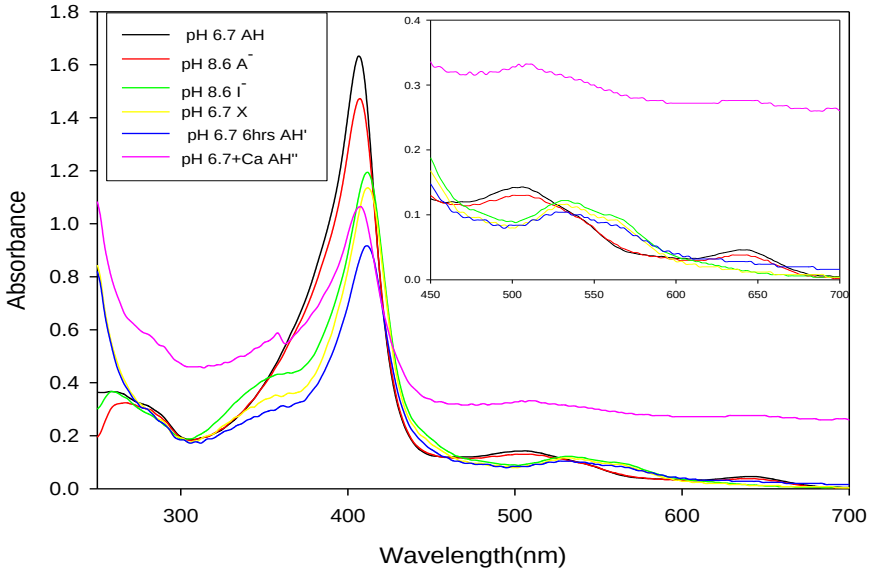

Figure 6.5: UV/visible spectra of pH cycled forms of MnP3 mutant, E40H/E44H. The spectra of A^- , I^- , X and AH' have been corrected for dilution caused by pH adjustment. AH, pH 6.7 (—); A^-, pH 8.6 (—); I^-, pH 8.6 (—) after 1 hour at 25°C; X, pH 6.7(—), AH' pH 6.7 (—) after 6 hours at 25°C and AH' (+ $CaCl_2$), pH 6.7(—).

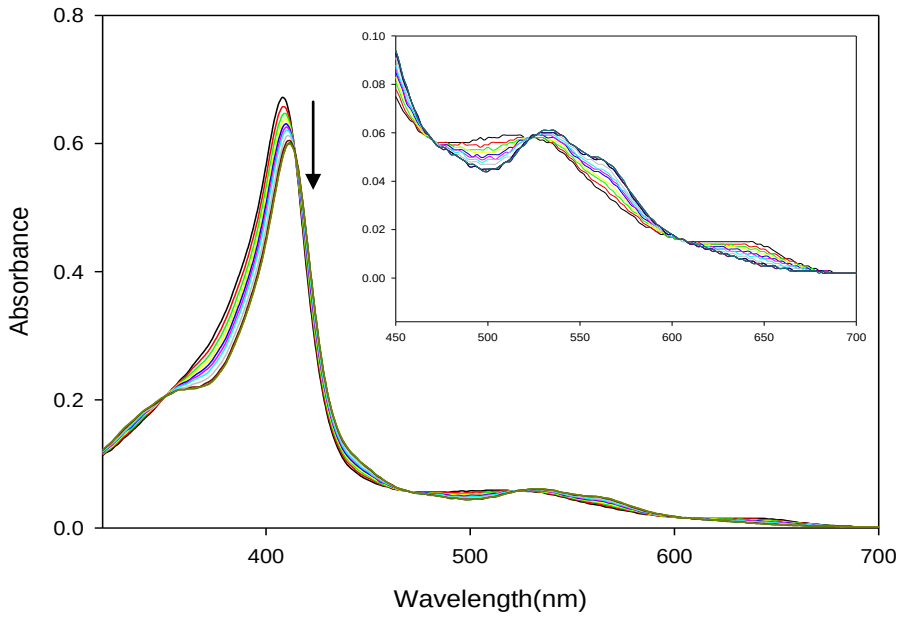

Figure 6.6: UV/visible spectra showing the conversion of form A^- of E40H/E44H to form I^- at pH 8.6. The enzyme was incubated for 40 mins at 25°C and scans repeated every 2 mins. Spectra show a gradual change from high- spin to low spin ferric iron in the haem group.

Table 6.2: Spectral characteristics, remaining activities and extinction coefficients of the different forms of E40H/E44H MnP3 mutant during pH transitions. The experiment was carried out in equal concentrations of MOPS and Bicine and the temperature was maintained at 25°C. The standard Mn (II) oxidation assay conditions were used. Characteristics were extracted from spectra depicted in Figure 6.5. Extinction coefficients were calculated using the concentrations of the various enzyme forms. Soret, β, α, CT II, CTI, and shoulder (on a major peak) denote the type of absorption band of the spectra. HS = spin. LS – low spin. + = the wild-type MnP3 would have been in the AH' state, the E40H/E44H in Figure 6.5 variant does not reattain this state.

pH	Predominant form	Percentage remaining activity	Soret (nm)	Extinction coefficient ($mM^{-1}cm^{-1}$)	β(nm)	α(nm)	Soret Shoulder (nm)	CT II (nm)	CT I (nm)	Spin state
6.7	AH	100	406	170	—	—	—	506	640	HS
8.6	A^-	22.4	408	154	—	—		500	640	HS
8.6	I^-	7	412	120	532	564	368	—	—	LS
6.7	X	0.7	412	114	532	564	368	—	—	LS
6.7	+ AH'	5	410	93	528	546	—	—	—	LS
6.7	+AH' + 0.4mM Ca^{2+}	17	408	112	—	—	—	502	640	HS

At pH 6.7, the E40H/E44H MnP3 mutant, resting state form AH spectrum has characteristic bands at 406 nm (Soret) and two charge transfer bands at 506 nm (CT II) and 640 nm (CT I), which are indicative of a high-spin mainly 6-coordinate haem protein.

Following alkaline transition to pH8.6 and formation of an A^- state, the spectrum (recorded within the first minute of exposure to alkaline conditions) showed absorption maximum slightly red-shifted in the Soret region to 408 nm, while the CT II blue-shifted from 506 nm to 500 nm and CT I remained at 640 nm. On incubating the E40H/E44H form A^- at pH 8.6 for about an hour, with repeat spectral scans every 120 seconds, significant changes similar to those observed for the wild-type were observed. The A^- form was converted to the I^- form with Soret red-shifted to 412 nm, a shoulder at 368 nm, CT bands I and II disappeared and α and β bands appeared at 532 and 564 nm indicating a low-spin haem iron. Five isosbestic points were also observed for the change at 352, 414, 472, 524 and 612 nm (Figure 6.6). The percentage activity remaining decreased to 7%.

The spectrum (taken within the first minute) of taking lowering the pH back to 6.7, showed that the haem iron was still in a predominantly low-spin state. Unlike the wild-type enzyme, incubating E40H/E44H at pH 6.7 for 24 hours led to very little recovery of activity or spectral features. Only 5% of the activity was recovered while the low spin α and β features persisted. The enzyme did not recover to the AH' state.

However, on addition of 0.4 mM Ca^{2+}, a significant recovery of the high-spin characteristics of the enzyme was observed (Figure 6.5, Table 6.2). The Soret absorption maximum blue-shifted back from 412 nm to 408 nm, the α and β bands at 528 nm and 564 nm disappeared, while the CT I and CT II reappeared at 640 and 502

nm, respectively. Hence, the X form of the mutant enzyme was presumably lacking a calcium ion presumably the less tightly bound distal calcium, which was then recovered from the excess calcium added.

An experiment was also conducted in which the A^- form of the mutant E40H/E44H was treated with 5 mM $CaCl_2$ and incubated at the H 8.6 for about one hour. Figure 6.7 shows the spectra obtained at various stages during the subsequent pH cycle, while Figure 6.8 shows the spectra obtained during incubation of the enzyme at alkaline pH. Similar to the wild-type only slight changes in the spectral features were observed, with no significant changes showing the presence of low spin haem. This means that the presence of Ca^{2+} prevents completely the A- to I' transition, maintaining the enzyme in the active high spin form.

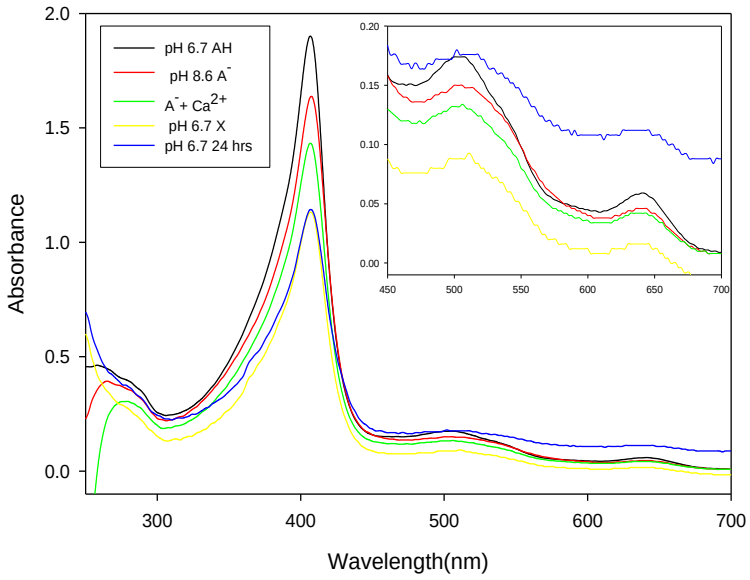

with addition of 5mM$CaCl_2$ to enzyme form A^-. The spectra of A^- , A^- + Ca^{2+}, X and AH' have been corrected for dilution caused by pH adjustment. AH, pH 6.7 (—); A^-, pH 8.6 (—); A^- + 5mM Ca^{2+}, pH 8.6 (—) after 1 hour at 25°C; X, pH 6.7(—), AH' pH 6.7 (—) after 24 hours at 25°C.

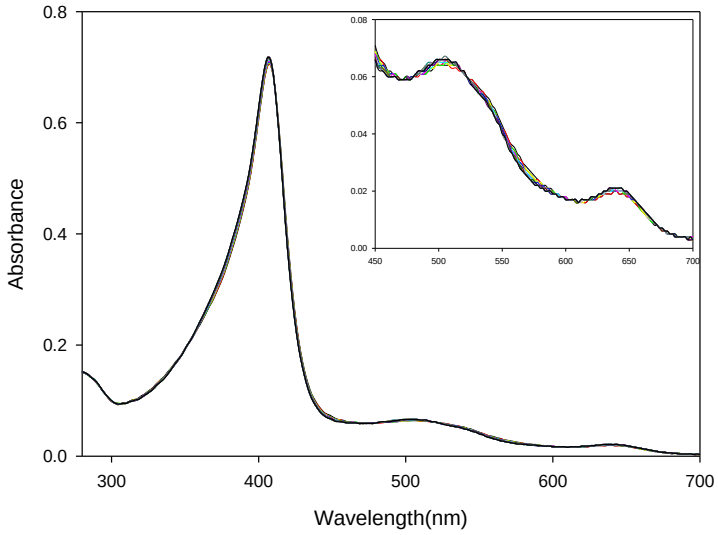

Figure 6.8: UV/visible spectra showing the conversion of form A^- of E40H/E44H to form I^- at pH 8.6. The enzyme was incubated for 40 mins. At 25°C and scans repeated every 2 mins. Spectra showed no obvious change from high-spin to low spin ferric iron in the haem group. The change here was much slower than when no Ca was added to enzyme form A^-.

6.2.4 D186H mutant MnP3 spectroscopic and activity changes during the pH cycle

The *P. radiata* MnP3 mutant D186H exhibited a high-spin ferric haem absorption spectrum with a Soret maximum at 406 nm and CT band maxima at 502 and 640 nm at pH 6.7 (form AH). On raising the pH to 8.6, the enzyme changed to form A^- with an 11 %, and 40% loss in Soret absorbance and activity, respectively. The spectrum (recorded within the first minute of enzyme's exposure to alkaline pH conditions) showed that the enzyme still maintained in the high-spin state (see Figure 6.9, Table 6.3). Incubating the enzyme for about one hour at pH 8.6 resulted in the A^- to I^- form conversion with spectral features indicative of a low-spin ferric haem (Figure 6.10 and Table 6.3). Incubating the enzyme for about one hour at pH 8.6 resulted in the A^- to I^- form conversion with spectral features indicative of a low-spin ferric haem (Figure 6.10 and Table 6.3).

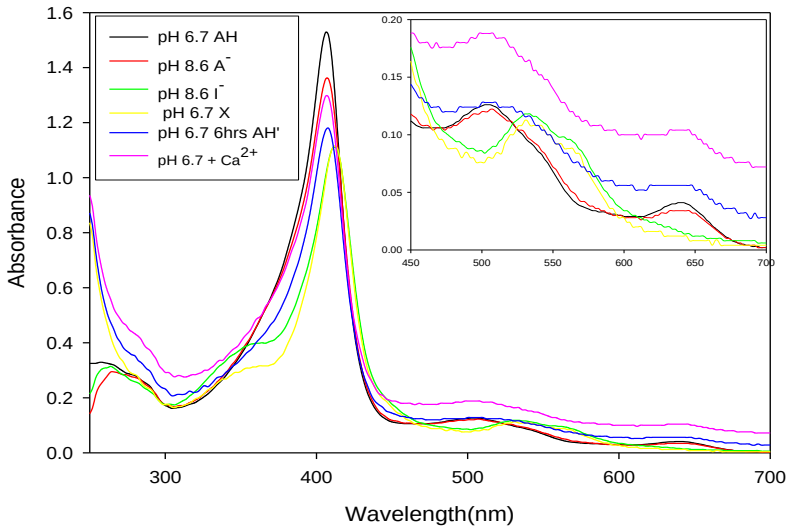

Figure 6.9: UV/visible spectra of the pH cycled forms of MnP3 mutant D186H. The spectra of A^- , I^- , X and AH' have been corrected for dilution caused by pH adjustment. AH, pH 6.7 (—); A^-, pH 8.6 (—); I^-, pH 8.6 (—) after 1 hour at 25°C; X, pH 6.7(—), AH' pH 6.7 (—) after 6 hours at 25°C and AH' + $CaCl_2$, pH 6.7 (—).

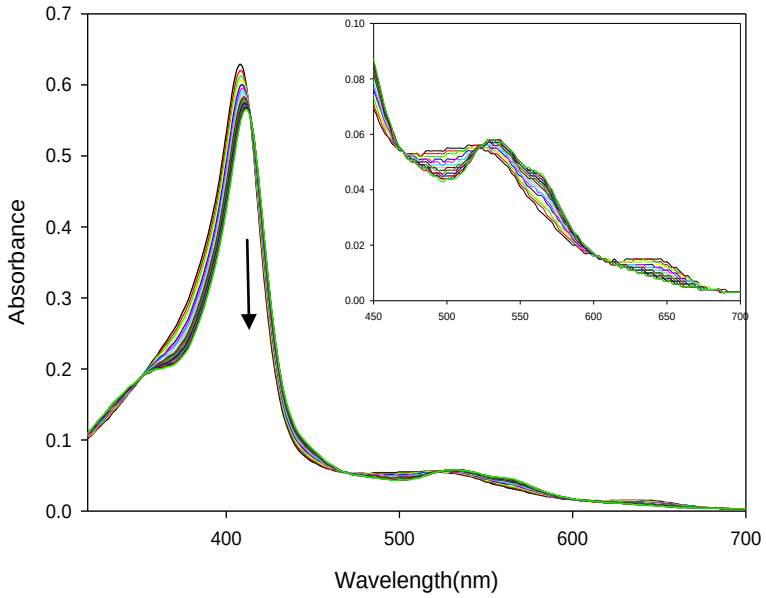

Figure 6.10: UV/visible spectra showing the conversion of form A^- of D186H to form I^- at pH 8.6. The enzyme was incubated for 40 mins at 25°C and scans repeated every 2 mins. Spectra show a gradual change from high-spin to low-spin ferric iron in the haem group.

Table 6.3: Spectral characteristics, remaining activities and extinction coefficients of the different forms of MnP3 mutant, D186H during pH transitions. The experiment was maintained at 25°C. The standard Mn (II) oxidation assay conditions were used. Characteristics were extracted from spectra depicted in Figure 6.9. Extinction coefficients were calculated using the concentrations of the various enzyme forms. Soret, β, α, CT II, CTI, and shoulder denote the type of absorption band of the spectrum. HS = high spin, low spin.

pH	Predominant form	Percentage remaining activity	Soret (nm)	Extinction coefficient ($mM^{-1}cm^{-1}$)	β(nm)	α(nm)	Shoulder (nm)	CT II (nm)	CT I (nm)	Spin state
6.7	AH	100	406	170	—	—	—	502	640	HS
8.6	A^-	60	408	152	—	—	—	506	638	HS
8.6	I^-	2	412	119	534	564	368	—	—	LS
6.7	X	2.4	412	118	542	562	370	—	—	LS
6.7	AH'	27	408	132	—	—	—	507	638	HS
6.7	AH' + 0.4mM Ca^{2+}	33	406	45	—	—	—	500	638	HS

An experiment was also conducted with the addition of 5mM $CaCl_2$ to the A^- form of the alkaline treated D186H and the enzyme was observed to behave in a similar manner to the wild-type and E40H/E44H enzymes, in that incubation of the enzyme form A^- at pH 8.6 in the presence of Ca^{2+} ions for about one hour resulted in no change in the absorption maxima of the spectrum observed (Table 6.4) with no evidence of a low-spin haem. A marked recovery of the Soret absorbance and activity that was lost on formation of the A^- form occured on lowering the pH back to 6.7 and incubating the enzyme for about six hours.

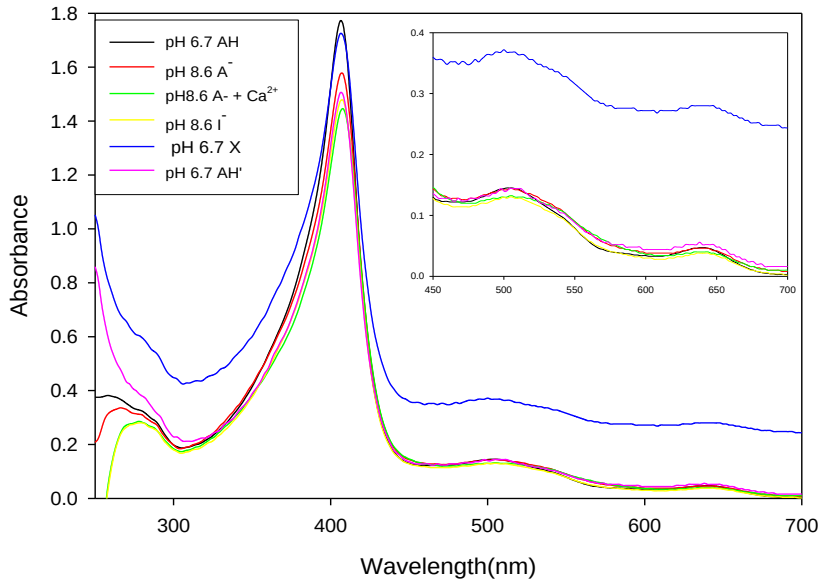

Figure 6.11: UV/visible spectra of the pH cycled forms of MnP3 mutant D186H with 5 mM $CaCl_2$ added to form A^-. The spectra of A^- , I^- , X and AH' have been corrected for dilution caused by pH adjustment. AH, pH 6.7 (—); A^-, pH 8.6 (—); I^-, pH 8.6 (—) after 1 hour at 25°C; X, pH 6.7(—), AH' pH 6.7 (—) at 25°C and AH' + $CaCl_2$, pH 6.7 (—).

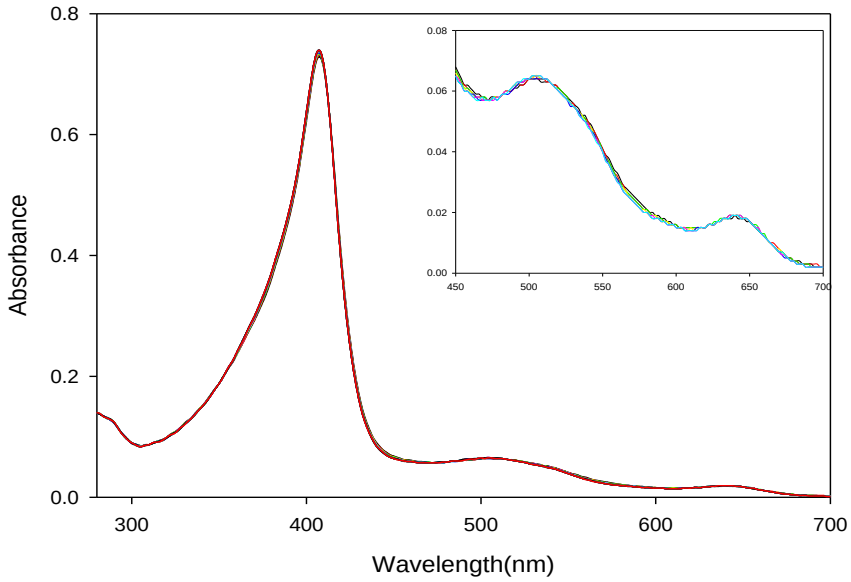

Figure 6.12: UV/visible spectra showing the conversion of form A^- of D186H to form I^- at pH 8.6. The enzyme was incubated for 40 mins at 25°C and scans repeated every 2 mins.

6.2.5 D186N mutant MnP3 spectroscopic and activity changes during the pH cycle.

The UV-Vis spectral features for MnP3 mutant, D186N at pH6.7 and 8.6 are shown in Figure 6.13 and Table 6.4.

On elevating the pH to 8.6, the enzyme converted to form A^- and the spectrum (obtained within first minute of enzyme's exposure to alkaline conditions) showed a red-shifted Soret, to 408nm and although the positions of the charge transfer bands at 640 and 504 nm remained unchanged, a shoulder at 374 nm appeared. At pH 8.6 the enzyme initially lost 55%, and 64% of its Soret absorbance and activity respectively.

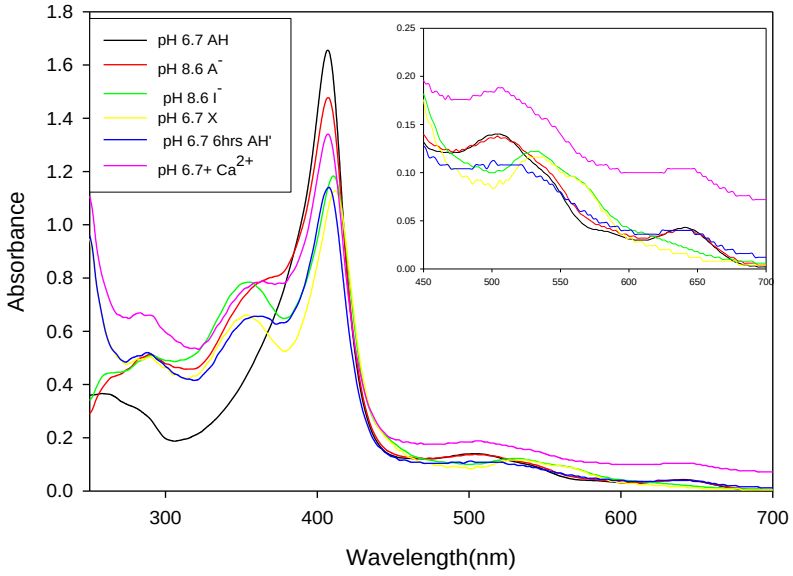

Figure 6.13: UV/visible spectra of the pH cycled forms of MnP3 mutant D186N. The spectra of A^- , I^- , X and AH' have been corrected for dilution caused by pH adjustment. AH, pH 6.7 (—); A^-, pH 8.6 (—); I^-, pH 8.6 (—) after 1 hour at 25°C; X, pH 6.7(—), AH' pH 6.7 (—) after 6 hours at 25°C and AH' + $CaCl_2$, pH 6.7 (—).

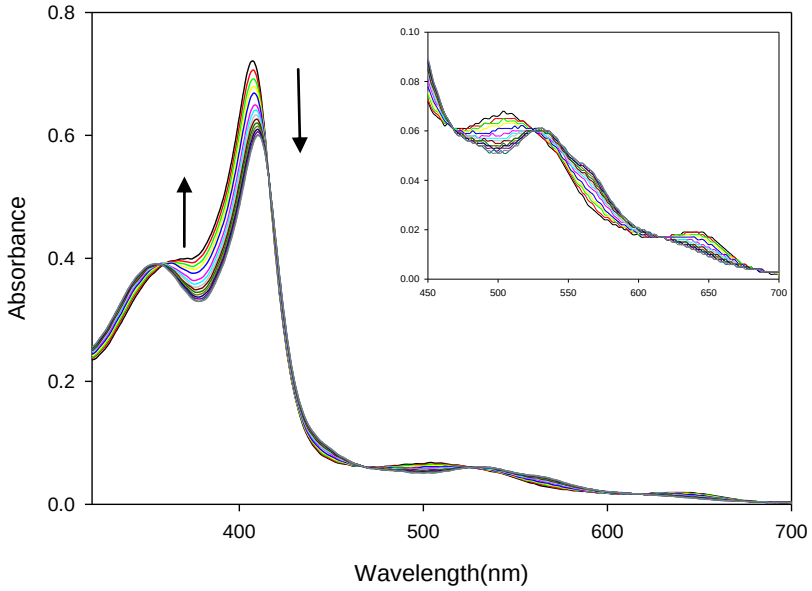

Figure 6.14: UV/visible spectra showing the conversion of form A^- of mutant D186N to form I^- at pH 8.6. The enzyme was incubated for 40 mins at 25°C and scans repeated every 2 mins. Spectra show a gradual change from high- spin to low spin ferric iron in the haem group.

Table 6.4: Spectral characteristics, remaining activities and extinction coefficients of the different forms of MnP3 mutant, D186N enzyme during pH transitions. The experiment was maintained at 25°C. The standard Mn (II) assay conditions were as use in the activity assay. The enzyme sample was diluted 50 times before a further 100 fold dilution into the activity assay. Characteristics were extracted from spectra shown in Figure 6.13. Extinction coefficients were calculated using the concentrations of the various enzyme forms. Soret, β, α, CT II, CTI, and shoulder denote the type of absorption band of the spectrum. HS = high spin. LS = low spin

pH	**Predominant form**	**Percentage remaining activity**	**Soret (nm)**	**Extinction coefficient ($mM^{-1}cm^{-1}$)**	**β (nm)**	**α (nm)**	**Soret Shoulder (nm)**	**CT II (nm)**	**CT I (nm)**	**Spin state**
6.7	AH	100	406	168	—	—	—	504	640	HS
8.6	A^-	36	408	150	—	—	374	504	640	HS
8.6	I^-	8	410	118	530	—	374	—	—	LS
6.7	X	6	412	110	532	—	374	—	—	LS
6.7	AH'	9	408	116	—	—	374	—	638	HS
6.7	AH' + 0.4mM Ca^{2+}	13	406	136	—	—	—	506	638	HS

Incubation of the D186N enzyme for one hour at alkaline pH resulted in form A^- to I^- conversion (Figure 6.14). The electronic spectrum for the I^- form of D186N was characteristic of a 6-coordinate low-spin species with maxima at 410 nm (Soret) and 530 nm (β band), and a shoulder at 374nm (Table 6.4). The charge transfer bands also disappeared and the percentage of remaining activity was reduced to 8 %.

On returning the enzyme back to the acidic pH 6.7, form I^- converted to form X and the spectrum (recorded within the first minute of downward pH jump) (Figure 6. 13) showed the Soret and the β peaks further red-shifted to 412 and 532 nm respectively and a shoulder at 374 nm, indicative of the enzyme still being in the low-spin haem state. Further incubation at pH 6.7 resulted in the Soret maximum blue-shifting to 408 nm, a disappearance of the α and β peaks and a reappearance of charge transfer bands, CT I at 638 nm, indicating an increased proportion of the high-spin form.

Addition of 0.4mM $CaCl_2$ restored the CT II at 506 nm and Soret peak back to its initial position at 406 nm and strengthened its intensity. However, initial activity of the enzyme was not significantly recovered (Table 6.4).

6.2.5.1 Addition of 5mM $CaCl_2$ to form A^- at pH 8.6 of D186N

To stabilise the spectral and kinetic characteristics of the mutant 5mM $CaCl_2$ was added to enzyme form A^-. Figure 6.15 show the spectra of the different forms of the enzyme. The initial pH 6.7 form of the enzyme (AH) has absorption maxima at 406 nm (Soret), 640 nm (CT I) and 504 nm (CT II), indicative of high-spin haem. The adjustment of pH to 8.6, again converted the AH form of the enzyme to form A^-.

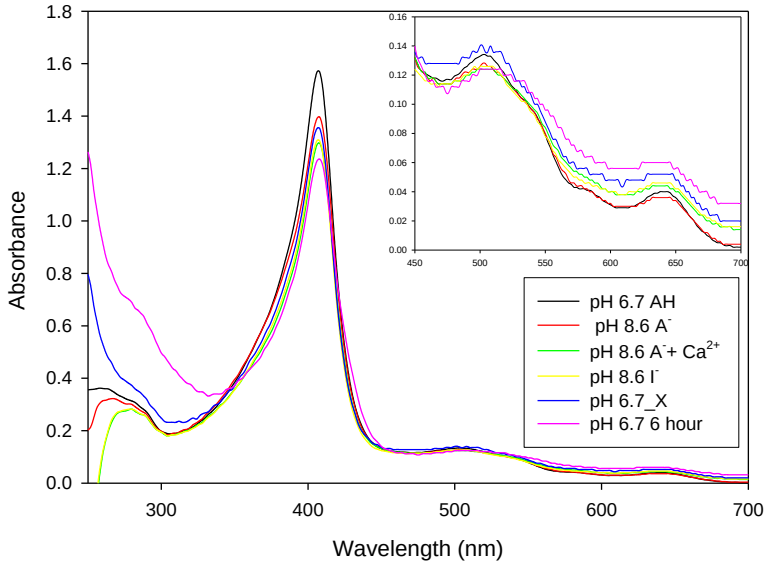

Figure 6.15: UV/visible spectra of the pH cycled forms of MnP3 mutant D186N with 5 mM $CaCl_2$ addition to form A^-. The spectra of A^- , I^- , X and AH' have been corrected for dilution caused by pH adjustment. AH, pH 6.7 (—); A^-, pH 8.6 (—); A^- + $CaCl_2$, pH 6.7 (—); I^-, pH 8.6 (—) after 1 hour at 25°C; X, pH 6.7(—), After 6 hours incubation pH 6.7 (—) at 25°C.

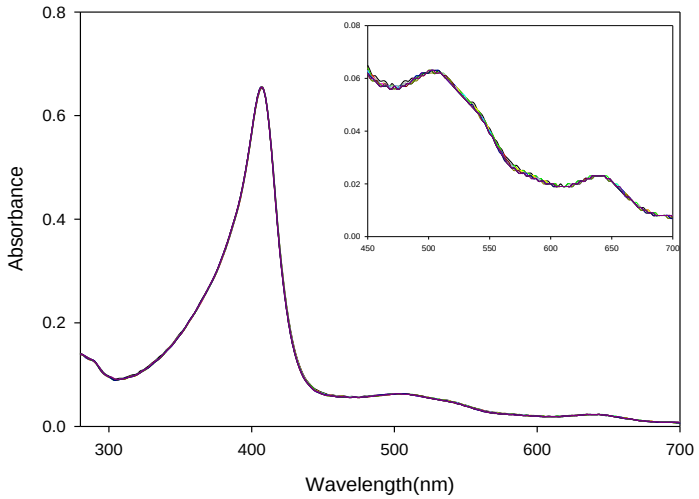

Figure 6.16: UV/visible spectra showing the conversion of form A^- of mutant D186N to form I^- at pH 8.6. The enzyme was incubated for 40 mins at 25°C and scans repeated every 2 mins.

The spectrum recorded within the first minute of exposure to alkaline conditions showed that the Soret position had not altered, but the charge transfer bands slightly shifted to 638 nm (CT I) and to 502 nm (CT II), with a significant decrease in the Soret absorbance and activity by 55% and 70% respectively, occured. Addition of 5mM $CaCl_2$ to enzyme form A^- stopped the transition to low-spin haem as for all other MnP3 enzymes. Returning the enzyme to pH 6.7, with incubation the absorption peaks were fully restored, to those of the AH state: 408 nm (Soret), 636 nm (CT I) and 508 nm (CT II).

6.3 Effect of calcium on alkali-treated MnP3

The alkali-treated MnP3 enzymes when returned to pH 6.7 all responded to the addition of exogenous calcium (5mM $CaCl_2$). It was observed that lowering the pH from 8.6 back to 6.7 without the addition of calcium at most partially restored the activity of the enzyme. However, incubating the enzyme with exogenous calcium at acidic pH for 24 hours restored the spectral features of the enzyme, i.e. high-spin compared to low spin, but still did not fully restore 100% enzyme's activity. Sutherland *et al*., (1996) showed that the extent of recovery of activity was inversely dependent upon the duration of exposure to the extreme condition, suggesting that other structural rearrangements were occurring within the protein, which predisposed the enzyme to irreversible inactivation.

Successful stabilization of peroxidase activity and electronic structure in alkaline pH was obtained by adding Ca ions to the sample. This observation is in agreement with the results reported for *P.chrysosporium* LiP (George *et al*., 1999). These experiments, where 5 mM $CaCl_2$ were added to A^- forms of the enzymes showed that alkaline inactivation of MnP3 could be avoided. The key point is that the addition of exogenous Ca^{2+} prevents the A^- to I^- *i.e.* high-spin transition to low-spin. The enzyme can then

almost completely be reactivated at return to low pH provided Ca^{2+} is present. Mutant enzymes were found to have an even more critical dependence on Ca^{2+}. The effect of Ca^{2+} on MnP3 in this study is consistent with previous reports (Canverso and Fernandez, 1996; Henriksen *et al*., 1998; Rasmussen *et al*., 1998; van Huystee *et al*., 2004).

Catalytic activity of MnP3 from *P. radiata* as in other peroxidases depends on Ca^{2+} ions embedded in the enzyme. Calcium release has previously been observed both during thermal and alkaline inactivation of MnP and LiP (Haschke and Friedhoff, 1978; Sutherland and Aust, 1996; Nie and Aust, 1997; George *et al.*, 1999). A previous inactivation model proposed an increase in distal histidine flexibility after Ca^{2+} loss, leading to a low-spin haem and to activity inhibition (Sutherland *et al.*, 1997; Nie and Aust, 1997). In addition, Howes *et al*., (2001) suggested that for Ca^{2+}-depleted HRP, other structural changes around the proximal histidine could occur and influence the catalytic performance of the enzyme.

The cause-consequence relationship between inactivation and Ca^{2+} loss has been established by reconstituting peroxidase activity in the presence of $CaCl_2$. In this study, the preservation of Soret absorption, and a high spin haem, as well as partial restoration of activity corroborate the direct dependence of catalytic activity on structural Ca^{2+} ions.

In this work, calcium loss has been shown to play an important role in the pH inactivation of MnP3. The data collected provide a viable explanation that calcium ion plays a role in conferring structural stability to the haem environment and in retaining the enzyme active site geometry. Calcium also functions in conversion of the haem iron from a low-spin state to a high-spin state following reversible inactivation.

6.4 Kinetics of the pH induced A^- to I^- conversion

In peroxidases, activity is dependent on the presence and correct conformation of the haem group and the residues forming the catalytic pocket. Conformational changes of the protein are likely affect enzyme activity (Neves-Petersen *et al.,* 2007)**.**

A slow pH-dependent spectral transition in such haem proteins as horseradish peroxidase (Araiso and Yamazaki, 1978; Kihara et al., 1978) and turnip peroxidase (Job et al., 1977) has been reported. Though the transitions previously reported were termed "slow", the time scale referred to is generally the order of milliseconds, that is, slow relative to many spectral changes but much faster than the changes reported in this work. It is interesting to note that one isozyme of turnip peroxidase, P_1, exhibited a very slow spectral change after a pH jump, with $T_{1/2} = \sim 0.05\ s^{-1}$ (Job *et al*., 1977). However, this change accounted for less than 10% of the total spectral alterations, most of which was orders of magnitude faster.

For MnP3 from *P. radiata,* the three mutants enzymes, E40H/E44H, D186H and D186N involved in this study had spectral changes that could be described as essentially first order reactions (Figures 6.17, a and b), but the wild-type which is essentially first order also shows evidence of second slow phase. Thus MnP3 appears to possess a unique mechanism of haem-protein interaction, involving both catalytic and spectral properties of the enzyme and occurring in a physiologically significant pH and time context.

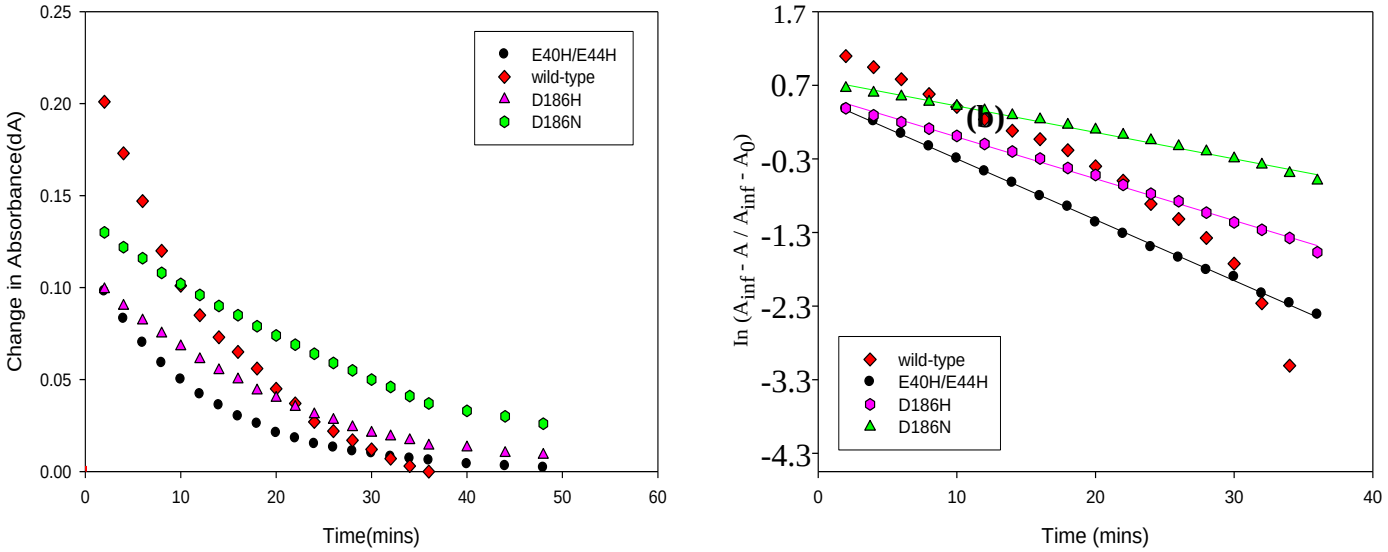

Figure 6.17: **(a)** Time- of change in absorbance at 408nm during the conversion of enzyme form A^- to I^- of wild-type, E40H/E44H, D186H and D186N MnP3 enzymes.

(b) Semi-log plots used to determine the first-order rate constants for the loss of haem at 408 nm during the conversion of enzyme form A^- to I^- of wild-type MnP3 and mutants E40H/E44H, D186H and D186N. The determined rate constants extracted from the gradients of the straight lines for wild-type, E40H/E44H, D186H and D186N are in Table.6.5 shows the rates and the decay constants obtained.

Table 6.5: Change in extinction coefficient, rate, rate constant and percentage (%) of remaining activity for the conversion of form A^- of wild-type MnP3 and mutants enzymes to form I^- after upward pH jump from pH 6.7 to pH 8.6.

MnP3	Change in extinction coefficient ($\Delta\ \varepsilon_o$)	Rate Constant ($_{Kd}$) (min^{-1})	Half-life($T_{1/2}$) (min)	Percentage (%) remaining activity	Second slow phase
Wild-type	45	0.25 ± 0.01	2.8	10	Yes
E40H/E44H	34	0.12 ± 0.0003	5.8	7	No
D186H	33	0.12 ± 0.002	5.8	2	Yes
D186N	32	0.15 ± 0.004	4.6	8	Yes

The decrease in Soret absorbance has been used as a convenient probe for the conformational stability of *Coprinus cinereus* peroxidase (CiP) (Tam and Welinder, 1996; Tam and Welinder, 1998) during high pH, urea, and heat treatments. This assumption was also employed by Lige *et al*., (2001) to determine the rate of irreversible unfolding of wild type and mutant peanut cationic peroxidase using guanidium chloride. The remaining fraction of native peroxidase (RP) at time t is described by equation thus:

$$RP = [native]_t / [native]_0 = (A_t - A_\infty) / (A_0 - A_\infty)$$

Where A_t is the absorbance at time t (during the unfolding reaction), A_0 is the initial absorbance at time 0, and A_∞ is the absorbance at the end of the reaction.

The pH inactivation of MnP3 followed first-order kinetics. Therefore, a plot of In (ΔA) versus time gave a straight line, Figure 6.17b from where rate constant of inactivation reaction (k) can be deduced and half-life ($t_{1/2}$) calculated. The loss of absorbance occurs with a rate constants (k) = 0.25 min^{-1}, and half-life ($T_{1/2}$) = 2.8 min; k = 0.12 min^{-1}, $T_{1/2}$ = 5.8 min; k = 0.12 min^{-1}, $T_{1/2}$ = 5.8 min; and k = 0.15 min^{-1}, $T_{1/2}$ = 4.6 min for wild-type MnP3 and mutants, E40H/E44H, D186H and D186N (Figure 6. 17and Table 6.5).

The comparison of stability of peroxidases has shown that many of these enzymes have similar stabilities. Only anionic peroxidase isolated from soybean hulls exhibits significantly higher pH and thermal stabilities (McEldoon *et al*., 1995; McEldoon and Dordick, 1996). Although the crystal structure of recombinant soybean peroxidase has been reported (Henriksen *et al*., 2001), reasons for the high stability of this peroxidase are not clear yet.

The effect of pH on wild type and mutant, E40H/E44H, D186H and D186N) MnP3 stability is shown in the Figures 6.1 - 6.16 as well as Tables 6.1 - 6.4 above. Identification of the various conformational forms of the enzymes in this work uses data based solely on the enzyme's activity and the UV/visible spectra. It has been observed that the wild-type and mutant MnP3 enzymes respond similarly to alkaline transition by activity loss and conformational changes evident in the spectral features. The presence of calcium was also observed to either prevent or minimise the extent of alkaline inactivation of these enzymes implying that calcium has a significant capacity to stabilise the enzyme's haem environment and prevent activity loss.

It was possible to detect four distinct spectroscopic species associated with enzyme state, which interconvert in a reversible manner between pH 6.7 and 8.6 during MnP3 pH transitions. The outstanding conformational enzymes forms were designated as AH, A^-, I^-, and X. Although the electronic spectra alone do not allow quantification of the relative proportion of these forms, results indicate that the high spin haem state is favoured at acidic pH and that the low spin haem form is favoured at alkaline pH.

The results suggest that forms AH and A^- are in a rapid pH-dependent equilibrium. Since all activity measurements were carried out at the enzymes optimum pH (5.0 for wild-type and 8.0 for the mutants enzymes), it can be seen from the current data that form A^- is less active relative to form AH. The current data is also suggestive of forms I- and X as enzymatically inactive. Undoubtedly, A^- to I^- conversion involves a conformational change. The appearance of β and α band, as well as a shoulder n the Soret peak is suggestive of I^- being a low-spin form of the enzyme.

The following Scheme extended from that of Sanders *et al* (1994) would appear to explain the basic pH cycle of MnP3.

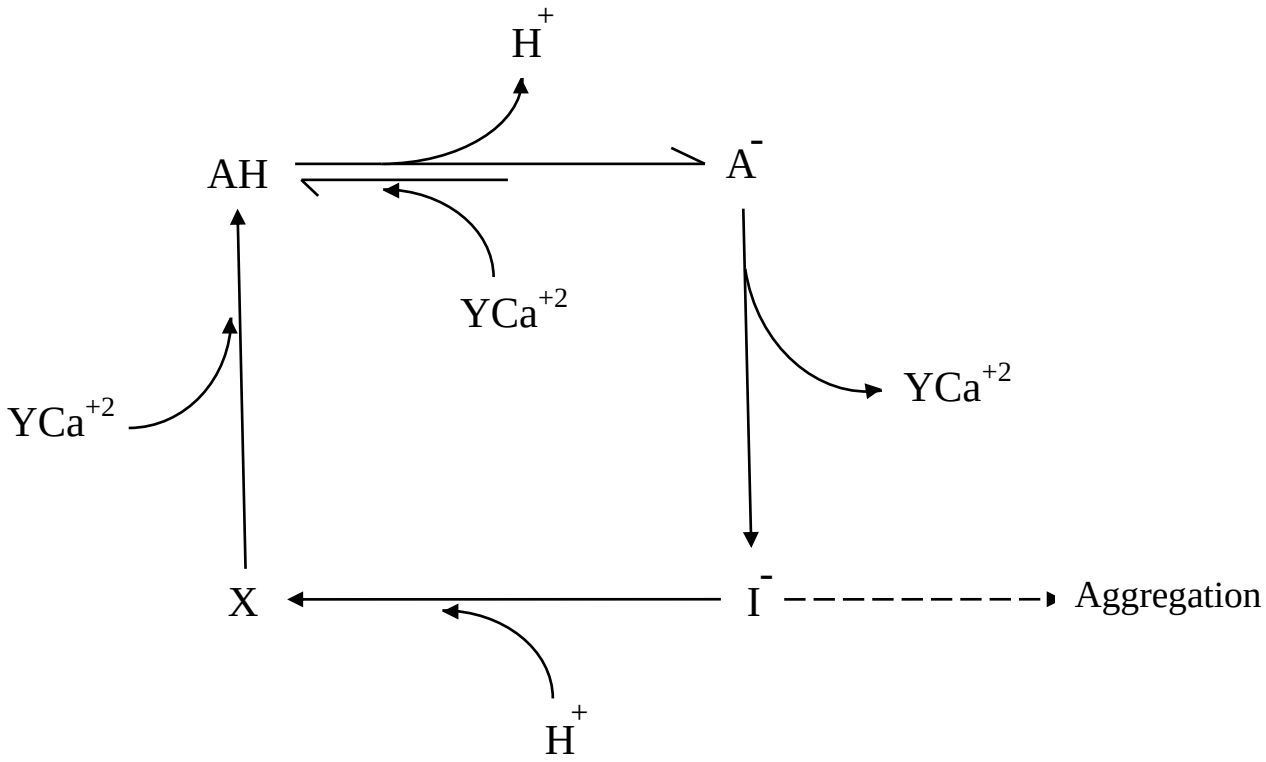

Scheme 6.2: A scheme describing the pH-dependent changes in the spectrum of *P.radiata* MnP3 enzymes. Reactions shown by solid arrow symbolise changes taking place when the pH is altered. Reaction indicated with broken arrow represent unfolding and aggregation following prolong incubation at alkaline pH.

(Where Y = 1 or 2)

1. It is hypothesised that state I^- and X have a collapsed haem pocket of some kind and it is not known whether the I^- or A^- states have lost one or two Ca^{2+} ions.
2. It is possible that the weaker site depleted in the A^- state and the more tightly bound site in the I^-form.
3. It is possible that protonation of the distal histidine in I^- drives the partial restoration of Soret features observed in X.

In view of the spectral properties of the enzyme forms described and in comparison to those of other haem proteins (Smith and Williams, 1970; Dunford and Stillman, 1976; Smulevich *et al*., 1988; Miller *et al*., 1990; Vitello *et al*., 1992) it is possible to imagine the nature, in the different enzyme forms, of the ligand occupying the sixth coordination position of the haem iron. At alkaline pH a transition to six-coordinate low spin has been observed where the sixth ligand is OH^- hydrogen bonded directly to distal arginine, and through a water molecule to distal histidine (Vitello *et al*., 1992). The alkaline transition of MnP3 is therefore proposed to be an abstraction of a hydrogen atom from a water molecule in the distal cavity with subsequent binding of OH^- group to the haem iron, rather than a deprotonation of an amino acid side chain. Hence, it is suggestive that, in form AH, a molecule of H_2O occupies the sixth coordination position. The possibility that an amino acid residue deprotonates in alkaline solution and becomes the sixth iron ligand cannot be excluded by the data obtained in this study

With the apparently simple relationship that exists between AH and A^-, it is assumed that, in the form A^-, the ligand should be OH^-. A β-absorption band closer to 540 nm favours the coordination of a hydrogen bonded OH^- ligand rather than an amino acid residue around 525 nm (Vitello *et al*., 1992). The conversion of form I^- to form X is considerably more rapid than that of form A^- to form I^- but still appears slower than the AH to A^- interconversion. It may likely involve a conformational change in addition to a protonation, which might prompt a further conformational change. As observed, the formation of form X is undoubtedly followed by further slower conformational changes, which result finally in the regeneration of form AH designated AH'.

With this background, it could be postulated that at alkaline pH, MnP3 is deprotonated Protonation of MnP3 at low pH may preclude or perturb such stabilizing interactions and thereby favour the high spin form of the enzyme.

Conclusion

The transition of MnP3 from A^- to I^- is strongly affected by the presence of calcium. When $CaCl_2$ was added to A^- form of the enzyme only slight changes in the spectral features were observed, hence, high-spin state of the enzyme was maintained. Therefore $CaCl_2$ has significantly stabilised the enzymes spectral features and reduced the loss of activity during the alkaline pH change. Calcium was also able to promote the recovery of most of the initial activity (reversible inactivation) but is not able to prevent the final irreversible denaturation and aggregation that is time dependent.

Chapter Seven

Effect of temperature on the stability of MnP3

7.1 Introduction and background

The optimum temperature for peroxidase activity depends on the source of the enzyme (Lamikanra and Watson, 2000), but has been reported to be 25 to 60 °C. (Campos *et al*., 1996). Studies have also shown some instances where peroxidase stability and activity has increased under cold conditions (Kremer, 1970; Cano *et al*., 1998)

In general peroxidases are known as very stable enzymes (Stegemann *et al*., 1973), the mechanism of which is largely controlled by their structure, although thermostability has also been associated with hydrophobic linkage (Daniel *et al*., 1996). Calcium has been shown to be involved in maintaining the haem configuration (van Huystee *et al*., 1992) and therefore the activity of peroxidases (Ogawa *et al*., 1979).

Purified MnP contains 2 moles of calcium per mole of enzyme but only 1 mole of calcium per mole enzyme was found to be removed during reversible thermal inactivation (Sutherland and Aust, 1996.) Thermal inactivation of MnP is thought to be due to the loss of the more weakly bound distal calcium (Nie and Aust, 1997). This calcium is coordinated to helix B, which contains the amino acid residues involved in the binding of H_2O_2 and Mn^{2+} and has been proposed to function in the maintenance of the integrity of the active site environment (Sundaramoorthy *et al*., 1994), particularly, the coordination and spin state of the haem iron. Therefore, the loss of the distal calcium may disrupt the position of helix B, resulting in activity loss and marked spectroscopic changes at higher wavelength (Sutherland and Aust, 1996). A similar situation has been reported for LiP (Nie and Aust, 1997) and HRP (Haschke and Friedhoff, 1978; Shiro *et*

al., 1986). Excess calcium has also been found to decrease the rate of thermal inactivation and stabilise peroxidase enzyme at higher temperature (Timofeevshi and Aust, 1997).

The amount of residual peroxidase activity after heat treatment is often used as an index of enzyme inactivation (Burnette, 1977). The identification of highly stable and thus active peroxidases remains a key step in the development of an enzyme catalyst with broad commercial appeal. In particular, the good stability of a peroxidase enzyme at elevated temperatures (Sakharov, *et al*., 2002; Zamorano *et al*., 2008) would make it more useful for industrial applications.

7.2 The effect of EDTA or Ca^{2+} on the temperature stability of *P. radiata* MnP3 enzymes

In pursuit of a detailed characterization of *P. radiata* MnP3 enzymes, the effect of additives $CaCl_2$ and EDTA on wild-type and E40H/E44H mutant thermal stability was investigated. Thermal inactivation of these *P. radiata* enzymes was carried out by monitoring the activity remaining over time during incubation of the enzyme alone, or in the presence of 5mM $CaCl_2$ or 0.5mM EDTA, at 25°C, 40°C and 50°C, respectively, as described in section 2.4.12.

Initial studies performed at 25°C showed that wild-type MnP3 underwent a period of increasing activity during the first 3 hours of the incubation and that activity was then unchanged for a further 21 hours. This behaviour implies that MnP3 is highly stable at 25°C. In addition, although some inactivation of the enzyme was seen at 40°C, a half-life of 20 hours was found for wild-type enzyme with no additive. Therefore it was decided to perform most thermal inactivation experiments at 50°C, where the equivalent half-life for wild-type enzyme with no additive was found to be 24 minutes.

The addition of Ca^{2+} to assays after thermal inactivation was also investigated to see if the presence of calcium would cause an immediate increase in activity. Assay values were found to be the same both with and without $CaCl_2$ addition. Therefore all activities given are for without calcium.

7.2.1 Wild-type MnP3 thermal inactivation in the presence and absence of Ca^{2+} or EDTA

The results for wild-type MnP3 inactivation at 50°C are summarised in Figure 7.1 and the left half of Table 7.1. As mentioned above, the measured half-life for wild-type MnP3 at 50°C was 24 minutes. This compares to a figure of 10 minutes when 0.5mM EDTA is present in the incubating enzyme; only 2% activity was left in the EDTA-treated sample after 75 minutes. This implies that, at least at high temperature, EDTA, a divalent cation-chelating agent, increases the rate of inactivation of MnP3, presumably by increasing the loss of calcium from the MnP3 enzyme.

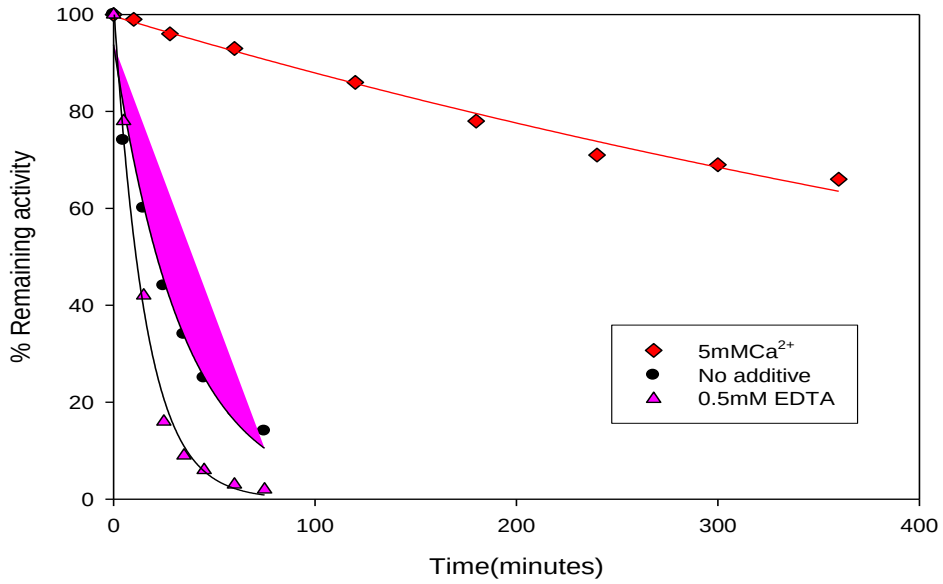

Figure 7.1: Temperature stability of *P. radiata* wild-type MnP3 at 50°C. Plots represent no additive, 5mM $CaCl_2$ added and 0.5mM EDTA added, to MnP3 during incubation. Enzyme concentration was 2.5 µM in 10mM sodium succinate buffer, pH 6.0. At specified times aliquots were measured for Mn (II) oxidation activity. Assay mixtures contained 0.4µM enzyme, 0.2mM $MnSO_4$, 0.1mM H_2O_2 and 100mM sodium tartrate, pH 5.0.

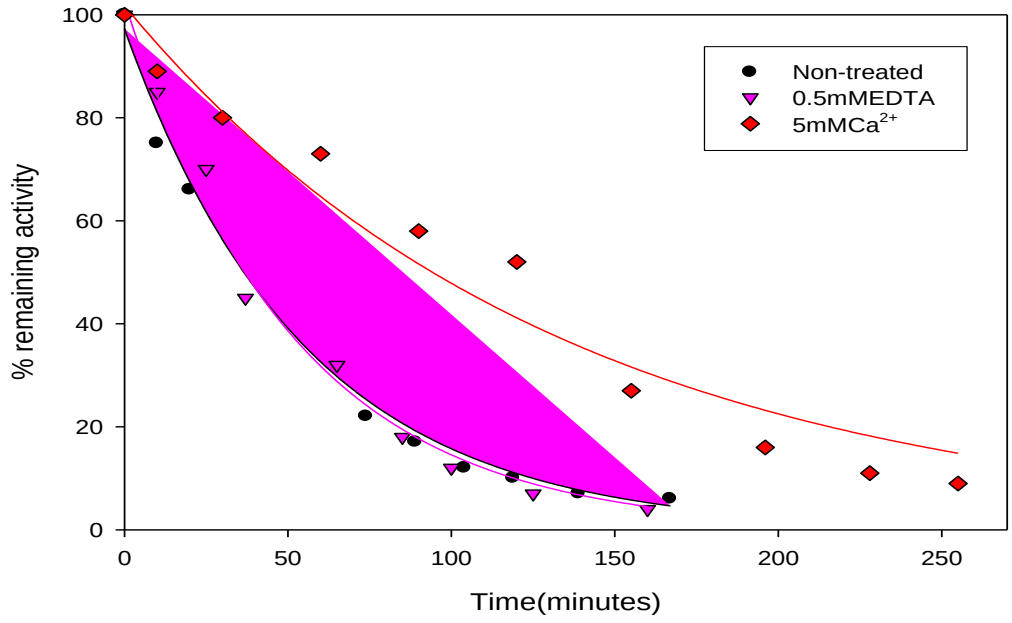

Figure 7.2: Temperature stability of *P. radiata* mutant E40H/E44H MnP3 at 50°C. Plots represent no additive, 5mM $CaCl_2$ added and 0.5mM EDTA added, to MnP3 during incubation. Enzyme concentration was 10µM in 10mM sodium succinate buffer, pH 6.0. At specified times aliquots were measured for Mn (II) oxidation activity. Assay mixtures contained 0.4µM enzyme, 40mM $MnSO_4$, 0.1mM H_2O_2 and 100mM sodium tartrate, pH 8.0.

Table 7.1 Decay constants (k_d) and half-life for wild-type MnP3 and mutant E40H/E44H in the presence or absence of additive, 5mM $CaCl_2$ or 0.5mM EDTA when incubated at 50°C.

Wild-type MnP3 sample	Decay constants(k_d) (min^{-1})	Half life($t_{1/2}$) (min)	pH	E40H/E44H MnP3 sample	Decay constants(k_d) (min^{-1})	Half life($t_{1/2}$) (min)	pH
Non-treated	0.029 ± 0.002	24	5.0	Non-treated	0.018 ± 0.001	39	8.0
$CaCl_2$ -treated	0.0013 ± 0.0001	533	5.0	$CaCl_2$-treated	0.0075 ± 0.001	92	8.0
EDTA-treated	0.070 ± 0.007	10	5.0	EDTA-treated	0.020 ± 0.0012	35	8.0

The results presented in Figure 7.1 and Table 7.1 also show that the presence of 5mM $CaCl_2$ in with the incubating wild-type MnP3 enzyme has a very large stabilising effect on the enzyme. The half-life has increased to 533 minutes, a 22-fold increase. Therefore calcium ions appear to be an important factor for the stabilization of this enzyme, like already known for other peroxidases (Barber *et al*., 1995; Tam and Welinder, 1996; Nie and Aust, 1997). The high concentration of calcium relative to enzyme is presumably allowing the distal calcium site to remain more fully occupied.

The results for both Ca^{2+} and EDTA additive experiments are consistent with the view that thermal denaturation of MnP3 is due to the loss of calcium from the protein, presumably the less tightly bound distal calcium, as found for other peroxidases (Sutherland and Aust, 1996; Nie and Aust, 1997). This in turn is suggested to keep the haem conformation correct.

7.2.2 E40H/E44H mutant MnP3 thermal inactivation in the presence or absence of Ca^{2+} and EDTA

MnP3 mutant enzyme, E40H/E44H, was also subjected to the same treatment as for the wild-type enzyme. The results are shown in Figure 7.2 and the right half of Table 7.1. Note that activity for the mutant enzyme was measured at pH 8.0, not pH 5.0 as for the wild-type. It should firstly be noticed that the mutant enzyme appears to be more stable than the wild-type with a half-life if no additive is present of 39 minutes, approximately 60% more than the wild-type. The basic effect of 5mM $CaCl_2$ additive to the incubating enzyme is also the same as wild-type, in that it increases the half-life to 92 minutes, almost 3-fold. However, this is much less than the 20-fold found for wild-type. This can easily be seen by comparing Figures 7.1 and 7.2.

The 0.5mM EDTA-added E40H/E44H sample also responded in a different way to that seen for the wild-type enzyme. As can be seen from Figure 7.2 EDTA has essentially not affected the rate at which the mutant enzyme is thermally inactivated, with a half-life for the EDTA treated sample of 35 minutes compared to 39 minutes for the untreated sample.

The higher stability of the E40H/E44H mutant enzyme under no additive conditions suggests that calcium loss from the mutant enzyme is more difficult than from the wild-type enzyme. This would appear to be confirmed by the smaller increase in stabilisation by calcium and the lack of inactivation by EDTA. This more heat-stable calcium site, presumably the distal site, may be explained by the mutations to the Mn (II) binding site as both the calcium site and Mn (II) binding site have ligands from helix B of the protein. The mutations to the manganese-binding site may have altered the position of helix B so that there is also a change in the helix B position relative to the distal calcium site. However, although the mutant enzyme is more heat-stable, it's much reduced activity (see chapter 4) makes it not a commercially useful enzyme.

7.3 Effect of pH of assay on the results for thermal denaturation of MnP3 enzymes

To ascertain the assay pH involvement in the measurement of the thermal inactivation of MnP3 from *P. radiata*, activity assays at pH 8.0 were conducted as well as assays at pH 5.0 using a wild-type MnP3 solution that had been incubated at 40°C with no additives. The results are shown in Figure 7.3 and Table 7.2. It can be seen that measuring the remaining activity of the enzyme solution at pH 8.0 gives a steeper rate of apparent inactivation than if the activity is measured at pH 5.0, with a pronounced immediate decrease in activity at the start. This is surprising, as although the actual activity measured for the wild-type enzyme will be much lower at pH 8.0 than pH 5.0, it would be expected that both would measure a similar rate of activity decrease.

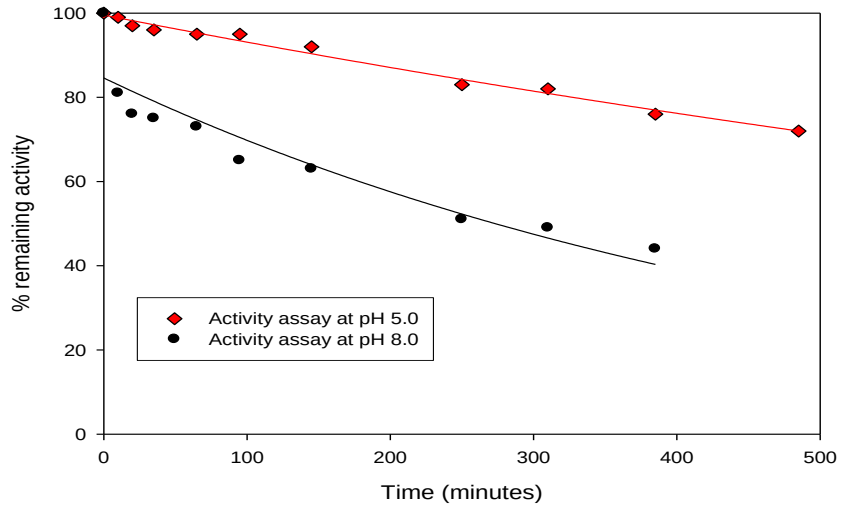

Figure 7.3: Temperature stability of *P. radiata* wild-type MnP3 at 40°C, with activity measured at pH 5.0 and 8.0. Enzyme concentration was 2.5µM in 10mM sodium succinate, pH 6.0. At specified times aliquots were measured for Mn (II) oxidation activity. Assay mixtures contained 0.4µM enzyme, 0.2mM $MnSO_4$, 0.1mM H_2O_2 ,100mM sodium tartrate buffer, pH 5.0 or pH 8.0.

Table 7.2: Effect of pH of assay on the thermal denaturation of wild-type MnP3 Two sets of enzyme samples, non-treated and EDTA-treated were used. The enzyme was incubated at 40°C, and Mn (II) oxidation activity assay conducted at pH 5.0 or 8.0 and at 25°C (2.4.12).

MnP3	Decay constants(k_d) (min^{-1})	Half life($t_{1/2}$) (min)	pH
Wild-type (non-treated)	0.0006 ± 0.0000	1155	5.0
	0.0016 ± 0.0002	433	8.0
Wild-type (EDTA-treated)	0.0024 ± 0.0001	289	5.0
	0.0039 ± 0.0002	178	8.0

This difference may, at least in part, be explained by a small fraction of each enzyme sample being inactivated when it is added to the pH assay buffer. Peroxidases are in general enzymes that are most active at acid pH. For *P. radiata* MnP3 this is at pH 5.0 for the wild-type enzyme. Indeed chapter 6 shows that the wild-type enzyme undergoes a gradual transition to a low-spin form at pH 8.6. If this is the case it also suggests that the half-lives calculated for the E0H/E44H enzyme, which are based on assays at pH 8.0, may in fact be slight underestimates.

7.4 The effect of added Ca^{2+} on the reactivation of thermally inactivated *P. radiata* wild-type MnP3.

Heat-treated peroxidases from several plant sources have shown an ability to recover their activity after being stored at ambient temperature (Schwimmer, 1944; Lu and Whitaker, 1974). However, only partial regeneration of peroxidase activity following heat treatment and

cooling also has been reported (McEldon and Dordick, 1996). In HRP, reactivation has been reported to occur after partial inactivation at 70, 90, or 110°C (Tamura and Morita, 1975). Rodrigo *et al*., (1997) showed that HRP treated at high temperatures (115 and 130°C) for short times (5 – 85 s) could recover up to 22% of its activity during incubation at 25°C. Similarly, a 15 – 30% restoration of original peroxidase activity was noted for the cationic isoenzyme of green peas after several hours of incubation at 25°C following a 50 – 70°C heat treatment for 1 – 10 minutes (Halpin *et al*., 1989).

The extent of reactivation depends on enzyme, heating conditions, temperature and time (Whitaker, 1974; Adams, 1978; Thong and Barret, 2005). It may be wise to suggest that reactivation of the peroxidase enzyme is a complex process that is influenced by several factors. In the majority of the cases studied, heat treatment even at low temperature for long times prevented full reactivation of the heated enzymes.

The structural calcium ions present in plant and fungal peroxidases are released during unfolding and can be efficiently bound by EDTA, leading to irreversible conditions. This permitted the measurement of the decay rate constant (k_D) independently of the refolding rate constant (k_f). Therefore, EDTA-treated enzyme was thermally inactivated by its incubation at 50°C for 55minutes, leaving enzyme with only 2% of its initial activity. A regain of peroxidase activity occurred in the sample, when when later treated with 5mM $CaCl_2$ and incubated at 4ºC. A total of 28 % of the original activity was obtained after 185 minutes, with a reactivation constant of 0.026 ± 0.01 min^{-1}, and half-life of 27 minutes (Figure 7.4).

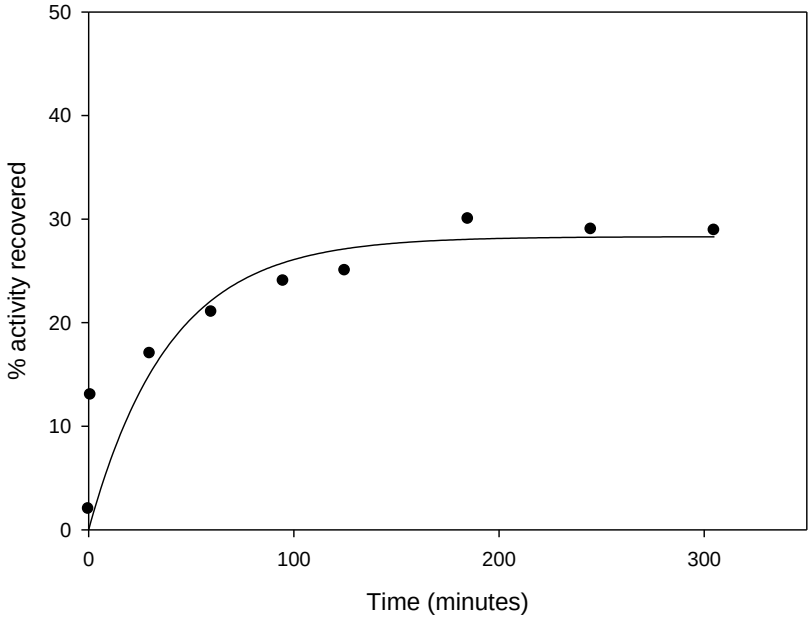

Figure 7.4: Recovery of activity in thermally-inactivated, EDTA-treated wild-type MnP3, as a function of added calcium. Reactivation of thermally inactivated enzyme (55min at 50°C with 0.5mM EDTA) was obtained by adding 5mM $CaCl_2$ to 2.5µM enzyme solution at 4°C for up to 5 hours. At specified times aliquots were measured for Mn (II) oxidation activity. Assay mixtures contained 0.4µM enzyme, 0.2 mM $MnSO_4$, 0.1 mM H_2O_2 and 100 mM sodium tartrate, pH 5.0.

Heat-denaturation of no additive wild-type MnP3 at 50°C gave first-order kinetics but the denaturation of MnP3 mutant E40H/E44H enzyme was observed not to be entirely first-order. The plot in Figures 7.2 seems to be displaying two distinct exponential decays that could best be described using a model involving a single enzyme form undergoing parallel denaturation steps to different forms.

Scheme 7.1 shows a summary of the proposed temperature induced enzyme changes.

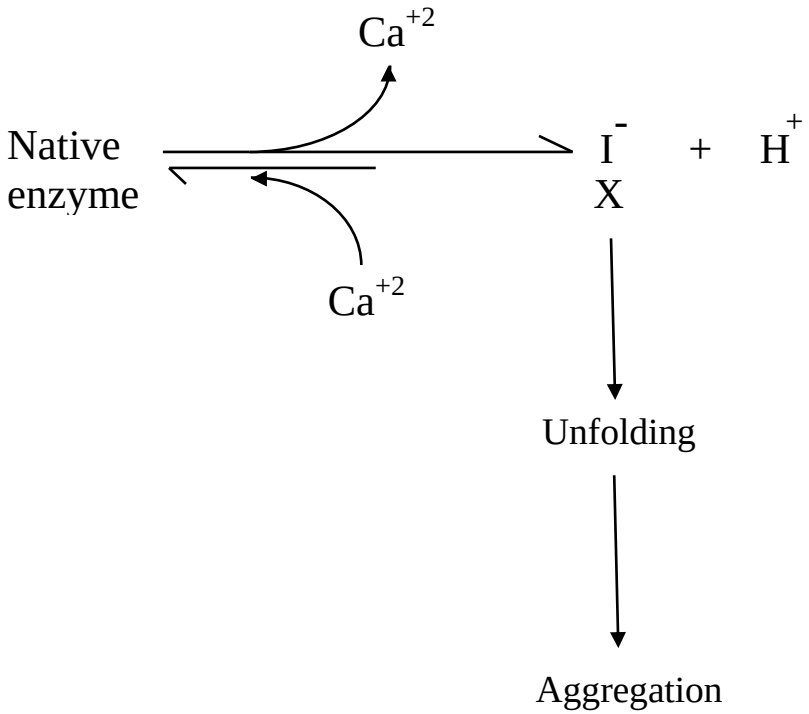

Scheme 7.1: A scheme describing the temperature-dependent changes in the resting state of *P.radiata* MnP3 enzymes. Reactions shown by solid arrows indicate changes taking place when the enzyme was heated.

This scheme shows the formation of probable multiple intermediate forms upon loss of Ca^{2+} following exposure to high temperature. If no calcium is available to the intermediate, it will eventually undergo denaturation and aggregation (irreversible inactivation). However, if calcium is available to the intermediate before irreversible denaturation occurs then the addition of calcium to the enzyme form leads back to active enzyme (irreversible inactivation).

Assay pH was also observed to impact significantly on the activity of the heat-treated enzymes. At 40°C, pH 5.0 the non-treated wild-type MnP3 showed high activity, which correlate high stability with half-life of 1155 minutes, while at pH 8.0 the thermal stability decreases appreciably with half-life of about 433 minutes. At 50°C, the thermal stability

decreased sharply. The enzymes lost activity almost completely in 75 minutes ($t_{1/2}$ = 24 minutes) but in the presence of EDTA, the inactivation was faster (occurring in 55 minutes with $t_{1/2}$ = 10 minutes). The wild-type MnP3 incubated at 50°C was observed to be more stable in the presence of excess exogenous calcium with the enzyme losing only 34% of its initial activity after 360 minutes (6 hours) with half-life of 533 minutes.

These results suggest that the MnP3 experimental conditions, pH 5.0; 25°C for the determination of the initial enzymatic activity are not the most useful with regard to thermal stability. Thus, the nature of the additive present in enzyme solution and controlling the time of exposure of MnP3 at reactor temperatures are critically important to maximizing or controlling its thermal stability. Regarding the combined effect of pH and temperature, it was observed that the relative maximum activity shifts to lower temperatures, below 40ºC with acidic pH value.

In conclusion, this study reveals that calcium is labile and is essential for the activity and stability of MnP3 from *P. radiata*. Therefore, while calcium is lost following thermal inactivation, irreversible inactivation can be prevented by the presence of exogenous Ca^{2+}. This has potential implication to the use of this enzyme in industrial applications

7.5 Determination of melting temperature of wild-type and E40H/E44H mutant MnP3 enzymes using circular dichroism (CD)

Measurement of melting temperature (T_m) as an index of thermodynamic stability of MnP3 was conducted for the wild-type MnP3 and E40H/E44H mutant enzymes using Circular dichroism (CD) technique. Also assessed was the effect of $CaCl_2$ or EDTA on the melting point of the enzymes. Figures 7.5 (a) and (b) show thermal melts for wild-type MnP3 and E40H/E44H mutant enzymes, both with no additive and with 5mM $CaCl_2$ or 0.5mM EDTA. Figure 7.5 (c) compares the no additive samples of the wild-type and mutant proteins. No aggregate or precipitate was seen at the end of the process, suggesting probable reversibility of the process. The reversibility of the unfolding makes the melting temperature directly related to conformational stability.

It can be seen from Figure 7.5 (c) and Table 7.3 that the E40H/E44H mutant enzyme is slightly more thermostable than the wild-type enzyme, with the T_m higher, 54°C compared to 58°C, similar to that determined for the catalytic stability of the two enzymes. The observed melting temperature of the no additive wild-type MnP3 protein sample is lower than that measured for CiP, T_m = 65 °C (McEldon and Dordick, 1996) and HRP- C, T_m = 60°C, and much lower than the value obtained for African palm tree peroxidase, T_m = 74°C (Rodriguez *et al*., 2002).

For both the wild-type and mutant enzyme, EDTA has no significant effect on the T_m, suggesting that any removal of calcium by the EDTA does not affect the general stability of the protein tertiary structure or that EDTA is not able to remove calcium from the protein under the experimental conditions.

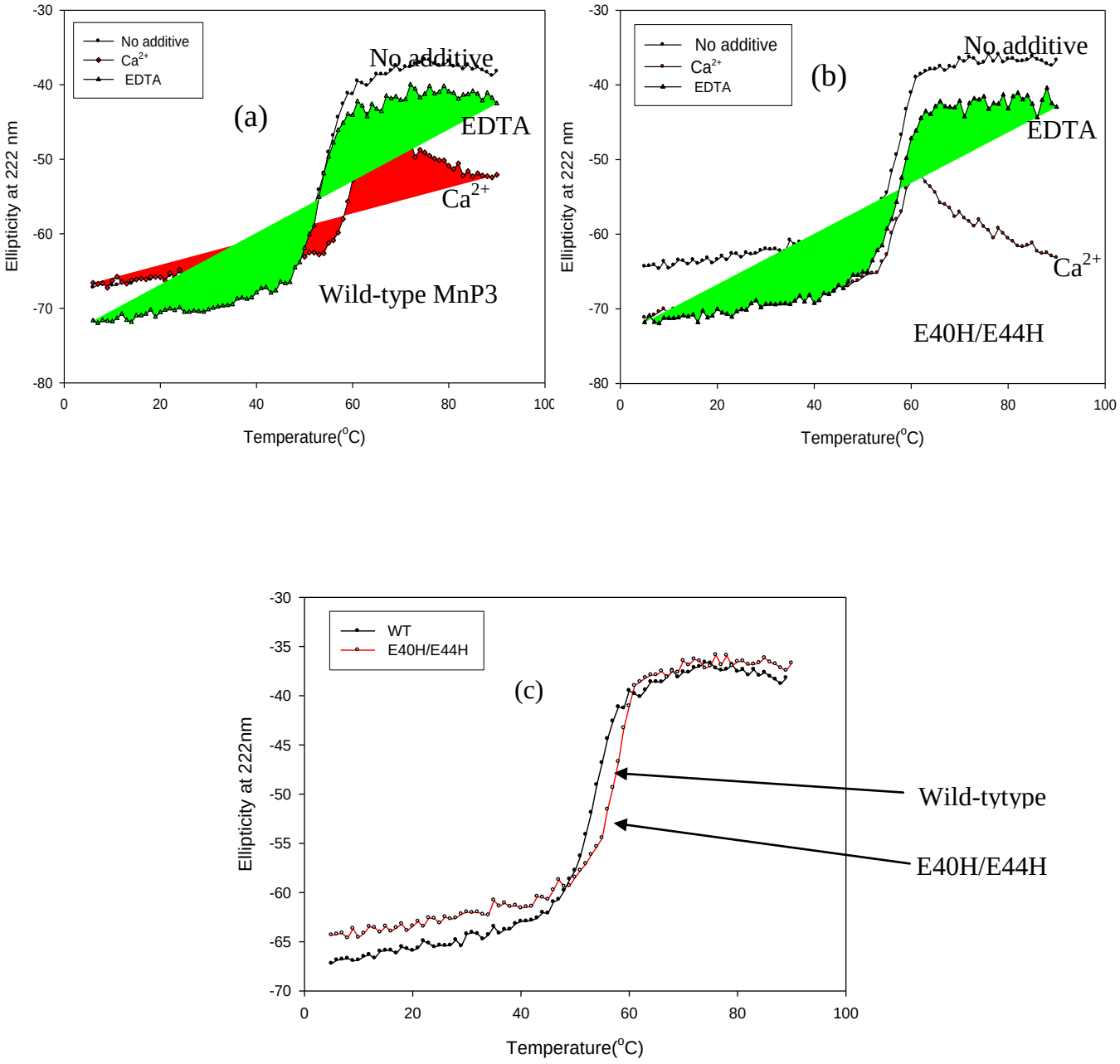

Figure 7.5: Thermal denaturation plots of wild-type and mutant E40H/E44H MnP3 as a function of temperature, as measured by CD. Plots **(a)** and **(b)** represent no additive, 5mM $CaCl_2$ added and 0.5mM EDTA added, to wild-type or E40H/E44H MnP3 during incubation. **(c)** is an overlay of wild-type and E40H/E44H mutant under no additive conditions. Enzyme concentration was 1.6µM each enzyme in 10mM sodium acetate, pH 6.0. Readings were taken at 222 nm as the temperature was raised from 5 to 90°C at a constant rate of 1°C / min, with 16 seconds of equilibration at each temperature.

Table 7.3: Melting temperature of *P. radiata* wild-type and E40H/E44H mutant MnP3 enzymes. T_m values are from derivatives of the melting profiles. Enzyme concentration was 1.6µM enzyme in 10 mM sodium acetate, pH 6.0. Additives were 0.5 mM EDTA or 5 mM $CaCl_2$. Ellipticities were recorded at 222 nm, as the temperature was raised from 5 to 90°C, at a constant rate of 1°C / min, with 16 seconds of equilibration at each temperature.

Sample	**Wild-type MnP3 Melting temperature (T_m) °C**	**E40H/E44H MnP3 Melting temperature (T_m) °C**
No additive	54	58
5 mM $CaCl_2$	60	58
0.5 mM EDTA	52	57

Calcium ions is protective of the unfolding of wild-type MnP3, increasing the T_m from 54°C to 60°C, but not of the unfolding of the E0H/E44H mutant. This is consistent with that found for the thermal inactivation of activity, when calcium addition protected activity loss by 22-fold for the wild-type enzyme but only 3-fold for the mutant enzyme. Presumably calcium loss from the wild-type enzyme is being lowered by the presence of the $CaCl_2$; the presence of calcium in the protein tertiary structure must therefore stabilise it, at least to some extent.

7.6 Conclusion

The results show that the presence of $CaCl_2$ has a very stabilising effect on wild-type MnP3 and mutants enzymes at high temperature. The basic effect of 5 mM $CaCl_2$ additive to the incubating E40H/E44H is also the same as the wild-type, in that, it increases the half-life to 92 minutes. However, the extent of the effect is not as large. It has also been observed that in the absence of calcium E40H/E44H MnP3 appears to be more stable than the wild-type with a half-life of 39 minutes (~ 60%). The higher stability of the E40H/E44H mutant enzyme under no additive conditions suggests that calcium loss from the mutant enzyme is more difficult than from the wild-type enzyme. Being that calcium is coordinated to helix B, mutations to the Mn-binding site may have altered the position of helix B, relative to the distal calcium site and removed electrostatic repulsion in the Mn site stabilising the enzyme. EDTA has essentially not affected the rate at which the mutant enzyme is thermally inactivated, with a half-life for the EDTA treated sample of 35 minutes compared to 39 minutes for the untreated sample.

Chapter Eight
Concluding discussion

This thesis has described work carried out on a novel manganese peroxidase, MnP3 from the major lignin degrader *Phlebia radiata*. This is the first example of a 'short' MnP which compared to the classical *P. Chrysosporium* MnP enzymes has a truncated C-terminus making it more similar in evolutionary terms to the so-called versatile peroxidases that are also MnP's but posses in addition, the redox active Trp residue characteristic of lignin peroxidases. The enzyme had been purified in very small amounts from the native fungus but in insufficient amounts to be fully characterised. *E.coli* expression from an engineered MnP3 gene and in vitro refolding have now allowed extensive biochemical characterisation of this new enzyme. Some new and interesting properties have been revealed.

The *Phlebia radiata* wild-type MnP3 gene was engineered so that the N-terminal region mimicked the N-terminus of the highly expressed CiP synthetic gene (Smith and Ngo, 2007). The engineered gene was cloned into pFLAG1, under the control of the *tac* promoter. A variety of Mn (II) binding site mutants were also generated by a PCR i.e. E40H, E44H, E40H-E44H, D186H and D186N MnP3. Both the wild-type and mutant MnP3 proteins were successfully expressed in *E. coli*, and the enzymes refolded and purified.

The UV/visible spectrum of wild-type MnP3 found to be typical of a large 6-coordinate high spin protein. It was also observed that the E40H, E44H, E40H/E44H, D186H and D186N mutant variants had a spectrum(see Figure 4.1 and Table 4.1) very similar to that of the wild-type enzyme, indicating that the haem environment was not substantially altered by mutations at the nearby Mn (II) binding site

The *P. radiata* recombinant wild-type MnP3 enzyme showed optimal activity with Mn (II) at pH 5.0 and remained moderately active (approximately 40%) in the pH range 6.0-8.5; the MnP3 mutants maximum activity ranged between 5.5 and 8.0. This activity at higher pH is not common and has not been reported for an MnP enzyme before and could have considerable interest for commercial uses. Wild-type MnP3 seemed to have a substantially higher pH optimum than the more classical *Phanaerochate* MnP enzyme. The MnP3 mutants exhibited a similar pH profile to wild-type, with an optimum at pH 3.0, for ABTS oxidation. This strongly suggests that ABTS is oxidised at the Mn (II) binding site, as charge neutralisation mutations decreased K_m for ABTS and improved effectiveness.

Mutation of the Mn^{2+} binding ligands had profound effects on the catalytic properties of the enzyme. The removal of a carboxylate ligand at the Mn (II)-binding site was found to severely depress the catalytic efficiency of E40H (1.0 $mM^{-1}s^{-1}$), E44H (1.5 $mM^{-1}s^{-}1$), E40H/E44H (0.08 $mM^{-1}s^{-1}$), D186 (0.04 $mM^{-1}s^{-1}$) and D186N (0.30 $mM^{-1}s^{-1}$) for Mn (II) compared to wild-type (1029 $mM^{-1}s^{-1}$) MnP3 at lower pH. Mutation specific preferences were also created with the MnP3 DI86N variant being the poorer kinetically than D186H at higher pH. Clearly His is a more acceptable alternative for catalysis than Asn. These changes in k_{cat} and the specificity constants for Mn (II) oxidation by MnP3 mutants were to some extent expected from the nature of the mutants involved and prior work on the *Phanerochaete chrysosporium* MnP enzymes **(**Kishi *et al*., 1996).

Interestingly, it was observed that histidine substitutions at the Mn (II) binding site lead to a mutant with a similar effectiveness ratio to the wild-type enzyme at higher pH, when the His ligands were in a deprotonated state. Activity towards Mn (II) at lower pH was greatly decreased, presumably due to the presence of the positively charged

histidine. In contrast to expectation, the enzyme can therefore function at higher pH with alternative ligands in the Mn^{2+} site and does not have an absolutely obligate requirement for an all carboxylate ligand set. The results obtained for wild-type MnP3 for Mn (II) oxidation at pH 5.0 and 8.0 also showed enhanced affinity for Mn (II) at alkaline pH. Progressive deprotonation of Mn ligands results in a progressively higher affinity for Mn, which is evident in a relatively good catalytic efficiency at higher pH, even for the mutants, E40H (92 $mM^{-1}s^{-1}$), E44H (244 $mM^{-1}s^{-1}$), E40H/E44H (29 $mM^{-1}s^{-1}$), D186H (128 $mM^{-1}s^{-1}$) and D186N (15 $mM^{-1}s^{-1}$) But none of the catalytic efficiencies of the mutants was in any way near the of the wild-type (3109 $mM^{-1}s^{-1}$) at alkaline pH.

Turnover numbers for some enzymes, wild-type (300 ± 11 s^{-1}) and D186H (10 ± 0.30 s^{-1}) were best in lactate buffer and lowest e.g. D186H (0.84 ± 0.1 s^{-1}) in tartrate buffer, thus confirming dependence on the type of Mn^{3+} chelating agent present. An exception was observed in the case of the double E40H/E44H variant, where reaction in lactate buffer gave the lowest k_{cat} (0.9 ± 0.04 s^{-1}) value relative to tartrate and malonate. It is tempting to suggest that the double mutant, with two negative charges missing, favoured a dicarboxylic chelator, implying that the chelating agent may in part be able to compensate for the loss of negative charges in the Mn (II) binding site.

Studies on the effect of metal ions during Mn (II) oxidation revealed that Cu^{2+} and Zn^{2+} function as mixed inhibitors of MnP3 enzymes, with Cu^{2+} having by far the strongest competitive effect. During ABTS oxidation, Na, Zn, Co and Cu again could be weakly stimulatory of ABTS activity possibly through more generalised ionic strength effects. The effects of Zn and Cu on Mn (II) oxidation appear however to be specific to the Mn (II) oxidation site. Investigations of metal binding to the wild-type enzyme showed multiple tight binding sites for Cu (II) and Zn (II). Zinc ions bound irreversibly and

somewhat non-specifically to MnP3, to sites other than the Mn (II) binding site. Mn (II)–MnP3 interactions were observed to be of lower affinity. The binding affinity of the putative Mn (II)-binding site to Mn (II) was grossly reduced following ligand mutation, particularly at lower pH. The double E40H/E44H variant was observed to have less ability to retain Mn than any of the single mutants. There was some evidence that the E40H/E44H variant may have a better affinity for Co than for Mn. This would need to be investigated further by ICP analysis.

Alkaline pH and high temperature (50°C) have been observed to reversibly alter the spin and / or activity of MnP3 enzymes from *Phlebia radiata*. Partial restoration of the high spin active form of the enzyme was achieved by lowering the pH or temperature with the addition of Ca^{2+}, implying that the reversible pH and temperature induced conformational change had involved Ca^{2+} loss. Addition of excess Ca^{2+} under equilibrium conditions prevents the formation of the low spin state at higher pH.

The ability of MnP3 enzymes from *Phlebia radiata* to be active over a wide pH range, particularly alkaline conditions makes it unique in comparison with other MnP enzymes. This is interesting in the light of potential industrial applications requiring alkaline conditions. The relative stability and pH profile of the enzyme make it a good candidate as a starting point for the 'Biorefinery' concept with reasonable effectiveness at alkaline pH and good stability in the presence of excess Ca^{2+}. The findings also form an excellent platform for further characterisation of the enzyme It would be interesting to test the enzyme further under applications based conditions as a delignifying enzyme in a pulp mill process.

References

Abelskov, A. K., Smith, A. T., Rasmussen, C. B., Dunford, H. B., Welinder, K. G. (1995) pH-dependence and structural interpretation of the reactions of *Corprinus cinereus* peroxidase with hydrogen peroxidase, ferulic acid, and 2,2'-azinobis(3-ethylbenzthiazoline-6-sufonic acid). *Biochemistry* 34: 4022 – 4029.

Abu-Soud, H. M., M. Y. Khassawneh, *et al*., (2001) Peroxidases inhibit nitric oxide (NO) dependent bronchodilation: Development of a model describing NO-peroxidase interactions. *Biochemistry* 40 (39): 11866-11875.

Adams, J. B. (1978) The inactivation and regeneration of peroxidase in relation to the high temperature-short time processing of vegetables. *J. Food Technol*. *13*, 281-297.

Aifa, S. M., Sayadi, S. and Gargouri, A. (1999) Heterologous expression of lignin peroxidase of *Phanerochaete chrysosporium* in *Aspergillus* niger. *Biotechnol Lett.* 21: 849-853.

Aitken, M. D. and Irvine (1990) Characterisation of reactions catalysed by manganese peroxidase from *Phanerochaete chrysosporium*. Archieves of Biochemistry and Biophysics, 276(2): 405-414.

Aitken, M. D., and Irvine, R. L. (1990) *Arch. Biochem. Biophys.* 276,405- 414.

Aitken, M. D., and R. I. Irvine. (1989). Stability testing of ligninase and Mn-peroxidase from Phanerochaete chrysosporium. *Biotechnol. Bioeng*. 34:1251-1260.

Aliaga, C., and Lissi, E. A. (1998) Reaction of 2, 2-azinobis (3-ethylbenzothiazoline-6-sulfonic acid (ABTS) derived radicals with hydroperoxides. Kinetics and mechanism, *Inter. J. Chem. Kinet*. 30: 565- 70.

Alic, M., Akileswaran, L. and Gold, M. H. (1997) Characterization of the gene encoding manganese peroxidase isozyme 3 from *Phanerochaete chrysosporium*. *Biochimica et Biophysica Acta* 1338: 1-7.

Ammann AA. 2007. Inductively coupled plasma mass spectrometry (ICP -MS): A versatile tool. *J Mass Spectrom* 42:419–427.

Ander, P., Eriksson, K.E. (1977) Selective degradation of wood components by white-rot fungi. *Physiologia Plantarum* 41:239-248.

Andersson, L. A., Renganathan, V., Loehr, T. M., and Gold, M. H. (1987) *Biochemistry* 26, 2258-2263.

Andersson, L.,A., Bylkas, S.A., and Wilson, A. E. (1996) Spectral analysis of lactoperoxidase. Evidence for a common haem in mammalian peroxidases. *J. Biol. Chem.* 271: 4211-8.

Andrawis, A., Pease, E., Tien, M. In Kirk, T. K. and Chang, H.M. (eds.) (1990) Biotechnology in Pulp and Paper Manufacture; Applications and Fundamental Investigations. Butterworth-Heinemann., Butterworth-Heinemann, Boston, 601.

Appleton, D. W. and Sarkar, B. (1971) *J. Biol. Chem*. 246: 5046.

Araiso, T., K. Miyoshi, et al., (1976) "Mechanisms of electron transfer from sulphite to horseradish peroxidase-hydroperoxide compounds" *Biochemistry*, 15 (14): 3059-63.

Arasio, T., and Yamazaki, I. (1978) *Biochemistry* 17: 942-946.

Arato C, Pye EK, Gjennestad G. 2005. The lignol approach to biorefining of woody biomass to produce ethanol and chemicals. *Appl Biochem. Biotechnol* 121/124:871–882.

Argyropoulos D. S., and Menachem, S. B. (1997) Lignin. In: Eriksoon K. E. L (ed.) *Advances in Biochemical Engineering/Biotechnology*. Springer-Verlag, Germany, 127-158.

Arias, M. E., Arenas, M., Rodriguez, J., Soliveri, A. S., Ball and Hernandez M. (2003) Kraft pulp bleaching and mediated oxidation of nonphenolic substrate by laccase from *streptomyces cyaneus* CECT 3335. *Applied and Environmental Microbiology* 69, 1953.

Arnhold, J., Furtmuller, P. G.and Obinger, C., (2003) Redox properties of myeloperoxidase, *Redox. Res*. 8: 179-86.

Arnold, F. H. and Zhang, J. H. (1994) Metal-mediated protein stabilization, *Trends Biotechnol*. 12, 189 - 192.

Arnone, A., Bier, C. J., Cotton, F. A., Day, V.W., Hazen, E. E., Jr., Richardson, D. C., Richardson, J. S. and Yonath, A. (1971) *J. Biol. Chem*. 246, 2302 – 2316.

Arora, D. S. and Sharma, R. K. (2010) Ligninolytic fungal laccases and their biotechnological applications. *Appl Biochem Biotechnol,* 160:1760–1788.

Bal, W., Christodoulou, J., Sadler, P.J. (1998). *J. Inorg. Biochem.* 70: 33.

Banci, L. (1997). Structural properties of peroxidases. *J. Biotechnol*. 53: 253–263.

Banci, L., Bertini, I., Bini, T., Tien, M. and Turano, P. (1993) Binding of horseradish, lignin and manganese peroxidases to their respective substrate. *Biochemistry* 32: 5825-5831.

Banci, L., Bertini, I., Dal Pozzo, L., Del Conte, R., and Tien, M. (1998) Monitoring the role of oxalate in manganese peroxidase, *Biochemistry* 37, 9009-9015.

Banci, L., Bertini, I., Pierattelli, R., Tien, M. and Vila, A.J. (1995) Factoring of the hyperfine shifts in the cyanideadduct of lignin peroxidase from *P. chrysosporium. J. Am.Chem. Soc.* 117: 8659–8667.

Barber, K. R., Jose, M. Maranon, R., Shaw G. S., Robert B., and Van Huystee, R. B. ('1995). Structural influence of calcium on the heme cavity of cationic peanut peroxidase as determined by 'H-NMR spectroscopy. *Eur. J. Biochem.* 232: 825-833.

Beauchemin D. 2006. Inductively coupled plasma mass spectrometry. *Anal Chem* 78:4111–4135.

Beguin, P., and Aubert, J. P. (1994) The biological degradation of cellulose. *FEMS Microbiol.* 62: 1723-1727.

Bennet, J.W. (1998) Mycotechnology: the role of fungi in biotechnology. *J. Biotechnol*. 66: 101-107.

Berman, H. M., Westbrook, J., Feng, Z., Gilliland, G. Bhat, T. N., Weissig, H., Shindyalov, I. N. and Bourne, P. E. (2000) The Data Bank. *Nucleic acids Res.* 28: 235-242.

Bertini, I., Briganti, F., Scozzafava, A.(1995) In Hanbook of metal-ligand interactions in Biological fluids; Berthon, G., Ed.; Marcel Dekker: New York, pp 81-91.

Bertini, I., Sigel, A., Sigel, H. eds. (2001). Handbook on Metalloproteins. New York: Marcel Dekker.

Besle, J. M., Cornu, A., Jouany, J. P. (1989) Roles of structural phenylpropanoids in forage cell wall digestion. *J. Sci. Food Agric.* 64: 171-190.

Biorenew: White Biotechnology for added value products from renewable plant polymers: Design of tailor-made biocatalyst and new industrial bioprocesses. NMP2-CT-2006-026456, Sixth Frame Programme. www.biorenew.org.

Birecka, H., Chasks, M. J. and Goldstein, J. (1979) Plant pathogen attack. *J. Exp. Bot*. 30: 565-573.

Black, C. B. and Cowan, J. A. (1994) *Inorg. Chem.* 33: 5805-5808.

Blanchette, R. A. (1995) Degradation of lignocelluloses complex in wood. *Can. J. Bot*., 73 (Suppl. 1) S999-S1010.

Blanchette, R.A. (1984) Screening wood decayed by white rot fungi for preferential lignin degradation. *Appl Environ Microbiol* 48:647-653.

Blanchette, R.A., Cease, K.R., Abad, A.R. (1991) An evaluation of different forms of deterioration found in archaeological wood. Inter. Biodeter. *Biodegrad.* 28: 3-22.

Bolscher, B. G. and Wever, r. (1984) A kinetic study of the reaction between human myeloperoxidase, hydroperoxides and cyanide. Inhibition by chloride and thiocyanate, *Biochmim. Acta* 788:1-10.

Bolscher, B. G., Plat, H., and Wever, R. (1984) Some properties of human eosinophil peroxidase, a comparison with other peroxidases, *Biochim. Biophys. Acta* 784: 177-86.

Bonnarme, P. and Jeffries, T. W. (1990) Mn (II) regulation of lignin peroxidase and manganese-dependent peroxidase from ligni-degrading white-rot fungi. Appl. Environ. Microbiol. 56(1): 210-217.

Bonnen, A. M., Anton, L.H. and Orth, A. B. (1994). Lignin-degrading enzymes of the commercial button mushroom, *Agaricus bisporus*. Appl. Environ. *Microbiol.* 60: 960 – 965.

Bono, J. J., Goulas, P., Doe, J. F., Portet, N. and Seris, J. L. (1990). Effect of Mn (II) on reactions catalysed by lignin peroxidase from *Phaneraochaete chrysosporium*. J. Bacteriol. 17222: 3125-3130.

Brill, A. S. and Williams, R. J. P. (1961) Absorption spectra, magnetic moments and binding of iron in some haemoproteins. *Biochemical Journal* 78(2): 246-253.

Browett, W. R., and Stillman, M. J., (1981) Evidence for haem p cation radical species in compound I of horseradish peroxidase and catalase, Biochimica et Biophysica. Acta. 660: 1-7.

Brown, A. (1985) Review of lignin in biomass. *J. Appl. Biochem.* **7**: 371-387.

Brown, J., Glenn, J. K. and Gold, M. H. (1990) Manganese regulates expression of manganese peroxidase by *Phanerochaete chrysosporium*. *J. Bacteriol* 172: 3125-3130.

Brunow, G. (2001) Methods to reveal the structure of lignin. In: Hofrichter M and Steinbüchel A (eds.) Biopolymers, vol.1. Wiley-VCH, Weinheim, Germany, pp. 89-116.

Burnette, F. S. (1977) *Food Sci.* 42, 1- 6.

Buswell, J.A., Odier, E. (1987) Lignin biodegradation. CRC *Crit Rev Microbiol*. 6:1-60.

Butler, A. (1998) Vanadium haloperoxidases, *Curr. Opin. Chem. Biol*. 2, 279-85.

Camarero, S., Sarkar, S., Ruiz-Duenas, F. J., Martinez, M. J. and Martinez, A. T. (1999) Description of versatile peroxidase involved in the natural degradation of lignin that has

both manganese peroxidase and lignin peroxidase substrate interaction sites. *J. Biol. Chem.* 274: 10324-10330.

Campos, A. M., and Lissi, E. A., (1997) Kinetics of the reaction between 2,2-azinobis (3-ethylbenzothiazoline-6-sulfonic acid (ABTS) derived radical cations and phenols, Int. *J. Chem. Kinet.* 29: 219 – 24.

Campos, C. F., Souza, P. E. A., Coelho, J. V. and Gloria, M. B. A. (1996) *J. Food Process, Preserv.* 20: 487 – 500.

Cano, M. P., Lobo, M. G. and de Ancos, B. (1998) *J. Sci. Food Agric.* 76: 135 – 141.

Caramelo, L., Martinez, M. J. and Martinez, A. T. (1999) A search for ligninolytic peroxidases in the fungus Pleurotus eryngii involving α-keto-γ-thiomethylbutyric acid and lignin model dimmers, *Appl. Environ. Microbiol*. 65: 916-922.

Carlile, M. J. and Watkinson, S.C. (1994) The Fungi. Academic Press, Great Britain.

Carlile, M.J., Watkinson, S.C., Gooday, G.W. (2001) The fungi. Academic press, London, 588.

Carlstrom, A. (1969) Lactoperoxidase. Some spectral properties of a haemoprotein with a prosthetic group of unknown structure, *Acta. Chem. Scand*. 23: 203-13.

Casadaban, M. J., Martinez-Arias, A., Shapira, S. K and Chou, J. (1983) b-galactosidase gene fusions for analyzing gene expression in *Escherichia coli* and yeast. *Methods Enzymol* 100, 293-310.

Chander, M., and Arora, D. S. (2007). Evaluation of some white rot fungi for their potential to decolorise industrial dyes, *Dyes and Pigments*, 72: 192–198.

Cherry, J., Lamsa, M., Schneider, P., Vind, J., Svendsen, A., Jones, A. and Pedersen A. H. (1999) Directed evolution of a fungal peroxidase *Nat. Biotechnol*. 17: 379-384.

Chiang (2006) Monolignol biosynthesis and genetic engineering of lignin in trees, a review, *Environ. Chem. Lett*. 4: 143.

Childs, R. E. and Bardsley, W. G. (1975) "The steady-state kinetics of peroxidase with 2, 2'-azino-di-(3-ethyl-benzthiazoline-6-suphonic acid) as chromogen," *Biochem. J.* 145(1): 93 -103.

Choi, H. J., Kang, S. W., Yang, C.-H., Rhee, S. G., and Ryu, S., E. (1998). Crystal structures of a novel human peroxidase enzyme at 2.0 A resolution, *Nature Struct. Biol*. 5: 400- 406.

Choinowski, T., Blodig, W., Winter, K. H., and Piontek, K., (1999) The crystal structure of lignin peroxidase at 1.70 Å resolution reveals a hydroxyl group on the cbeta of tryptophan 171: a novel radical site formed during the redox cycle, *J. Mol. Biol*. 286: 809-27.

Christianson, D.W., Cox J.D. (1999). Catalysis by metal-activated hydroxide in zinc and manganese metalloenzymes, *Annu. Rev. Biochem.* 68:33–57.

Chriswell, D.J. (1988) *Eur. Pat.* 029968-A1.

Ciullini, I., Tilli, S., Scozzafava, A., & Brigant, F. (2008). Fungal laccase, cellobiose dehydrogenase, and chemical mediators: Combined actions for the decolorization of different classes of textile dyes. *Bioresource Technology,* 99: 7003–7010.

Colas, C., Kuo, J. M., and Oritz de Montellano, P. R., (2002) Asp-225 and Glu-375 in autocatalytic attachment of the prosthetic haem group of lactoperoxidase. *J. Biol. Chem* 277: 7191-200.

Conesa, A. van den Honde,l C.A.M.J.J., Punt, P.J. (2000) Studies on the production of fungal peroxidases in *Aspergillus niger*. *Appl. Environ. Microbiol*. 66: 3016-3023.

Conesa, A., Punt, P.J., van den Hondel CAM.J.J. (2002) Fungal peroxidases: Molecular aspects and applications. *J Biotechnol* 93:143-158.

Converso, D. A. & Fernandez, M. E. (1996) Ca^{2+} activation of wheat peroxidase: a possible physiological mechanism of control. *Arch Biochem Biophys* 333: 59–65.

Converso, D. A. & Fernandez, M. E. (1996) Ca^{2+} activation of wheat peroxidase: a possible physiological mechanism of control. *Arch Biochem Biophys* 333: 59–65.

Coolbear, T., Whittaker, J. M. & Daniel, R. M. (1992) The effect of metal ions on the activity and thermostability of the extracellular proteinase from a thermophilic Bacillus, strain EA.1. *Biochem J.* 287: 367 – 374.

Cotton, F. A., and Wilkinson, G. (1988) Advanced inorganic Chemistry, 5th ed., John Wiley, New York.

Cowan, J. A. (1995) Biological chemistry of magnesium; VCH; New York.

Cramer, S.P., Dawson, J.H., Hodgson, K.O. and Hager, L.P. (1978) Studies on the ferric forms of cytochrome *P*-450 and chloroperoxidase by extended X-ray absorption fine structure. Characterization of the Fe-N and Fe-S distances. *J. Am. Chem. Soc.* 100: 7282–7290.

Cregg, J. M., J. L. Cereghino, J. Shi, and D. R. Higgings. 2000. Recombinant protein expression in *Pichia pastoris*. *Mol. Biotechnol.* 16: 23-52.

Criquet, S., Farnet, A.M., Tagger, S., Le Petit, J**.** (2000) Annual variations of phenoloxidases activities in an evergreen oak litter: influence of certain biotic and abiotic factors. *Soil. Biol. Biochem.* 32:1505–1513.

Cui, F., and Dolphin, D. (1990) *Holzforschung*, 44: 279-283.

Dalton, D. A., Diaz del Castillo, L., Kahn, M. L., Jouner, S. L., Chatfield, J. M. (1996) Heterologous expression and characterisation of soybean cytosolic ascorbate peroxidase. Arch. Biochem. Biophys. 328: 1-8.

Daly, R, and Hearn, M. T. W. (2005) Expression of heterologous proteins in *Pichia pastoris*: a useful experimental tool in protein engineering and production. *J Mol Recognit,* 18: 119–38.

Daniel, G. (2003) Microview of wood under degradation by bacteria and fungi. In: Goodell B, Nicholas DD and Schultz TP (eds.) Wood deterioration and preservation. ACS Symposium series 845, Washington DC, USA, pp. 34-72.

Daniel, R. M., Dines, M. and Petach, H (1996) The denaturation and degradation of stable enzymes at high temperatures. *Biochem. J.* 317:1-17.

Davey, C. A., and Fenna, R. E. (1996) 2.3 Å resolution X-ray crystal structure of bisubstrate analogue inhibitor salicylhydroxamic acid bound to human myeloperoxidase: a model for a prereaction complex with hydrogen peroxide, *Biochemistry* 35: 10967–10973.

De Gioia, L., Ghibaudi, E. M., Laurenti, E., Salmona, M., and Ferrari, R. P. (1996) *J. Biol. Inorg. Chem.* 1: 476–485.

de Jong, E., Field, J.A., Spinnler, H.-E., Wijnberg, J.B.P.A., de Bont, J.A.M. (1994) Significant biogenesis of chlorinated aromatic by fungi in natural environments. *Appl. Environ. Microbiol.* 60: 264-270.

De Ropp, J. S., La Mar, G. N., Wariishi, H. and Gold, M. H. (1991) NMR study of the active site of resting state and cynide-inhibited lignin peroxidase from Phanerochaete chrysosporium. Comparison with Horseradish peroxidase. *J. Biol. Chem.* 266: 15001-15008.

De Ropp, J. S., Mandal, P., Brauer, S. L., and La Mar, G. N., (1997) Solution NMR study of the Electronic and molecular structure of the Haem cavity in High-spin, Resting state Horseradish peroxidase, *J. Am. Chem. Soc.* 119: 4732-4739.

Dean, F. D., Eriksson, K. E. L. (1992). Biotechnological modification of lignin structure and composition in forest trees. *Holzforschung*, 46: 135-147.

Delves, H. T. (1988) Biomedical applications of ICP-MS. *Chem. Brit.*, I10: 1009.

Demmer, H., Hinz, I., Keller-Rudek, H., Koeber, K., Kottelwesch, H., and Schneider, D. (1980) in Coordination compounds of manganese (Schleitzer-Rust, E. ed) vol. 56, 8th Ed., pp 1-185, Springer-Verlag, New York.

Demmer, H., Hinz, I., Keller-Rudex, H., Koeber, K., Kottelwesch, H. and Schneider, D. (1980) in Coordination Compounds of manganese (Schleitzer-Rust, E., (Ed) 8th ed, Springer-Verlag, New York, vol. 56: 1-185.

DePillis, G. D., Ozaki, S., Kuo, J. M., Maltby, D.A., and Ortiz de Montellano, P. R. (1997) Autocatalytic processing of haem lactoperoxidse produces the native protein-bound prosthetic group. *J.Biol. Chem.* 272: 8857-60.

Diamantidis, G., Effosse, A., Potier, P and Bally, R. (2000) *Soil Biology and Biochemisrty*, 32, 919.

Dicko, M. H. Gruppen, H., Hilhorst, R., Voragen, A. G. J. Willem J. H. van Berkel, W.J.H. (2006) Biochemical characterization of the major sorghum grain peroxidase. *FEBS Journal* 273, 2293–2307.

Dix, N.J., Webster. J. (1995) Fungal ecology. Chapman & Hall, London, Cambridge, Great Britain, 549 p.

Dolphin, D. (ed) (1978) The porphyrins, Vol. 5, Academic Press, New York.

Dolphin, D., Forman, A., Borg, D. C., Fajer, J. and Felton, R. H. (1971) Compound I of catalase and horseradish peroxidase: Pi-cation radicals, Proc. Natl. Acad. Sci. USA. 68: 614-8.

Donnelly, P. K., Entry, J. A., Crawford, D.L., Cromack, Jr. K. (1990) Cellulose and lignin degradation in forest soils: Response to moisture, temperature, and acidity. *Microbial Ecol.* 20: 289–295.

Doyle W A and Smith A T. (1996) Expression of lignin peroxidase H8 in *Escherichia coli*: folding and activation of the recombinant enzyme with Ca^{2+} and haem. *Biochem J.* 315:15–19.

Doyle, W. A., Blodig, W., Veitch, N. C., Piontek, K., and Smith, A. T., (1998) Two substrtate interaction sites in lignin peroxidase revealed by site-directed mutagenesis, Biochemistry 37: 15097-105.

Dudev, T. and Lim, C. (2001) *J. Phys. Chem.* B 105: 4446.

Dudev, T. and Lim, C. (2003) Principles Governing Mg, Ca, and Zn Binding and Selectivity in proteins. *Chem. Rev.* 103: 773-787.

Dudev, T. and Lim, C. (2006) ADFT/CDM study of metal-carboxylate interactions in metalloproteins: factors governing the maximum number of metal-bound carboxylates. *J. Am. Chem. Soc.* 128: 1553-61.

Dudev, T. and Lim, C. (2006) Competition between protein ligands and cytoplasmic inorganic anions for the metal cation: a DFT/CDM study. *J. Am. Chem. Soc.* 128: 10541-48.

Dudev, T., Raghunathan, G. and Bahar, I. (1994) *Curr. Op. Struct. Biol.* 4: 256.

Dunford, H. B. (1982). "Peroxidases". *Advances in Inorganic Bichemistry* 4: 41-68,

Dunford, H. B. (1991). Horseradish peroxidase: Structure and kinetic properties. Peroxidses in chemistry and biology. J. Everse and M.B. Gisham. Boca Raton, CRC Press: 1-24.

Dunford, H. B. (1999a). Spectroscopy of horseradish peroxidase. I: Optical, Resonance Raman, Magnetic circular dichroism, X-ray absorption, and Diffraction, in: Heme peroxidase, WILEY-VCH, New York, pp. 135-174.

Dunford, H. B. (1999c) Myeloperoxidase and Eosinophil peroxidase: Pagocytosis and Microbial killing, in Haem peroxidase, WILEY-VCH, New York, pp. 349-385.

Dunford, H. B. (2010) Peroxiases and Catalases. Biochemistry, Biophysics, Biotechnology and Physiology. Wiley, A John Wiley and Sons, Inc., Publication, Hoboken, New Jersey, pp. 179-227.

Dunford, H. B. and Stillman, J. S. (1976) *Coord. Chem. Rev.* 19, 187 – 251.

Dunford, H. B., (1999b) Horseradish peroxidase. I: Ligand binding, Redox potentials, formation of its Compound, and some of their reactions, in: Haem peroxidase, WILEY-VCH, New York, pp. 58-91.

Eaton, R.A., Hale, M.D.C. (1993) Wood: Decay, pests and protection. Chapman & Hall, Cambridge, Great Britain.

Eichhorn, G. L. (1973) "Inorganic Biochemistry", G. L. Eichhorn, ed., Elsevier, Amsterdam, Ch. 33,

English, A. M., & Tsaprailis, G. (1995) Adv. Inorg. Chem. 43: 79-125.

Epstein, N. and Schejter, A. (1972) Magnetic circular dichrosim studies on acid and alkaline forms of horseradish peroxidase, . *FEBS Lett.* 25: 46-48.

Eriksson K.-E.L., Blanchette R.A., Ander P. (1990) Microbial and enzymatic degradation of wood and wood components. Springer-Verlag, Berlin, Germany.

Erman, J. E., L. B. Vitello, et al., (1989). Detection of an oxyferryl porphyrin pi-cation-radical intermediate in the reaction between hydrogen peroxide and a mutant yeast cytochrome *c* peroxidase. Evidence for tryptohan-191 involvement in the radical site of Compound I. *Biochemistry* 28 (20): 7992-5.

Everse, J., Everse, K.E. (1991). Peroxidases in Chemistry and Biology, vols. 1–2. CRC Press, Boca Raton, FL.

Everse, J., K. E. Everse, *et al*., (1991) Peroxidases in chemistry and Biology, Boca Raton, FL.

Faix, O., Mozuch, M. D., and Kirk, T. K. (1985) Degradation of gymnosperm (guaiacyl) vs. Angiosperm (syringly/guaiacyl) lignins by *Phanerochaete chrysosporium*. *Holzforschung* 39: 203-208.

Falke, J. J., Thatcher, K. C. and Voertler, C. S. (1991) *Biochemistry*, 30: 8690.

Farrell, R. (2007) Cartapip/ Sylvanex™ Ophiostoma fungal product for coomercial pulp and paper and solid wood applications. In: 10th International congress on biotechnology in pulp and paper industry. 10-15. Madison, WI, United states, Book of abstracts. Pp. 63-64.

Feijoo, G., Moreira, M.T., Álvarez, P.A., Lú-Chau, T., Lema, J.M. (2008) Evaluation of the enzyme manganese peroxidase in an industrial sequence for the lignin oxidation and bleaching of eucalyptus kraft pulp. *J. Appl. Polym. Sci*. 109:1319-1327.

Feis, A., Rodriguez-Lopez, J. N., Thorneley, R. N. F., Smulevich, G. (1998) *Biochemistry*, 37:13575-13581.

Felton, R. H., Romans, A. Y., Yu, N. T., Schonbaum, G. R. (1976) Laser Raman spectra of oxidized hydroperoxidases. *Biochim Biophys Acta.* 434 (1):82-9.

Fengel, D., Wegener, G. (1989) Wood: Chemistry, ultrastructure, reactions. Walter de Gruyter, New York, Berlin, Germany, 613 p.

Ferrari, R. P., Laurenti, E., Cecchini, P. I., Gambino, O., Sondergaard, I. (1995) Spectroscopic investigations on the highly purified lactoperoxidase Fe(III)-haem catalytic site, *J. Inorg. Biochem*. 58: 109-27.

Ferrer, I., Dezotti, M. and Duran, N. (1991) Decolorization of kraft effluent by free and immobilized lignin peroxidases and horseradish peroxidase. *Biotechnol. Lett.* 13:577-582.

Finzel, B. C., Poulos, T. L., and Kraut, J., (1984) Crystal structure of yeast cytochrome c peroxidase refined at 1.7 Å resolution, *J. Biol. Chem*. 259: 13027-36.

Fishel, L. A., Villafranca, J. E., Maurao, J. M., Kraut, J. (1987) *Biochemistry*, 26: 351-360.

Forrester, I.T., Grabski, A.C., Mishra, C., Kelly, B.D., Striekl, W. N., Leatham, G. E, and Burgess, R. R**.** (1990) Characteristics and N-terminal amino acid sequence of a manganese peroxidase purified from *Lentinula edodes* culture grown on a commercial wood substrate. *Appl. Microbiol. Biotechnol*., 33: 359-365.

Frausto da Silva, J.J.R, Williams, R. J. P. (1991). The Biological Chemistry of the Elements. Oxford: Oxford Univ. Press.

Fuhrhop, J., and Smith, K., (1975). Laboratory methods in porphyrin and metalloporphyrin research, ESPC, Oxford.

Furtmuller, J. Arnhold, W. Jantschko, M. Zederbauer, C. Jakopitsch, C. Obinger, J. (2005) Standard reduction potentials of all couples of the peroxidase cycle of lactoperoxidase. J. *Inorg. Biochem*. 99, 1220–1229.

Furtmuller, P. G., Burner, U., Jantschko, W., Regelsberger, G. and Obinger, C., (2000) The reactivity of myeloperoxidase compound I formed with hypochlorous acid, Redox. Rep. 5: 173-8.

Furtmuller, P. G., Jantschko, W., Zederbauer, M., Jakopitsch, C., Arnhold, J., and Obinger, C. (2004) *Jpn. J. Infect. Dis.* 57**:** S30–S31.

Furtmuller, P. G.,Arnhold, J., Jantschko, W., Pichler, H. and Obinger, C. (20030 Redox properties of the couples compound I/compound II and compound II/ native enzyme of human myeloperoxidase, *Biochem. Biophys. Res. Commun*. 301: 551-7.

Gajhede, M., Schuller, D. J., Henriksen, A., Smith, A. T., and Poulos, T. L. (1997) *Nat. Struct. Biol.* 4**:** 1032–1038.

Garcia, J. S., de Magalhaes, C. S. Arruda, M. A. (2006) Trends in metal-binding and metalloprotein analysis. *Talanta*, 69: 1-15.

Garmer, D. R. and Gresh, N. (1994) *J. Am. Chem. Soc*. 116: 3556.

Gazaryan, I. G. (1994) LABPV New sl., 4: 8-15.

Gelpke, M. D. S., Mayfield-Gambill, M., Cereghino, G. P. L. and Gold, M. H. (1999) Homologous Expression of Recombinant Lignin Peroxidase in *Phanerochaete chrysosporium*. *Appl Environ Microbiol*. 65(4): 1670–1674.

Gelpke, M. D. S., Moenne-Loccoz, P., and Gold, M. H. (1999) Arginine 177 is involved in Mn (II) binding by manganese peroxidase, *Biochemistry* 38: 11482-11489.

George, S. J., Kvaratskhelia, M., Dilworth, M. J., Thorneley, R. N.F (1999). Reversible alkaline inactivation of lignin peroxidase involves the release of both the distal and proximal site calcium ions and bishistidine co-ordination of the haem. *Biochem J* 344:237–244.

Gill, P. K., Arora, D. S., & Chander, M. (2002). Biodecolorisation of azo and triphenyl-methane dyes by *Dichomitus squalens* and *Phlebia* spp. Journal of Industrial *Microbiology & Biotechnology*, 28: 201–203.

Gilson, M. K. and Honig, B. H. (1986) The dielectric constant of a folded protein. *Biopolymers* 25 (11) 2097-2119.

Girous, E.L., Schoun, J. (1981). *J. Inorg. Biochem*. 14, 359.

Glenn, J. K., Akileswaran, L., & Gold, M. H. (1986) *Arch. Biochem. Biophys. 251*: 688-696.

Glenn, J. K., and Gold, M. H. (1985) Purification and Characterization of an extracellular Mn (II)-dependent peroxidase from the lignin–degrading basidiomycete, *Phanerochaete chrysosporium*. *Arch. Biochem. Biophys. 242*: 329-341.

Gold, H. M., Youngs, H. L., and Sollewijn Gelpke, M. D. (2000). Manganese peroxidase. Metal Ions in Biological Systems, 37: 559–586, Medline.

Gold, M. H., and Alic, M. (1993) Molecular biology of the lignin-degrading basidiomycete *Phanerochaete chrysosporium*. *Microbiol. Rev.* 57: 605- 622.

Gold, M. H., Kuwahara, M., Chiu, A. A., and Glenn, J. K. (1984**)** *Arch. Biochem. Biophys.* 234: 353-362.

Gold, M. H., Wariishi, H. and Valli, K. (1989) Extrcellular peroxidases involved in lignin degradation by the white rot basidiomycete *Phanerochaete chrysosporium*, ACS Symp. Ser. 389: 127 -140.

Goodin, D. B. and McRee, D. E. (1993) The Asp-his-Fe triad of cytochrome c peroxidase controls the reduction potential , electronic structure and coupling of the tryptophan free radical to the heme. *Biochemistry* 32: 3313 – 3324.

Gouterman, M. J. (1961) *Mol. Spectrosc*. 6:138.

Gray, K.A., Zhao, L.S., Emptage, M. (2006) Bioethanol. *Curr Opin Chem Biol* 10:141-146.

Gregg, J. M., Vedvick, T. S. and Raschke, W. C. (1993) Biotechnol. Bioengineering, 30: 31-36.

Gregory, D. S., Martin, A. C. R., Cheetham, J. and Rees, A. R (1993) The prediction and characterisation of metal sites in proteins. *Protein Engineering* , 6 : 29-35.

Gu, L., Lajoie, C. and Kelly, C. (2003) Expression of a *Phanerochaete chrysosporium* manganese peroxidase gene in the yeast *Pichia pastoris*. *Biothecnol. Prog.* 19, 1403-1409.

Guex, N. and Peitsch, M. C. (1997). SWISS-MODEL and the Swiss-PdbViewer: An environment for comparative protein modeling. Electrophoresis 18: 2714-2723.

Hakala, T.K. (2007) Characterization of the lignin-modifying enzymes of the selective white-rot fungus *Physisporinus rivulosus*. Dissertationes Bioscientiarum Molecularium Universitatis Helsingiensis in Viikki, 21/2007. PhD Thesis. Department of Applied Chemistry and Microbiology, University of Helsinki, Helsinki. 60 p.

Halpin, B.; Pressey, R.; Jen, J.; Mondy, N. (1989) Purification and characterization of peroxidase isoenzymes from green peas (*Pisum sati*V*um*). *J. Food Sci. 54*, 644-649.

Hammel, K. E. and Cullen, D. (2008) Role of fungal peroxidases in biological ligninolysis. *Curr. Opin. Plant Biol.* 11:349-355.

Haritash, A. K. and Kaushik, C. P. (2009) Biodegradation aspects of polycyclic aromatic hydrocarbons (PAHs): A review. *J. Hazard. Mater*. 169: 1-15.

Harris, P.J., Stone, B.A. (2008) Chemistry and molecular organization of plant cell walls. In: Himmel M., editor. Biomass recalcitrance: deconstructing the plant cell wall for bioenergy. Blackwell Pub., Oxford, UK, pp. 61-93.

Harris, R. Z., Wariishi, H., Gold, M. H. and Ortiz de Montellano, P. R. (1991) The Catalytic Site of Manganese Peroxidase: Regiospecific addition of sodium azide and alkylhydrazines to the heme group. *The journal of Biological chemistry*, 266 (14): 8751 – 8758.

Hartmann, C. and Ortiz de Montellano, P.R. (1992) Baculovirus expression and characterization of catalytically active horseradish peroxidase. *Arch. Biochem. Biophys.* 297: 61-72.

Harvey, P. J., Schoemaker, H. E., Palmer, J. M. (1986) Veratryl alcohol as a mediator and the role of radical cations in lignin biodegradation by *Phanerochaete chrysosporium*. *FEBS Lett* 195: 242-246.

Haschke, R. H., and Freidhoff, T. M. (1978) *Biochem*. *Biophys*. *Res*. *Commun*. *80*, 1039-1042.

Hatakka A.I., Mohammadi, O.K., Lundell, T.K. (1989) The potential of white-rot fungi and their enzymes in the treatment of lignocellulosic feed. *Food Biotechnol* 3:45-58.

Hatakka, A. I. & Uusi-Rauva, A. K. (1983) Degradation of IT labelled poplar wood lignin by selected white-rot fungi, *Eur*. J. *Appl. Microbiol. Biotechnol.* 17, 235 -242.

Hatakka, A. I. And Lundell, T. (1989) Degradation of lignin model compounds by ligninolytic enzymes of the white-rot fungus *Phlebia radiata*. In: Kennedy, J. F., Philips, G. O. and Williams, P. A. (eds) Wood processing and utilization. Ellis Horwood Publ. Ltd., Chichester, pp. 333-340.

Hatakka, A., Buswell, J. A., Pirhonen, T. I., Uusi-Rauva, A.K. (1983) Degradation of ^{14}C-labelled lignins by white-rot fungi. In: Higuchi T., Chang H. M., Kirk, T. K. (eds) Recent advances in lignin biodegradation research, UNI Publishers Co., Tokyo, Japan, pp. 176-187.

Hatakka, A., Lundell, T., Hofrichter, M., Maijala, P. (2003) Manganese peroxidase and its role in the degradation of wood lignin. In: Mansfield S.D., Saddler J.N., editors. ACS Symposium series 855, Applications of Enzymes to Lignocellulosics.

Hatakka, A.I. (1994) Lignin-modifying enzymes from selected white-rot fungi – production and role in lignin degradation. *FEMS Microbiol Rev* 13:125-135.

Hatakka, A.I. (2001) Biodegradation of lignin. In: Hofrichter M and Steinbuchel A (eds.) Biopolymers. Vol 1: Lignin, humic substances and coal. Wiley-VCH, Weinheim, Germany, pp. 129-180.

Hatakka, A.I., Kantelinen, A., Tervila-Wilo, A., Viikari, L. (1987) Production of ligninases by *Phlebia radiata* in agitated cultures. In: Odier E (ed) Lignin enzymic and microbial degradation. INRA, Paris, pp. 185-189.

Hatakka, A.I., Uusi-Rauva, A.K. (1983) Degradation of 14C-labeled poplar wood lignin by selected white-rot fungi. *Eur J Appl Microb* Biotechnol 17:235-242.

Hatfield, R.D. (1989) Structural polysaccharides in forages and their degradability. *Argon. J.* 81: 39-46.

Henriksen A, Welinder, K. G & Gajhede, M. (1998) Structure of barley grain peroxidase refined at 1.9-A˚ resolution: a plant peroxidase reversibly inactivated at neutral pH. *J Biol Chem. 2*73, 2241–2248.

Henriksen, A., Mirza, O., Indiani, C., Teilum, K. Smulevich, G. Karen G. Welinder, K. G and Gajhede, M. (2001) Structure of soybean seed coat peroxidase: A plant peroxidase with

unusual stability and haem-apoprotein interactions. Protein Sci. 2001 January; 10(1): 108–115.

Henriksson, G., Sild, V., Szabo, I. J., Pettersson, G. and Johansson, G. (1998b). Substrate specificity of cellobiose dehydrogenase from *Phanerochaete chrysosporium*. *Biochim. Biophys. Acta* 1383**:**48–54.

Higuchi, T., Shimada, M., Nakatsubo, F., Tanahashi, M**.** (1977) Differences in biosynthesis of guaiacyl and syringyl lignin in wood. *Wood Sci. Technol*. 11: 153–167.

Hilden, K., Martinez, A.T., Hatakka, A., Lundell, T. (2005) The two manganese peroxidases pr-MnP2 and pr-MnP3 of *Phlebia radiata*, a lignin-degrading basidiomycete, are phylogenetically and structurally divergent. *Fungal Genet Biol* 42:403-419.

Hilden, K.S., Bortfeldt, R., Hofrichter, M., Hatakka, A., Lundell, T.K. (2008) Molecular characterization of the basidiomycete isolate *Nemataloma frowardii* b19 and its manganese peroxidase places the fungus in the corticioid genus *Phlebia*. *Microbiology* 154:2371-2379.

Hilden, K.S., Makela, M.R., Hakala, T.K., Hatakka, A., Lundell, T. (2006) Expression on wood, molecular cloning and characterization of three lignin peroxidase (LiP) encoding genes of the white rot fungus *Phlebia radiata*. *Curr Genet* 49:97-105.

Himmel, M.E., Ding, S.Y., Johnson, D.K., Adney, W.S., Nimlos, M.R., Brady, J.W., Foust, T.D. (2007) Biomass recalcitrance: Engineering plants and enzymes for biofuels production. *Science* 315:804-807.

Hinder, A. N. P., Ruiz, J. H., Lopez, J. N. R. Canovas, F. G., Brisset, N. C., Smith, A. T., Arnao, M. B., Acosta, M. (2002). Reactions of the class II peroxidase, lignin peroxidase and Arthro ramosus peroxidase with hydrogen peroxidase. *J. Biol. Chem*. 277: 26879 – 26885.

Hiraga, S., Sasaki, K., Ito, H., Ohashi, Y. and Matsui, H. (2001) A large family of class III plant peroxidases. *Plant and Cell Physiology*, 42 (5) 462-468.

Hitzeman, R.A., Chen, C.Y., Dowbenko, D.J. (1990). Use of heterologous and homologous signal sequences for secretion of heterologous proteins from yeast. *Meth. Enzymol.* 185, 421–440.

Hoegger, P.J., Kilaru, S., James, T.Y., Thacker, J.R., Kües, U. (2006) Phylogenetic comparison and classifi cation of laccase and related multicopper oxidase protein sequences. *FEBS J.* 273:2308-2326.

Hofrichter, M. (2002) Review: Lignin conversion by manganese peroxidase (MnP). *Enzyme Microb Technol* 30:454-466.

Hofrichter, M., Scheibner, K., Bublitz, F., Schneegaß, I., Ziegenhagen, D., Martens, R., Fritsche, W. (1999a) Depolymerization of straw lignin by manganese peroxidase from *Nematoloma frowardii* is accompanied by release of carbon dioxide. *Holzforschung* 53, 161-166.

Hofrichter, M., Vares, K., Scheibner, K., Galkin, S., Sipila, J., Hatakka, A. (1999) Mineralization and solubilization of synthetic lignin by manganese peroxidases from *Nematolomafrowardii* and *Phlebia radiata. J Biotechnol* 67:217-228.

Hofrichter, M., Vares, T., Kalsi, M., Galkin, S., Scheibner, K., Fritsche, W., Hatakka, A. (1999b) Production of manganese peroxidase and organic acids and mineralization of14C-labelled lignin (14C-DHP) during solid-state fermentation of wheat straw with the white rot fungus *Nematoloma frowardii*. Appl. Environ. Microbiol. 65, 1864-1870.

Houk, R. S. (1986). Mass spectrometry of inductively coupled plasmas. *Anal. Chem.* **58**, 97A–105A.

Houk, R. S., Fassel, V. A., Flesch, G. D., Svec, H. J., Gray, A. L and Taylor, C. E., (1980), *Anal. Chem.*, 52, 2283-2289.

Howest, B. D., Feis, A., Raimond, L. Indiani, C. and Smulevich, G. (2001). The critical role of the proximal calcium ion in the structural properties of horseradish peroxidase. *J. of Biological chemistry*, 276 (44): 40704 – 40711.

Huang, D. T. C., Thomas, M. A. W. and Christopherson, R. I. (1999) *Biochemistry*, 38: 9964.

Husain, Q. (2006) Potential applications of the oxidoreductive enzymes in the decolorization and detoxifi cation of textile and other synthetic dyes from polluted water: A review. *Crit. Rev. Biotechnol*. 26:201-221.

Huynh, V.B. and Crawford, R.L. (1985) Novel extracellular enzymes (ligninases) of *Phanerochaete chrysosporium*. *FEMS. Microbiol. Lett.* 119-123.

Ibers, J. A. and Holm, R. H. (1980). Modelling coordination sites in metallobiomolecues. *Science*, 209, 223, 4453.

Ikeda-Saito, M., and Prince, R. C. (1985) The effect of chloride on the redox and EPR properties of myeloperoxidase, *J. Biol. Chem.* 260: 8301-5

Ikehata, K., Buchanan, I. D., Pickard, M. A., and Smith, D. W. (2005) *Bioresource Technol*. 96: 1758-1770.

Ilgenfritz, G. and Cshuster, T. M. (1961) in: Probes in structure and function of macromolecules membranes. Vol. II. Chance, B., Yonetani, T. and Mildvan, A.S. eds.) Academic Press, New York, London. pp 299 – 310.

Iori, R., Cavalieri, B., & Palmieris, S. (1995) *Cereal Chem. 72*, 176-181.

Irving, H. and Williams, R. J. P. (1948). Order of stability of metal complexes. *Nature;* 162: 746-7.

Jentzen, W.; Ma, J. G. (1998) Shelnutt, J. A. *Biophys. J.* 74: 753.

Jernigan, R., Raghunathan, G. and Bahar, I. (1994) Characterisation of interactions and metal ions binding sites in proteins. *Current Opinion in Structural Biology*, 4 (2): 256-263.

Jiang, F., Kongsaeree, P., Charron, R., Lajoie, C., Xu, H. Scott, G. and Kelly, C. (2008) Production and separation of manganese peroxidase from haem amended yeast cultures, *Biotechnol Bioeng* 99: 540–549.

Job, D., Richard, J., and Dunford, H. B. (1977) *Arch. Biochem. Biophys.* 179: 95-99.

Johjima, T., Itoh, N., Kabuto, M., Tokimura, F., Nakagawa, T., Wariishi, H., Tanaka, H. (1999) Direct interaction of lignin and lignin peroxidase from *Phanerochaete chrysosporium*. *Proc Natl Acad. Sci*. USA, 96: 1989-1994.

Johnson, C. R., Cullen, D., and Lamar, R.T. (1994). Manganese peroxidases of the white rot fungus *Phanerochaete sordida. Appl. Environ. Microbiol*, 60, 599-605.

Johnson, T. M. and Li, J. K. (1991) Heterologous expression and characterisation of an active lignin peroxidase from *Phanerochaete chrysosporium* using recombinant barculovirus. *Arch Biochem. Biophys.* 291: 371-378.

Johnson, T., Pease, E., Li, J. and Tien, M. (1992) Production and characterisation nof recombinant lignin peroxidase isozymes H2 from *Phanerochaete chrysosporium* using recombinant baculovirus. *Arch Biochem Biophys*. 296: 660-666.

Jülich, W., J. A. Stalpers (1980) *The Resupinate Non-poroid Aphyllophorales of the Temperate Northern Hemisphere*. North-Holland Publishing Company, Amsterdam, Oxford, New York.

Kamm, B., Kamm, M. (1994) Principles of biorefi neries. Appl. Microbiol. *Biotechnol.* 64:137-145.

Kanayama, N., Suzuki, T., Kawai, K. (2002) Purification and characterization of an alkaline manganese peroxidase from *Aspergillus terreus* LD-I. *J. of Biosci. Bioeng*. 93 (4), 405 – 410.

Kane, J. F. And Hartley, D. L. (1988). Formation of recombinant protein inclusion bodies in Escherichia coli. *Trends Biotech*. 6: 95-101.

Kantelinen, A., Hatakka, A., Viikari, L. (1989) Production of lignin peroxidase and laccase by *Phlebia radiata*. *Appl Microbiol Biotechnol* 31:234-239.

Kantelinen, A., Waldner, R., Niku-Paavola, M.L., Leisola, M.S.A. (1988) Comparison of two lignin-degrading fungi: *Phlebia radiata* and *Phanerochaete chrysosporium*. *Appl Microbiol Biotechnol* 28:193-198.

Kapich, A., Hofrichter, M., Vares, T., Hatakka, A. (1999) Coupling of manganese peroxidasemediated lipid peroxidation with destruction of nonphenolic lignin model compounds and 14C-labeled lignins. *Biochem Biophys Res Commun* 259:212-219.

Kaposi, A. D.; Wright, W. W., Fidy, J., Stavrov, S. S., Vanderkooi, J. M. and Rasnik, I. (2001) *Biochemistry*, 40: 3483.

Karhunen, E., Kantelinen, A. and Niku-Paavola, M. (1990) Mn-dependent peroxidase from the lignin-degrading white rot fungus *Phlebia radiata*. *Archives of Biochemistry and Biophysics*, 279 (1): 25 – 31.

Kaschl, A., Romheld, V., Chen, Y. (2002) The influence of soluble organic matter from municipal solid waste compost on trace metal leaching in calcareous soils. *Sci. Total Environ.* 291: 45–57.

Kennedy, M. L. and Gibney, B. R. (2000). Metalloprotein and redox protein design. *Current Opinion in Structural Biology* 2001, 11:485–490.

Kersten, P. J., Tien, M., Kalyanaraman, B., & Kirk, T. K. (1985). The ligninase of *Phanerochaete chrysosporium* generates cation radicals from methoxybenzenes. *Journal of Biological Chemistry*, 260, 2609–2612.

Kersten, P., & Cullen, D. (2007). Extracellular oxidative systems of the lignin-degrading Basidiomycete *Phanerochaete chrysosporium*. Fungal Genetics Biology, 44, 77–87.

Kiiskinen, L.-L., Palonen, H., Linder, M., Viikari, L., Kruus, K**.** (2004) Laccase from *Melanocarpus albomyces* binds effectively to cellulose. *FEBS Lett.* 576: 251–255.

Kim, S. J, Lee, J. A., Won, K., Kim, Y. H., Song, B. K. (2009) Functional expression of *Coprinus cinereus* peroxidase in *Pichia pastoris. Process Biochemistry* 44 (2009) 731–735.

Kimura, S., and Ikeda-Saito, M. (1988) *Proteins* 3**,** 113–120.

Kimura, S., and Yamazaki, I. (1979), Comparison between hog intestinal peroxidase and bovine lactoperoxidase-compound I formation and inhibition by benhydroxamic acid, *Arch. Biochem. Biophys*. 198: 580-8.

Kirk, T. K. (1983). Degradation and conversion of lignocelluloses. In J. E. Smith, D. R. Berry and B. Kristiansen (Eds.), The filamentous fungi (Vol. 4, pp. 266–295). London: Edward Arnold.

Kirk, T.K., Brunow, G. (1988) Synthetic 14C-labeled lignins. *Method Enzymol* 161:65-73.

Kirk, T.K., Farrell, R.L. (1987) Enzymatic combustion - the microbial-degradation of lignin. *Annu Rev Microbiol* 41:465-505.

Kishi, K., Hildebrand, D. P., Kusters-van Someren, M., Gettemy, J., Mauk, A. G., and Gold, M. H. (1997) *Biochemistry* 36: 4268 – 4277.

Kishi, K., Kusters-van Someren, M., Mayfield, M. B., Sun, J., Loehr, T. M., and Gold, M. H. (1996) Characterization of manganese(II) binding site mutants of manganese peroxidase, *Biochemistry* 35: 8986-8994.

Kishi, K., Wariishi, H., Marquez, L., Dunford, H. B. and Gold, M. H. (1994) Mechanism of manganese peroxidase compound II reduction. Effect of organic acid chelators and pH. *Biochemistry*, 33: 8694-8701.

Kjalke, M., Andersen, M.B., Schneider, P., Christensen, B., Schulein, M., Welinder, K.G.(1992). Comparison of structure and activities of peroxidases from *Coprinus cinereus*, *Coprinus macrorhizus* and *Arthromyces ramosus*. *Biochim. Biophys. Acta* 1120: 248–256.

Kremer, M. L. (1970) Biochem. Biophy. Acta. 198: 199-209.

Kremer, S. and Anke, H. (1997) Fungi in bioremediation. In T. Anke (ed), Fungal Biotechnology. Chapman and Hall, Weinheim, Germany. P 275-295.

Kuan, I. C. and Tien, M. (1993a) Stimulation of Mn peroxidase activity: a possible role for oxalate in lignin biodegradation. *Proc. Natl. Acad. Sci.* USA, 90: 1242 – 1246.

Kuan, I.C., Johnson, K. A., & Tien, M. (1993). Kinetic analysis of manganese peroxidase. *Journal of Biological Chemistry*, 268: 20064–20070.

Kuchar, J. and Hausinger, R. P. (2004) Biosynthesis of metal sites. *Chem. Rev.* 104: 509-525.

Kuhad, R.C., Singh, A., Eriksson, K.E. (1997) Microorganisms and enzymes involved in the degradation of plant fiber cell walls. *Adv Biochem Eng Biotechnol* 57:45-125.

Kuila, D., Tien, M., Fee, J. a., and Ondrias, M. R. (1985) *Biochemistry* 24: 3394-3397.

Kumar, R., Singh, S., Singh, O.V. (2008) Bioconversion of lignocellulosic biomass: biochemical and molecular perspectives. *J. Ind. Microbiol. Biotechnol*. 35:377-391.

Kunishima, N., Amada, F., Fukuyama, K., Kawamoto, M., Matsunaga, T., and Matsubara, H. (1996) *FEBS Lett.* 378: 291–294.

Kunishima, N., Fukuyama, K. and Matsuara, H. (1994) *J. Mol. Biol*. 235: 331-344.

Kuo, M. (2008). *Phlebia radiata.* Retrieved from the *MushroomExpert.Com* Web site: http://www.mushroomexpert.com/phlebia_radiata.html

Kupke, D. W. and Dorrier, T. E. (1978) *Methods Enzymol*. 48: 155-162.

Kusters-van Someren, M., Kishi, K., Lundell, T., and Gold, M. H. (1995) The manganese binding site of manganese peroxidase: Characterization of an Asp179Asn site-directed mutant protein, *Biochemistry 34*:10620-10627.

Kuwahara, M., Glenn, J.K., Morgan, M.A. and Gold, M.H. (1984) Separation and characterization of two extracellular H_2O_2-dependent oxidases from ligninolytic cultures of *Phanerochaete chrysosporium*. *FEBS Lett*. 169: 247–250.

Lackner, R. et al., (1991) Oxidative degradation of high molecular weight chlorolignin by MnP. *Biochem. Biophys. Res. Commun*. 178: 1092-1098.

Lamikanra, O. and Watson, M. A. (2000) Cantaloupe melon peroxidase: Characterisation and effects of additives on activity. *Nahrung* 44: 168-172.

Lardinois, O. M., and Ortiz de Montellano, P. R. (2000) EPR spin-trapping of a myeloperoxidase protein radical, Biochem. Biophys. Res. Commun. 270: 199-202.

Laureti, E. and Ghibaudi, E. (2003) Unraveling the catalytic mechanism of lactoperoxidase and myeloperoxidase: A freflection on some controversial features, Review Article, *Eur. J. Biochem*. 270: 4403-12.

Laurie, S. H. and Pratt, D.E. (1986) *J. Inorg. Biochem.* 28: 431.

Lee, L. V., Poyner, R. R., Vu, M. V., Cleland, W. W. (2000) *Biochemistry*, 39: 4821.

Leone, M., A. Cupane, E. Vitrano, and L. Cordone. 1992. Strong vibronic coupling in haem proteins. *Biophys. Chem.* 42:111-115.

Leontievsky, A.A., Vares, T., Lankinen, P., Shergill, J.K., Pozdnyakova, N.N., Myasoedova, N.M., Kalkkinen, N., Golovleva, L.A., Cammack, R., Thurston, C.F., Hatakka, A. (1997) Blue and yellow laccases of ligninolytic fungi. *FEMS Microbiol. Lett.* 156:9-14.

Li, H. and Poulos, T.L. (1994) Structural variation in heme enzymes: a comparative analysis of peroxidase and *P*450 crystal structures. *Structure 2,* 461–464.

Lige, B., Ma, S. W. and Huystee, R. B. (2001) Glycosylation of the cationic peanut peroxidase gene expressed in transgenic tobacco. *Plant Sci*. 156: 55-63.

Lippard, S. J, Berg, J. M. (1994). Principles of Bioinorganic Chemistry. Mill Valley, CA: Univ. Science Books.

Littlechild, J. (1999) Haloperoxidases and their role in biotransformation reactions, *Curr. Opin. Chem. Biol.* 3: 28-34.

Liu, C. and Xu, H. (2002). *J. Inorg. Biochem*. 88, 77.

Lokman, B. C., V. Joosten, J. Hovenkamp, R. J. Gouka, C. T. Verrips, and C. A. van den Hondel. (2003) Efficient production of *Arthromyces ramosus* peroxidase by *Aspergillus awamori*. *J Biotechnol*. 103:183-190.

Lopez, P. and Burgos, J. (1995) Peroxidase stability and reactivation after heat treatment and manothermosonication. *Journal of Food Science*, 60 (3) 451-455.

Loschen, G., Azzi, A., Richter, C., and Flohe, L., (1974) Superoxide radicals as precursors of mitochondrial hydrogen peroxide, *FEBS, Lett.* 42: 68-72.

Lovell, T., Himo, F., Han, W. G., Noodleman, L. (2003). Density functional methods applied to metalloenzymes. *Coord. Chem. Rev.* 238-239: 211- 32.

Lu, A. T.; Whitaker J. R. (1974) Some factors affecting rates of heat inactivation and reactivation of horseradish peroxidase. *J. Food Sci*. *39*, 1173-1178.

Lu-Chau, T.A., Ruiz-Dueñas, F. J., Camarero, S. Feijoo, G. Martínez, M. J Lema, J. M. and Martínez, A.T. (2004) Effect of pH on the stability of *Pleurotus eryngii* versatile peroxidase during heterologous production in *Emericella nidulans*, *Bioprocess Biosyst. Eng.* 26: 287–293.

Lundell, T. (1993) Ligninolytic system of the white-rot fungus *Phlebia radiata*: Lignin model compound studies. PhD Thesis, Department of Applied Chemistry and Microbiology, University of Helsinki, Helsinki. 90 p.

Lundell, T., Hatakka, A. (1994) Participation of Mn (II) in the catalysis of laccase, manganese peroxidase and lignin peroxidase from *Phlebia radiata*. *FEBS Lett* 348:291-296.

Lundell, T., Leonowicz, A., Rogalski, J., Hatakka, A. (1990) Formation and action of ligninmodifyingenzymes in cultures of *Phlebia radiata* supplemented with veratric acid. *Appl Environ Microbiol* 56:2623-2629.

Macauley-Patrick, S., Fazenda, M. L., McNeil, B., Harvey, L. M (2005). Heterologous protein production using the *Pichia pastoris* expression system. Yeast; 22:249–70.

Magliozzo, R. S. and Marcinkeviciene, J. A. (1997) The role of Mn (II)-peroxidase activity of mycobacterial catalase-peroxidase in activation of the antibiotic isoniazid, J. Biol. Chem. 272: 8867-8870.

Magliozzo, R. S., and Marcinkeviviene, J. A. (1997) The role of Mn (II)-peroxidase activity of mycobacterial catalase-peroxidase in activation of the antibiotic isoniazid, *J. Biol.* Chem. 272: 8867-8870.

Maijala, P., Kleen, M., Westin, C., Poppius-Levlin, K., Herranen, K., Lehto, J.H., Reponen, P., Mäentausta, O., Mettala, A., Hatakka, A. (2008) Biomechanical pulping of softwood with enzymes and white-rot fungus *Physisporinus rivulosus. Enzyme Microb. Technol*. 43:169-177.

Makela, M. R. (2009) The white-rot fungi *Phlebia radiata* and *Dichomitus squalens* in wood-based cultures: expression of laccases, lignin peroxidases, and oxalate decarboxylase. Academic dissertation presented to the Faculty of Agriculture and Forestry, University of Helsinki.

Makinen, M. W.; Churg, A. K. (1983) Structural and analytical aspects of the electronic spectra of haemproteins. In *Iron Porphyrins*; Lever, A. B. P., Gray, H. B., Eds.; Addison-Wesley: Reading MA, p 141.

Maltempo, M. M. (1976) Visible absorption spectra of quantum mixed-spin ferric heme proteins. *Biochim. Biophys. Acta*. 434:513–518.

Maltempo, M. M., (1976) Visible absorption spectra of quantum mixed-spin ferric haem proteins. *Biochemica et Biophysica Acta*, 434: 513-518.

Manas, E. S., Wright, W. W., Sharp, K. A., Friedrich, J., Vanderkooi, J. M.(2000) *J. Phys. Chem. B 104*, 6932.

Manas, E. S.; Vanderkooi, J. M.; Sharp, K. A. (1999) *J. Phys. Chem. B* 103, 6334.

Maneiro, M., Ruettinger, W. F., Bourle, E., Mclendon, G. L. and Dismukes, G.C. (2003). *Proc. Natl. Acad. Sci.* USA 100: 3707 – 3712.

Maranon, M. J. R. and Huystee, R. B. (1994) Plant peroxidase interaction between their prosthetic groups. *Phytochemistry* 37: 1217-1225.

Maranon, M. J. R., Stillman, M. J., & van Huystee, R. B. (1993). *Biochem. Biophys. Res. Commun. 194*, 326-333.

Marquez, L. A., and Dunford, H. B. (1995) *J. Biol. Chem.* 270, 30434–30440.

Marquez, L. A., and Dunford, H. B., (1994) Chlorination of taurine by myeloperoxidase. Kinetic evidence for an enzyme-bound intermediate, J. Biol. Chem. 269: 7950-6.

Martínez Á.T., Ruiz-Dueñas F.J., Martínez M.J., del Rio J.C., Gutierrez A. (2009) Enzymatic delignification of plant cell wall: From nature to mill. *Curr. Opin. Biotechnol.* 20:348-357.

Martinez, A.T. (2002) Molecular biology and structure-function of lignin-degrading heme peroxidases. *Enzyme Microb Technol* 30:425-444.

Martinez, A.T., Camarero, S., Guillen, F., Gutierrez, A., Munoz, C., Varela, E. (1994) Progress in biopulping of non-woody materials: Chemical, enzymatic and ultrastructural aspects of wheat-straw delignification with ligninolytic fungi from the genus *Pleurotus*. *FEMS Microbiol Rev* 13:265-274.

Martins, L.O., Soares, C.M., Pereira, M.M., Teixeira, M., Costa ,T., Jones, G.H., Henriques, A.O. (2002) Molecular and biochemical characterization of a highly stable bacterial laccase that occurs as a structural component of the *Bacillus subtilis* endospore coat. *J. Biol. Chem.* 277: 18849–18859.

Matsubara, M., Suzuki, J., Deguchi, T., Miura, M. and Kitaoka, Y. (1996). Characterization of manganese peroxidases from the hyperlignolytic fungus IZU-154. *Appl. Environ. Microbiol.* 62, 4066-4072.

Mauro, J. M., L. A. Fishel, et al., (1988). Tryptophan-191----Phenylalanine, a proximal-side mutation in yeast cytochrome *c* peroxidase that strongly affects the kinetics of ferrocytochrome oxidation. *Biochemistry* 27 (17): 6234-56.

Mayeno, A. N., Curran, A. J., Roberts, R. L., and Foote, C. S. (1989). *J. Biol. Chem*. 264, 5660–5668.

Mayfield, M.B., Kishi, K., Alic, M., Gold, M.H. (1994). Homologous expression of recombinant manganese peroxidase in *Phanerochaete chrysosporium*. *Appl. Environ. Microbiol.* 60, 4303–4309.

Mc Eldoon, J. P. and Dordick, J. S. (1996) Unusual thermal stability of soybean peroxidase. *Biotechnool. Prog*. 12: 555-558.

McClelland, M. and Nelson, M. (1992) Effect of site-specific methylation on DNA

McDougall, G.J., Morrison, I.M., Stewart, D., Weyers, J.D.B., Hillman, J.R. (1993) Plant fibres: Botany, chemistry and processing for industrial use. *J. Sci. Food Agric*. 62, 1-20.

McEldoon, J.P., Pokora, A.R., and Dordick, J.S. (1995). Lignin peroxidase-type activity of soybean peroxidase. *Enzyme Microb. Technol.* 17**:** 359–365.

McLellan, K. M.; Robinson, D. S. (1987) Purification and heat-stability of Brussels-sprout peroxidase isoenzymes. *Food Chem. 23*, 305-319.

McClelland, M. and Nelson, M. (1992) Effect of site-specific methylation on DNA modification methyltransferases and restriction endonucleases. *Nucleic Acids Res.* 20**,** 2145–2157.

Mellor, D. P., and Maley, L. (1947). *Nature*, 159, 370.

Mellor, D. P., and Maley, L. (1948). *Nature*, 161, 436.

Messerschmidt and Huber, R. (1990) *European Journal of Biochemistry* 187: 341.

Messner, K. and Srebotnik. E**. (**1994**)** Biopulping: an overview on developments in an environmentally save paper-making technology. *FEMS Microbiol. Rev*. 13**:**351–364.

Mester, T., & Field, J. A. (1998). Characterization of a novel manganese peroxidase-lignin peroxidase hybrid isozyme produced by Bjerkandera species strain BOS55 in the absence of manganese. *Journal of Biological Chemistry*, 15412–15417.

Mielgo, I., Lopez, C., Moreira, M. T., Feijoo, G., Lema, J. M. (2003) Oxidative degradation of azo dyes by manganese peroxidase under optimized condition. *Biotechnol Prog*. 19, 325 0 – 31.

Miller, M. A., Coletta, M., Mauro, J. M., Putman, I. D., Farnum, M. F., Kraut, J. and Traylor, T. G. (1990) *Biochemistry* 29: 1777-1791.

Miller, M. A., Coletta, M., Mauro, J. M., Putman, I. D., Farnum, M. F., Kraut, J. and Traylor, T. G. (1990) *Biochemistry* 29: 1777-1791.

Mino, Y., Wariishi, H., Blackurn, N. J., Loehr, T. M. and Gold, M. H. (1988) Spectral characterization of manganese peroxidase, an extracellular heme enzyme from the Lignin-degrading Basidiomycete, *Phanerochaete chrysosporium*. *The journal of Biological Chemistry*, Vol. 263, (15), 7029-7036.

modification methyltransferases and restriction endonucleases. *Nucleic Acids Res.*

Moilanen, A.M., Lundell, T., Vares, T., Hatakka, A. (1996) Manganese and malonate are individual regulators for the production of lignin and manganese peroxidase isozymes and in the degradation of lignin by *Phlebia radiata*. *Appl Microbiol Biotechnol* 45:792-799.

Monties, B., Fukushima, K. (2001) Occurence, function and biosynthesis of lignins. In: Steinbüchel A. (ed.) Biopolymers. Vol 1: Hofrichter M., Steinbuchel A. (eds.) Lignin, Humic Substances and Coal. Wiley-VCH, Germany, pp. 1-64.

Morawski, B., Lin, Z., Cirino, P., Joo, H., Bandara, G., Arnold, F.H. (2000). Functional expression of horseradish peroxidase in *Saccharomyces cerevisiae* and *Pichia pastoris. Protein Eng*. 13, 377–384.

Moreira, M. T., Feijoo, G., Canaval, J. and Lema, J. M. (2003) Semipilot-scale bleaching of kraft pulp with manganese peroxidase. *Wood Sci. Technol*. 37: 117-121.

Moreira, M.T., Feijoo, G., Mester, T., Mayorga, P., Sierra-Alvarez, R. and Field, J.A. (1998) Role of organic acids in the manganese-independent biobleaching system of *Bjerkandera* sp. strain BOS55. *Appl. Environ. Microbiol.* 64:2409-2417.

Morishima, I., Kurono, M. and Shiro, Y. (1986) J. *Biol. Chem*. 261: 9391-9399.

Morozova, O.V., Shumakovich, G.P., Shleev, S.V., Yaropolov, Y.I. (2007b) Laccase-mediator systems and their applications: A review. *Appl. Biochem. Microbiol*. 5:523-535.

Moss, T. H., Ehrenberg, A.and Bearden, A. J., (1969) Mossbauer spectroscopic evidence for the electronic configuration of iron in horseradish peroxidase and its peroxide derivatives, Biochemistry 8: 4159-62.

Munoz, C., Guillen, F., Martínez, A.T. and Martínez, M.J**.** (1997) Laccase isoenzymes of *Pleurotus eryngii*: characterization, catalytic properties, and participation in activation of molecular oxygen and Mn2+ oxidation. *Appl. Environ. Microbiol*. 63:2166-2174.

Mura A, Medda R, Longu S, Floris G, Rinaldi AC, Padiglia A. 2005. A Ca2+/calmodulin-binding peroxidase from Euphorbia latex: novel aspects of calcium–hydrogen peroxide cross-talk in the regulation of plant defenses. *Biochemistry* 44, 14120–14130.

Nakajima, R., Yamazaki, I., and Griffin, B. W. (1985) *Biochem. Biophys. RES. Commun*. 128, 1-6.

Nakasone, K.K., Sytsma, K.J. (1993) Biosystematic studies on *Phlebia acerina*, *P. rufa*, and *P. radiata* in North America. *Mycologia* 85:996-1016.

Nakayama, T., and Amachi, T., (1999) Fungal peroxidase: its structure, function and application, *J. Mol. Catal B: Enzymatic*, 6: 185- 98.

Nelms, S. M. (editor), (2005). Inductively coupled plasma mass spectrometry handbook. Oxford: Blackwell Publishing Ltd, p. 485.

Nelson, D. P.and Kiesow, L. A. (1972) Enthalpy of decomposition of hydrogen peroxide by catalase at 25 degrees C (with molar extinction coefficient of H_2O_2 solutions in the UV), *Anal. Biochem.* 49: 474-8.

Ng, T. B., & Wang, H. X. (2004). A homodimeric laccase with unique characteristics from the yellow mushroom Cantharellus cibarius. *Biochemical and Biophysical Research Communications*, 313, 37–41.

Nie, G. and Aust, S. D. (1997) Effect of calcium on the reversible thermal inactivation of lignin peroxidase. *Arch. Biochem. Biophys*. 337: 225-231.

Nie, G. and Aust, S. D. (1997a). Spectral changes of lignin peroxidase during reversible inactivation. *Biochemistry*, 36, 5113 – 5119.

Nie, G. and Aust, S. D. (1997b) Effect of Calcium on the Reversible Thermal Inactivation of Lignin Peroxidase. *Arch. Biochem. Biophys*. 337, 225 – 231.

Nie, G., Reading, N. S., and Aust, S. D. (1999) Engineering a Disulfide Bond in Recombinant Manganese Peroxidase Results in Increased Thermostability. *Arch. Biochem. Biophys*. 365, 328 – 334.

Niemenmaa, O., Uusi-Rauva, A.K., Hatakka, A. (2006) Wood stimulates the demethoxylation of [O14CH3]-labeled lignin model compounds by the white-rot fungi *Phanerochaete chrysosporium* and *Phlebia radiata*. *Archives of Microbiology* 185:307-315.

Niku-Paavola, M.L., Karhunen, E., Kantelinen, A., Viikari, L., Lundell, T., Hatakka, A. (1990) The effect of culture conditions on the production of lignin modifying enzymes by the white-rot fungus *Phlebia radiata. J Biotechnol* 13:211-221.

Niku-Paavola, M.L., Karhunen, E., Salola, P., Raunio, V. (1988) Ligninolytic enzymes of the white-rot fungus *Phlebia radiata*. *Biochem J* 254:877-883.

Nissum, M., A. Feis, and G. Smulevich. (1998) Characterization of soybean seed coat peroxidase: resonance Raman evidence for a structurebased classification of plant peroxidases. *Biospectroscopy.* 4:355–364.

Obinger, C., Burner, U., Ebernmann, R., Penel, C. and Greppin, H. (1996). Plant peroxidases. Biochemistry and Physiology Geneva- Vienna Univ. Agriculture and Univ. Geneva, Vienna and Geneva.

Ogawa, S., Shiro, Y. and Morishma, J. (1979) *Biochem*. *Biophys*. *Res*. *Commun*. *90*, 674-678.

Orgel, L. E. (1966) An Introduction to Transition Metal Chemistry. 2nd Edition. John Wiley and Sons, Inc., New York, pp 186.

Orth, A.B., Pease, E.A., Tien, M. (1994) Properties of lignin-degrading peroxidases and their use in bioremediation. In: Chaudhry G.R. (ed.) Biological Degradation and Bioremediation of Toxic Chemicals. Chapman & Hall, London, pp. 345-363.

Orth, A.B., Royse, D.J. and Tien, M. (1993) Ubiquity of lignin-degrading peroxidases among various wood-degrading fungi. *Appl. Environ. Microbiol*. 59:4017-4023.

Ortiz de Montellano, P. R. (1992) *Annu. Rev. Pharmacol. Toxicol.* 32, 89–107.

Otjen, L., Blanchette, R., Effland, M., Leatham, G. (1987) Assessment of 30 white rot basidiomycetes for selective lignin degradation. *Holzforschung* 41:343-349.

Otjen, L., Blanchette, R., Effland, M., Leatham, G. (1987) Assessment of 30 white rot basidiomycetes for selective lignin degradation. *Holzforschung* 41:343-349.

Oxvig, C., Thomsen, A. R., Overgaard, M. T., Sorensen, E.S., Hojrup, P., Bjerrum, M. J., Gleich, G. J., and Sottrup-Jensen, L., (1999) Biochemical evidence fro haem linkage through esters with Asp-93 and Glu-241 in human eosinophil peroxidase. The ester with Asp-93 is only partially formed in vivo. *J. Biol. Chem*. 274: 16953-8.

Ozaki, S. and Ortiz de Montellano, P. R. (1995) Molecular engineering of horseradish Peroxidase: Thioanisole sulfoxidation and styrene epoxidation by Phe-41 leucine and threonine Mutants. *J. Am. Chem. Soc.* 117: 7056-7064.

Paice, M. G. et al., (1993) Manganese peroxidase, produced by Trametes versicolor during pulp bleaching demethylates and delignifies Kraft pulp. *Appl. and Environ. Microbiology*, p. 260-265.

Palcic, M. M., Rutter, R., Araiso, T., Hager, I. P., Dunford, H. B. (1980) *Biochem. Biophys. Res. Commun*. 94: 1123-1127.

Palma, C., Martinez, A. T., Lema, J. M., and Martinez. M. J. (2000). Different fungal manganese-oxidizing peroxidases: a comparison between Bjerkandera sp. and *Phanerochaete chrysosporium*. *J. Biotechnol*. 77, 235-245.

Palmer, G. (1985) *Biochem. Soc. Trans.* 13: 548-560.

Pappa, H., R. Patterson, et al., (1996). The homologous tryptophan critical for cytochrome *c* peroxidase function is not essential for ascorbate peroxidase activity. *Journal of Biological Inorganic Chemistry* 1(1): 61-66.

Pasczynski, A., Huynh, V. B., and Crawford, R. (1986) *Arch. Biochem. Biophys*. 244, 750 – 765.

Passardi, F., Bakalovic, N., Teixeira, f. K., Margis-Pinheiro, M., Penel, C. and Dunand, C. (2007) Prokaryotic origins of the peroxidase superfamily and organellar-mediated transmission to eukaryotes, *Genomics* 89 (2007), pp. 567–579.

Paszczynski, A., Crawford, R.L. (1995) Potential for bioremediation of xenobiotic compounds by the white-rot fungus *Phanerochaete chrysosporium*. *Biotechnol. Prog*. 11, 368-379.

Patterson, W.R. and Poulos, T.L. (1995) Crystal structure of recombinant pea cytosolic ascorbate peroxidase. *Biochemistry* 34, 4331–4341.

Pease, E. A., Aust, S. D. and Tien, M. (1991) Heterologous expression of active manganese peroxidase from Phanerochaete chrysosporium using the baculovirus expression system. *Biochem. Biophys. Res. Commun*. 179: 897-903.

Pease, E.A., Andrawis, A. and Tien, M. (1989) Manganese-dependent peroxidase from *Phanerochaete chrysosporium*. Primary structure deduced from complementary DNA sequence. *J. Biol. Chem*. 264(23), 13 531–13 535.

Pecoraro, V.L.; Hsieh, W-Y; (2000) The Use of Model Complexes to Elucidate the Structure and Function of Manganese Redox Enzymes, Chapter 14 in *Metals in Biological Systems*, Astrid Sigel and Helmut Sigel (eds.) Marcel-Dekker, Inc., Basel, Switzerland 37: 429-504.

Peitsch, M. C. (1996). ProMod and Swiss-Model: Internet-based tools for automated comparative protein modeling. *Biochem. Soc. Trans.* 24: 274-279.

Pere-Boada, M., Doyle, W. A., Ruiz-Duenas, F. J., Martinez, Martinez, Martinez, A. T. and Smith , A. T. (2002) Expression of Pleurotus eryngii versatile peroxidase in *Escherichia coli* and optimization of in vitorn folding. *Enzyme Microb Technol* 30: 518-524.

Perez, J. and Jeffries, T. W. (1990) Mineralization of 14C-ring-labeled synthetic lignin correlates with the production of lignin peroxidase, not Mn-peroxidase or laccase. *Appl. Environ. Microbiol.* 56:1806-1812.

Perez, J. and Jeffries, T.W. (1992). Roles of manganese and organic acid chelators in regulating lignin degradation and biosynthesis of *Phanerochaete chrysosporium. Appl. Environ. Microbiol*. 58, 2402-2409.

Perez-Boada, M., Ruiz-Duenas, F. J., Pogni, R., Basosi, R., Thomas Choinowski, T., Martínez, M. J., Piontek, K. and Angel T. Martínez, A.T. (2005) Versatile Peroxidase Oxidation of High Redox Potential Aromatic Compounds: Site-directed Mutagenesis,

Spectroscopic and Crystallographic Investigation of Three Long-range Electron Transfer Pathways. *J. of Molecular Biology*, 354 (2), 385-402.

Perie, F.H., Sheng, D., and Gold, M.H. (1996) Purification and characterization of two manganese peroxidase isozymes from the white-rot basidomycete *Dichomitus squalens. Biochem. Biophys. Acta*, 1297, 139-148.

Petersen, J. F. W., Kadziola, A. and Larsen, S. (1994) Three-dimensional structure of a recombinant peroxidase from Coprinus cinereus at 2.6 Å resolution. *FEBS LETT*. 339: 291-296.

Petersen, J. F., J. W. Tams, J. Vind, A. Svensson, H. Dalboge, K. G. Welinder, and S. Larsen. 1993. Crystallization and X-ray diffraction analysis of recombinant *Coprinus cinereus* peroxidase. *J. Mol. Biol.* 232: 989-991.

Piontek, K., Choinowski, T., Perez-Boada, M. Ruiz-Duenas, F. J., Martinez, M. J., Plattmer, D. A. and Martiunez, A. T. (2009) Structural and site-directed mutagenesis study of versatile peroxidase oxidizing both Mn (II) and aromatic substrates (unpublished). Pdb 3FJW_A. http://www.ncbi. Nlm.nih.gov/protein/3FWA.

Piontek, K., Glumoff, T., and Winterhalter, K. (1993). Low pH crystal structure of glycosylated lignin peroxidase from *Phanerochaete chrysosporium* at 2.5 Â resolutions. *FEBSLett.* 315, 119-124.

Pointing, S. B. (2001). Feasibility of bioremediation by white rot fungi. *Applied Microbiology and Biotechnology*, 57, 20–33.

Popp, J. L., Kalyanaraman, B. and Kirk, T. K. (1990) Lignin peroxidase oxidation of Mn2+ in the presence of veratryl alcohol, malonic or oxalic acid, and oxygen. *Biochem*. 29: 10475-10480.

Poulos, T. L. and Finzel, B. C. (1984) Haem enzyme structure and function. In M. T. Mean (ed), peptide and protein Reviews, vol. 4. Marcel Dekker, New York, pp. 115-171.

Poulos, T. L., Patterson, W. R. and Sundaramoothy, M. (1995) The crystal structure of acsorbate and manganeseperoxidase: the role of non-haem metal in the catalytic mechanism. *Biochem. Soc. Trans*. 23: 228-232.

Poulos, T.L. and Kraut, J. (1980) The stereochemistry of Peroxidase catalysis. *J. Biol. Chem.* 255, 8199–8205.

Prabhu, N. V., Dalosto, S. D., Sharp, K. A., Wright, W. W., Vanderkooi, J. M. (2002) *J. Phys. Chem. B* 106, 5561.

Puglisi, A., Tabbi, G., and Vecchio, G. (2004). *J. Inorg. Biochem*. 98: 969 – 976.

Punt, P. J., van Biezen, N., Conesa, A., Albers, A., Mangnus, J. and van den Hondel, C.A.M. J J. (2002) Filamentous fungi as cell factories for heterologous protein production, *Trends Biotechnol.* 20: 200–206.

Rae, T. D., and Goff, H. M. (1996) Lactoperoxidase haem structure characterized by Paramagnetic Proton NMR Spectroscopy, *J. Am. Chem Soc.* 118:2103-4.

Raghukumar, C., D'Souza-Ticlo, D., Verma, A. (2008) Treatment of coloured effluents with lignin-degrading enzymes: An emerging role of marine-derived fungi. *Crit. Rev. Microbiol.* 34:189-206.

Rakhit, G., Antholine, W.E., Froncisz, W., Hyde, J.S., Pilbrow, J.R., Sinclair, G.R., Sarfar, B. (1985). *J. Inorg. Biochem*. 25, 217.

Ralph, J.P. and Catcheside, D.E.A**.** (2002) Biodegradation by white-rot fungi. In H. D. Osiewacz (ed.), The Mycota, vol. X. Springer-Verlag, Germany. p. 303-326

Rao, M.S.N., Lal, H. (1958). *J. Am. Chem. Soc*. 80 (1958) 3226.

Rasmussen, C. B, Hiner, A. N. P., Smith, A. T. and Welinder K.G. (1998) Effect of calcium, other ions, and pH on reactions of barley peroxidase with hydrogen peroxidase and fluoride: control of activity through conformational change. *J Biol Chem* 273, 2232–2240.

Rayner, A.D.M., Boddy, L. (1988) Fungal decomposition of wood. John Wiley & Sons, Great Britain.

Renganathan, V. And Gold, M. H. (1986) Spectral characterization of the oxidized states of lignin peroxidase, an extracellular heme enzyme from the white rot basidiomycete Phanerochaete chrysosporium *Biochemistry* 25: 1626 – 1631.

Renganathan, V., Miki, K. and Gold, M.H. (1985) Multiple molecular forms of diarylpropane oxygenase, an H_2O_2-requiring, lignin-degrading enzyme from *Phanerochaete chrysosporium*. *Arch. Biochem. Biophys*. 241, 304–314.

Rodrigo, C.; Rodrigo, M.; Alvarruiz, A.; Frigola, A. (1996) Thermal inactivation at high temperatures and regeneration of green asparagus peroxidase. *J. Food Prot. 59*, 1065-1071.

Rodrıguez, A, Pina, D. G, Yelamos, B., Leon, J. J. C, Zhadan, G. G., Villar, E, Gavilanes F, Roij, M. G, Sakharov, I. Y. & Shnyrov, V. L. (2002) Thermal stability of peroxidase from the African oil palm tree Elaeis guinensis. *Eur J Biochem* 269, 2584–2590.

Rodriguez, J., Ferraz, A., Nogueira, R.F.P., Ferrer, I., Esposito, E., Duran, N**.** (1997) Lignin degradation by the ascomycete *Chrysonilia sitophila*. *Appl. Biochem. Biotechnol*. 62: 233–242.

Rodriguez-Lopez, J. N., Lowe, D. J., Hernandez-Ruiz, J., Hiner, A. N., Garcia-Canovas, F., and Thorneley, R. N. (2001) Mechanism of reaction of hydrogen peroxide wih horseradish peroxidase: identification of intermediates in the catalytic cycle, J. Am. Chem. Soc. 123: 11838-47.

Roman, R., and Dumbord, H. B., (1972) pH dependence of the oxidation of iodide by Compound I of horseradish peroxidase, *Biochemistry* 11: 2076-82.

Ruiz-Duenas, F. J., Martinez, M. J. and Martinez. A.T. (1999c). Molecular characterization of a novel peroxidase isolated from the ligninolytic fungus *Pleurotus eryngii. Mol. Microbiol.* 31, 223- 235.

Ruiz-Dueñas, F.J., Martínez, Á.T (2009) Microbial degradation of lignin: how a bulky recalcitrant polymer is effi ciently recycled in nature and how we can take advantage of this. *Microb. Biotechnol*. 2:164-177.

Ruiz-Duerias, F. R., Morales, M., Perez-Boada, M., Choinowski, T., Martinez, M. J., Piontek, K. and Martinez, A. T. (2007) Manganese oxidation site in pleurotus eryngii versatile peroxidase: A site-directed mutagenesis, kinetic, and crystallographic study. *Biochemistry*, 46: 66-77.

Rulisek, L. and Vondrasek, J. (1998) Coordination geometries of selected transition metal ions (Co2+, Ni2+, Cu2+, Zn2+, Cd2+, and Hg2+) in metalloproteins. *J. Inorg. Biochem.* 71:155.

Rulisk, L. and Havlas, Z. (2002) Theoretical studies of metal ion selectivity: DFT calculations of camplexation energies of selected transition metal ions (Co^{2+}, Ni^{2+}, Cu_{2+}, Zn^{2+}, Cd^{2+}, and Hg^{2+}) in metal-binding sites of metalloproteins. *J. Phys. Chem. A.* 106: 3855-3866,.

Ryall, X. (1974), Competitive dialysis studies of metal–protein equilibria, Ph.D. thesis, Australian National University, Canberra.

Ryan, O., Smyth, M. R., O Fagain, C., (1994) Essays in Biochemistry, Ballou, D. P., ed., Portland Press: London, 28: 129-146.

Sakharov, I. Yu.; Sakharova, I. V. (2002) Extremely high stability of African oil palm tree peroxidase. *Biochim. Biophys. Acta 1598,* 108-114.

Saloheimo, M., Barajas, V., Niku-Paavola, M.L., Knowles, J.K. (1989) A lignin peroxidase encoding cDNA from the white-rot fungus *Phlebia radiata*: characterisation and expression in *Trichoderma reesei*. *Gene* 85: 343-351.

Saloheimo, M., Barajas, V., Niku-Paavola, M.L., Knowles, J.K.C. (1989) A lignin peroxidase en-coding cDNA from the white-rot fungus *Phlebia radiata*: Characterization and expression in *Trichoderma reesei*. Gene 85:343-351.

Sambrook, J., Fritsch, E., and Maniatis, T. (1989) Molecular cloning: A Laboratory Manual, CSH, USA.

Sander, S. A., Brays, R. C., and Smith, A. T., (1994) pH-dependent properties of a mutant horseradish peroxidase isoenzyme C in which Arg38 has been replaced with lysine, *Eur. J. Biochem.* 224: 1029-37.

Sanz, L., Nielsen, P. R., Villar, O., Gavel, E., Roig, M.G., Watanabe, V., Polikarpov, I., Shnyrov, V.L. (2008) *Biochimie* 90: 1737–1749.

Sanz, L., Nielsen, P. R., Villar, O., Gavel, E., Roig, M.G., Watanabe, V., Polikarpov, I., Shnyrov, V.L. (2008) *Biochimie* 90: 1737–1749.

Sarkar, B. (1987). Metal protein interactions. *Prog Food Nutr Sci.* ; 11(3-4):363-400.

Sarkar, S., Martinez, A. T., and Martinez, M. J**.** (1997). Biochemical and molecular characterization of a manganese peroxidases isoenzyme from *Pleurotus ostreatus. Biochim. Biophys. Acta*, 1339, 23-30.

Sawai-Hatanaka, H., Ashikari, T., Tanaka, Y., Asada, Y., Nakayama, T., Minakata, H., Kunishima, N., Fukuyama, K., Yamada, H., Shibano, Y., et al., (1995) Cloning, sequencing, and heterologous expression of a gene coding for *Arthromyces rasmosus* peroxidase. *Biosci. Biotechnol. Biochem*. 59, 1221-1228.

Sawai-Hatanaka, H., Ashikari, T., Tanaka, Y., Asada, Y., Nakayama, T., Minakata, H., Kunishima, N., Fukuyama, K., Yamada, H., Shibano, Y., Amachi, T., (1995). Cloning, sequencing and heterologous expression of a gene coding for Arthromyces ramosus peroxidase. *Biosci*. *Biotechnol. Biochem.* 59, 1221- 1228.

Schneegaβ, I., Hofrichter, M., Scheibner, K. and Fritsche. W. (1997). Purification of the main manganese peroxidase isozyme MnP2 from the white-rot fungus *Nematoloma frowardii* b19. *Appl. Microbiol. Biotechnol*. 48, 602-605.

Schuller, D. J., Ban, N., van Huystee, R. B., McPherson, A., and Poulos, T. L. (1996) *Structure* 4**,** 311–321.

Schwimmer, S. (1944) Regeneration of heat inactivated peroxidase. *J. Biol. Chem. 154*, 487.

Scott, G.M., Akhtar, M. and Kirk, T.K**.** (2000) An update on biopulping commercialization. In Proceedings of the 2000 Pulping Conference. Tappi Press, Atlanta, GA.

Serpersu, E. H., Shortle, D. and Mildvan, A. S. (1986) *Biochemistry* 26: 68-77.

Shah, V. and Nerud, F. (200) Lignin degrading system of white-rot fungi and its exploitation for dye decolourization. *Can. J. Microbiol*. 48:857-870.

Sharp, K. H., Moody, P. C. E., Brown, K. A. and Raven, E. L. (2004) Crystal structure of the ascorbate peroxidase-salicylhydroxamic acid complex. Biochemistry, 43(27):8644

Shatzman, A. R. and Rosenberg, M. (1987) Expression, identification, and characterization of recombinant gene products in *Escherichia coli*. *Methods Enzymol.* 152: 661-73.

Shiro, Y., Kurono, M., & Isao, M. (1986) Presence of endogenous calcium ion and its function and structural regulation in horseradish peroxidase, *J. Biol. Chem. 261*, 9382- 9390.

Sibbet, S.S. and Hurst, J.K. (1984) Structural analysis of myeloperoxidase by resonance Raman spectroscopy. Biochemistry 23, 3007–3013.

Sivaraja, M., Goodin, D.B., Smith, M. and Hoffman, B. M. (1989) Identification by of Trp191 as the Free-Radical Site in Cytochrome *c* Peroxidase Compound ES. Science, 245: 730-740.

Sjostrom, E. (1993) Wood Chemistry, Fundamentals and Applications. 2. ed., San Diego: Academic press, Inc. P.54.

Smith, A. T. and Veitch, N. C. (1998) Substrate binding and catalysis in haem peroxidases. *Current opinion in chemical Biology* 2 (2): 269- 278.

Smith, A.T. and Ngo, E. (2007) Novel peroxidases and uses, Patent number: WO/2007/020428

Smith, A.T., Santama, N., Decay, S., Edward, M., Bray, R.C., Thorneley, R. N. F. and Burke, J. F. (1990). Expression of a synthetic gene for horseradish peroxidase-C inn *Escherichia coli* and folding and activation of the recombinant protein with Ca^{2+} and hem, *J. Biol. Chem.* 265: 13335-43.

Smith, D. W. and Williams, R. J. P. (1970) The spectra of ferric haem and haemproteins. Sruct. Bonding 7: 1-45.

Smulevich, G., Martini, A. R., English, A. M. & Mauro, J. M. (1989) Effects of temperature and glycerol on the resonance Raman spectrum of cytochrome c peroxidase and selected mutants, *Biochemistry* 28, 5058 – 5064.

Smulevich, G., Mauro, J. M., Fishel, L. A., English, A. M., Kraut, J. & Spiro, T.G. (1988) Heme pocket interactions in cytochrome c peroxidase studied by site-directed mutagenesis and resonance Raman spectroscopy, *Biochemistry* 27, 5477 – 5485.

Sollewijn Gelpke, M. D., Moenne-Loccoz, P., and Gold, M. H. (1999) Arginine 177 is involved in Mn (II) binding by manganese peroxidase, *Biochemistry* 38, 11482-11489.

Srajer, V., and Champion, P. M. (1991) *Biochemistry 30*: 7390.

Stadman, T. C. (1990) Selenium biochemistry, *Annu. Rev. Biochem*. 59: 111-27.

Stavrov, S. S. 2001. Optical absorption band III of deoxyheme proteins as a probe of their structure and dynamics. Chem. Phys. 271:145–154.

Stewart, P., Whitwam, R.E., Kersten, P.J., Cullen, D., Tien, M. (1996) Efficient expression of a *Phanerochaete chrysosporium* manganese peroxidase gene in *Aspergillus oryzae*. *Appl. Environ. Microbiol*. 62:860-864.

Sundaramoorthy, M. Kiishi, K. Gold, M. H. and Thomas L. Poulos, T. L. (1994). The cystal structure of manganese peroxidase from *Phanerochuete chrysosporium* at 2.06-A resolution. The *J. of Biol. Chem*. Vol. 269, No. 52: 32759 – 32767.

Sundaramoorthy, M., Kishi, K., Gold, M. H., Poulos, T. L. (1997). *J. Biol. Chem*. 272: 17574 – 17580.

Sundaramoorthy, M., Youngs, H. L., Gold, M. H. & Poulos, T. L. (2005) High-Resolution crystal structure of manganese peroxidase: Substrate and inhibitor complexes. *Biochemistry*, 44, 6463-6470.

Surino, G., Watanabe, S., Ghibaudi, E. M., Bollen, A., Ferrari, R. P., and Moguilevsky, (2001) Glu375Gln and Asp225Val mutants: about the nature of the covalent linkages between haem group and apo-protein in bovine lactoperoxidase, *Bioorg. Med. Chem. Lett.* 11: 2827-3.

Sutherland, G. and Aust, S. D. (1996) The effects of calcium on the thermal stability and activity of manganese peroxidase. *Arch. Biochem. Biophys*, 332: 128-134.

Sutherland, G. R. J., Zapanta, L. S., Tien, M., and Aust, S. D. (1997) *Biochemistry*, 36, 3654–3662.

Tam, J. W. and Welinder (1996) Unfolding and refolding of Coprinus cinereus peroxidase at high pH, in urea, and at high temperature. Effect of organic and ionic additives on these processes. *Biochemsitry* 35: 7573-7579.

Tams, J. W., and Welinder, K. G. (1998) Glycosylation and thermodynamic versus kinetic stability of horseradish peroxidase, *FEBS, Lett.* 421: 234-6.

Tams, J. W., Vind, J., and Welinder, K. G. (1999) Adapting protein solubility by glycosylation. N-glycosylation mutants of *Coprinus cinereus* peroxidase in salt and organic solutions, *Biochem. Biophys. Acta.* 1432: 214-21.

Tamura, M., Asakura, T., and Yonetmi, T. (1972) *Biochim. Biophys*. 268,292-304 3977.

Tamura, Y.; Morita Y. (1975) Thermal denaturation and regeneration of Japanese-radish peroxidase. *J. Biochem. (Tokyo*) *78*, 561-571.

Taurog, A. (1999) Molecular evolution of thyroid peroxidase, *Biochimie* 81: 557 – 62.

Teer, T., Pentila, M., Keranen, S., Nevalainen, H., Knowles, J. K.C. (1992) Structure, function, and genetics of cellulose. In Finkelstein D. B., Ball, C. (eds). *Biotechnology of Filamentous Fungi*. Butterworth-Heinemann, Boston, pp. 417-445.

Teeri, T. (1997) Crystalline cellulose degradation: New insight into the function of cellobiohydrolases. *Trends Biotechnol* 15:160.

ten Have, R., Hartmans, S., Teunissen, P.J., Field, J.A**.** (1998) Purification and characterization of two lignin peroxidase isozymes produced by *Bjerkandera* sp. Strain BOS55. *FEBS Lett.* 422: 391–394.

Teske, J. G., Savenkova, M. I., Mauro, J. M., Erman, J. E. and Satterlee, J. D. (2000). Yeast cyrochrome c peroxidase expression in *Escherichia coli* and rapid isolation of various highly pure holoenzymes. *Protein expression and purification* 19:139-147.

Thong, T. and Barrett, D. M. (2005) Heat inactivation and reactivation of broccoli peroxidase. *J. Agric. Food Chem*. 53: 3215- 3222.

Thurston, C. F. (1994). The structure and function of fungal laccases. *Microbiology*, 140, 19 – 26.

Tien, M. (1987) Properties of ligninases from *Phanerochate chrysosporium* and their possible application. *Crit. Rev. Microbiol*. 15, 141-168.

Tien, M. and Kirk, T. K. (1983) Lignin-degrading enzyme from the hymenomycete *Phanerochaete chrysosporium* burds, *Science* **221** (1983), pp. 661–663. *Methods Enzymol*. 161: 238 – 249.

Tien, M. and Kirk, T.K. (1984) Lignin-degrading enzymes from *Phanerochaete chrysosporium*: purification, characterization, catalytic properties, of a unique H_2O_2-requiring oxigenase. *Proc. Natl. Acad. Sci*. U.S.A. 81: 2280-2284.

Timofeevski, S.L., and Aust, S. D. (1997) *Biochem. Biophys. Res. Commun*. 239, 645-649.

Tuisel, H., Sinclair, R., Bumpus, J. A., Ashbaugh, W., Brock, B. J. and Aust, S. D. (1990) Lignin peroxidase H2 from *Phanerochaete chrysosporium*: purification, characterization and stability to temperature and pH. *Archives of Biochemistry and Biophysics*, 279 (1), 158 – 166.

Vahatalo, A.V., Salonen, K., Salkinoja-Salonen, M., Hatakka, A. (1999) Photochemical mineralization of synthetic lignin in lake water indicates rapid turnover of aromatic organic matter under solar radiation. *Biodegradation* 10: 415-420.

Van Aken, B., Hofrichter, M., Scheibner, K., Hatakka, A.I., Naveau, H., Agathos, S.N**.** (1999) Transformation and mineralization of 2,4, 6-trinitrotoluene (TNT) by manganese peroxidase from the white-rot basidiomycete *Phlebia radiata. Biodegradation* 10:83-91.

Van den Hondel C. J. J., Punt, P. J. and Van Gorcom R. F. M. (1991) Heterologous gene expression in filamentous fungi. In: Bennett JW and Lasure LL (Eds) More Genetic Manipulation of Filamentous Fungi (pp 396-428). Academic Press, Orlando.

van Huystee, R. B., Roi, M. G., Shnyrov, V. L. & Sakharov, I. Y (2004) Peroxidase stability related to its calcium and glycans. *Phytochem Rev* 3: 19–28.

Van Huystee, R. B., Xu, Y. and O'Donnel, J. P. (1992) *Plant Physiol. Biochem*. 30: 293-297.

Vares, T. and Hatakka, A. (1997) Lignin-degrading activity and ligninolytic enzymes of different whit-rot fungi: Effects of manganese and malonate. Can J. Bot 75: 61-71.

Vares, T., Kalsi, M., Hatakka, A. (1995) Lignin peroxidases, manganese peroxidases, and other ligninolytic enzymes produced by *Phlebia radiata* during solid-state fermentation of wheat-straw. *Appl Environ Microbiol* 61: 3515-3520.

Veitch, N.C. (2004) Horseradish peroxidase: a modern view of a classic enzyme. *Phytochemistry* 65 (3): 249-259.

Villaasenor, F., Lorea, O., Campero, A., & Viniegra-Gonzalez, G. (2004). Oxidation of dibenzothiophene by laccase or hydrogen peroxide and deep desulfurization of diesel fuel by the latter. *Fuel Processing Technology*, 86: 49–59.

Vitello, L. B., Erman, J. E. *et al*., (1992) Effect of Asp-235→Asn substitution on the absorption spectrum and hydrogen peroxide reactivity of cytochrome c peroxidase. Biochemistry, 31 (46): 11524-35.

Voet, D. & Voet, J. G. (2003). Biochemistry, Wiley, USA.

Waldron, K. J. and Robinson, N. J. (2009). How do bacterial cells ensure that metalloproteins get the correct metal? Nature reviews/Microbiology, Macmillian Publishers Ltd. 6: 25 – 35.

Wang, M., Feng, W., Zhao, Y. & Chai, Z. (2009). ICP-MS-Based strategies for protein quantification. *Mass Spectrometry Reviews*, Wiley periodicals, Inc

Wang, Y., Vazquez-Duhalt, R. and Pickard. M.A. (2002). Purification, characterization, and chemical modification of manganese peroxidase from *Bjerkandera adusta* UAMH 8258. *Curr. Microbiol*. 45, 77-87.

Wantanabe, S., Murata, S., Kumura, H., Nakamura, S., Bollen, A., Moguilevsky, N., and Shimazaki, K. (2000) Bovine lactoperoxidase and its recombinant: comparison of structure and some biochemical properties. *Biochem. Biophys. Res. Commun*. 274: 756-61.

Wariishi, H., Akileswaran, L., and Gold, M. H. (1988) *Biochemistry* 27, 5365 – 5370.

Wariishi, H., Dunford, H. B., MacDonald, I. D., and Gold, M. H. (1989) *J. Biol. Chem*. 264, 3335 – 3340.

Wariishi, H., Gold, M. H., Valli, K. (1991) In vitro depolymerisation of lignin by manganese peroxidase of *Phanerochaete chrysosporium*. *Biochem. Biophys. Res. Commun.*176:269-276.

Wariishi, H., Huang, J., Dunford, B. H. and Gold, M. H. (1991) Reactions of lignin peroxidase compounds I and II with veratryl alcohol: Transient-state kinetic characterisation. *J. Biol. Chem.* 286: 20694-20699.

Wariishi, H., Valli., K., and Gold, M. H. (1992). *J. Biol. Chem*. 267, 23688 – 23695.

Welinder, K. G., Gajhede, M. In "Plant peroxidases: Biochemistry and Physiology", Welinder, K. G., Rasmussen, S. K., Penel, C., Greppin, H., Eds; University of Geneva: Geneva, 18: 35-42.

Welinder, K. G., Rasmussen, S. K., Penel, C. and Greppin, H. (1993). Plant peroxidases. Biochemistry and Physiology, Univ. Of Copenhagen and Univ. Geneva, Copenhagen and Geneva.

Welinder, K.G. (1992) Superfamily of plant, fungal and bacterial peroxidases. *Curr. Op. Struct. Biol.* 2, 388–393.

Whitaker, J. R. (1994). Effect of pH on enzyme catalysed reactions. In: Principles of enzymology for the food science, 2nd edn. Marcel Dekker, New York, pp 271-300.

Whitwam, R. and Tien, M. (1996) Heterologous expression and reconstitution of fungal Mn peroxidase. *Arch. Biochem. Biophys*, 333: 439-446.

Whitwam, R. E., Gazarian, I. G. and Tien, M. (1995) Expression of fungal manganese peroxidase in *E.coli* and refolding to yield active enzyme. *Biochemical and biophysical research communications*. 216 (3), 1013-1017.

Whitwam, R., Brown, K. R., Musick, M., Natan, M. J., Tien, M., (1997) Mutagenesis of the Mn^{2+}- binding site of manganese peroxidase affects oxidation of Mn^{2+} by both compound I and compound II. *Biochemistry* 36: 9766-9773.

Xu, P., Yu, B., Li, F. L., Cai, X. F., and Ma, C. Q. (2006). Microbial degradation of sulfur, nitrogen and oxygen heterocycles. *Trends in Microbiology*, 14: 398–405.

Yamashita, .M. M., Wesson, L., Eisenman, G. and Eisenberg, D. (1990) Where Metal Ions Bind in Proteins, *Proc Natl Acad Sci.* 87: 5648–5652.

Yang, S.Q., Yan, Q.J., Jiang, Z.Q., Li, L.T., Tian, H.M., Wang, Y.Z. (2006) High-level of xylanase production by the thermophilic *Paecilomyces thermophila* J18 on wheat straw in solid-state fermentation. *Bioresource Technol*. 97: 1794–1800.

Youngs, H. L., Moe nne-Loccoz, P., Loehr, T. M., Gold, M. H (2000). Formation of a bis (histidyl) heme iron complex in manganese peroxidase at high pH and restoration of the native enzyme structure by calcium. *Biochemistry* 39: 9994–10000.

Youngs, H. L., Sollenijn Gelpke, M. D., Li, D., Sundaramoorthy, M. and Gold, H. (2001) The role of Glu39 in Mn (II) binding and oxidation by manganese peroxidase from *Phanerochaete chrysosporium*. *Biochemistry* 40: 2243-2250.

Youngs, H. L., Sollewijn Gelpke, M. D., Li, D., Sundaramoorthy, M., and Gold, M. H. (2001) The role of Glu39 in Mn (II) binding and oxidation by manganese peroxidase from *Phanerochaete chrysosporium*, *Biochemistry* 40: 2243-2250.

Zamorano, L. S., Vilarmau, S. B., Arellano, J. B., Zhadan, G. G., Cuadrado, N. Bursakov, S. A. Roig, M. G. and Shnyrov, V. L. (2009). Thermal stability of peroxidase from *Chamaerops excelsa* palm tree at pH 3. *International Journal of Biological Macromolecules* 44: 326–332.

Zamorano, L.S., Pina, D.G., Arellano, J.B., Bursakov, S.A., Zhadan, A.P. , Calvete, Sanz, L., Nielsen, P. R., Villar, O., Gavel, E., Roig, M.G., Watanabe, V., Polikarpov, I., Shnyrov, V.L. (2008) *Biochimie* 90: 1737–1749.

Zoorob, G. K., Mckiernan, J. W. and Caruso, J. A (1998) Fundamental Review: ICP-MS or elemental speciation studies. *Mikrochim. Acta.* 128: 145-168.